# Chapter 1

# Introduction to Fiber Optic Sensors, Cholesterol and Chitosan

*Abstract*

*This introductory chapter begins with a general description of fiber optic sensors. Common classifications of fiber optic sensors are also discussed in this section. It gives a brief description about the photosensitivity in optical fibers and various methods employed for the fabrication of optical fiber gratings. Subsequently, the importance of cholesterol detection is outlined, which is the main theme of this thesis. Different methods for the detection of cholesterol and their limitations are also briefed in this chapter. Chitosan, the biopolymer used in the experimental investigation for the enhancement of the cholesterol sensitivity of the sensor heads is also introduced in this chapter.*

## 1.1 Introduction

Charles K Kao and Hockham proposed the idea of optical fiber in 1966 [1]. In this paper, they evaluated the materials and loss mechanisms in waveguides and concluded that a dielectric fiber "represents a possible medium for the guided transmission of energy at optical frequencies." They also concluded that, "The required loss figure of around 20 dB/km is much higher than the lower limit of loss figure imposed by fundamental mechanisms." Optical fibers have emerged as the most suitable medium for light delivery and have become an integral and indispensable part of the communication systems. Induction of optical fibers revolutionized the communication network in all aspects like speed, bandwidth, coverage area etc. and the world witnessed breath-taking changes in every walks of life. C K Kao was bestowed with the 2009 Nobel Prize in Physics for this ground breaking invention in the history of science.

Even though optical fiber was proposed way back in 1966, the development of such a waveguide was limited by the huge transmission loss of the order of $10^3$ dB/km. The problem for this heavy attenuation was later identified as the impurities in silica which could not be removed with the then prevailing techniques. With the advancements in technologies in the area of material science, Kapron, Keck, and Maurer [2] came up with new optical fiber design in 1970 breaking the barrier of 20 dB/km suggested earlier by Kao et al. Since the development of the first low loss silica based optical fiber for communication systems, the optical fiber technology witnessed explosive developments and refinements and became the backbone of the communication networks of the modern world.

As suggested by Kao and Hockham, optical fibers were employed as a light guiding waveguide during the early development stages. During

early seventies, when the optical fiber communication technology was in its budding stages, the sensitivity of optical fibers to certain external perturbations like bending, stress etc. became evident in the transmission characteristics of the fiber. A great deal of research was done at that time to reduce these effects through suitable fiber and cable designs. Capitalizing on these observations of exceptional sensitivity of optical fibers to external perturbations, an alternate school of thought began to emerge, exploiting this feature. This offshoot of optical fiber technology soon saw a flurry of research and development activities around the world, which led to the emergence of a new stream of research, namely: fiber optic sensor technology.

As technology advanced, more and more applications for optical fibers evolved. Today, optical fibers are employed in numerous applications including communications, medicine, energy, manufacturing, sensing, transportation, entertainment etc. [3]. Fiber optic sensor technology became a full-fledged branch of research in the field of optical sensors with the nourishments provided by the developments in the field of optoelectronics and lasers.

Modulation of the properties like intensity, phase, polarization, wavelength etc., of the light propagating through the fiber, and its measurement forms the basis of a fiber optic sensor [4-6]. In the current scenario, fiber optic devices play a leading part in optical sensing and optical communication systems. The versatility of optical fiber based devices found diverse applications in almost all fields like electrical, mechanical, civil, nuclear, aerospace, chemical and biomedical sensing [4-6]. A brief introduction to various types of fiber optic sensors is provided in the succeeding section.

## 1.2 Fiber Optic Sensors - An Overview

In parallel with these developments in the field of communication, researchers also found applications for optical fibers in various field like optical sensors, lighting etc. Fiber optic sensor (FOS) can be simply described as an optical sensor system, which utilizes optical fiber as a part of it. Either the measurand or the perturbance interacts with the light being guided inside an optical fiber or the light is guided to an interaction region by an optical fiber, where it is modulated according to the parameter of interest. An illustration of a general fiber optic sensor is given in Fig. 1.1. The modulated light from the sensing site is coupled to a receiver where, it is detected and demodulated for the analysis.

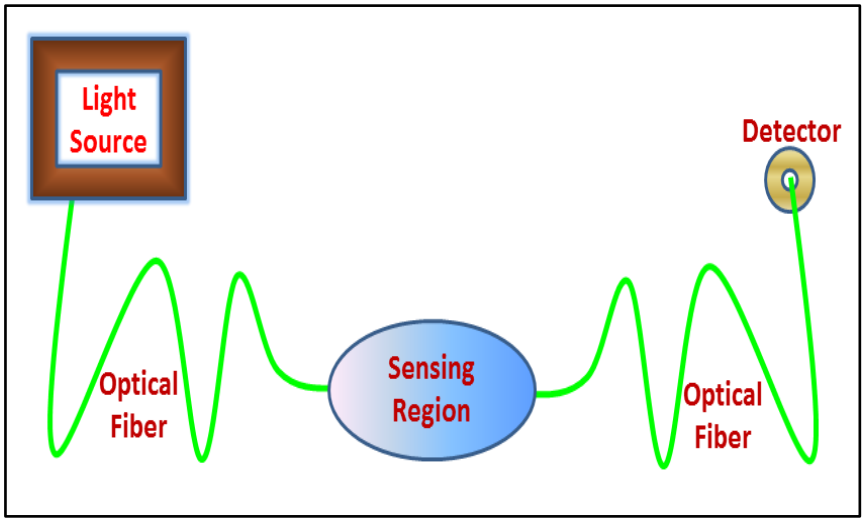


***Figure 1.1:*** *Illustration - FOS system.*

Sooner, optical fiber based sensing systems replaced many electrical, electronic and mechanical sensors because of their inherent advantages. The main attractions of fiber optic sensors over the conventional electrical, electronic and mechanical sensors are listed below [3-9].

(i) No EMI: The most important advantage of fiber optic sensor system is that, it is insensitive to electro-magnetic interference (EMI) and its dielectric characteristics. This makes the sensing mechanism tamper proof with lesser errors and can avoid accidents due the electric shocks and short circuits.

(ii) Smaller and light weight: In this era of micro and nano scaling, smaller size and lighter weight of fiber optic sensors make it attractive in the development of compact systems suitable for reduced size device.

(iii) Remote sensing: Remote sensing is another possibility of fiber optic sensors. It is possible to deploy a fiber optic sensor remotely, at one end of a long communication fiber, which can be used to convey the sensed parameters to the control room located miles away. Developments in the field of optical fiber technology led to the fabrication of transmission cables with significantly lower signal loss, maintaining higher values of signal-to-noise ratio (SNR). This also made sensing easier at locations, which are in accessible to human beings.

(iv) Hazardous environmental operations: Owing to the ability of fiber optic sensors to perform well under extreme conditions such as, high toxicity, high temperatures and pressures, corrosive environments, high radiation levels, large electromagnetic fields etc., they are being deployed to operate in these hazardous environments.

(v) Large bandwidth: The operating bandwidth of fiber optic systems is very huge and it is yet to be tapped fully, for want of the associated electronic devices at the transmitter and receiver sides, which can perform at par with the optic fiber cables.

(vi) High sensitivity: Fiber optic sensors are highly sensitive to small perturbations.

(vii) Distributed sensing: Being a part of an optical fiber, fiber optic sensors can be distributed along the cable to have localized measurements at different points along the transmission line without considerable loss. This provides a system

to monitor and investigate the parameter being measured over a stretched length like in the case of pipelines or an extended area.

(viii) Low maintenance: Since the health of fiber optic sensors is not influenced much by the operating conditions, these systems do not require frequent maintenance and recalibration. This reduces the operating cost and time consumed for the patch ups.

As mentioned earlier, FOSs have been used in diverse fields extending from monitoring of structures for the prediction of earthquakes and volcanic activity [10] to clinical diagnosis [11]. Fiber optic strain sensors are extensively used to monitor the health of buildings, other structures, bridges etc. [12-21]. FOS devices for sensing temperature [21-26], vibration [27], biological parameters [28-36], gaseous species [37,38], chemicals and pH [39-45], displacement [46], metrological parameters [47] etc., were also reported earlier.

### 1.2.1 Fiber Optic Sensors: Classifications

Fiber optic sensors are generally classified based on (a) the function of the optical fiber used, (b) the scheme of modulation used and (c) the principle employed in realization of the sensor. A brief description of these classifications is presented below.

#### 1.2.1.1 Based on the Function of the Fiber

The very basic classification is based on the functionality of optical fiber in the sensing system as: (*a*) Intrinsic sensor and (*b*) Extrinsic sensor [4-8, 42]. In an intrinsic FOS system, the sensor head or the sensing element is a part of the fiber and the light is modulated within the fiber itself [26, 42-47]. Hence, they are termed as all fiber sensors.

In an extrinsic FOS system, the sensor head is not a part of the fiber, as shown in Fig 1.2. Optical fiber functions as an optical waveguide for the

transport of the light signals from the source to the sensing site and from there to the detector. At the sensing area, the light carried by the optical fiber is taken out of the fiber and is modulated by the measurand. This measured light is coupled to the detector for further analysis and recording.

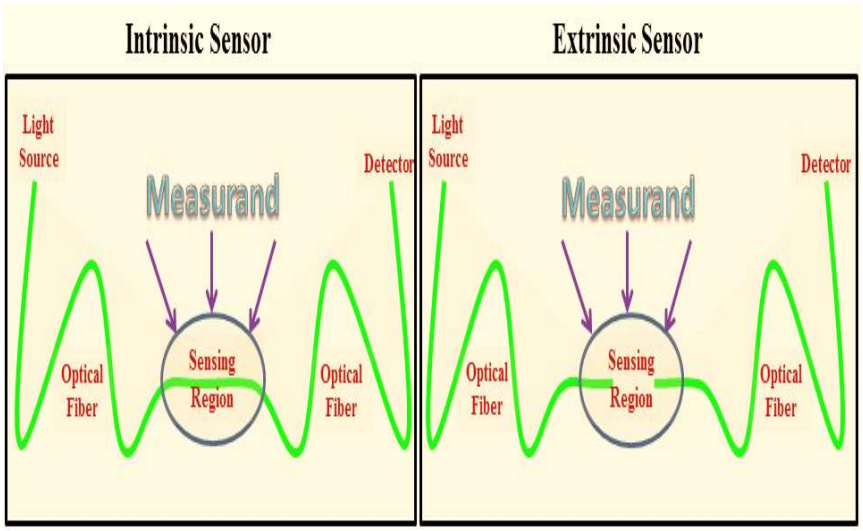


***Figure 1.2:*** *Intrinsic and extrinsic fiber optic sensor systems.*

#### 1.2.1.2 Based on the Scheme of Modulation

As light traverses the sensing region, the external perturbances influence the light to alter some of its properties. The characteristic property of the light signal, which is modulated by the perturbation, forms the basis of another classification of FOS systems. Based on the type of modulation schemes employed, FOSs are classified as: (*a*) Intensity modulated sensors, (*b*) Phase modulated sensors, (*c*) Polarization modulated sensors and (*d*) Wavelength modulated sensors [4-8, 42]. The perturbations from the surrounding environment interact with the sensor head, to modulate or alter at least one of the above four factors. The success of the FOS depends on its ability to convert the measurands into these parameters reliably and correctly.

Measurement of these modulations imparted on the light signal forms the basis of these types of FOSs.

**(a) Intensity Modulated Sensors**

In intensity modulated fiber optic sensors, the amplitude of the light signal is altered or varied by the perturbations or the measurand [42, 46, 48, 49]. The measurement of intensity or the signal strength is comparatively easier than the measurements associated with changes in phase or wavelength. This makes the entire system simpler and can be realized at a lower cost. The perturbation initiated mechanisms like reflection, transmission, bending or other optical phenomenon such as absorption, fluorescence, or scattering can be associated with the intensity modulation of the light delivered by the optical fiber.

Several intrinsic and extrinsic configurations are proposed for the intensity modulated FOSs based on these mechanisms. The most primitive type of these employ the intensity based reflective sensors and are the most widely used sensors [4-8, 35, 36, 47-49]. Since these sensors rely on the intensity measurements, they make use of optical fibers with comparatively larger core dimensions or a bundle of fibers, so that more power can be delivered to the measurement site.

The simple configuration, low fabrication cost, multiplexing possibilities, robustness and flexibility makes this scheme popular. In addition, the intensity modulated fiber optic sensors do not require any special components or fibers other than a stable optical source and a reliable photo-detector with a good signal processing unit. The major limitation of intensity based fiber optic sensors is the possibility of erroneous readings due to the influence of environmental factors other than the measurand, which can easily affect the intensity of the optical signal.

Major sources of errors include variable losses due to light sources and detectors, joints, misalignments and bends, wear and tear of optical fiber etc. Fluctuations at the source output can also lead to faulty readings, unless a referencing system is employed [48-50].

**(b) Phase Modulated Sensors**

The principle of operation of phase modulated sensors relies on the scrutiny of the alterations imposed on the phase of light coupled by the optical fiber. Optical phase modifications induced on the light passing through a fiber by the external perturbation of interest is decoded or demodulated, in comparison with the phase of the light passed through a reference optical fiber. Very high resolution measurements; feasible by virtue of its intrinsically high sensitivity to environmental fluctuations, make it very attractive.

Interferometric detection schemes are utilized in general with phase modulated sensors. In this method, the light is split into two halves, where one of the beams coupled to an optical fiber, is exposed to the external perturbation and undergoes phase modifications. The other beam, coupled through another fiber which is used as a reference, is isolated from the sensing environment. These two signals from the two fibers are made to recombine at the detector end, to form interference patterns [4, 5, 42-53]. These patterns are analyzed to measure the external perturbations like rotation, pressure, tilt, weight, magnetic field, etc. Various interferometers like Michelson, Sagnac, Fabry-Perot, Mach-Zehnder, etc. are the commonly used configurations. These interferometric sensors have wide applications in scientific, industrial and other technical fields [4, 5, 48-58]. In general, the phase modulated FOS is more sensitive than the intensity modulated sensors.

**(c) Polarization Modulated Sensors**

Since the fabrication material of optical fiber, namely silica, exhibit the phenomenon of photo elastic effect, its RI characteristics varies under the influence of stress, strain or pressure. This induced RI changes with respect to the external effects will in turn alter the polarization state of the light carried by fiber. These changes in polarization can be monitored to sense the perturbation [6, 8, 42].

A variety of physical phenomena like, electro optic effect, Faraday rotation and photo elastic effect, influence the state of polarization of light. Application of stress and twisting of the fiber can also alter the polarization state of the light being guided. Magnetic fields, electric fields, temperature, chemical species etc. can be measured by these polarization modulated sensors [8, 42, 49, 51, 52].

**(d) Wavelength Modulated Sensors**

If any external perturbation can alter the wavelength of the transmitted or the reflected light signal guided through an optical fiber, it can perform well as a wavelength modulated sensor. Wavelength modulated devices use the alterations in the wavelength of coupled light for the detection of parameters. Basically, these sensors make use of optical fiber gratings written inside the optical fiber as the sensing tool. A grating is a periodic arrangement that alters the light signal, depending on the periodicity of the grating.

**1.2.1.3 Based on the Principle of Operation**

Based on the operating principle, fiber optic sensors are classified as: (*a*) Evanescent Wave sensors (EWS), (*b*) Surface Plasmon Resonance (SPR) sensors and (*c*) Fiber Grating sensors.

**(a) Evanescent Wave Sensors**

Light signals traveling through the optical fiber by total internal reflection (TIR). In the process of TIR, interface specific electromagnetic disturbances are generated along the core cladding boundary. The transverse component of the reflecting beam generates standing waves at every point of strike on the interface. A portion of this harmonic wave penetrating out of the fiber structure, spreads to the surrounding medium, and decays exponentially with distance from the interface [59]. Evanescent wave sensors make use of this exponentially decaying tail for sensing. The power carried by the evanescent wave is influenced by the external medium, altering the characteristics of the light coupled through the fiber and this forms the basis of the EWS. The power carried by the evanescent tail can be modulated by various properties of the external medium like, absorbance, reflectance, RI etc. EWS is one of the mostly researched fiber optic sensor [4-9, 11, 35-40, 45, 48, 49, 59-68], owing to its possibility of sensing versatile parameters and materials, simpler structure, cost effectiveness and ease of use.

**(b) Surface Plasmon Resonance (SPR) Sensors**

A surface Plasmon Polariton (SPP) is an electromagnetic excitation at a metal-dielectric interface, consisting of a surface charge density oscillation coupled to the electromagnetic fields [69, 70]. The SPP field components have their maxima at the interfaces and it decay exponentially in the metallic layer and the surrounding media just like the evanescent waves. In the case of a planar structure, the SPP can exist in the form of S or P polarized (TM) wave [71].

SPP is a promising tool for sensing applications to probe the medium adjacent the interface as it is a localised phenomenon at the metal-

dielectric interface [72-77]. Many configurations of SPP sensors like bulk, planar, and fiber geometries are in practice today [69-83].

Since the first report on fiber optic SPR sensors published in 1990 [82], intense research brought about several modifications in the fiber structure and the geometry used. The simplest optical fiber SPR configuration makes use of a standard optical fiber to replace the coupling prism [82, 83]. A small portion of the fiber is uncladded and a metallic layer is coated in this region around the core. The guided optical wave traveling through the fiber hits the interface of core and the metallic coating to develop evanescent waves in this region. These evanescent waves in turn excite the surface plasmon waves. These resonating surface plasmon waves are highly susceptible to external perturbations like refractive index. This forms the basis of fiber optic SPR sensors. In order to enhance the sensitivity of the sensor head, several modifications such as, side polished fiber [83], tapered fiber [84], FBG [85-87], LPG [88], TFBG [89, 90], bend fiber geometry [91], sensitive coating over the metallic layer [92] etc. are being employed.

**(c) Fiber Grating Sensors**

As discussed earlier, the intensity based sensor systems are highly prone to errors arising from the variable losses due to light sources and detectors, joints, misalignments and bends, wear and tear of optical fiber etc. [48-50]. Light intensity fluctuations at the source output can also significantly influence the performance of these sensors. Phase and polarization measurements require sophisticated equipment and are also affected by minute vibrations and deviations in temperature of the operating environment. The solution for the above limitations is to use referenced measurements or change the geometry of the sensor such that,

the errors are minimized. Fiber gratings sensing systems turn out to be highly relevant in this context.

An optic fiber grating is fabricated by making intermittent refractive index perturbations on an optical fiber [93-95]. An optical fiber grating works by the coupling of power from the fundamental core mode to forward or backward propagating modes, depending upon the type of the grating. This power coupling from the core mode is strongly influenced by external perturbations like stress, strain, pressure, temperature, refractive index of the medium around the grating, bend of the fiber etc. Measurement of these alterations is the foundation of sensing with optical fiber gratings. The fiber gratings are mainly classified into two depending on the grating periodicity and nature of mode coupling:

**Fiber Bragg Gratings (FBGs)** are also referred as reflection gratings or short period gratings. FBGs work by the coupling of power between two core modes travelling in opposite directions termed as contra-directional coupling [93-96].

**Long Period Gratings (LPGs)** or transmission gratings work by the principle of co-directional coupling. Here, the coupling is from the core mode to the cladding modes that travel in the same direction as the core mode [96-99]. These cladding modes attenuate quickly on propagation, which results in loss bands at separate wavelengths in the transmission spectrum of the grating.

Fiber gratings are being widely used as sensing element for physical, chemical, biochemical and biological species and various physical parameters. Numerous parameters like stress, strain, temperature, displacement, vibration, radiation dosage etc. are monitored with the help of fiber gratings. Generalized discussion on the fabrication of optical fiber gratings is presented in the next section.

## 1.3 Optical Fiber Gratings

Photosensitivity in optical fibers was reported by Hill et al. in the year 1978 [100, 101]. They reported a permanent grating written in the core of germenosilicate fibers by the irradiation of an argon ion laser output. They were studying the nonlinear effects of germanium doped silica fiber by coupling the visible light from the argon ion laser into it. Prolonged coupling of the laser resulted in the reduction in the intensity of the transmitted signal and an enhancement in the reflected intensity. This grating written with a wavelength of 488 nm, resulted in a notch filter at this wavelength. These gratings were termed as self-organized or self-induced gratings as they were developed naturally without any human interventions. After these reports, related researches were comparatively thin for want of a suitable grating writing method till, Meltz et al. demonstrated the side writing technique in 1989 [102]. Towards the end of the last century, many other techniques for the direct fabrication of gratings were proposed. Along with this, optical fiber grating technology became one of the most researched fields owing to its innumerable applications in the field of communication, lighting, sensing etc.

### 1.3.1 Photosensitivity in Optical Fibers

The refractive index alterations induced on the core of the fiber resulting from the exposure to light radiations are termed as photosensitivity in optical fibers. In 1981, Lam and Garside [103] proposed a two-photon process as the probable mechanism for the induced RI modulation reported by Hill et al. But in 1987, J Stone established that, the mechanism behind the refractive index modulation is because of the photosensitivity of fibers due to the presence of higher concentrations of germanium [104]. He studied several fibers with germanium doped in the

core and observed similar phenomenon. As stated earlier, the work of Meltz et al. introduced a new technique for grating fabrication in optical fibers using 240-250 nm, UV wavelengths, close to the absorption peak of germanium related defects [102]. The peak of the absorption of the GeO defect was reported around 240 nm [105].

Several theories have been proposed to explain these photo induced RI changes, such as colour-center model [106], electron charge migration model [107], compaction model [108], dipole model [109], stress relief model [110], ionic migration model [111] and Soret effect [112]. The common component in these models is the germanium-oxygen vacancy defects in the glass lattice structure. The colour-center model proposed by Hand and Russel [106] is the most commonly accepted model in explaining the refractive index modulation in optical fiber gratings especially in germanosilicate fibers. According to the colour-center model, the defects present in glass core of the fiber leads to its photosensitivity.

Defects in optical fibers were subjected to strict scrutiny because of their unwanted strong absorption bands leading to attenuation of signals transmitted. These defects, which are often termed as colour centers, are the outcome of the fabrication method: The Modified Chemical Vapour Deposition (MCVD) process. During the high temperatures of MCVD process, $GeO_2$ dissociates to form GeO. These GeO species are manifested as Ge-Si and Ge-Ge bonds, when incorporated into the glass lattice.

It is proven that the Ge-Si and Ge-Ge bonds are responsible for the photosensitivity in germanosilicate fibers [113, 114]. The Ge-Si bond is the most efficient mechanism triggering the processes of refractive index changes through photoionization. Irradiation with wavelengths nearer to 240 nm ionizes these bonds releasing an electron to form paramagnetic GeE' centers. This electron may recombine immediately with the formed GeE' defect center

or it may diffuse through the lattice until it is trapped at a defect site, altering it to a paramagnetic defect center [115, 116]. Minimization of these defects has been a thrust area of research during the budding stages of optical fiber technology, in which the researchers have succeeded to a great extent. By the advent of optical fiber gratings, these defects turned out to be a blessing in disguise, changing their role in optical fiber radically. There are also published reports proposing that the refractive index modulation of UV exposed germanium doped silica fibers may be due to the structural rearrangement of glass matrix, like densification [117].

Silica fibers with doping materials other than germanium like, europium-alumina, erbium-germanium, cerium, antimony, germanium-boron, germanium-tin, germanium-phosphorous etc. in the core also exhibited photosensitivity [118-124]. Other optical fibers like ZBLAN fluorozirconate glass fibers and cerium doped fibers were also reported to exhibit photosensitivity [125, 126]. The photosensitivity of all fibers with these dopants was comparatively very low except for the germanium-boron co-doped fiber. Optical fibers also exhibited photosensitivity under the exposure to several other wavelengths of radiations (157 nm, 193 nm, 248 nm, 325 nm, 351 nm etc.) [127-130].

#### 1.3.1.1 Enhancement of Photosensitivity in Optical Fibers

The process and physics of photosensitization in optical fibers under the irradiation of UV light has been studied very well since its discovery. A great amount of time and research has been spent on developing easier ways of grating fabrication. These thoughts led to the development of methodologies to improve the photosensitivity of germanosilicate optical fibers. The three mainly used methods are: (*a*) Hydrogen Loading, (*b*) Flame Brushing and (*c*) Boron Co-doping.

### (a) Hydrogen Loading

Hydrogenation or hydrogen loading of the optical fibers is the easiest method to enhance the UV sensitivity of germanosilicate fibers. This is carried out by exposing the fiber to hydrogen gas during which the hydrogen molecules diffuse into the fiber core [130-133]. It is believed that, these hydrogen molecules react with the normal Si-O-Ge sites to form OH species, creating severe oxygen deficiency inside the fiber core leading to the development of defect centers with Ge-Si and Ge-Ge bonds. These bonds have strong absorption centered around 240 nm and can be easily altered by the UV exposure giving rise to the required refractive index changes [131-133]. This forms the basis of the enhancement in the photosensitivity in hydrogen loaded optical fibers. At normal temperature and pressure, the hydrogenation process is quiet lengthy with duration of one to two weeks. This can be reduced largely by increasing the temperature or pressure or both, which is practiced usually [132].

The most important advantage of hydrogen loading is that, it enhances the photosensitivity in germanosilicate fiber to a great extent, making the grating fabrication much easier in standard telecommunication optical fibers. Also, gratings with better characteristics like high reflectivity and smaller bandwidth can be fabricated at ease. Another advantage is that the grating is formed only in the regions exposed to UV. The unreacted hydrogen molecules inside the fiber core, after the grating fabrication, diffuse out of the fiber core gradually and will not contribute to the absorption losses of the fiber in the optical communication window. The requirement of using UV wavelengths, which coincides with defect absorption bands is also removed by the hydrogen loading process [133].

There are also several demerits for the hydrogenation process. The first and foremost disadvantage is the high pressure and temperature requirements.

Hydrogen is flammable and these elevated temperatures and pressures make the process more vulnerable to the risk of fire. Hence, extra care and precautions are to be taken during the process of hydrogen loading. The OH radicals developed in the process have a strong absorption at 1550 nm, which falls in the mostly used third window for optical communication. The impregnated hydrogen molecules slowly diffuse out of the core as time progress. This in turn leads to the gradual reduction in the enhanced photosensitivity of the fiber.

As stated earlier, the excess unreacted hydrogen molecules retained inside the fiber core after the grating fabrication process diffuses out as time progress. This in turn leads to shifts in the wavelength characteristics of the grating. This shift in the resonant peaks of the grating spectrum is more pronounced when the gratings are operating at high temperatures. This largely affects the repeatability and stability of measurements. This can be reduced by thermally annealing the gratings prior to its deployment in sensing applications. In the process of thermal annealing, the gratings are heated to temperatures much higher than the operating temperature conditions of the sensor. This enables the removal of the excess hydrogen molecules, before the deployment of the gratings in sensing applications, and thus reduces the shifts in the wavelength characteristics.

**(b) Flame Brushing**

This is a rather simpler method to enhance the photosensitivity in germanium doped silica fibers following the same concept as in the case of hydrogen loading. Here also, hydrogen is made to chemically react with the silica core of the optical fiber. In the flame brushing method, the fiber is repeatedly brushed by flame fueled by hydrogen [134]. The flame of hydrogen burning in the presence of oxygen elevates the temperatures to very high values around $1700^0$C. At this temperature, hydrogen molecules diffuse inside

the core very quickly and react with the germanosilicate glass material developing the defect sites, which can be altered by the subsequent exposure to UV radiations. These modifications in the bonds lead to RI changes in the fiber core, resulting in the formation of a grating.

The flame brushing technique can enhance the photosensitivity by a factor of more than 10 times that of the standard telecommunication fiber. This enables easier fabrication of gratings in standard optical fibers. Another advantage of this method is the permanency in the enhanced photosensitivity induced, as there is no retention of hydrogen molecules Also the process is much faster, as it takes only lesser time of around 20 minutes for the entire process. The photosensitized area can be controlled more precisely by adjusting the flame size.

The disadvantage of flame brushing is the weakening of fiber at the flamed sites leading to breakage. The exposure to high temperature flames significantly decreases its physical strength and durability, which increases the chances of damage to the fiber. In addition, there are chances to alter the dimensions of the fiber in the flamed region.

**(c) Boron Co-doping**

Researchers were working hard in developing a technique to enhance the photosensitivity, other than the processes involving hydrogen. In this quest, different research groups have tried various doping materials to improve the photosensitivity in optical fibers [118-124]. Silica fibers with various doping materials like, europium-alumina, erbium-germanium, cerium, antimony, germanium-boron, germanium-tin, germanium-phosphorous etc. were tried out. Out of these, the method of doping boron along with germanium into the silica fiber core during the time of preform fabrication was found to be the best for the enhancement in photosensitivity [122]. In

contrary to the increase in refractive index achieved through hydrogen loading and flame brushing, boron addition to the germanosilicate fiber core reduced its refractive index. This result was quiet expected, because of the fact that, addition of boron oxide to silica glass results in a low refractive index compound glass [135].

Boron co-doping results in large differences in the thermo-mechanical properties of the silica cladding and the doped core of the fiber. This difference arises because of the thermo-elastic stresses built up in the boron doped core. It is well known that tension lessens the RI through the stress-optic effect. Absorption studies revealed that, the boron cooping did not affect the absorption band of the defect sites around 240 nm in magnitude and shape [122]. Hence, it is clear that the enhancement in the photosensitivity was not because of the creation of excess defect sites as in the case of flame brushing and hydrogen doping. It is believed that the enhancement in photosensitivity is due to the process of stress relaxation in the fiber core under the exposure to UV radiations.

### 1.3.2 Fabrication of Optical Fiber Gratings

The discovery of photosensitivity in optical fibers revolutionized the research and developments in the area of optical fiber technology. Since the discovery, great amount work and money has been spent not only in developing newer applications for fiber gratings, but also in methodizing better ways to fabricate optical fiber gratings. The fabrication process is quiet tiresome for want of stable and reliable equipment to provide the required submicron periodic patterns. The fabrication methods are broadly classified as: (*a*) internal inscription methods and (*b*) external inscription or side writing method [94, 100, 101].

The internal inscription method was the formerly used version of the grating fabrication. In this method, the standing ways formed inside the fiber core imprints the grating on to the core by altering the refractive index pattern of the core [100, 101]. This method was quiet difficult, as its efficiency was very low. Researchers thought of better ways of grating fabrication and Meltz et al. in 1989 came up with the much easier side writing technique [102], which took over the internal inscription method naturally. The fiber to be inscribed with the grating is illuminated by the UV pattern from one side. These patterns create the needed refractive index variations in the fiber core to develop a grating inside. Only a few external inscription methods are devised, and are broadly classified as: (*a*) Holographic methods [93, 136] and (*b*) Non-interferometric method [93, 137]. In the holographic techniques, a beam splitter is used to divide the incoming UV beam into two, which are later made to interfere at the core of the photosensitive fiber to develop the grating. In the non-interferometric methods, the fiber is exposed, periodically to pulsed sources or through a spatially periodic amplitude mask to create the grating pattern inside the fiber core.

In general, the four mainly adopted methods for the fabrication of optical fiber gratings are: (*a*) Interferometric technique, (*b*) Phase mask method, (*c*) Amplitude mask method and (*d*) Point-by-point fabrication technique. The former two method are relatively tedious and are generally used to write the short period grating or fiber Bragg gratings (FBGs) and the latter two simpler methods are used for the fabrication of long period gratings (LPGs).

**(a) Interferometric Technique**

The very first grating fabrication method using the interferometric method was demonstrated by Meltz et al. in 1989 [102]. In this method of grating fabrication the UV light from a coherent source is split into two using

an interferometer. These beams are then made to interfere to form alternate dark and white fringes. The photosensitive optical fiber is then exposed to this fringe pattern, so that the RI of the fiber core is modified accordingly to create the grating inside the core of the fiber. Interferometric methods are generally used for the fabrication of Bragg gratings. In interferometric methods, the incoming UV beam is split either by Amplitude spitting interferometers or by Wave-front splitting interferometers. Both these techniques have their own advantages and disadvantages.

In amplitude splitting method, the UV light is divided into two equally intense beams. These beams traverse separate paths and are recombined to form the interference fringes at the fiber core later. Cylindrical lenses are normally used along with this setup, to focus the interfering UV beams to a fine line matching the dimensions of the fiber core. The formed grating pitch is exactly same as that of the interference pattern formed and is given by [93, 94]:

$$\Lambda = \frac{\lambda_{uv}}{2 \sin \alpha} \quad \text{..... (1.1)}$$

where, $\lambda_{uv}$ is the wavelength of the UV light, and α is the half angle between the interfering beams. It is clear from the above expression that, the pitch of the grating can be altered by changing the angle between the interfering beams or by tuning the wavelength of the light used. Since, the wavelength tuning is limited by the photosensitivity of the fiber core material, the angle α is always varied for the required grating pitch.

Advantage of this method is its ability to inscribe the grating with any period. This method also allows the fabrication of gratings with variable length, which opens up the possibilities to tune the grating characteristics. Special gratings like chirped grating can also be fabricated with this method by using suitable optical components like lenses, reflectors etc., in the beam paths. The major drawback of this method is its susceptibility to vibrations.

The very fine vibrations acting on the optical components largely affect the fringe pattern and thereby the grating formation. Since, the beams traverse longer optical paths, the local drift in the air column in their path can also affect the system. In addition, the system rely heavily on the qualities of the UV source like, stability spatial coherence, temporal coherence etc.

The wave front splitting interferometric method makes use of a prism interferometer [138, 139] or a Lloyd's interferometer [140]. Compared to the amplitude splitting method, these are rarely used due to their complexity. The main benefit of wave front splitting method is that, only one optical element is employed in the fabrication setup. This reduces the susceptibility to mechanical vibrations and air current induced wave front distortions to some extent. Another advantage is that, angle of the interfering beam can be controlled easily by rotating the prism assembly. The major drawback of this method is that the length of the grating is restricted to half of the beam width. In addition, the beam coherence length limits the Bragg wavelength tunability.

**(b) Phase Mask Method**

Excimer laser sources like KrF (248 nm) are usually employed along with the phase mask method. At times cylindrical lenses are used to focus the incoming UV beam on to the phase mask. A schematic sketch of grating fabrication setup using phase mask method and 248 nm KrF excimer UV laser source (CGCRI, Kolkata) is given in Fig 1.3.

The phase mask technique makes use of a diffractive optical element to modulate the incoming UV beam [93, 94, 141-146]. FBGs are fabricated usually with this most widely employed method for grating fabrication. The phase mask is a grating structure or corrugations developed on a UV transparent fused silica substrate, either by holographic imprinting or by electron beam lithography [144-146]. The phase mask is fabricated in such a

way that, the first order diffracted beams are maximized suppressing the zero order beam.

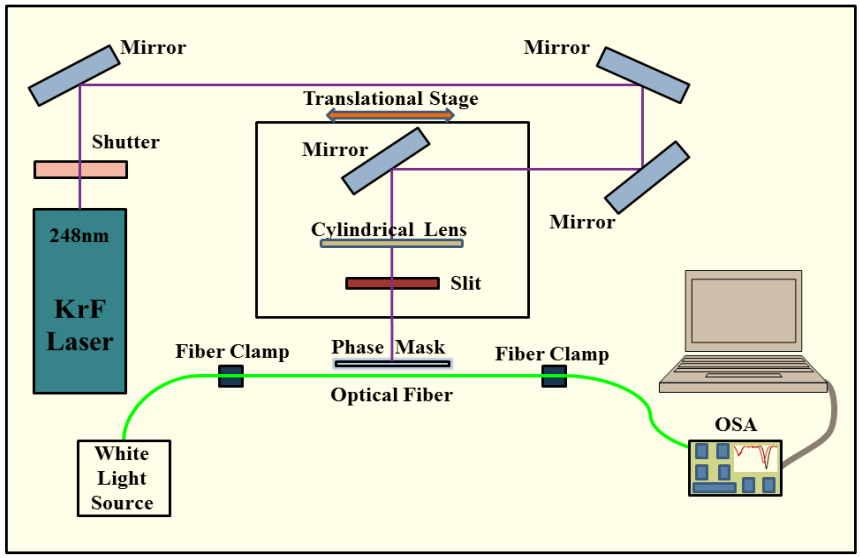


***Figure 1.3:*** *Generalized grating fabrication setup using phase mask. (CGCRI, Kolkata)*

A schematic representation of the phase mask assembly for writing gratings on an optical fiber is given in in Fig 1.4.

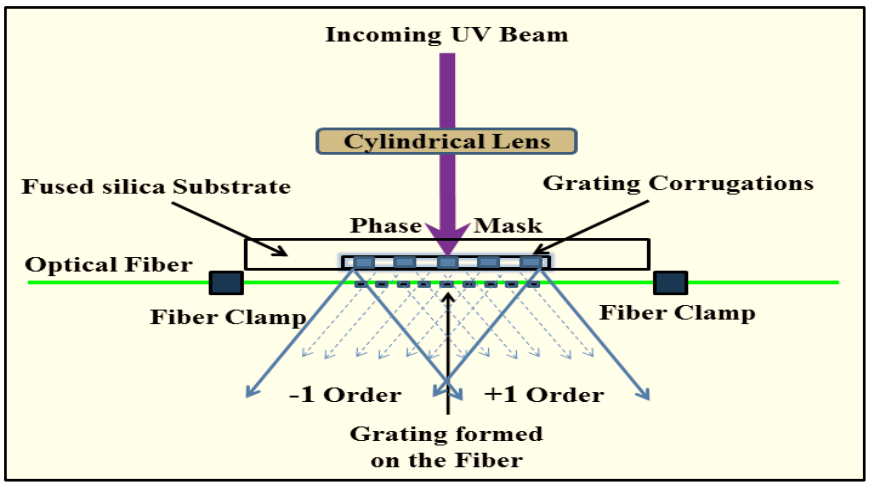


***Figure 1.4:*** *Phase mask assembly for optical fiber grating fabrication.*

The suppression of the zero order diffraction is achieved by controlling the engraving depth (d) of the relief grating or corrugations in the phase mask. The depth of the corrugations on the phase mask is limited by [93]:

$$d = \frac{\lambda_{uv}}{2} \quad \text{(1.2)}$$

where, $\lambda_{uv}$ is the wavelength of UV irradiation. The first order diffracted beams (+1 and -1 orders) are made to interfere on the fiber core to form the required grating pattern with pitch half of that of the phase mask.

$$\Lambda = \left(\frac{\Lambda_{PM}}{2}\right) \quad \text{(1.3)}$$

where, $\Lambda$ is the period of the grating formed (Also the period of the interference fringe pattern) and $\Lambda_{PM}$ is the period of the corrugations on the phase mask. This near field fringe pattern, photo imprints the RI modulation on to the fiber core placed in contact or in close proximity directly behind the phase mask.

The separation from the fiber is a critical parameter in maintaining the quality of the grating fabricated. This dependence of the Bragg wavelength on the separation can be expressed as [94]:

$$\lambda_B = 2n\Lambda\sqrt{1 + (\frac{r}{l})^2} \quad \text{(1.4)}$$

where, $\lambda_B$ is the Bragg wavelength, $\Lambda$ is the grating period, r is the distance between the fiber and the phase mask and *l* is the length of the phase mask.

The advantage of using the phase mask method is that, it greatly reduces the complexity of the setup. Also, the effect of mechanical vibrations and the temporal coherence of the laser sources are reduced to a great extent. Another advantage of this method is the freedom to fabricate Tilted FBG (TFBG) or slanted gratings. Complex structures, such as chirped and apodized gratings can also be fabricated by the phase-mask method [146-148].

From equation 1.2, it is clear that, depth of the corrugations on the phase mask is dependent on the wavelength of the UV light used. Hence, for different UV laser sources operating at different wavelengths, separate phase masks are to be used for the fabrication of FBGs. i.e. For FBG fabrication, same phase mask cannot be used with different laser sources. This is the main limitation of the phase mask method of grating fabrication.

**(c) Amplitude Mask Method**

The amplitude mask method for the fabrication of LPG was first demonstrated by Vengsarkar et al. [97, 149-151]. An amplitude mask is a thin metallic or ceramic sheet, having adjacent slits or the grating pattern imprinted, with the required period of the grating. The UV laser beam is directed on to the amplitude mask through a cylindrical lens, which alters the beam shape and size, to suit the dimensions of the fiber core. A generalized grating fabrication set up can be realized by replacing the phase mask assembly shown in Fig. 1.3, with the amplitude mask of required pitch as shown in Fig. 1.5.

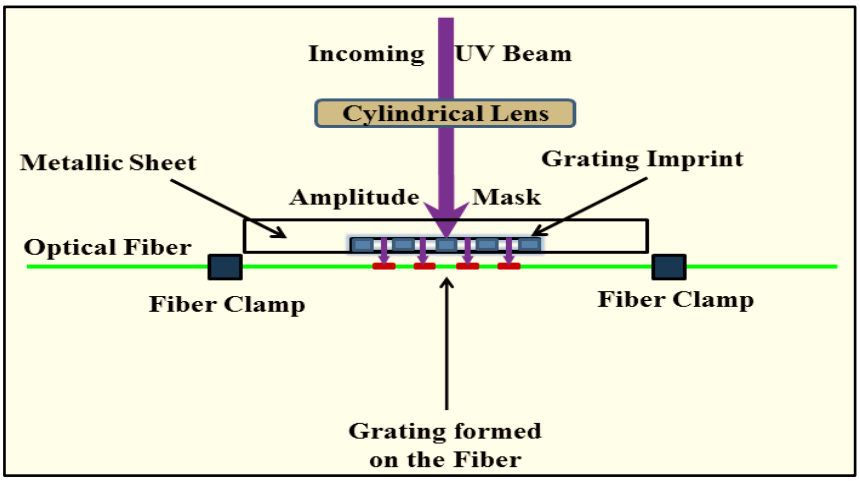


***Figure 1.5:*** *Amplitude mask assembly for optical fiber grating fabrication.*

The shadow of the amplitude mask formed by the incoming UV radiation is made to fall on the fiber. The UV light falling on the mask is transmitted at the slits and is blocked elsewhere. These transmitted wave fronts hit the fiber core (at the focus of the cylindrical lens) altering the RI at these irradiated points. The refractive index profile of the fiber core remain undisturbed at the points were the dark shadow is hitting. Thus, the grating pattern is inscribed on to the fiber core.

The amplitude mask method is widely used for grating fabrication due to its fundamental reliability and simplicity. This technique permits the repeated use of amplitude masks to produce multiple long period gratings of same pitch, enabling batch production of LPGs. The alignment of the setup is much easier than that for the other interferometric techniques. In addition, the same amplitude mask can be used with any laser source for the fabrication of the gratings. The main drawback of this technique is that the amplitude mask is to be replaced with another one for gratings with other periodicities. i.e. Separate amplitude masks are to be used for gratings with different periods. This is expensive and realignment is necessary after every mask replacement.

**(d) Point-by-Point Fabrication**

The point-by-point technique for the fabrication of grating is done by inducing the refractive index variations in a step-by-step manner [93, 94, 152-154]. The UV laser pulse is focused tightly on to the fiber core, whose transmission characteristics are being monitored. The fiber is then displaced by the required length depending on the period of the grating to be written so that, an adjacent new spot is illuminated by the next pulse to enhance the

refractive index at this spot. This process of advancing the fiber and irradiating with the UV pulse is continued until the required characteristics are obtained.

The simplest point-by-point set for the fabrication consists of an excimer laser whose pulses are focused on to the fiber core after passing through a slit. The fiber fixed on a translational stage is moved through a distance matching to the period of the grating, in a direction parallel to the fiber axis. This process is repeated to inscribe the entire grating pattern on the core of the fiber. A representation sketch of the setup is given in Fig. 1.6. The flexibility in the point-by-point writing setup to alter the grating parameters is its main advantage. Since no special optical components are used, it is easy to vary the pitch, length and characteristics of the grating. In addition, the RI profile of the grating can be customized by controlling the pulse energy and exposure time. It also provides options to fabricate gratings with periods ranging from micrometers to millimeters.

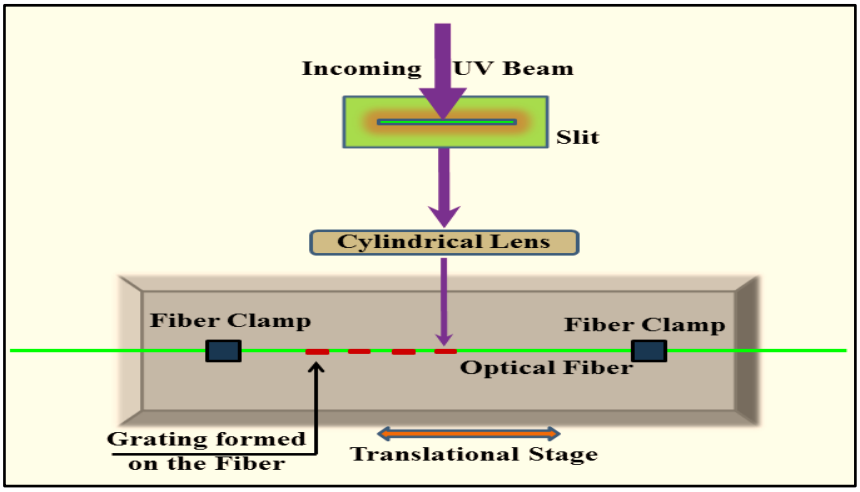


***Figure 1.6:*** *Point-by-point method of optical fiber grating fabrication.*

This enables the easier development of rocking filters and mode converters [153,154]. The main disadvantage of this method is that the process is tedious. High performing translational stages with precise control and

accurate displacement is also a prerequisite for this method. Since the grating is developed in a step-by-step method, the process is time consuming. Chances for errors are more with point-by-point writing method due to the variations in the pitch of grating under the influence of sudden temperature and stress on the fiber.

All the methods described above, exploit the photosensitivity of optical fibers and rely on the use of UV sources for the fabrication of gratings. Apart from these, several other methods were also reported in literature for the fabrication of gratings, generally LPGs. These non-UV methods include, $CO_2$ laser irradiation [155-158], electric arc discharge [159, 160], infrared femtosecond laser pulse exposure [146, 148, 161-164], mercury-arc lamp light focusing [165], ion implantation [166,167], and dopant diffusion in nitrogen-doped fibers [168]. In the first four methods, permanent physical alterations are induced on the fiber core using of the higher powers of the sources, to create the grating. The gratings fabricated by these technologies have found a variety of high temperature applications, as they have better and stable performance at these temperatures. The later techniques create the refractive index changes in the fiber by embedding selected dopants at specific points on the core. The possibility of writing gratings on almost any kind of fibers makes the ion implantation technique better over other methods. The major demerit of these methods is the increase of the average effective cladding RI, which in turn leads to losses in the spectrum. The necessity for specialized equipment to fabricate gratings is another drawback of these methods.

Mechanical deformation of the fibers can also lead to periodic structures behaving like gratings [169-180]. The simplest form of physical deformation can be induced by pressing the fiber between periodically grooved metallic/ceramic blocks, which can change the RI profile of the

core of the fiber. Dynamic LPGs with tunable characteristics were also reported earlier [172, 175, 177-180]. Temporary LPGs developed by means of acoustic modulation of a small length of optical fiber is also available in literature [181, 182].

Excimer laser sources working in the emission range of 240-250 nm are the popular sources for the grating fabrication. The basic reason for this is the photosensitivity of the fiber at these wavelengths. Even then, literature reports on the use of several other lasers sources and wavelengths, for the fabrication of gratings were published earlier. Apart from the femto second lasers and $CO_2$ lasers mentioned earlier, these lasers include $F_2$ lasers (157nm) [183-185], copper vapour lasers (211 and 255nm) [186] and argon lasers like, ArF lasers (193nm) [187], frequency doubled argon ion lasers (244 nm) [188] and 324/351 nm output from an Ar ion laser [130, 189]. This list also include near UV lasers at 334nm [190] and Nd lasers like, frequency quadrupled diode pumped $Nd^{3+}$:YLF laser (262 nm) [191], $IV^{th}$ harmonic of Nd:YAG (266 nm) [192], tripled Nd:YAG laser at 355nm [193] etc.

Sensing with optical fiber gratings is the main theme of this thesis. Three types of gratings (LPG, FBG and TFBG) were employed in the experimental investigations presented in the subsequent chapters. The LPGs and FBGs used for the measurement of cholesterol were fabricated at CGCRI-Central Glass and Ceramic Research Institute, a CSIR-Council of Scientific and Industrial Research laboratory at Kolkata, India.

A schematic sketch of the setup for the inscription of gratings at CGCRI, is given in Fig. 1.3. In the setup, the laser source is a KrF excimer laser (TeraXion: Bragg Star 500) with specifications: Wavelength: 248 nm, Pulse duration: 20 ns, Energy per pulse: 18 mJ and Maximum pulse repetition rate: 500 Hz. A shutter blocks the laser when not in use. For FBG

fabrication, phase mask method was employed. The UV laser beam is directed to the phase mask after many reflections at several mirrors and focused on to the fiber core at the final stage, with the help of a cylindrical lens. The cylindrical lens and preceding mirror was mounted on a motorized translational stage with precision controls. This was to enable the movement of the laser beam along the fiber (for point-by-point inscription). The fiber was mounted on another small translational stage for precise alignment and to adjust the separation between the fiber and the phase mask. The movement of the perfectly aligned fiber and phase mask was monitored using a camera.

Standard single mode optical fibers (SMF-28e, Corning), with lengths about 1m were used for the fabrication of gratings. The fibers used had a core diameter of 8.2 micron and the cladding diameter was 125 micron. The numerical aperture value of the fiber was 0.14. The core and the cladding RIs were 1.461 and 1.456, respectively. The photosensitivity of the fibers was enriched by the method of hydrogen loading at 100$^{o}$C and a pressure of 1500 psi, for 24 hours before the fabrication process. The epoxy coating layers on the fiber were removed from the middle section, around 5-7 cm, using an automated thermo-mechanical stripper (TeraXion). The fiber was attached on the setup using magnetic clamps after thorough cleaning of the stripped section using isopropyl alcohol (IPA). Vertical and horizontal alignments of the fiber were done to focus the beam vertically on to the fiber. The ends of fiber were spliced to patch cords and were connected to a broadband white light source (Yokogawa – AQ 4305) and an Optical Spectrum Analyzer (OSA) (Ando – AQ 6317B) to monitor the characteristics continuously. A circulator was used during FBG fabrication, to monitor the transmission or the reflection spectra. A governing software run on a computer also records the spectrum for

analysis. The whole system was kept inside a UV protective enclosure on a vibration free laboratorial breadboard.

For the point-by-point method employed for the fabrication of the LPGs, the final stages of the setup (cylindrical lens, slit and phase mask) shown in Fig. 1.3 was replaced with an arrangement similar to that shown in Fig. 1.6. The fiber was kept stationary while the focused UV beam was made traverse over the fiber by the movement of the lens and the mirror assembly as mentioned earlier. The spectrum was continuously recorded and monitored for the required characteristics of the grating. The residual molecular hydrogen that was not used in the photochemical reaction at the time of grating fabrication, was removed by the process of annealing at $200^0$C for 7 hours, using a high temperature oven, before the deployment of gratings for the cholesterol sensing applications.

As mentioned earlier, the last chapter of this thesis discusses the principle of operation of TFBG sensor and its application as a cholesterol sensor. TFBGs with a reflected Bragg wavelength of 1557 nm and a tilt angle of $15^0$ were fabricated at Polytechnique, Montréal, Canada, through phase mask method on standard telecommunication (SMF-28e, Corning) fiber [194,195].

In general, TFBGs are written by tilting the fiber at an angle to phase mask. One end of the fiber being exposed, is placed very close to the mask while the other end is kept at a distance (suiting tilt angle requirements) from the phase mask as shown in Fig 1.7 (A). This enables the formation of slanted gratings on the fiber core. However, this method of fabrication requires larger beam cross sectional area so that, the beams may overlap [93]. The focusing done by the cylindrical lens makes this intangible under normal operating conditions.

A better configuration for the TFBG fabrication is given in Fig. 1.7 (B) [196]. In this setup the first order diffracted beams from the phase mask is guided by a pair of mirrors and made to interfere, inducing the required RI modulation on the core of the fiber. In this method, the coherence properties of the source and the depth of the fringe pattern determine the quality of the fringe pattern formed at the fiber core [93].

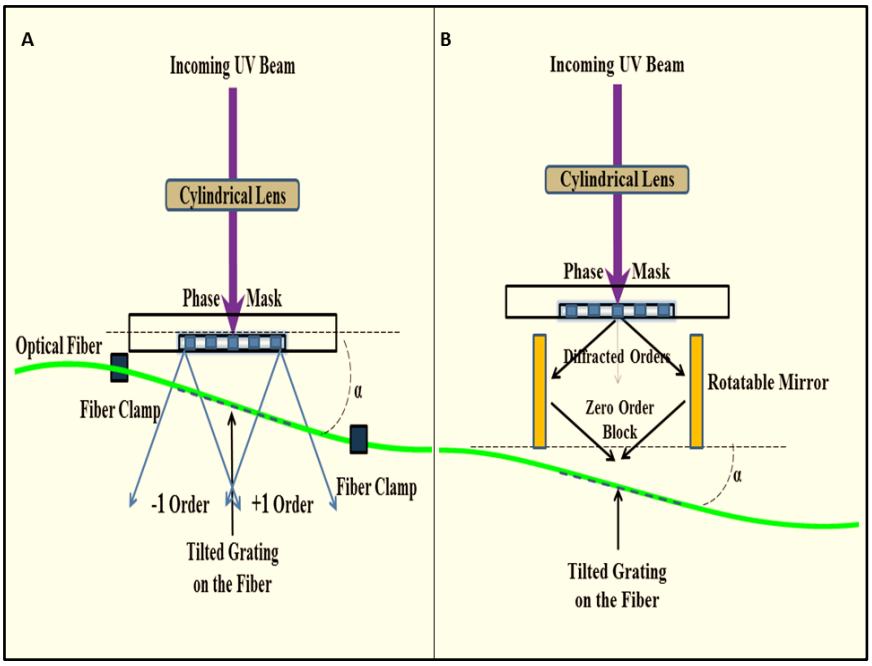


***Figure 1.7:*** *Generalized* TFBG *fabrication setups using phase mask.*

The depth (D) of the fringe pattern formed by the interference of the diffracted beams can be expressed as [93]:

$$D \leq \frac{W}{\tan\left(\frac{\theta_m}{2}\right)} \quad \text{..... (1.5)}$$

where, W is the width of the diffracted beams and ($\theta_m$ / 2) is the angle of diffraction, as shown in Fig. 1.8. The coherence (both temporal and spatial) of the laser beam used, limits the magnitude of the depth of overlap of the beams (D).

Since the fiber is placed at an angle to the fringes, gratings are formed with the tilt, to the direction of the propagating mode inside the fiber core. For small tilt angles α, the period of the tilted grating formed on the fiber core Λ is given by:

$$\Lambda \approx \frac{\Lambda_g}{\cos \alpha} \quad \text{.....(1.6)}$$

where, Λ is the pitch of the tilted grating in the fiber core and $\Lambda_g$ is the period of the corrugations on the phase mask.

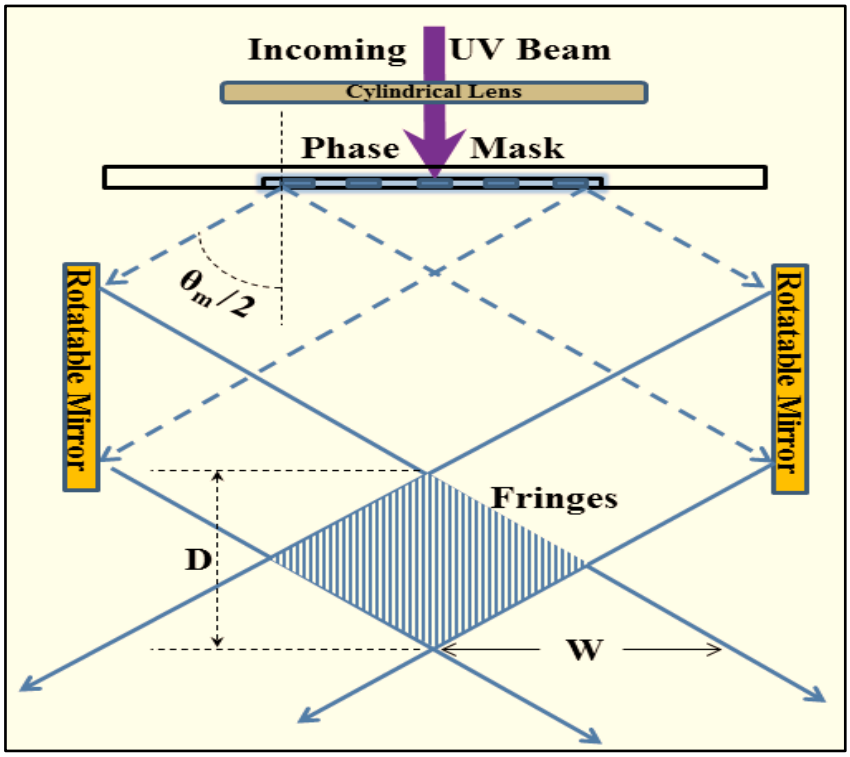


***Figure 1.8:*** *Formation of fringe pattern - TFBG fabrication.*

The basic theory of operation of the gratings (LPG, FBG and TFBG) and their sensitivities to external perturbations are discussed in the subsequent chapters. Brief report on the sensing applications of these types of gratings is also presented.

## 1.4 Cholesterol

François Poulletier de la Salle in 1769, was the first to identify cholesterol in solid form in gall stones. The name has its origin from the Greek chole - (bile) and stereos (solid), and the suffix – ol, for the chemically alcoholic nature. In 1815, Eugène Chevreul: a chemist, named the compound "cholesterine"[197, 198].

Cholesterol is a waxy organic compound with a whitish crystalline appearance, found in all animal tissues and blood. It is a cyclic hydrocarbon alcohol, with molecular formula $C_{27}H_{46}O$, having four carbon rings in the structure.

The systematic name of this steroid is (3β)-cholest-5-en-3-ol. Cholesterol is commonly classified as a lipid, as it is insoluble in water but soluble in a number of organic solvents. The structure of cholesterol molecule is given in Fig. 1.9 and the important properties are tabulated in Table 1.1.

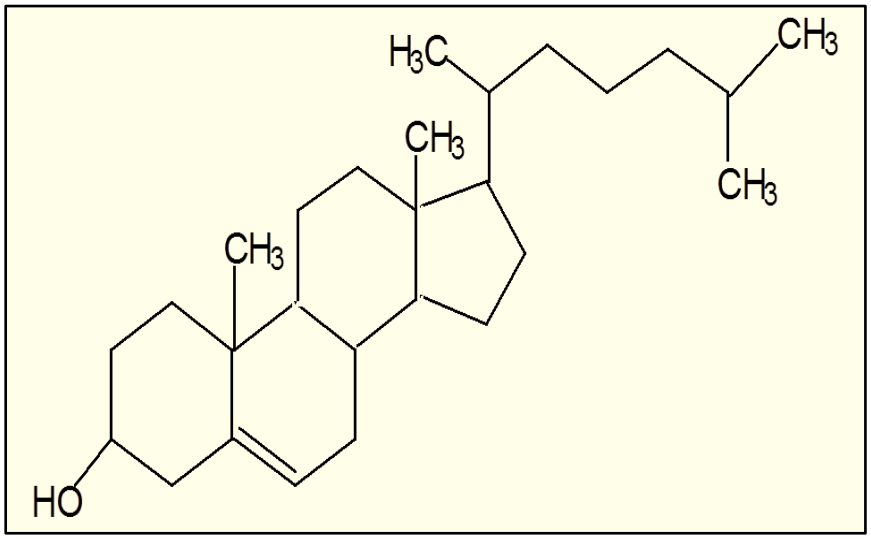


***Figure 1.9:*** *Molecular structure of cholesterol.*

Cholesterol is a combination of steroid and alcohol (sterol), and a fatty lipid found in the cell membranes of all body tissues. The body synthesizes most of the cholesterol and some are derived from food. Cholesterol is more abundant in tissues where it is synthesized more or has ample densely packed membranes for storage like, brain, liver, spinal cord etc. The liver is the most important site of cholesterol biosynthesis. By means of several enzymatic reactions, cholesterol can also be synthesized from acetic acid. It is transported along the blood plasma in all vertebrates and animals. Trace amounts of cholesterol are also found in the cell membranes of plants and fungi.

| | |
|---|---|
| **Molecular Formula** | $C_{27}H_{46}O$ |
| **Chemical Name** | Cholest-5-en-3b-ol |
| **Molar Mass** | 386.654 |
| **Refractive Index** | 1.525 |
| **Density** | 1.052 g/cm3 |
| **Melting Point** | 146-147 °C |
| **Boiling Point** | 360°C (decomposes) |
| **Solubility in Water** | 0.095mg/l (30 °C) |

***Table.1.1:*** *Properties of cholesterol.*

Cholesterol plays a vital role in many biochemical processes. The action of cholesterol is indispensable for the functioning of some glandules. It also work together with many compounds such as the lipids and other cell components. In addition, they are also the elementary constituents of nerve and brain cells [199]. They are also the precursors for

other biological materials, such as bile acid and steroid hormones [200, 201]. Cholesterol is required to build and maintain cell membranes and it regulates membrane fluidity over a wider range of temperatures. Antioxidant action of cholesterol was also reported in 1991[202]. The cholesterol concentration in the blood of a healthy human adult is in the range of 140 to 200 mg/dL [203]. This corresponds to a range of 1400 to 2000 ppm of cholesterol. Excess amount of cholesterol may lead to a number of health complications.

Public became more concerned about the risks of high blood cholesterol levels by 1980s. Hypercholesterolemia was identified as one of the many independent risk factors that may lead to coronary heart diseases. This in turn made, the elevated levels of blood cholesterol and its transport mechanisms aided by various lipoprotein in association with cardiovascular ailments, as the most researched problem associated to cholesterol. The combination of protein carriers and cholesterol is termed as lipoproteins. In the last three decades, numerous investigations performed in this regard clearly established the relationship between increased cholesterol concentration and the occurrence of cardiovascular diseases like arteriosclerosis and hypertension [204-208]. The deposition of cholesterol and other fatty acids on the inner walls of major blood vessels is called arteriosclerosis, which is usually associated with coronary heart diseases. Another factor in the growth of atherosclerosis is the insolubility of cholesterol in water. This buildup of plaques in the blood vessels may constrict the channels significantly and obstruct the free flow of blood to and from the heart. Researches have brought out the attachment of cholesterol to relatively abundant protein complexes (lipoproteins) in blood, as the real reason for cholesterol accumulation in the blood vessels [209].

The total cholesterol contained in the blood plasma is a mixture of two basic components namely; Low Density Lipoprotein (LDL) and High Density Lipoprotein (HDL). The desired levels of these components in the blood of human beings is presented in Table. 1.2.

| Category | Range (mg/dL) | Inference |
|---|---|---|
| **Total Cholesterol** | < 200 | Desirable |
| | 200-239 | Borderline |
| | > 240 | High, Risky |
| **HDL** | < 40 | Major Risk |
| | 40-59 | Desirable<br>The higher the better |
| | > 60 | Protective to Heart Diseases |
| **LDL** | < 100 | Optimal |
| | 100-129 | Above optimal |
| | 130-159 | Borderline |
| | 160-189 | High, Risky |
| | > 190 | Very High, Very Risky |

***Table 1.2:*** *Cholesterol components in the blood of adult human beings and their indications.*

Nowadays, the term “bad cholesterol” has been used to refer to the LDL components, which is thought to have harmful actions and “good cholesterol” has been used to denote the HDL component, which is believed to be beneficial. HDL carries cholesterol out of the bloodstream into the liver where it is broken down for excretion. The LDL components carry it back into the blood stream for use by numerous body cells, which in turn leads to the deposition inside the blood vessels, when in excess.

The unit of parts per million (ppm), used for the measurement of cholesterol described in the subsequent chapters, is related to the clinically used unit of mg/dL as per the following expression.

10ppm = 1mg/dL ……..... (1.7)

Reduced consumption of foods having cholesterol and saturated fat has been found to be effective in lowering the blood cholesterol levels. Cholesterol levels can also be controlled by the administration of drugs.

Hence, the measurement of blood cholesterol has gained much attention as it gives an indication on the chances of occurrence of cardiovascular disease. Also, estimation of cholesterol and its byproducts in food is important, as it may enhance the blood cholesterol levels. For these reasons, cholesterol has become one of the main factors to be analyzed in routine clinical, pharmaceutical, biomedical research and food processing laboratories. Consequently, an ever-increasing demand for cholesterol testing technology has been observed in the last few years.

### 1.4.1 Detection of Cholesterol

Various methods for the detection and estimation of cholesterol were reported earlier in the literature. Fluorescence detection, electrophoresis method, amperometric detection, Raman spectroscopy, high performance liquid chromatography, fiber optic, gas-liquid chromatography etc. are a few of them [210-217]. Most of them rely on the chemical methods centered around the classical Libermann- Burchard reaction [218] which has been conventionally employed for total cholesterol measurements. These approaches do not assure any onsite checking of cholesterol and are time consuming. Besides the lack of specificity, these methods also require costlier equipment and trained personnel, which in turn increases the cost of the tests. Due to these

shortcomings, enzymatic techniques have virtually replaced the chemical methods, as enzymes guarantee the required specificity and selectivity for these kinds of tests. Other advantages of immobilized enzymes are their repetitive usage, easiness in the separation of enzyme and products, greater stability and considerable reduction in the operation cost.

Several methods based on enzymatic reactions with cholesterol esterase, cholesterol oxidase [219], cytochrome P450scc [213] etc. were reported earlier. Of which, the mostly employed enzymatic method is based on the cholesterol oxidase based detection. Cholesterol oxidase ($ChO_x$) is one of the technologically significant enzymes that catalyze the oxidation of cholesterol to form equimolar quantities of cholest-4-en-3-one and hydrogen peroxide. This enzymatic estimation of cholesterol monitors the oxygen consumption or the production of hydrogen peroxide during the enzymatic reaction given in equation 1.7.

$$\text{Cholesterol} + O_2 \xrightarrow{ChO_x} \text{Cholest} - 4 - \text{en} - 3 - \text{one} + H_2O_2 \ldots (1.8)$$

The major drawback of the enzymatic methods is the difficulties in the fabrication and usage of the sensor head. Extra care should be taken at the time of measurements and afterwards to keep the enzymes intact so that it can be preserved for repeated uses. In addition, the use of these enzymes makes the sensor head costlier.

An optical detection method for cholesterol was first proposed by Allain et al. [220]. In this 1974 paper, colorimetry was used for the first time for the enzymatic determination of total cholesterol. In 1986, Akiyoshi et al. developed a laboratory-built, chemi-luminescence system for cholesterol determination [221]. This was followed by several reports on photochemical methods for cholesterol measurements from various research groups [222, 223]. The photochemical biosensors exhibited more sensitivity

and stability over the enzymatic procedures. They were also easy to wash and have good optical biocompatibility, which is required for in vivo detection. A report on a voltammetric sensor for the detection of total cholesterol, fabricated by co-immobilization of two enzymes: cholesterol oxidase (ChOx) and horseradish peroxidase (HRP) on porous graphite was published in 2014 [224]. G Kaur et al. developed a microfluidic biosensor based on surface plasmon resonance technique, for quantification of cholesterol using nanostructured ZnO thin film [225]. Cholesterol oxidase (ChOx) enzyme was immobilized on the ZnO coated Au prism for the detection of cholesterol. In 2016, X Lin et al. proposed an enzymatic electrochemical cholesterol sensor [226]. Q Wu et al. demonstrated amperometric cholesterol sensor using silver nanowire and zinc oxide films on an indium tin oxide (ITO) electrode modified with graphene oxide and chitosan [227]. S Alexander et al. developed another non enzymatic electrochemical cholesterol sensor [228]. They developed a modified grapheme oxide based molecular imprinted polymer for cholesterol sensing.

In the year 2000, Kim et al. demonstrated a fiber optic calorimetric spectrometer for the detection of cholesterol [229]. Concentration was measured based on changes in the absorbance of a cholesterol compound formed as a byproduct of a chemical reaction. In this paper, optical fiber was utilized merely as a light guiding waveguide. Fluorescence quenching technique clubbed with optical fiber for cholesterol determination was introduced by Yan et al. [230]. After the invention of carbon nanotubes, Tan et al. employed it in the detection of total cholesterol in the year 2005 [231]. D A R Medina et al. have reported the design and fabrication of optrodes using photonic crystal fiber and cholesterol enzyme to monitor cholesterol in 2015 [232]. In 2017, Yunianto et al. came up with another fiber optic sensor for the estimation of cholesterol [233]. In this paper, the authors report the

usage of bent optical fiber with scratches on its surface, for the measurement of blood cholesterol. M Budiyanto et al. proposed an intensity modulated sensor employing an optical fiber bundle for the determination of cholesterol [234]. Recently, V Semwal and B D Gupta, proposed the development and characterization of highly sensitive fiber optic cholesterol sensor configurations [235]. These sensorheads employing the principle of surface plasmon and localized surface plasmon utilizes the enzyme cholesterol oxidase (ChOx) for the measurement of cholesterol.

## 1.5 Chitosan

Chitosan is used as a bio polymeric coating to improve the sensitivity of the developed cholesterol sensor heads presented in this thesis. Chitosan is a polysaccharide prepared by the deacetylisation of chitin, which is the main constituent of the exoskeleton of crustaceous water creatures [236- 245]. Chitin is a nitrogenous polysaccharide, which is white in appearance, hard and inelastic in nature. It is considered as a major source of surface contamination in coastal areas [236]. Chitin, the second most abundant organic complex in nature after cellulose, is also present in aquatic invertebrates, insects, fungi, and yeast [237]. Chemically, chitin is β-(1→4)-linked N-acetyl-D-glucosamine and its structure is given in Fig. 1.10.A.

Chitin is made up of a linear chain of acetyl glucosamine groups while chitosan is obtained by removing enough acetyl groups ($CH_3$-CO) from the molecular chain. This process is called deacetylation. The actual difference between chitin and chitosan is the acetyl content of the chitin polymer. The removal of acetyl groups makes the derivatives soluble in almost all diluted acids. Chitosan, with one free amino group in the molecular chain is the most useful derivative of chitin [245].

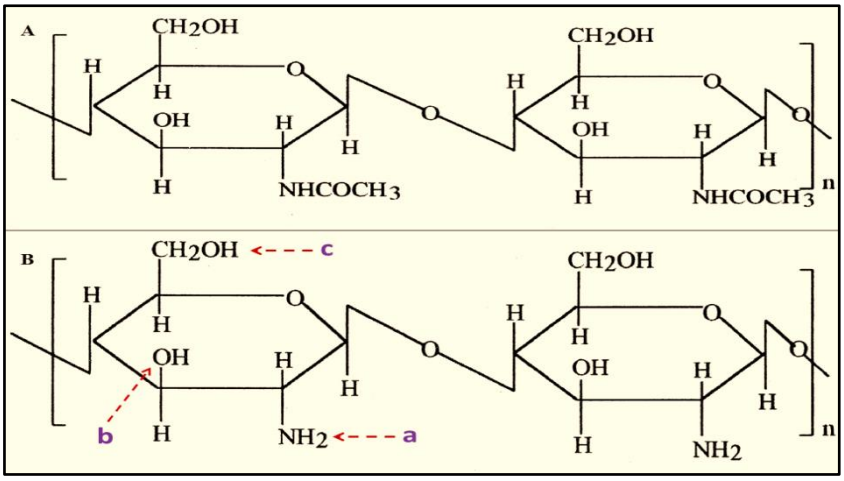


***Figure 1.10:*** *Molecular structure - (A) Chitin and (B) Chitosan.*

Chitosan can selectively bind with materials, such as cholesterol, fat, metal ion and protein [246, 247]. The fat and cholesterol binding capabilities of chitosan is exploited to develop cholesterol lowering supplements. Chitosan attaches itself to fat in the stomach before it is broken down, forming a mass, which the body cannot absorb, and is excreted from the body. Thus the trapping of fat by chitosan, prevents its assimilation to the digestive system.

Chitosan contains three types of reactive functional groups, which are an (a) amino/acetamido group, (b) a primary hydroxyl group and (c) a secondary hydroxyl groups as depicted in Fig. 1.10.B. These active sites in chitosan acts as the binding sites for cholesterol [247]. The combined effects of electrostatic attraction, embedding, adsorption and entrapment are the probable mechanisms for the cholesterol binding effects of chitosan [248]. Chitosan fiber having a positive ionic charge also gives the ability to chemically bond with the negatively charged lipids, fats and bile acids [249–251].

This fat and protein binding characteristics of chitosan stimulated the research in studying the hypocholesterolaemic activity of chitosan in birds,

animals and human beings. Several studies have revealed that it is a potential candidate, which can reduce the cholesterol levels [247-263].

This cholesterol binding effect of chitosan is exploited in enhancing the selectivity as well as the sensitivity of the cholesterol sensors presented in the succeeding chapters of this thesis. A layer of chitosan was coated over the optical fiber gratings for the development of cholesterol sensor heads. In our experiments, it was found that the grating based cholesterol sensor heads with chitosan coatings exhibited an enhancement in the sensitivity in the cholesterol measurements compared to the sensor heads without chitosan coating

Sensing with optical fiber gratings is the focus of this thesis. The main objective of the research was to design and develop grating based fiber optic sensors for the measurement of cholesterol in the desired range with the required acuuracy and sensitivity, so that these studies can be extended to the real time measurements of cholesterol in blood. Approaches to improve the sensitivity and selectivity of the sensor heads also became an objective in the due course of the research activities. Long period gratings with pitches ranging from 435 μm to 550 μm were employed in the experimental analyses described this thesis. This selection was random, keeping the ease of fabrication in mind. The Bragg grating pitches were selected such that reflected Bragg wavelengths lie in the commonly used communication bandwidth.

Sensing capabilities and principle of operation of optical fiber grating based sensors are covered in detail in the subsequent chapters of this thesis. Chapter 2 outlines the principle of operation of LPG sensors, while the next chapter discusses the performance improvement of LPG sensors by the application of suitable coatings. Chapter 4 describes the principle of FBG based sensors and a typical application. TFBG based

refractive index sensor for the detection of cholesterol is presented in chapter 5 along with the supportive theory of operation.

## 1.6 Summary

Fiber optic devices have become an integral and indispensable part of the sensor industry. Right from the days of Kao, optical fiber has been employed in the sensing field for the detection of a variety of parameters and species including, physical, chemical and biological entities. This introductory chapter was intended to present a short technical insight into the major subjects dealt in this thesis.

This chapter discussed the development of fiber optic sensors as a leading research area with vast possibilities. The basic classifications of fiber optic sensors were discussed with an emphasis to the fiber grating based sensors. A discussions on photosensitivity of the optical fibers and the methods of enhancing the photosensitivity was included. Discussion on the various fabrication methods of optical fiber gratings was presented in this chapter. The setup for fabricating the gratings used in the experimental sections was discussed in detail.

The gratings fabricated were employed for the development of sensor heads for the detection of cholesterol. The properties and functions of cholesterol were outlined in this chapter. The importance of the measurement of cholesterol was highlighted. Brief report on the various cholesterol detection mechanisms was also presented.

Chitosan, the biopolymer employed as an overlay coating around the grating sensor heads used in the experiments was introduced in this chapter. The structure of chitosan was also discussed, bringing out its ability to bind with cholesterol. A literature report on the hypocholesterolaemic activity of chitosan was also presented here.

## References


[1]. K C Kao and G A Hockham, "*Dielectric-fiber surface waveguides for optical frequencies*", Proc. IEEE, 113 (7), pp. 1151-1158 (1966).

[2]. F Kapron, D Keck, and R Maurer, "*Radiation losses in glass optical waveguides*", Appl. Phys. Lett., 17, pp. 423–425 (1970).

[3]. National Research Council, "*Optics and Photonics: Essential Technologies for Our Nation*", The National Academies Press, Washington DC, (2013)

[4]. B Culshaw and J Dakin, "*Optical Fiber Sensors System and Applications*", Vol 2, Artech House (1989).

[5]. Eric Udd and William B Spillman, "*Fiber Optic Sensors: An Introduction for Engineers and Scientists*", John Wiley & Sons (2011).

[6]. S Yin, P B Ruffin and F T S Yu, "*Fiber Optic Sensors*", 2nd ed, Taylor & Francis, CRC Press (2008).

[7]. T G Giallorenzi, J A Bucaro, A Dandridge, J H Cole, S C Rashley and R G Priest, "*Optical fiber sensor technology*", IEEE Trans. Microwave Theory and Tech., 30, pp. 472-511 (1982).

[8]. K T V Grattan and B T Meggitt, "*Optical Fiber Sensor Technology: Applications and systems*", Kluwer Academic Publishers (2000).

[9]. B Lee, "*Review of the present status of optical fiber sensors"*, Opt. Fiber Tech., 8, pp. 57-79 (2003).

[10]. E Udd, R G Blom, D Tralli, E Saaski and R Dokka, "A*pplication of the Sagnac interferometer based strain sensor to an earth movement detection system*", Proc. SPIE, 2191, pp. 126-136 (1994).

[11]. J R Griffiths and S P Robinson "The Oxy Lite: A *fiber optic oxygen Sensor*", The British J. of Radiology, pp. 627-630 (1999).

[12]. W Habel and D Hofmann "*Determination of structural parameters concerning load capacity based on fiber Fabry-Perot-interferometers*", Proc. SPIE, Vol. 2361, pp. 176-179 (1994).

[13]. P Ferdinand, S Magne, V Dewynter Marty, C Martinez, S Rougeault and M Bugaud, "*Application of Bragg grating sensors in Europe*", 12th Int. Conf. on OFS '97- Optical Fiber Sensors, Williamsbourg, OSA Technical Digest Series, Vol. 16, pp. 14-19 (1997).

[14]. D Inaudi and B Gllisic "*Long range pipeline monitoring by distributed fiber optic sensing*", J. Pressure Vessel Tech., Vol. 132(1), 011701, pp. 596-599 (2009).

[15]. D Inaudi, "*Field testing and application of fiber optic displacement sensors in civil structures*", 12th Int. conf. on OFS '97- Optical Fiber Sensors, Williamsbourg, OSA Technical Digest Series, Vol. 16, pp. 596-599 (1997).

[16]. D Inaudi, N Casanova, P Kronenberg, S Vurpillot and S Marazzi "*Embedded and surface mounted fiber optic sensors for civil structural monitoring*", Smart Struct. & Mat. Conf., San Diego, SPIE Vol. 3044, pp. 236-243 (1997).

[17]. L Thévenaz, M Facchini, A Fellay, P Robert, D Inaudi and B Dardel, "*Monitoring of large structure using distributed Brillouin fiber sensing*", SPIE 13th Int. Conf. on Opt. Fiber Sens OFS-13., Kyongju, Korea, Vol. 3746, pp. 345-348 (1999).

[18]. K Hotate and S L Ong, "*Distributed dynamic strain measurement using a correlation-based Brillouin sensing system*", IEEE Photonics Technology Letters, 15, pp. 272–274 (2003).

[19]. S Villalba and J R Casas, *"Application of optical fiber distributed sensing to health monitoring of concrete structures",* Mech. Sys. and Sig. Processing, 39, pp. 441–451 (2013).

[20]. C K Y Leung, N Elvin, N Olson, T F Morse and H Y Fei, "*A novel distributed optical crack sensor for concrete structures"*, Engineering Fracture Mechanics, Vol. 65, pp. 133-148 (2000).

[21]. Y Dong, L Chen and X Bao, "*High-spatial-resolution simultaneous strain and temperature sensor using Brillouin scattering and birefringence in a polarization-maintaining fiber*", IEEE Photonics Technology Letters, 22, pp. 1364–1366 (2010).

[22]. M Niklès, L Thevenaz and P A Robert, "*Simple distributed temperature sensor based on Brillouin gain spectrum analysis*", SPIE OFS-10, 10th Int. Conf. on Opt. Fiber Sens., Glasgow, UK, Vol. 2360, pp. 138-141 (1994).

[23]. J Geng, S Stanies, M Blake and S Jiang, "*Distributed fiber temperature and strain sensor using coherent radio frequency detection of spontaneous Brillouin scattering",* Appl. Opt., Vol. 46 (23), pp. 5928-5932 (2007).

[24]. J S Seler, L Thevenaz, H Huwald, A Mallet, W Luxemberg, N V Geisen, M Stejskal, J Zeman, M Wasthoff and M B Parlange, "*Distributed fiber optic temperature sensing for hydrologic systems"*, Water resources Research, Vol. 42 (12), (2006).

[25]. Y Dong, X Bao and L Chen, "*Distributed temperature sensing based on birefringence effect on transient Brillouin grating in a polarization-*

*maintaining photonic crystal fiber",* Optics Letters, 34, pp. 2590–2592 (2009).

[26]. H Guo and S Tao, "*An active core fiber optic temperature sensor using an Eu(III)-doped sol-gel silica fiber as a temperature indicator*", IEEE Sensors J., 7, pp. 953-954 (2007).

[27]. D Zhou, Z Qin, W Li, L Chen and X Bao, "*Distributed vibration sensing with time-resolved optical frequency-domain reflectometry*", Optics Express, Vol. 20, pp.13138–13145 (2012).

[28]. S Yan, L Mingming, Z Hong, Y Y Xiao and Z Lu*," Optical fiber direct sensing biosensor applied in detecting biolayer thickness of nanometer grade*", Proc. SPIE, 6150 II (2006).

[29]. T Scheper and A F Buckmann, "*A fiber optic biosensor based on fluorometric detection using confined macromolecular nicotinamide adenine dinucleotide derivatives*", Biosensors and Bioelectronics, 5, pp. 125-135 (1990).

[30]. C Schelp, T Sheper, F Buckmann and K F Reardon, "*Two fiber optic sensors with confined enzymes and coenzymes: Development and application*", Analytica Chimica Acta, Vol. 255, pp. 223- 229 (1991).

[31]. S G Ignatov, J A Ferguson and D R Walt, "*A fiber optic lactate sensor based on bacterial cytoplasmic membranes",* Biosensors and Bioelectronics, Vol. 16, pp. 109-113 (2001).

[32]. T Sheper, W Brandes, C Graw, H G Hundeck, B Reinhardt, F Ruther, F Plotz, C Shelp, K Schugerl, K H Schenider, F Giffhorn, B Rehr and H Sahm, "*Applications of biosensor systems for bioprocess monitoring*", Analytica Chimica Acta, 249, pp. 25-34 (1991).

[33]. J A Ferguson, T C Boles, C P Adams and D R Walt, "*A fiber optic DNA biosensor microarray for the analysis of gene expression*", Nature Biotechnology, Vol. 14, pp. 1681-1684 (1996).

[34]. B G Healy, L Li, and D R Walt, "*Multianalyte biosensors on optical imaging bundles",* Biosensors and Bioelectronics, Vol. 12, pp. 521-529 (1997).

[35]. H S Haddock, P M Shankar and R Mutharasan, "*Evanescent sensing of biomolecules and cells",* Sensors and Actuators B: Chemical, Vol. 88, pp. 67-74 (2003).

[36]. P V Preejith, C S Lim, A Kishen, M S. John and A Asundi, "*Total protein measurement using a fiber optic evanescent wave based biosensor*", Biotechnology Letters, Vol. 25, pp.105-110 (2001).

[37]. G Stewart, W Jin and B Culshaw, "*Prospects for fiber optic evanescent-field gas sensors using absorption in the near-infrared*", Sensors and Actuators B: Chemical, Vol. 38, pp. 42-47 (1997).

[38]. H Jiang, R Yang, X Tang, A Burnett, X Lan, H Xiao and J Dong, "*Multilayer fiber optic sensors for in situ gas monitoring in harsh environments"*, Sensors and Actuators B: Chemical, Vol. 177, pp. 205–212 (2013).

[39]. F B Xiong, W Z Zhu, H F Lin, X G Merg, "*Fiber optic sensor based on evanescent wave absorbance around 2.7 μm for determining water content in polar organic solvents",* Appl. Phy. B, Vol. 115, pp. 129-135 (2014).

[40]. O S Wolfbeis, "*Fiber optic chemical sensors and biosensors",* Analytical Chem., Vol. 76, pp. 3269-3284 (2004).

[41]. A M Dietrich, J N Jensen and W F Da Costa, "*Measurement of pollutants: Chemical species*", Water Environmental Research, Vol. 68, pp. 391-406 (1996).

[42]. B D Gupta, and Banshi Das, "*Fiber Optic Sensors: Principles and Applications*", New India Pub. (2006).

[43]. M Archenault, H Gagnaire, J P Goure and N Jaffrezic-Renault, "*A simple intrinsic optical fiber refractometer",* Sensors and Actuators B: Chemical, Vol. 5, pp. 173-179 (1991).

[44]. J Yuan and M A El-Sherif, "*Fiber optic chemical sensor using polyaniline as modified cladding material*", IEEE Sensors, Vol. 3, pp. 5-12 (2003).

[45]. C Egami, K Takeda, M Isai and M Ogita, "*Evanescent wave spectroscopic fiber optic pH sensor",* Optics Communications, Vol. 122, pp. 122-126 (1996).

[46]. J Zhang and S Albin, "*Self-referenced reflective intensity modulated fiber optic displacement sensor*", Optical Engineering, Vol. 38, pp. 227-232 (1999).

[47]. S Jhonson, "*Fiber displacement sensor for metrology and control",* Optical Engineering, Vol. 24, pp. 961-965 (1985).

[48]. B Culshaw, "*Fiber optics in sensing and measurement"*, IEEE Selected Topics in Quantum Electronics, Vol. 6, pp. 1014-1021 (2000).

[49]. D A Krohn, "*Fiber Optic Sensors: Fundamentals and Applications"*, 3rd edition, Instr. Systems (2000).

[50]. J R Casas, and J S Paulo, "*Fiber optic sensors for bridge monitoring*", J. of Bridge Engineering, Vol. 8, pp. 362-373 (2003).

[51]. S M Jeon and Y P Kim, "*Temperature measurement using fiber optic polarization interferometer*", Optics and Laser Technology, Vol. 36, pp. 181-185 (2004).

[52]. Y Lung Lo and T Chih Yu, "*A polarimetric glucose sensor using a liquid-crystal polarization modulator driven by a sinusoidal signal*", Optics Communications, Vol. 259, pp. 40-48 (2006).

[53]. H Y Fu, H Y Tam, Li Y Shao X Dong, P A Wai, C Lu and S K Khijwania, "*Pressure sensor realized with polarization maintaining photonic crystal fiber based Sagnac interferometer*", Appl. Opt., Vol. 47 ( 15), pp. 2835-2839 (2008).

[54]. M Deng, C P Tang, T Zhu and Y J Rao, "*Highly sensitive bend sensor based on Mach-Zehnder interferometer using photonic crystal fiber*", Opt. Commu. Vol. 284 (12), pp. 2849-2853 (2011).

[55]. P Lu, L Men, K Sooley and Q Chen, "*Tappered fiber Mach-Zehnder interferometer for simultaneous measurement of refractive index and temperature*", Appl. Phys. Lett. 94, 131110 (2009).

[56]. T Yoshino, K Kurosawa, K Itoh and T Ose, "*Fiber optic Fabry-Perot interferometer and its sensor applications*", IEEE Trans. On Microwave Theory and Tech. Vol. 30 (10), pp. 1612-1621 (1982).

[57]. H Lefevre, "*The Fiber Optic Gyroscope*", Artech, Norwood (1993).

[58]. W K Burns (Editor), "*Optical Fiber Rotation Sensing*", Academic Press, San Diego (1994).

[59]. P H Paul and G Kychakoff, "*Fiber optic evanescent field absorption sensor*", Appl. Phys. Lett. Vol. 51, pp. 12–14 (1987).

[60]. V Ruddy, B D McGrath and J A Murphy, "*Evanescent wave absorption spectroscopy using multimode fibers*", J. Appl. Phys. Vol. 67 (10), pp. 6070–6074 (1990).

[61]. G Keiser, "*Optical Fiber Communications*", Mc Graw-Hill, Singapore, (2000).

[62]. AW Snyder and J D Love, "*Optical Waveguide Theory*", Chapman and Hall, (1983).

[63]. W Love, L Button and R Slovacek, "*Optical Characteristics Of Fiber Optic Evanescent Wave Sensors: Biosensors With Fiber Optics*", Humana Press, Totowa, NJ, p. 139 (1991).

[64]. K Rijal, A Leung, P M Shankar and R Mutharasan, "*Detection of pathogen Escherichia coli O157:H7 at 70 cells/mL using antibody immobilized*

*biconical tapered fiber sensors*", Biosens. Bioelectron., Vol. 21, pp. 871–880 (2005).

[65]. M D DeGrandpre and L W Burgess, "*Long path fiber optic sensor for evanescent field absorbance measurements*", Anal. Chem., Vol. 60, pp. 2582–2586 (1988).

[66]. B D Gupta, H Dodeja and A K Tomar, "*Fiber optic evanescent field adsorption sensor based on a U-shaped probe*", Opt. Quantum Electron. Vol. 28, pp. 1629–1639 (1996).

[67]. D Littlejohn, D Lucas and L Han, "*Bent silica fiber evanescent absorption sensors for near-infrared spectroscopy*", Appl. Spectrosc. Vol. 53 (7), pp. 845–849 (1999).

[68]. A G Mignani, R Falciai and L Ciaccheri, "*Evanescent wave absorption spectroscopy by means of bi-tapered multimode optical fibers*", Appl. Spectrosc. Vol. 52, pp. 546–551 (1998).

[69]. H Raether, "*Surface Plasmons*", Springer, Berlin, Germany (1988).

[70]. H Raether, "*Surface Plasmons on Smooth and Rough Surfaces and on Gratings*", Springer, Berlin, Germany (1988).

[71]. K Park, B J Lee, C Fu, and Z M Zhang, "*Study of the surface and bulk polaritons with a negative index metamaterial*", J. Optical Society of America B, Vol. 22, pp. 1016– 1023, (2005).

[72]. C Nylander, B Liedberg, and T Lind, "*Gas detection by means of surface plasmon resonance*", Sensors and Actuators, Vol. 3, pp. 79–88, (1982).

[73]. H Kano and W Knoll, "*Locally excited surface plasmon polaritons for thickness measurement of LBK films*", Optics Communications, Vol. 153, No. 4–6, pp. 235–239, (1988).

[74]. H Kano and W Knoll, "*A scanning microscope employing localized surface plasmon polaritons as a sensing probe*", Optics Communications, Vol. 182, No. 1–3, pp. 11–15, (2000).

[75]. S Patskovsky, A V Kabashin, M Meunier, and J H T Luong, "*Silicon-based surface plasmon resonance sensing with two surface plasmon polariton modes*", Applied Optics, Vol. 42, No. 34, pp. 6905–6909, (2003).

[76]. S Patskovsky, A V Kabashin, and M Meunier, "*Properties and sensing characteristics of surface plasmon resonance in infrared light*" J. of the Optical Society of America A, Vol. 20, pp. 1644–1650, (2003).

[77]. G Nemova and R Kashyap, "*Theoretical model of a planar integrated refractive index sensor based on surface plasmon polariton excitation*", Optics Communications, Vol. 275, no. 1, pp. 76–82, (2007).

[78]. G Nemova and R Kashyap, "*A compact integrated planar waveguide refractive index sensor based on a corrugated metal grating*", J. of Lightwave Technology, Vol. 25, No. 8, pp. 2244–2250, (2007).

[79]. G Nemova, A V Kabashin, and R Kashyap, "*Surface plasmon polariton Mach-Zehnder refractive index sensor*", J. of the Optical Society of America B, Vol. 25, pp. 1673– 1677, (2008).

[80]. A K Sheridan, R D Harris, P N Bartlett, and J S Wilkinson, "*Phase interrogation of an integrated optical SPR sensor"*, Sensors and Actuators B, Vol. 97 (1), pp. 114–121, (2004).

[81]. A V Kabashin, V E Kochergin, and P I Nikitin, "*Surface plasmon resonance bio- and chemical sensors with phase polarization contrast"*, Sensors and Actuators B, Vol. 54 (1), pp. 51–56, (1999).

[82]. F Vlluendas and J Pelayo, "*Optical fiber device for chemical seming based on surface plasmon excitridon*", Sensors and Actuators A, Vol, 23, pp. 1142-1145, (1990).

[83]. J Homola and R Slavik, "*Fiber optic sensor based on surface plasmon resonance*", Electronics Letters, Vol. 32, pp. 480–482 (1996).

[84]. D Monzon-Hermandez, J Villatoro, D Talavera, and D Luna- Moreno, "*Optical fiber surface plasmon resonance sensor with multiple resonance peaks*", Applied Optics, Vol. 43 (6), pp. 1216–1220, (2004).

[85]. D Kim, "*Effect of the azimuthal orientation on the performance of grating coupled surface plasmon resonance biosensors*", Applied Optics, Vol. 44 (16), pp. 3218–3223, (2005).

[86]. G Nemova and R Kashyap, "*Fiber Bragg grating assisted surface plasmon polariton sensor"*, Optics Letters, Vol. 31(14), pp. 2118–2120, (20060.

[87]. G Nemova and R Kashyap, "*Modeling of plasmon polariton refractive index hollow core fiber sensors assisted by a fiber Bragg grating*", J. of Lightwave Technology, Vol. 24 (10), pp. 3789–3796, (2006).

[88]. Y J He, Y L. Lo, and J F Huang, "*Optical fiber surface plasmon resonance sensor employing long period fiber gratings in multiplexing*", J. of the Optical Society of America B, Vol. 23 (5), p. 80, (2006).

[89]. Y Y Shevchenko and J Albert, "*Plasmon resonances in gold coated tilted fiber Bragg gratings*", Optics Letters, Vol. 32 (3), pp. 211–213, (2007).

[90]. T Allsop, R Neal, S Rehman, D J Webb, D Mapps, and I Bennion, "*Generation of infrared surface plasmon resonances with high refractive index sensitivity utilizing tilted fiber Bragg gratings*", Applied Optics, Vol. 46 (22), pp. 5456–5460, (2007).

[91]. V V R Sai, T Kundu and S Mukherji, *"Novel U-bent fiber optic probe for localized surface plasmon resonance based biosensor*", Biosens. Bioelectron., Vol. 24, pp. 2804–2809 (2009).

[92]. P S Grant, S Aul, S Cinnayelka and M J McShane, "*Fiber optic biosensors comprising nanocomposite multilayered polymer and nanoparticle ultrathin films*", Proc. IEEE 25th Annu. Int. Conf. Vol. 4, pp. 2987-2990 (2003).

[93]. R Kashyap, "*Fiber Bragg Gratings*", 2nd Edition, Academic Press (2010).

[94]. A Othonos, "*Fiber Bragg gratings*", Review of Scientific Instruments, Vol. 68, pp.4309-4341 (1997).

[95]. T Erdogan, "*Fiber grating spectra*", J. of Lightwave Technology, Vol. 15, pp. 1277-1294 (1997).

[96]. T Erdogan, "*Cladding mode resonances in short and long period fiber grating filters*", J. Optical Society of America A, Vol. 14, pp. 1760–1773 (1997).

[97]. A . Vengsarkar, P J Lemaire, J B Judkins, V Bhatia, T Erdogan and J E Sipe, "*Long period fiber gratings as band rejection filters*", J. of Lightwave Technology, Vol. 14, pp. 58-65 (1996).

[98]. S W James and R P Tatam, "*Optical fiber long period grating sensors: Characteristics and applications",* Measurement Science and Technology, Vol. 14, pp. 49-61 (2003).

[99]. X Shu, L Zhang and I Bennion, "*Sensitivity characteristics of long period fiber gratings*", J. of Lightwave Technology, Vol. 20, pp. 255-266 (2002).

[100]. K O Hill, Y Fujii, D C Johnson and B S Kawasaki, "*Photosensitivity in optical fiber waveguides: Application to reflection filter fabrication"*, Applied Physics Letters, Vol. 32, pp. 647-649 (1978).

[101]. B S Kawasaki, K O Hill, D C Johnson and Y Fujii, "*Narrow band Bragg reflectors in optical fibers*", Optics Letters, Vol. 3, pp. 66-68 (1978).

[102]. G Meltz, W W Morey and W H Glenn, "*Formation of Bragg gratings in optical fibers by a transverse holographic method*", Optics Letters, Vol. 14, pp. 823-825 (1989).

[103]. D K W Lam and B K Garside, "*Characterization of single mode optical fiber filters",* Applied Optics, Vol. 20, pp. 440-445 (1981).

[104]. J Stone, "*Photorefractivity in $GeO_2$ doped silica fibers*", Applied Physics, Vol. 62, pp. 4371-4374 (1987).

[105]. M J Yeun, "*Ultraviolet absorption studies of germanium silicate glasses*", Appl. Opt., Vol. 21 (1), pp.136-140 (1982).

[106]. D P Hand and J S. Russell, "*Photoinduced refractive index changes in fiber Bragg gratings",* Applied Physics Letters, Vol. 15, pp. 102-104 (1990).

[107]. A Attard, "*Fermi level shift in $Bi1_2SiO_20$ via photon induced trap level occupation*", Applied Physics, Vol. 71, pp. 933-937 (1992).

[108]. H G Limberger, P Y Fonjallaz, R P Salathe and F Cochet, "*Compaction and photoelastic induced index changes in fiber Bragg gratings",* Applied Physics Letters, Vol. 68, pp. 3069-3071 (1996).

[109]. D L Williams, "*Photosensitive index changes in germania doped silica fibers and waveguides*", Proc. Photosensitivity and Self Organization in Optical Fibers and Waveguides, Quebec, Canada, SPIE, 2044, pp. 55-68 (1993).

[110]. D Wong, S B Poole, and M G. Sceats, "*Stress birefringence reduction in elliptical core fibers under ultraviolet irradiation*", Opt. Letters, Vol. 17, pp. 1773-1775 (1992).

[111]. N Lawandy, "*Light induced transport and delocalization in transparent amorphous systems",* Optics Communication, Vol. 74, pp. 180-184 (1989).

[112]. A Miotello and R Kelly, "*Laser irradiation effects in $Si^+$ implanted $SiO_2$*", Nuclear Instruments & Methods in Physics Research. Sect. B, Vol. 65, pp. 217-222 (1992).

[113]. D L Griscom and E J Friebele, "*Fundamental radiation induced defect centers in synthetic fused silicas: Atomic chlorine, delocalized E' centers and triplet state*", Phy. Rev. B, 34 (11), pp. 7524-7533 (1986).

[114]. R M Atkins, V Mizrahi and T Erdogan, "*248 nm induced vacuum UV spectral changes in optical fiber preform cores: support for a colour center model of photosensitivity*", Electronics Letters, 29, pp. 385-387 (1993).

[115]. P St J Russell, D P Hand, Y T Chow and L J Poyntz-Wright, "*Optically induced creation, transformation and organization of defects and color centers in optical fiber*", Proc. SPIE, Vol. 1516, pp.47-54 (1991).

[116]. T E Tasi, G M Williams and E J Friebele, "*Index structure of fiber Bragg gratings in Ge-$SiO_2$ fibers*", Opt. Lett. Vol 22, pp. 224-226 (1997).

[117]. B Poumelie, P Guenot, I Riant, P Sansonetti and P Niay, "*UV induced densification during Bragg grating inscription in Ge-SiO2 preforms*". Opt. Mat., Vol. 4, pp. 441-449 (1995).

[118]. K O Hill, B Malo, F Bilodeau, D C Johnson, J F Morse, A Kilian, L Reinhart and K Oh, "*Photosensitivity in $Eu^{2+}$:$Al_2O_3$ doped core fiber*", Proc. Conf. on Optical Fiber Communication OSA, 14, pp. 14-21 (1991).

[119]. F Bilodeau, D C Johnson, B Malo, K A Vineberg, K O Hill, T F Morse, A Kilian and L Reinhart, "*Ultraviolet light photosensitivity in $Er^{3+}$-Ge-doped optical fiber*", Optics Letters, Vol. 15, pp. 1138-1140 (1990).

[120]. M M Broer, R L Cone and J R. Simpson, "*Ultraviolet-induced distributed feedback gratings in $Ce^{3+}$ doped silica optical fibers*", Opt, Let., Vol. 16, pp. 1391-1393 (1991).

[121]. K Oh, P S Westbrook, R M Atkins, P Reyes, R S Windeler, W A Reed, T E Stockert, D Brownlow and D DiGiovanni, "*Ultraviolet photosensitive response in an antimony doped optical fiber*", Optics Letters, Vol. 27, pp. 488-490 (2002).

[122]. D L Williams, B J Ainslie, J R Armitage, R Kashyap and R Campbell, "*Enhanced UV photosensitivity in boron co-doped germanosilicate fibers*", Electronics Letters, Vol. 29, pp. 45-47 (1993).

[123]. L Dong, J L Cruz, L Reekie, M G Xu and D Payne, "*Enhanced photosensitivity in tin co-doped germanosilicate optical fibers*", IEEE Photonics Technology Letters, Vol. 7, pp. 1048-1050 (1995).

[124]. L Dong, L Reekie, L Cruz and D N. Payne, "*Grating formation in a phosphorus doped germanosilicate fiber*", Proc. Conf. on Optical Fiber Communication, pp. 82-83 (1996).

[125]. G M Williams, T E Tsai, C I Merzbacher and E J Friebele "*Photosensitivity of rare earth doped ZBLAN fluoride glasses*", J. Lightwave Technology, Vol. 15, pp.1357-1362 (1997).

[126]. T Taunay, P Niay, P Bernage, E X Xie, H Poignant, S Boj, E Delevaque and M Monerie, "*Ultraviolet induced permanent Bragg grating in cerium doped ZBLAN glasses or optical fibers",* Opt. Lett., Vol. 19 (17), pp. 1269-1271(1994)

[127]. P R Herman, K Beckley and S Ness, "*157nm photosensitivity in germanosilicate waveguides*", Proc. Conf. on Lasers and Electro-Optics, California, Technical Digest Series, pp. 513 (1998).

[128]. J Albert, B Malo, F Bilodeau, D C Johnson, K O Hill, Y Hibino and M Kawachi, "*Photosensitivity in Ge doped silica optical waveguides and fibers with 193nm light from an ArF excimer laser*", Optics Letters, Vol. 19, pp.387-389 (1994).

[129]. R M Atkins, V Mizrahi and T Erdogan, "*248 nm induced vacuum UV spectral changes in optical fiber preform cores: Support for a colour center model of photosensitivity*", Electronics Letters, Vol. 29, pp. 385-387 (1993).

[130]. R M Atkins and R P Espindola, "*Photosensitivity and grating writing in hydrogen loaded germanosilicate core optical fibers at 325 and 351nm*", Applied Physics Letters, Vol. 70, pp. 1068-1069 (1997).

[131]. P J Lemaire, R M. Atkins, V Mizrahi and W A Reed, "*High pressure $H_2$ loading as a technique for achieving ultrahigh UV photosensitivity and thermal sensitivity in $GeO_2$ doped optical fibers*", Electronics Letters, Vol. 29, pp. 1191-1193 (1993).

[132]. R M Atkins, P J Lemaire, T Erdogan and V A Mizrahi, "*Mechanisms of enhanced UV photosensitivity via hydrogen loading in germanosilicate glasses*", Electronics Letters, Vol. 29, pp. 1234-1235 (1993).

[133]. V Grubsky, D S Starodubov, J Feinberg, "*Photochemical reaction of hydrogen with germanosilicate glass initiated by 3.4 - 5.4-eV ultraviolet light*", Optics Letters, Vol. 24, pp. 729-731 (1999).

[134]. F Bliodeau, B Malo, J Albert, D C Johnson, K O Hill, Y Hibino, Y Abe and M Kawachi, "*Photosensitization of optical fiber and silica on silicon/silica waveguides*", Optics Letters, Vol. 18, pp. 953-955 (1993).

[135]. I Camlibel, D A Pinnow and F W Dabby, "O*ptical aging characteristics of borosilicate clad fused silica core fiber optical waveguides",* Appl. Phys. Lett., Vol. 26 (4), pp. 185-187 (1975).

[136]. W W Morey, G Meltz, and W H Glenn, "*Holographically generated gratings in optical fibers*", Optics & Photonics News, Vol. 1(7), p.8 (1994).

[137]. K O Hill, B Malo, K A Vineberg, F Bilodeau, D C Johnson, and I Skinner, "*Efficient mode conversion in telecommunication on fiber using externally written gratings*", Electron. Tech. Lett., Vol. 26 (16), pp. 1270- 1272 (1990).

[138]. R Kashyap, J R Armitage, R W Wyatt, S T Davey and D L.Williams, "*All fiber narrow band reflection gratings at 150 nm"*, Electronics Letters, Vol. 26, pp.730-732 ( 1990).

[139]. B J Eggleton, P A Krug and L Poladian, "*Experimental demonstration of compression of dispersed optical pulses by reflection from self-chirped optical fiber Bragg gratings*", Optics Letters, Vol. 19, pp. 877-880 (1994).

[140]. H G Limberger, P Y Fonjallaz, P Lambelet, C Zimmer, R P Salathe and H H Gilgen, "*Photosensitivity and self-organisation in optical fibers and wave guides*", Proc. SPIE 2044, pp. 272-285 (1993).

[141]. K O Hill, B Malo, F Bilodeau, D C. Johnson and J Albert, "*Bragg gratings fabricated in monomode photosensitive optical fiber by UV exposure through a phase mask*", Appl. Phy. Lett., Vol. 62, pp. 1035-1037 (1993).

[142]. D Z Anderson, V Mizrahi, T Erdogan and A E White, "*Phase mask method for volume manufacturing of fiber phase gratings*", OSA Tech. Digest, Vol. 4, pd16 (1993).

[143]. M L Dockney, J W James and R P Tatam, "*Fiber Bragg grating fabricated using a wavelength tunable source and a phase mask based interferometer*", Measurement Sci. and Technology, Vol. 7, pp. 445-448 (1996).

[144]. D Z Anderson, V Mizrahi, T Erdogan and A E White, "*Production of in-fiber gratings using a diffractive optical element*", Electronics Letters, Vol. 29, pp. 566-568 (1993).

[145]. J Albert, S Theriault, F Bilodeau, D Johnson, K Hill, P Sixt and M Rooks, "*Minimization of phase errors in long fiber Bragg grating phase masks made using electron beam lithography*", IEEE Photonics Technology Letters, Vol. 8, pp. 1334–1336 (1996).

[146]. J Thomas, C Voigtländer, D Schimpf, F Stutzki, E Wikszak, J Limpert, S Nolte and A Tünnermann, "*Continuously chirped fiber Bragg gratings by femtosecond laser structuring*", Optics Letters, Vol. 33, pp. 1560–1562, (2008).

[147]. R Kashyap, P F McKee, R J Campbell and D L Williams, "*A novel method of writing photo induced chirped Bragg gratings in optical fibers",* Electron Lett., Vol. 30 (12), pp. 996-997 (19940

[148]. C Voigtländer, J Thomas, E Wikszak, P Dannberg, S Nolte and A Tünnermann, "*Chirped fiber Bragg gratings written with ultrashort pulses and a tunable phase mask*", Opt. Lett., Vol. 34, pp. 1888-1890 (2009).

[149]. A M Vengsarkar, P J Lemaire, G Jacobovitz-Veselka, V Bhatia, and J B. Judkins, "*Long period fiber gratings as gain flattening and laser stabilizing devices*", Proc. Conf. on Integrated Optics and Optical Fiber Commu., PD1, (1995).

[150]. A M Vengsarkar, P J Lemaire, J B Judkins, V Bhatia, J E. Sipe, and T E. Ergodan, "*Long period fiber gratings as band rejection filters*", Proc. Conf. on Optical Fiber Communications, PD4, (1995).

[151]. A M Vengsarkar, J R Pedrazzani, J B Judkins, P J Lemaire, N S Bergano and C Davidson, "*Long period fiber grating based gain equalizers*", Opt. Lett., Vol. 21, pp. 336–338 (1996).

[152]. B Malo, K O Hill, F Bilodeau, D C Johnson and J Albert, "*Point-by-point fabrication of micro Bragg gratings in photosensitive fiber using single excimer pulse refractive index modification techniques*", Electronics Letters, Vol. 29, pp.1668-1669 (1993).

[153]. K O Hill, B Malo, K A Vineberg, F Bilodeau, D C Johnson and I Skinner, "*Efficient mode conversion in telecommunication fiber using externally written gratings"*, Electron. Lett., Vol. 26 (16), pp. 1270-1272 (1990).

[154]. K O Hill, F Bilodeau, B Malo, and D C. Johnson, "*Birefringent photosensitivity in monomode optical fiber: application to external writing of rocking filters*", Electron. Lett., Vol. 27 (17), pp. 1548-1550 (1990).

[155]. D D Davis, T K Gaylord, E N Glytsis and S C Mettler, "*$CO_2$ laser induced long period fiber gratings: Spectral characteristics, cladding modes and polarization independence*", Electronics Letters, Vol. 34, pp. 1416-1417 (1998).

[156]. D D Davis, T K Gaylord, E N Glytsis and S C Mettler, "*Very high-temperature stable $CO_2$ laser induced long period fiber gratings*", Electronics Letters, Vol. 35, pp. 740-742 (1999).

[157]. J L Tang, S F Cheng, W T Hsu, T Y Chiang and L K Chau, "*Fiber optic biochemical sensing with a colloidal gold modified long period fiber grating*", Sensors & Actuators B. Chemical, Vol. 119, pp. 105-109 (2006).

[158]. D D Davis,T K Gaylod, E N Glytsis, S G Kosinski, S C Mettler and A M Vengsarkar, "*Long period fiber grating fabrication with focused CO2 laser pulses*", Electron. Lett., Vol. 34, pp. 302-303 (1998).

[159]. G Rego, O Okhotnikov, E Dianov and V Sulimov, "*High temperature stability of long period fiber gratings produced using an electric arc*", J. Lightwave Technology, Vol. 19, pp. 1574-1579 (2001).

[160]. A Malki, G Humbert, Y Ouerdane, A Boukhenter and A Boudrioua, "*Investigation of the writing mechanism of electric arc induced long period fiber gratings*", Applied Optics, Vol. 42, pp. 3776–3779 (2003).

[161]. Y Kondo, K Nouchi, T Mitsuyu, M Watanabe, P G Kazansky and K Hirao, "*Fabrication of long period fiber gratings by focused irradiation of infrared femtosecond laser pulses*", Opt. Letters, Vol. 24, pp. 646-648 (1999).

[162]. F Hindle, E Fertein, C Przygodzki, F Dürr, L Paccou, R Bocquet, P Niay, G Limberger and M Douay, "*Inscription of long period gratings in pure silica and germane silicate fiber cores by femtosecond laser irradiation*", IEEE Photonics Technology Letters, Vol. 16, pp. 1861–1863 (2004).

[163]. J Thomas, E Wikszak, T Clausnitzer, U Fuchs, U Zeitner, S Nolte and A T¨unnermann,"*Inscription of fiber Bragg gratings with femtosecond pulses using a phase mask scanning technique*", Applied Physics A, Vol. 86, pp. 153–157 (2007).

[164]. S J Mihailov, D Grobnic, C W Smelser, P Lu, R B Walker and H Ding, "*Bragg grating inscription in various optical fibers with femtosecond infrared lasers and a phase mask*", Optical Materials Express, Vol. 1, pp. 754–765 (2011).

[165]. Y Jiang, C Tang, J Xu, "*Fabrication of long period gratings with a mercury arc lamp*", Optics Communications, Vol. 283, pp. 1311–1315 (2010).

[166]. M Fujimaki, Y Ohki, J L Brebner and S Roorda, "*Fabrication of long period optical fiber gratings by use of ion implantation*", Optics Letters, Vol. 25, pp. 88-89 (2000).

[167]. M Fujimaki, Y Nishihara, Y Ohki, J L Brebner and S Roorda, "*Ion implantation induced densification in silica based glass for fabrication of optical fiber gratings*", J. of Applied Physics, Vol. 88, pp. 5534-5537 (2000).

[168]. V I Karpov, M V Grekov, E M Dianov, K M Golant, S A Vasiliev, O I Medvedkov and R R Khrapko, "*Mode field converters and long period gratings fabricated by thermo-diffusion in nitrogen doped silica core fibers*", Proc. Opt. Fiber Commu. Conf. and Exhibition, OFC '98, Technical Digest, pp. 279–280 ( 1998).

[169]. C Narayanan, H M Presby and A M Vengsarkar, "*Band rejection fiber filter using periodic core deformation*", Electronics Letters, Vol. 33, pp. 280-281 (1997).

[170]. C D Poole, H M Presby and J P Meester, "*Two mode fiber spatialmode converter using periodic core deformation*", Electronics Letters, 30, pp. 1437- 1438 (1994).

[171]. C Y Lin, G W Chern and L A Wang, "*Periodical corrugated structure for forming sampled fiber Bragg grating and long period fiber grating with tunable coupling strength*", J. Lightwave Technology, Vol. 19, pp. 1212-1220 (2001).

[172]. S Savin, M J F Digonnet, G S Kino and H J Shaw, "*Tunable mechanically induced long period fiber gratings*", Optics Letters, Vol. 25, pp. 710-712 (2000).

[173]. I K Hwang, S H Yun and B Y Kim, "*Long period fiber gratings based on periodic microbends*", Optics Letters, Vol. 24, pp. 1263-1265 (1999).

[174]. M Kim, D Lee, B I Hong and H Chung, "*Performance characteristics of long period fiber gratings made from periodic tapers induced by electric arc discharge*", J. Korean Physical Society, Vol. 40, pp. 369–373 (2002).

[175]. Y Jiang, Q Li, C H Lin, E Lyons, I Tomov and H P Lee, "*A novel strain induced thermally tuned long period fiber grating fabricated on a periodic*

*corrugated silicon fixture*", IEEE Photonics Technology Letters, Vol. 14, pp. 941-943 (2002).

[176]. G Kakarantzas, T E Dimmick, T A Birks, R Le Roux and P St. J Russell, "*Miniature all-fiber devices based on $CO_2$ microstructuring of tapered fibers*", Optics Letters, Vol. 26, pp. 1137-1139 (2001).

[177]. J K Bae, S H Kim, J H Kim, J H Bae, S B Lee and J M. Jeong, "*Spectral shape tunable band rejection filter using a long period fiber grating with divided coil heaters*", IEEE Photonics Technology Letters, Vol. 15, pp. 407-409 (2003).

[178]. T Y Tang, P Y Tseng, C Y Chiu, C N Lin, C C Yang, Y W Kiang and K J Ma, "*Long period fiber grating effects induced by double sided loading*", Optical Engineering, 42, pp. 1910-1914 (2003).

[179]. Y C Jeong, B C Yang, B H Lee, H S Seo, S S Choi and K W Oh, "*Electrically controllable long period liquid crystal fiber gratings*", IEEE Photonics Technology Letters, Vol. 12, pp. 519-521 (2000).

[180]. R Faced, C Alegria, M N Zervas and R I Laming, "*Acousto optic attenuation filters based on tapered optical fibers*", IEEE J. Selected Topics in Quantum Electronics, Vol. 5, pp. 1278-1288 (1999).

[181]. A Diez, T A Birks, W H Reeves, B J Mangan and P St. J Russell, "*Excitation of cladding modes in photonic crystal fibers by flexural acoustic waves*", Optics Letters, Vol. 25, pp. 1499-1501 (2000).

[182]. G Rego, R Falate, J L Santos, H M Salgado, J L Fabris, S L Semjonov and E M Dianov, "*Arc induced long period gratings in aluminosilicate glass fibers*", Optics Letters, Vol. 30, pp. 2065- 2067 (2005).

[183]. P R Herman, K Beckley and S Ness, "*157 nm Photosensitivity in germanosilicate and fused silica glasses*", Proc. Conf. on Lasers and Electro-Optics, San Francisco, CA, pp.4-8 (1998).

[184]. K P Chen, P R Herman and R Tam, "*Strong fiber bragg grating fabrication by hybrid 157 and 248 nm laser exposure*", IEEE Photonics Technology Letters, Vol. 14, pp 170-172 (2002).

[185]. K P Chen, P R Herman, and J Zhang, "*Fabrication of strong long period gratings in hydrogen free fibers with 157 nm $F_2$ laser radiation*", Opt. Lett. Vol. 26 (11), pp. 771-773 (2001).

[186]. C J Paddison, J M Dawes, D J W Brown, M J Withford, R I Trickett, P A Krug, "*Multiple fiber gratings fabricated using frequency doubled copper vapour lasers*", Electronics Letters, Vol. 34, pp. 2407-2408 (1998).

[187]. L Dong, W F Liu and L Reekie, "*Negative index gratings formed by a 193-nm excimer laser*", Optics Letters, Vol. 21, pp. 2032- 2034 (1996).

[188]. H Patric and S L Gilbert, "*Growth of Bragg gratings produced by continuous wave ultraviolet light in optical fibers*", Optics Letters, Vol. 18, pp. 1484-1486 (1993).

[189]. G D Peng, Z Xiong and P L Chu, "*Photosensitivity and gratings in dye doped polymer optical fibers*", J. Optical Fiber Technology, Vol. 5 (2), pp. 242-251 (1999)

[190]. D S Starodubov, V Grubsky, J Feinberg, "*Bragg grating fabrication in germanosilicate fibers by use of near-UV light: A new pathway for refractive index changes*", Optics Letters, Vol. 22, pp. 1086-1088 (1997).

[191]. J R Armitage, "*Fiber Bragg reflectors written at 262nm using a frequency quadrupled diode pumped $Nd^{3+}$:YLF laser*", Electronics Letters, Vol. 29, pp. 1181-1183 (1993).

[192]. C Y Wei, C C Ye, S W. James, R P Tatam and P E Irving. "*The influence of hydrogen loading and the fabrication process on the mechanical strength of optical fiber Bragg gratings*", Optical Materials, Vol. 20, pp. 241–51 (2002).

[193]. J Blows and D Y Tang, "*Gratings written with tripled output of Q-switched Nd;YAG laser*", Electronics Letters, Vol. 36, pp. 1837-1839 (2000).

[194]. M D Baiad, M Gagné, W-J Madore, E De Montigny, N Godbout, C Boudoux and R Kashyap, "*Surface plasmon resonance sensor interrogation with a double-clad fiber coupler and cladding modes excited by a tilted fiber Bragg grating*", Optics Letters, Vol. 38, No. 22, pp. 4911-4914 (2013).

[195]. M D Baiad and R Kashyap, "*Concatenation of surface plasmon resonance sensors in a single optical fiber using tilted fiber Bragg gratings*", Optics Letters, Vol. 40, No. 1, pp. 115-118 (2015).

[196]. R Kashyap, R Wyatt and P F McKee, "*Wavelength flattened saturated erbium fiber amplifier using multiple side tap Bragg gratings",* Electron. Lett., Vol. 29 (11), pp. 1025-1026 (1993).

[197]. R E Olson, "*Discovery of the lipoproteins, their role in fat transport and their significance as risk factors*", J. Of Nutrition, Vol. 128 (2), pp. 439S-443S (1998).

[198]. J L Schlienger, "*The edifying cholesterol story: From gall stone to the LDL receptor*", Med. Des Maladies Metaboliques, Vol. 6 (1), pp. 97-103 (2012).

[199]. N B Myant, "*The Biology of Cholesterol and Related Steroids*", Willium Heinemann, London, (1981).

[200]. D S Fredrickson, R I Levy, J B Wyngarden and D D Fredrickson, "*The Metabolic Basis of Inherited Disease*", McGraw-Hill, New York, (1972).

[201]. D S Fredrickson, R I Levy and R S Lee, "*Fat transport in lipoproteins-An integrated approach to mechanisms and disorders*", The New England J. of Med., Vol. 276 (1), pp. 34-42 (1967).

[202]. L L Smith, "*Another cholesterol hypothesis: Cholesterol as antioxidant*", Free Radical Bio. and Med., Vol. 11 (1), pp. 47-61 (19910.

[203]. B Wang, J Huang, M Li and X Zhou, "*Multifunctional sensing film used for fiber optic cholesterol sensor*", Proc. SPIE, Vol. 7278, pp. 72780Q-1-12 (2009).

[204]. G Wick, G Schelt, A Amberger, R Kleindienst and Q Xu, "*Is atherosclerosis an immunologically mediated disease?* ", Immun. Today Vol. 16, pp. 27–33, (1995).

[205]. A I Fyte, J H Qiao and A J Lusis, "*Immunodeficient mice develop typical atherosclerotic fatty streak when fed an atherogenic diet*", J Clin. Invest Vol. 94, pp. 2516–2520, (1994).

[206]. J D Laman, B J G L deSmet, A Schoneveld and M V Meurs, "*CD4o-CD40L interaction in atherosclerosis*", Immunology Today, Vol. 18, pp. 272–277, (1997).

[207]. A Keys, "*Coronary heart disease – the global picture*", J. Atherosclerosis Vol. 22, pp. 149–192, (1975).

[208]. D Kaul, "*Molecular link between cholesterol, cytokines and atherosclerosis*", J. Molecular and Cellular Biochemistry, Vol. 219, pp. 65–71 (2001).

[209]. The Columbia Electronic Encyclopedia, Columbia University Press (2007).

[210]. T N Flink, A Oraevsky and S L Jacques, "*Autofluorescence detection of oxidized LDL in monocytes: a novel risk factor for the assessment of atherosclerosis?*", Proc. SPIE, Vol. 2679, pp.34-39 (1996).

[211]. Y H Yan, Y H Xu and S P Li, "*Development of fiber optical biosensor of cholesterol based on fluorescence quenching*", Chinese J. of Biomedical Engineering, 23 (1), p. 44-48 (2004).

[212]. I H Lee, D Pinto, E A Arriaga, Z Zhang and N Dovichi, "P*icomolar analysis of proteins using electrophoretically mediated microanalysis and capillary electrophoresis with laser induced fluorescence detection"*, J. Anal. Chem., Vol. 70 (10), pp. 4546- 4548 (1998).

[213]. V Shumyantseva, G Deluca, T Bulko S Carrara, C Nicolini, S A Usanov and A Archakov, "*Cholesterol amperometric biosensor based on cytochrome P450scc*", Biosens. Bioelectron., Vol. 19 (9), pp. 971-976 (2004).

[214]. P L Cacheux, G Menard, H N Quang, P Weinmann, M Jouan and N Q Dao, "*Quantitative analysis of cholesterol and cholesterol ester mixtures using near infrared Fourier transform Raman spectroscopy"*, Appl. Spectrosc., Vol. 50 (10), pp. 1253-1257 (1996).

[215]. W W Wong, D L Hachey, L L Clark, S Zhang, M Llaurador and W G Piond, "*An improved HPLC method to purify erythrocyte cholesterol for estimation of in vivo cholesterol synthesis using the deuterium method*", Appl. Radial Isotopes, Vol. 45 (4), pp. 529-533 (1994).

[216]. M D Marazuela, B de la Calle, A Quejido, M C Moreno-Bondi, "*Free cholesterol fiber optic sensor for serum samples with simplex optimization*", Biosens. Bioelectron., Vol. 12, pp. 233-241 (1997).

[217]. E Agullo, and B Susna, "*Gas liquid chromatographic determination of total and free cholesterol in egg pastas*", Food Research. Int., 2 Vol. 9, p. 77 (1996).

[218]. G Lia, J M Liao, G Q Hu, N Z Ma and P J Wu, "*Study of carbon nanotube modified biosensor for monitoring total cholesterol in blood*", Biosens. Bioelectron., Vol. 20, pp. 2140–2144 (2005).

[219]. I Karube, K Hara, H Matsuoka and S Suzuki, "*Amperometric determination of total cholesterol in serum with use of immobilized cholesterol esterase and cholesterol oxidase*", Anal. Chim. Acta, Vol. 13, pp. 127-132 (1982).

[220]. C C Allain, L S Poon, C S Chan, W Richmond, and P C Fu, "*Enzymatic determination of total serum cholesterol*", Clinical Chemistry., Vol. 20(4), pp. 470-475 (1974).

[221]. T Akiyoshi, H Yuzuru, and Y Hidetaka, "*Determination of cholesterol with a laboratory built chemiluminescence system*",Analytica Chimica Acta. 188, 95-100 (1986).

[222]. A Krug , R Gobel and R Kellner, "*Flow injection analysis for total cholesterol with photometric detection*", Analytica Chimica Acta. Vol. 287, pp. 59-64 (1994).

[223]. J H Mike and T J Cleland, "*Temperature enhanced chemiluminescence for determination of cholesterol*", Analytica Chimica Acta., Vol. 259, pp. 73-78 (1992).

[224]. K V Derina, E I Korotkova, E V Dorozhko , O A Voronovaa and D A Vishenkova, "*Voltammetric sensor for total cholesterol determination*", Procedia Chemistry, 10, pp. 513 – 518 ( 2014 ).

[225]. G Kaur, M Tomar and V Gupta, "*Nanostructured Zinc Oxide Thin Film for Application to Surface Plasmon Resonance based Cholesterol Biosensor*", Proc. SPIE, Vol. 9667, pp. 966706-1-4 (2015).

[226]. X Lin, Y Nia and S Kokot, "*Electrochemical cholesterol sensor based on cholesterol oxidase and $MoS_2$-AuNPs modified glassy carbon electrode*", Sens. and Act.. B : Chem. Vol. 233, 5, pp. 100-106 (2016).

[227]. Q Wu, YHou,b M Zhang, X Hou, L Xu, N Wang, J Wanga and W Huang, "*Amperometric cholesterol biosensor based on zinc oxide film at silver nanowires - graphene oxide modified electrode*", Anal. Methods, 8, pp. 1806-1812 (2016)

[228]. S Alexander, P Baraneedharan, S Balasubrahmanyan and S Ramaprabhu, "*Modified graphene based molecular imprinted polymer for electrochemical nonenzymatic cholesterol biosensor*", European Polymer J. Volume 86, pp. 106-116 (2017).

[229]. S H Kim, S M Nam, G S Byeon, S Y Yeong, and H S Sik, "*Determination of cholesterol by a diode laser/fiber optic colorimetric spectrometer*", Bull. Korean Chem. Soc., Vol. 21 (4), pp. 389-392 (2000).

[230]. Y H Yan, Y H Xu and S P Li, "*Development of fiber optical biosensor of cholesterol based on fluorescence quenching*", Chinese J. of Biomedical Engineering, Vol. 23 (1), (2004).

[231]. X Tan, M Li, P Cai, L Luo and X Zou, "*An amperometric cholesterol biosensor based on multiwalled carbon nanotubes and organically modified sol-gel/chitosan hybrid composite film*", Anal. Biochem., Vol. 337, pp. 111-120 (2005).

[232]. D A R Medina, E A Méndeza and M T Durán, "*Thin film of sol-gel deposited in photonic crystal fiber for cholesterol detection*", Proc. SPIE Vol. 9434, pp. 943417-1-6 (2015).

[233]. M Yunianto, A N Permata, D Eka, D Ariningrum, S Wahyuningsih and A Marzuki, "*Design of a fiber optic biosensor for cholesterol detection in human blood*", IOP Conf. Series: Materials Science and Engineering, Vol. 176, 012014 (2017).

[234]. M Budiyanto, Suhariningsih and M Yasin, "*Cholesterol detection using optical fiber sensor based on intensity modulation*", J. Phys.: Conf. Ser. Vol. 853, Conf. 01 (2017).

[235]. V Semwal and B D Gupta, "*LSPR- and SPR-based fiber-optic cholesterol sensor using immobilization of cholesterol oxidase over silver nanoparticles coated graphene oxide nanosheets*", J. IEEE Sensors, Vol. 18, No. 3, pp.1039-46 (2018).

[236]. R A A Muzzarelli (Ed.), "*Natural Chelating Polymers*", Pergamon Press, New York, p. 83 (1973).

[237]. P R Austin, C J Brine, J E Castle and J P Zikakis, "*Chitin: New facets of research*", Science, Vol. 212 (4498), pp. 749-753 (1981).

[238]. J P Zikakis (Ed.), "*Chitin, Chitosan and Related Enzymes*", Academic Press, Orlando (1984).

[239]. W A Mass, A Mass and B Tighe, "*A review of biodegradable polymers: uses, current developments in the synthesis and characterization of biodegradable polyesters, blends of biodegradable polymers and recent advances in biodegradation studies*", Polym. Int., Vol. 47 (2), pp. 89-144 (1998).

[240]. L Illum, "*Chitosan and its use as pharmaceutical excipient*", Pharma. Res. Vol. 15 (9), pp. 1326-1331 (1998).

[241]. S Nishimura, O Kohgo, K Kurita and H Kuzuhara, "*Chemospecific manipulations of a rigid polysaccharide synthesis of novel chitosan derivatives with excellent solubility in common organic solvents by region selective chemical modifications*", Macromolecules, Vol. 24 (17), pp. 4745-4748 (1991).

[242]. A Toffey, G Samaranayake, C E Frazier and W G Glasser, "*Chitin derivatives. I. Kinetics of the heat induced conversion of chitosan to chitin*", J. Appl. Polym. Sci., Vol. 60 (1), pp. 75-85 (1996).

[243]. S J Kim, S S Kim and Y M Lee, "*Synthesis and characterization of ether type chitin derivatives*", Macromol. Chem. Phys., Vol. 195 (5), pp. 1687-1693 (1994).

[244]. H K No and S P Meyers, "*Preparation and characterization of chitin and chitosan- A review*", J. Aquatic Food Product Tech., Vol. 4 (2), pp. 27-52 (1995).

[245]. Y I Cho, H K No and S P Meyers, "*Physiochemical characteristics and functional properties of various commercial chitin and chitosan products*", J. of Agricultural Food Chemistry, Vol. 46 (9), pp. 3839-3843 (1998).

[246]. X Y Lü, Y Huang and C Q Ma, "*Evaluation of protein adsorption on chitosan surfaces with reflectometry interference spectroscopy*", Sensors, Vol. 1, pp. 148-160 (2001).

[247]. I Aranaz, M Mengíbar, R Harris, I Paños, B Miralles, N Acosta, G Galed and Á Heras, "*Functional Characterization of Chitin and Chitosan*", Current Chemical Biology, Vol. 3, No. 2, pp. 203-230(28) (2009).

[248]. M S Rodriguez and L E Albertengo, "*Interaction between chitosan and oil under stomach and duodenal digestive conditions*", J. Biosci., BioTech. and Biochem., Vol. 69 (11), pp. 2057-2062 (2005).

[249]. R A A Muzzarelli, "*Management of hypercholesterolemia and overweight by oral administration of chitosans*", New Biomedical Materials-Applied and Basics, D Chapman, P I Haris (Eds.), POI Press, London, (1998).

[250]. R A A Muzzarelli, "*Chitosan based dietary foods*", Carbohydrate Polymers, Vol. 28 (4), pp. 309-316 (1996).

[251]. J Liu, J Zhang and W Xia, "*Hypocholesterolaemic effects of different chitosan samples in vitro and in vivo*", J. Food Chemistry, Vol. 107, pp. 419–425 (2008).

[252]. J K Lee, S U Kim and J H Kim, "*Modification of chitosan to improve its hypocholesterolemic capacity*", J. Biosci. Biotech. Biochem., Vol. 63 (5), pp. 833-839 (1999).

[253]. S Nagaoka, Y Futamura, K Miwa, T Awano, K Yamauchi and Y Kanamaru, "*Identification of novel hypocholesterolemic peptides derived from bovine milk beta-lactoglobulin*", Biochemical and Biophysical Research Communications, Vol. 281(1), pp. 11–17 (2001).

[254]. A Razdan and D Pettersson, "*Effect of chitin and chitosan on nutrient digestibility and plasma lipid concentrations in broiler chickens*", British J. of Nutrition, Vol. 72 (2), pp. 277–288 (1994).

[255]. A Razdan and D Pettersson, "*Hypolipidaemic, gastrointestinal and related responses of broiler chickens to chitosans of different viscosity*", British J. of Nutrition, Vol. 76 (3), pp. 387–397 (1996).

[256]. J Simunek and H Bartonova, "*Effect of dietary chitin and chitosan on cholesterolemic of rats*". Acta Veterinarian Brno, Vol. 74, pp. 491–499 (2005).

[257]. M Sugano, T Fujikawa, Y Hiratsuji, K Nakashima, N Fukuda and Y Hasegawa, "*A novel use of chitosan as a hypocholesterolemic agent in rats*", The American J. of Clinical Nutrition, 33(4), pp. 787–793 (1980).

[258]. M Sugano, S Watanabe, A Kishi, M Izume, and A Ohtakara, "*Hypocholesterolemic action of chitosans with different viscosity in rats*", Lipids, Vol. 23 (3), pp. 187–191 (1988).

[259]. G V Vahouny, S Satchithanandam, M M Cassidy, F B Lightfoot and I Furda, "*Comparative effects of chitosan and cholestyramine on lymphatic absorption of lipids in the rats*", The American J. of Clinical Nutrition, Vol. 38, pp. 278–284 (1983).

[260]. C M Gallaher, J Munion, R Jr Hesslink, J Wise and D D Gallaher, "*Cholesterol reduction by glucomannan and chitosan is mediated by changes in cholesterol absorption and bile acid and fat excretion in rats*", J. of Nutrition, Vol. 130 (11), pp. 2753–2759 (2000).

[261]. Y Maezaki, K Tsuji, Y Nakagawa, Y Kawai, M Akimoto and T Tsugita, "*Hypocholesterolemic effect of chitosan in adult males*", Bioscience Biotechnology and Biochemistry, Vol. 57 (9), pp. 1439–1444 (1993).

[262]. H Zhang and S H Neau, "*In vitro degradation of chitosan by a commercial enzyme preparation: effect of molecular weight and degree of deacetylation*", Biomaterials, Vol. 22, pp. 1653–1658 (2001).

[263]. K Zhou, W Xia, C Zhang and L Yu, "*In vitro binding of bile acids and triglycerides by selected chitosan preparations and their physicochemical properties*", LWT-Food Science and Technology, Vol. 39, pp. 1087–1092 (2006).

Chapter **2**

# Long Period Grating: Basic Theory and its Application as a Cholesterol Sensor

*Abstract*

*This chapter gives an overview of the basic principle of operation of fiber optic long period gratings. This chapter also deals with the sensitivities of LPGs to external perturbances namely, temperature, strain and refractive index. A review of LPG sensors, highlighting their applications as RI sensors for chemical as well as bio-sensing is presented. This chapter also provides the design and development of cholesterol sensors exploiting the refractive index sensitivity of LPG.*

1). ***C Bobby Mathews*** *et al., Sensors & Transducers, Vol. 149 (2), pp. 83-88 (2013).*

2***). B Mathews*** *et al., Proc. Photonics 2012: 11th Int. Conf. on Fiber Optics and Photonics, OSA Tech. Digest, OSA, TPo.23 (2012).*

## 2.1 Introduction

The invention of optical fiber has revolutionized the world of communication towards the end of last century. Optical fiber was also employed in various sensing applications due to its numerous advantages over the conventional electrical, mechanical and chemical sensors. The discovery of photosensitivity in optical fibers was a major lead in the development of fiber gratings. Nowadays fiber grating based sensors have replaced majority of the conventional sensors because of their flexibility, versatility and ease of use.

This section introduces the sensing characteristics of long period gratings. The principle of operation of, LPG and LPG based sensors are discussed initially and then the application of LPG based refractive index sensor for the detection and estimation of cholesterol is presented. It is shown that for an LPG, the wavelength shifts are functions of external perturbations like temperature, strain and surrounding refractive index modulations. The strain and temperature responses of the LPGs along with their highly sensitive nature to the changes in refractive index of the medium around the grating are discussed in detail.

## 2.2. LPG for Sensing Applications

LPGs were first demonstrated by Vensarakar et al. as a spectrally selective band rejection filter for telecommunication application in 1996 [1, 2]. Followed by this, the very first LPG device for sensing application was developed by Vikram Bhatia in the same year [3]. The paper discusses the sensitivity of LPGs to strain, temperature and refractive index, opening up important new potential sensing applications. Since then, LPGs have been extensively deployed in optical communication systems and fiber optic sensor systems. In the field of sensing, they were employed as

temperature sensors, axial strain sensors, structural bend sensors etc. [3-10]. They are used for structural health monitoring of buildings, dams and roads. In the field of automobiles, LPGs are used as sensing elements in spacecrafts, ships, trains and vehicles on road. These widespread applications make it one of the stable and versatile technologies in optical field.

LPG is very beneficial as a refractometer when the RI of the medium surrounding the grating changes. The changes in ambient RI, alter the effective cladding mode index and will lead to shifts in both the amplitude and the wavelength of the resonant dips in the transmission spectrum. As the higher ordered cladding modes in LPGs are less bound to the waveguide structure of the fiber, they exhibit greater ambient refractive index sensitivity [3-5]. These spectral changes with respect to the surrounding medium RI are measured when LPGs are used as a transducer. These characteristics of LPG have been exploited in many sensors reported for the measurement of the RI of the external medium surrounding the grating [11-17]. RI sensing is very significant for applications in the fields of chemical, biological, biochemical sensing since a wide range of parameters can be detected and quantized through RI measurements.

Several sensors exploiting the effect of the ambient refractive index on LPGs have been reported in literature [18-27]. Libish has employed LPGs for the measurement of glucose concentration and adulteration in edible oil utilising its refractive index sensitivity [18]. Shu et al. [19] proposed a concentration sensor for sugar solutions in 1999. Sensors for the detection and measurement of organic aromatic compounds [20] and for the measurement of concentrations of solutions of sodium chloride, calcium chloride, ethylene glycol [12, 21] were also reported earlier. Hydrogen sensors [22], liquid level sensor [23] and measurement of

chloride-ion concentration [24] with long period grating technology were also reported in literature. Chong et al. [25] demonstrated the discrimination of salt, sugar and ethylene glycol solutions and determination of the concentration of the analytes. Falate et al.[26] measured the concentration of turpentine, naphtha, paint thinner and anhydrous alcohol in fuel, water and air using a sensor based on LPGs. Determination of the quality of gasoline and its compliance with legal standards using long period gratings written on standard telecommunication fiber was presented by the same group [27].

In the field of bio sensing Cheng et al. [28], proposed an LPG sensor for real time detection of DNA interaction. Bacterial detection schemes using LPGs were demonstrated by Brzozowska et al. [29], Tripathi et al. [30, 31] and Mateusz et al. [32]. Glucose detection accomplished using LPG was presented by Deep et al. [33]. LPG based sensor for the detection of triacylglycerides was reported by Anjali et al. [34] in 2016. Several other applications of LPG in the area of biosensing were also published earlier [35-37].

To enhance chemical selectivity, the long period gratings can be coated with different polymers having distinct affinities for selected analytes. This is covered in subsequent chapters.

## 2.3 Long Period Grating – Basic Theory

As explained earlier, long period gratings (LPGs) are prepared by inscribing periodic or quasi-periodic RI modulation inside the core of an optical fiber. The periodic modulation can be induced either by a permanent alteration of the RI of the fiber core or by physical deformation. The refractive index changes are normally imposed on the optical fiber core by exposing it to intense UV radiations through an

amplitude mask of specific period or by the point-by-point writing method. The UV illumination creates a permanent increase in the RI of the core of the fiber, creating a fixed RI modulation according to the exposed pattern. This fixed RI modulation developed on the fiber core is called a grating [38]. For LPGs, the period or the pitch of the RI modulation inscribed on the core of the optical fiber is higher than 100 μm [4].

### 2.3.1 Mode Coupling in LPG

The working principle of LPGs can be described by the coupled mode theory of optical fiber gratings. In an optical fiber grating, the modes couple at discrete wavelengths, which can be derived from the phase matching equation given by [3]:

$$\beta_1 - \beta_2 = \Delta\beta = \frac{2\pi}{\Lambda} \quad \text{.....(2.1)}$$

where $\beta_1$ and $\beta 2$ are the propagation constants of the modes between which the power is coupled and $\Lambda$ denotes the grating period [39, 40].

In LPGs, the power from the forward propagating core mode is coupled to the co-propagating cladding modes of order m, as illustrated in Fig. 2.1. Then,

$$\beta_{co} - \beta_{cl,m} = \Delta\beta = \frac{2\pi}{\Lambda} \quad \text{.....(2.2)}$$

where, $\beta_{co}$ and $\beta_{cl,m}$ are the propagation constants of core and that of $m^{th}$ order cladding mode respectively. For normal LPGs, $\Delta\beta$ is small, making the grating pitch to be very large, in comparison with FBGs. Substituting the values of propagation constants, $\beta_{co}$ and $\beta_{cl,\ m}$, the resonance wavelength condition can be simplified as [1, 3]:

$$\lambda_m = \left[n_{eff}^{co} - n_{eff,m}^{cl}\right]\Lambda \quad \text{.....(2.3)}$$

where $\lambda_m$ is the resonant wavelength corresponding to coupling to the $m^{th}$ order cladding mode, $\Lambda$ is the period of the grating, $n_{eff}^{co}$ is the effective RI

of the fundamental core mode ($LP_{01}$), $n_{eff,m}^{cl}$ is the effective RI of the $m^{th}$ order cladding mode ($LP_{0m}$). Thus, LPG operates by the coupling of power from the fundamental core mode (i.e. the $LP_{01}$ mode) to the co-propagating cladding modes ($LP_{0m}$ mode with m = 2, 3, 4 . . .).

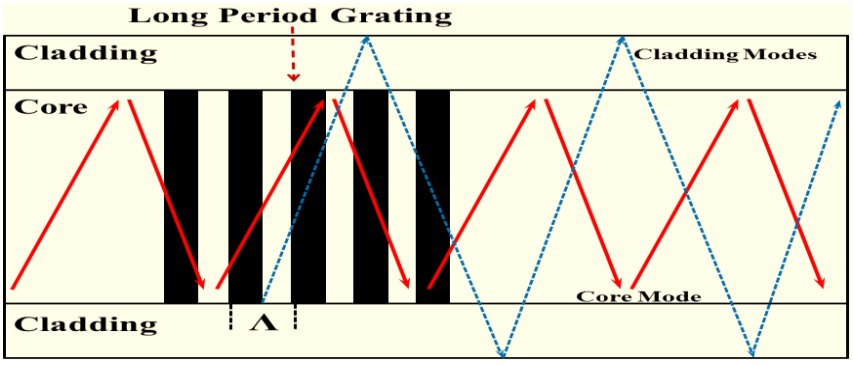


***Figure 2.1:*** *Illustration - Mode coupling in long period grating.*

For a typical long period grating, more than one cladding mode can satisfy the phase matching condition (equation (2.3)) at discrete wavelengths, and the guided mode will be coupled to all those cladding modes. Because of this, rejection bands around specific wavelengths (resonant wavelengths) are formed in the transmission spectrum of the LPG. A typical LPG transmission spectrum is given in Fig. 2.2.

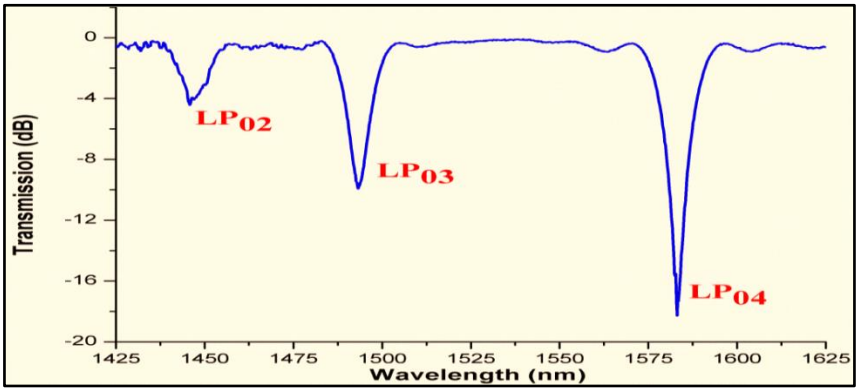


***Figure 2.2:*** *Typical LPG transmission spectrum (Λ=550μm)*

Detailed descriptions and analysis of mode coupling mechanisms in gratings and the principle of operation of LPGs are available in books [41, 42]. Further references are also available in published literature [5, 39, 43, 44, 45].

### 2.3.2 Phase Matching Curve (PMC)

The PMC is a plot of the grating period, $\Lambda$ as a function of the resonant wavelength, $\lambda_m$ for various modes propagating inside an optical fiber. The $n_{eff}$ corresponding to the resonant wavelengths can be computed after identifying the modes. Using the calculated value of $n_{eff}$, of each cladding mode at different wavelengths, grating pitch against wavelength can be plotted using the equation (2.3), which can be rearranged as:

$$\Lambda = \frac{\lambda_m}{[n_{eff}^{co} - n_{eff,m}^{cl}]} \quad \text{.....(2.4)}$$

For various modes, periodicity versus resonant wavelength can be plotted and is referred to as the Phase Matching Curve. The PMC for LPGs written on SMF-28e fiber is shown in Fig. 2.3 [18].

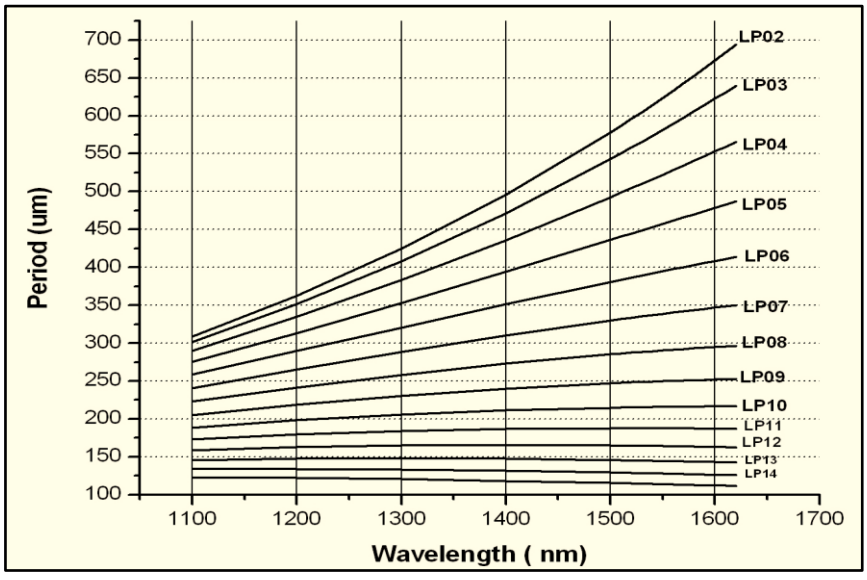


***Figure 2.3:*** *Phase matching curve: SMF-28 fiber [18]*

For an LPG, the resonant wavelengths correspond to the intersection points of the curve with the period of the grating. The reciprocal of the slope, $d\lambda/d\Lambda$ from the PMC is an indication on the sensitivity of the cladding mode to exterior perturbations. The highest order cladding mode with the largest $d\lambda/d\Lambda$ will exhibit maximum sensitivity [39, 40, 43].

For an LPG, the resonant wavelengths correspond to the intersection points of the curve with the period of the grating. The reciprocal of the slope, $d\lambda/d\Lambda$ from the PMC is an indication on the sensitivity of the cladding mode to exterior perturbations. The highest order cladding mode with the largest $d\lambda/d\Lambda$ will exhibit maximum sensitivity [39, 40, 43].

For a grating with a specific period, the LPG the energy is coupled from the fundamental core mode to several cladding modes simultaneously at different wavelengths. Number of resonant wavelengths at which the coupling occurs depends on the grating period. The shorter the grating period, the higher the number of resonant bands or wavelengths at which coupling occurs. The resonant wavelength at which the coupling required can be designed by properly selecting the grating period.

The slope, $d\Lambda/d\lambda$ gradually increases from the higher order modes to the lower order modes. As a result, $d\lambda/d\Lambda$ progressively decreases with the decrease in the order mode. ie. The shift in $\lambda$, due to the change in period ($\Lambda$) gets smaller as the order of the coupled mode decreases for the same LPG. The change in $\Lambda$ can be a result of the change in strain, pressure, temperature etc. on the grating. Consequently, the sensitivity of the LPG to these external perturbations, decreases with decrease in the order of the cladding mode for the same LPG.

## 2.4 Principle of Operation of LPG Based Sensor

The phase matching equation (equation (2.3)) governs the wavelengths at which the guided mode couples to the cladding modes [1, 3]: $\lambda_m = \left[n_{eff}^{co} - n_{eff,m}^{cl}\right]\Lambda$

The phase matching equation can also be rewritten as:

$$\lambda_m = (\delta n_{eff})\,\Lambda \quad \text{.....(2.5)}$$

where, $\delta n_{eff}$ is the difference of the effective index of the guided mode and the cladding mode ($n_{eff}^{co} - n_{eff,m}^{cl}$) at the wavelength $\lambda_m$.

The transmission strength of the coupled modes [4] can be written as: $T_m = 1 - \sin^2(k_m L)$ ……...…… (2.6)

where, L represents the length of the grating and $k_m$ denotes the coefficient of coupling to the $m^{th}$ order cladding mode. Hence, it is clear that, the percentage of power coupled is related to L and $k_m$. The parameter $k_m$ however depends on the specific cladding mode and the magnitude of the RI modulation inscribed in the core ($\Delta n_{co}$) at the time of grating fabrication.

In an LPG, the coupling between the core mode and cladding modes is strongly dependent on external influences like strain [43], temperature [3], bending [12] and surrounding refractive index (SRI) [21]. The strength of coupling is strongly influenced by these external perturbations. This influence in turn leads to shifts in both wavelength and amplitude of the resonant bands in the transmission spectrum of LPG [46, 47]. Measurement of these spectral parameters with respect to the environment, around the grating forms the basis of sensors based on LPGs. These shifts in the coupled wavelength and its amplitude can be interrogated with an optical spectrum analyzer (OSA) to develop simple LPG based sensors.

The shift in the resonant wavelength in the transmission spectrum of LPGs under the influence of strain, temperature and external RI variations, can be expressed as [47]:

$$\Delta\lambda_m = \left(\frac{d\lambda_m}{d\varepsilon}\right)\Delta\varepsilon + \left(\frac{d\lambda_m}{dT}\right)\Delta T + \left(\frac{d\lambda_m}{dn_{sur}}\right)\Delta n_{sur} \quad \text{.....(2.7)}$$

where, $\left(\frac{d\lambda_m}{d\varepsilon}\right)$, $\left(\frac{d\lambda_m}{dT}\right)$ and $\left(\frac{d\lambda_m}{dn_{sur}}\right)$ are the strain, temperature and surrounding RI sensitivities of the LPG at the resonant wavelength, respectively. In the succeeding sections, a brief study about the sensitivity of LPG to these external perturbations is presented.

### 2.4.1 Strain Sensitivity of LPG

Strain acting on an optical fiber, induces significant variations in the RI values of the core and the cladding as well as the physical dimensions of the fiber. This in turn alters the coupling conditions in an optical fiber resulting in the variations in the transmission spectrum.

The strain response of a LPG arises due to two factors: 1) the physical elongation of the fiber, leading to a change in the grating periodicity and 2) the change in the effective RI of the core and cladding due to the elasto-optic effect [48]. Differentiating the phase matching, with respect to axial strain-ε, the shift in resonant wavelength with axial strain can be written as: [5, 49, 50].

$$\frac{d\lambda_m}{d\varepsilon} = \frac{d\lambda_m}{d(\delta n_{eff})}\left[\frac{dn_{co}^{eff}}{d\varepsilon} - \frac{dn_{cl,m}^{eff})}{d\varepsilon}\right] + \Lambda\frac{d\lambda_m}{d\Lambda} \quad \text{..... (2.8)}$$

The terms on the right hand side of the above equation, which affect the axial strain sensitivity, are termed as the material effect and the waveguide effect. The change in the dimension of the fiber (Poisson's effect) and the strain-optic effect (RI variations) are the factors contributing to the material effects. The waveguide effect is a function of the slope of the dispersion term, $\frac{d\lambda_m}{d\Lambda}$, for a specific cladding mode [43, 51, 52, 53]. In

short, resonant wavelength ($\lambda_m$) shift in of the LPG transmission spectrum is highly dependent on the order of the coupled cladding mode (m) and the grating pitch ($\Lambda$).

The contributions of the material and waveguide effects to the strain induced wavelength shift are either "+" or "-", depending on the pitch of the grating and the mode order (m). In general, LPGs having longer pitch (>100 μm) have negative material contribution and the contribution to the waveguide effect is positive. When the grating periodicity is small (<100 μm), both the contributions of material and waveguide effects to the strain sensitivity are negative. Thus, the shift of the resonant wavelength to blue or red region is determined by the relative magnitudes of these contributions from the material and waveguide effects.

### 2.4.2 Temperature Sensitivity of LPG

The major factors contributing to the temperature sensitivity of LPGs are: 1) changes in the difference in the RI of the core and the cladding due to thermo optic effects, and 2) variations in the periodicity of LPG with the temperature. The temperature sensitivity of an LPG can be described by taking the derivative of the phase matching condition, with respect to temperature [5, 52-55].

$$\frac{d\lambda_m}{dT} = \frac{d\lambda_m}{d(\delta n_{eff})}\left[\frac{(dn_{co}^{eff})}{dT} - \frac{(dn_{cl,m}^{eff})}{dT}\right] + \Lambda\frac{d\lambda_m}{d\Lambda}\frac{1}{L}\frac{dL}{dT} \quad \text{.....(2.9)}$$

where, T denotes the temperature, L represents the length of LPG, and $\delta n_{eff} = (n_{co}^{eff} - n_{cl,m}^{eff})$ is the effective RI difference between the coupled core mode and the cladding modes. Thus the wavelength shift due to temperature changes is mainly influenced by the grating pitch ($\Lambda$) [4], the order of the cladding mode (m) [5] and the composition of the fiber [52].

Similar to the strain sensitivity of LPGs (equation (2.8)), there are two terms influencing the temperature sensitivity of LPGs. The composition of the fiber affects the wavelength shift and is defined as the material contribution, which is represented as the first term in equation (2.9). This material contribution arises from the change in the differential RI of the core and cladding due to the thermo optic effect, which varies with different dopants in the fiber. The direction of shift in the resonant wavelength depends on the value of the thermo optic coefficients of the core and cladding [52, 56]. $GeO_2$ has a larger thermo optic coefficient compared to $SiO_2$ whereas; $B_2O_3$ has a negative thermo optic coefficient. In the case of standard fiber, the core constituents are $SiO_2$ and $GeO_2$ and the cladding contains $SiO_2$ only. Therefore, the thermo optic coefficient of the core will be greater than that of the cladding. This results in the red shift of the wavelength, when the temperature is increased [54, 56]. For boron co-doped fibers, the resonant wavelength shifts towards shorter wavelengths (blue shift) due to the negative thermo optic coefficient of the boron dopant [52, 56, 57].

The second term on the right hand side of equation (2.9) is termed as the waveguide contribution to the temperature dependence. This arises from changes in the grating pitch and can be either positive or negative depending on the cladding mode order [41]. Different temperature dependent spectral responses can be observed when coupling occurs at lower-order cladding modes as opposed to modes with higher orders [5, 49, 50]. For coupling to cladding modes with lower orders, which are accessed using a large grating pitch (>100 μm), the material effect dominates. Instead, when coupling to higher ordered cladding modes occur in gratings with relatively shorter pitches (<100 μm); the material contribution can become negligible compared to the waveguide effect.

Thus, the thermal responses of LPGs vary depending upon the type of the fiber and the grating periodicity. The sensitivity of the LPGs to temperature changes can be enhanced by providing coating the LPGs with polymeric materials that have high thermo optic coefficients [58, 59] or by reducing the thickness of the fiber cladding [60]. LPGs written in micro structured fibers, with holes in the cladding filled with UV curable acrylate based polymer also demonstrated higher temperature sensitivity [48].

### 2.4.3 Sensitivity to Surrounding Medium Refractive Index

Conventional fiber optic RI sensors works on the principle of evanescent wave detection. These sensors make use of modifications on the cladding of the fiber to access the evanescent field of the guided mode. In surface plasmon sensors, the fiber cladding is removed partially or completely and a thin layer of appropriate metal is deposited on the polished fiber surface [61]. Limitations of these types of devices are non-repeatability and lack of mechanical strength. In addition, the measurements with these devices are highly influenced by the external power fluctuations. In an LPG, the light guided within the fiber interacts with the surrounding medium without any modifications of the fiber.

The transmitted signal from an LPG is highly sensitive to the RI of the medium around the LPG. The RI sensitivity of an LPG arises due to the dependence of the phase matching condition on $n_{cl,m}^{eff}$ (effective RI of the cladding modes), which are depends on the RIs of the cladding material and the external medium around the cladding. LPG is highly useful as a SRI sensor when the RI of the medium around the grating varies. The alterations in the ambient refractive index changes the $n_{cl,m}^{eff}$ and this in turn leads to shifts in both the amplitude and the wavelength of the resonant loss bands in the transmission spectrum of LPG. This feature

of LPGs can be utilized in the development of various sensors for the measurement of RI, biological parameters, liquid sensors, chemical concentration sensors etc. [3, 12, 52, 62-64].

The effect of SRI on the resonant wavelengths can be expressed as [5]: $\frac{d\lambda_m}{dn_{sur}} = \frac{d\lambda_m}{dn_{eff,m}^{cl}}\left[\frac{dn_{eff,m}^{cl}}{dn_{sur}}\right]$ ..... (2.10)

where, $n_{sur}$ denotes the RI of the medium around the grating. For each cladding mode, the term $\left[\frac{dn_{eff,m}^{cl}}{dn_{sur}}\right]$ is unique and hence for an LPG, the RI sensitivity is expected to depend strongly on the value of m (order of the coupled cladding mode). Higher order cladding modes are likely to exhibit greater sensitivity to SRI, as they extend further out into the area exterior to the fiber [5, 12, 52]. The RI sensitivity of the resonance wavelengths of LPGs can also be expressed as: [52, 53]

$$\frac{d\lambda_m}{dn_{sur}} = \lambda_m \gamma \Gamma_{sur} \quad \text{.....(2.11)}$$

where, $\gamma = \frac{\frac{d\lambda_m}{d\Lambda}}{n_{co}^{eff} - n_{cl,m}^{eff}}$ is the general sensitivity factor related to the waveguide dispersion of the fiber and $\Gamma_{sur}$ is the specific sensitivity factor. The specific sensitivity factor, $\Gamma_{sur}$ for surrounding RI is given by:

$$\Gamma_{sur} = -\frac{u_m^2 \lambda_m^3 n_{sur}}{8\pi r_{cl}^3 n_{cl} \left(n_{co}^{eff} - n_{cl,\ m}^{eff}\right)\left(n_{cl}^2 - n_{sur}^2\right)^{3/2}} \text{.....(2.12)}$$

where, um is the mth root of the zeroth-order Bessel function of the first kind, rcl and ncl are the radius and refractive index of the fiber cladding, respectively. From equation (2.12), it is clear that the sensitivity is lower for lower order cladding modes. Also, it can be enhanced by reducing the cladding thickness, as it is proportional to $r_{cl}^{-3}$ [52, 64].

The spectral variations of LPG sensors can be characterized in terms of the SRI. The experimental verification of these spectral variations of LPG sensors with respect to the RI changes of the surrounding medium is shown in Fig. 2.4 [18]. When the RI of the medium around the grating is lower than the RI of the cladding ($n_{sur}<n_{cl}$), mode guidance can be described using total internal reflection. Under this condition the resonant wavelengths in the transmission bands shift towards the lower wavelength region (blue shift), as the refractive index of the external medium is increased up to the refractive index of the cladding of the fiber [52, 63]. The closer the SRI to the cladding RI, the higher the sensitivity and exhibit larger wavelength shifts.

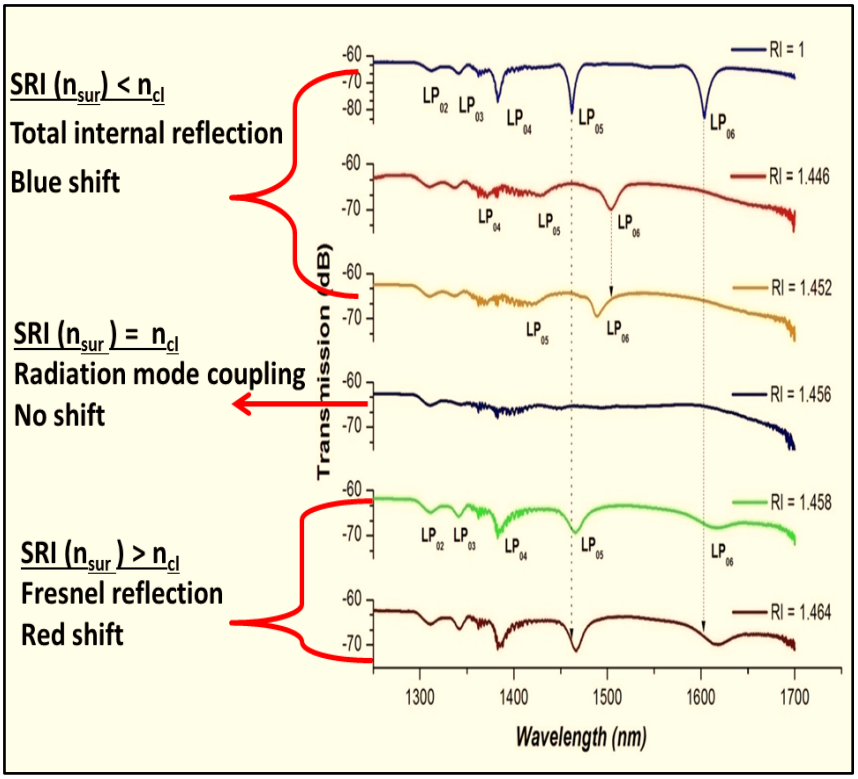


***Figure 2.4:*** *LPG Transmission spectra for different SRI conditions [18].*

Once the SRI matches with refractive index of the cladding, the cladding along with the external medium acts as an infinitely extended layer and then no discrete cladding modes are supported. Under this condition, radiation mode coupling occurs without any distinct attenuation bands [16]. In short, when the SRI is equal to the RI of the cladding, the resonant loss bands disappear, making the transmission spectrum flat.

When the ambient RI value is above the RI of the cladding ($n_{sur}>n_{cl}$), the cladding modes no longer experience total internal reflection and Fresnel reflection can be used to describe the mode structure [62]. For surrounding media with RI values greater than that of the cladding, a part of the transmitted energy is reflected at the interface of the cladding layer and the external medium. The streangth of the reflection will be determined by the Fresnel coefficients.

For $n_{sur}>n_{cl,}$ the resonant peaks get slightly red shifted compared to those measured with air as the surrounding medium [65, 66]. The amplitude of these attenuation peaks increases with further increase in SRI. This increase in amplitude is attributed to the larger Fresnel reflection coefficients at the interface that yield enhanced reflection [65-67].

## 2.5 Cholesterol Sensor

As explained earlier in chapter 1, cholesterol sensing has gained great attention, as excess cholesterol levels can lead to fatal cardiovascular diseases. Several methods including fiber optic techniques were reported earlier for the detection and measurement of cholesterol. Fiber optic sensors, especially LPG sensors offer greater ease of use and accurate, onsite measurements with instantaneous responses. In this context fiber optic long period gratings were employed in the detection and measurement of cholesterol levels.

Cholesterol sensors exploiting the LPG sensitivity to the concentration of the sample solution under test is presented in this section. As the cholesterol concentration levels are altered, a RI variation occurs, which in turn induce shifts in the resonant wavelength and change the depth (amplitude) of the resonant bands in the transmission spectrum of LPG. Cholesterol levels can be detected and estimated by analyzing these changes in the spectrum. The device performance is evaluated in terms of its sensitivity and resolution.

### 2.5.1 LPG Fabrication

The LPGs used in these experiments were fabricated with a KrF-Excimer laser source (248 nm), through point-by-point writing method at CGCRI, Kolkata. The standard single mode Fiber, SMF-28 (SMF-28e, Corning), used for the LPG fabrication had a core diameter of 8.2 micron and cladding diameter of 125 micron. The numerical aperture was 0.14 and the refractive index values were 1.461 and 1.456, for the core and the cladding respectively. Hydrogen loading was done at a temperature of $100^0$C and 1500 psi pressure for 24 hours, prior to the fabrication of LPG to enhance the photosensitivity of the used fiber. The residual molecular Hydrogen, retained after the photochemical reactions, which occur during the process of grating fabrication, was removed by annealing the grating, at a temperature of $200^0$C for 7 hours, using a high temperature oven. LPGs with grating periods of 515 μm (LPG-1) and 550 μm (LPG-2) were selected for the experimental investigations.

### 2.5.2 Experimental Setup

An optical spectrum analyzer (OSA) (Yokogawa - AQ 6319) and a white-light source (Yokogawa - AQ 4305) were used to study the transmission characteristics of the sensor head. The OSA used, works in the range of 600 nm to 1700 nm and has a resolution of 0.001 nm. The white light source

operates in the range of 400 nm to 1800 nm. The refractive index measurements were done using an Abbe refractometer with a measuring range of 1.3000 to 1.7000 and an accuracy of 0.001 by direct measurements and 0.0001 by estimation.

The LPG sensor head was fixed inside a specially designed glass cell. Provision for filling the sample and draining it out as and when desired was provided with in the cell. Fluctuations in the external parameters like temperature, strain, bending etc., can affect the characteristics of the LPG. Epoxy glue was used to fix the fiber in the glass cell to avoid the effect of strain and bending. In doing so, the grating section was aligned straight at the center of the cell. The fiber inscribed with LPG was connected to the light source on one end and to the OSA on the other side as shown in Fig. 2.5.

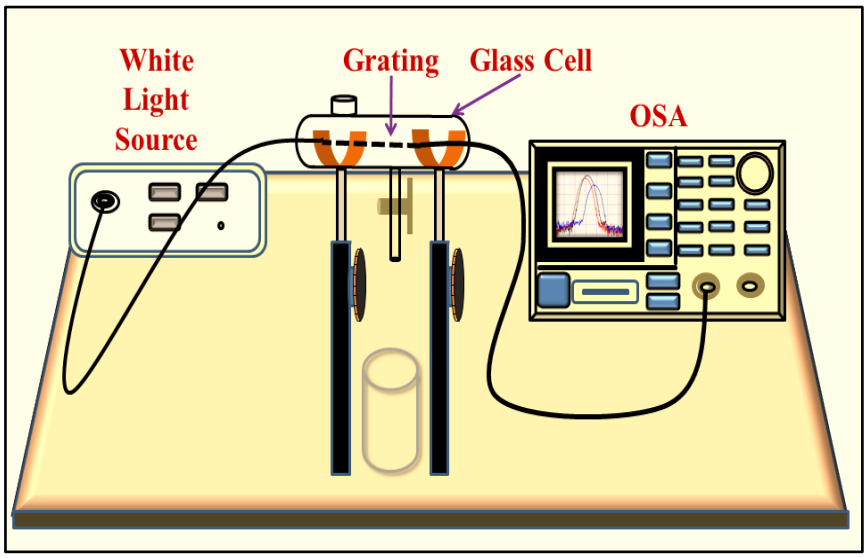


***Figure 2.5:*** *Experimental setup*

The effect of temperature was taken care by maintaining the temperature of the experimental setup and sample solution at 25.0 ± 0.5°C. In addition, a volume of around 20 ml of the test sample was used throughout the

experiments in order to maintain uniformity of the measurements. The shifts in the resonant wavelength and changes in the amplitude of the attenuation dips were measured by immersing the fiber section containing the LPG completely in the sample solution. The cladding around the grating was exposed directly to the sample under test.

### 2.5.3 Materials and Methods

The cholesterol level in the blood of a normal human being is in the range of 1400 ppm to 2000 ppm [68]. Hence, the measurements were restricted to a maximum cholesterol concentration of 5000 ppm, which covers the normal levels of cholesterol. Extra pure cholesterol ($C_{27}H_{46}O$), purchased from Merck was used for the studies. Cholesterol sensing experiments were carried out using two solvents, namely petroleum ether and coconut oil. Spectroscopic grade petroleum ether (purity > 99% ) with a RI of 1.341, purchased from Sigma Aldrich was used to prepare cholesterol sample solutions for the first set of experiments. The second set of experiments were conducted using coconut oil having a RI of 1.448, as the solvent for sample preparation. Samples with concentrations ranging from 0 ppm to 5000 ppm, prepared by dissolving cholesterol in the respective solvents, were subjected to analysis. The prepared solutions were stirred well for an hour at room temperature, so that the cholesterol powder is dissolved completely in the solvent. Spectral changes were detected as soon as the samples were introduced into the glass cell. A stabilization period of one minute was provided after the LPGs were immersed in the solution before recording the spectrum. Once the readings were taken, the sample solution was drained out and the glass cell along with the sensor head was washed repeatedly with distilled water and isopropyl alcohol. This is to ensure that the LPG attenuation dips return to the initial values in the spectrum observed in air, which is used as the primary reference spectrum for further analysis.

## 2.5.4 Results and Discussion

As mentioned earlier the first set of experiments were carried out with petroleum ether as the solvent for cholesterol. An LPG with a grating period of 515 μm (LPG-1) was used in this experiment. The transmission spectrum of the LPG fixed inside the glass cell without any sample is given in Fig. 2.6. The transmission spectrum had three resonant peaks corresponding to the $LP_{0m}$ modes, at 1445.73 nm ($LP_{02}$) 1493.64 nm ($LP_{03}$) and 1583.27 nm ($LP_{04}$). Out of these modes the highest order mode, i.e, the $LP_{04}$ mode at 1583.27 nm, showed maximum sensitivity as expected. Hence further investigations were centered around this resonant wavelength of $LP_{04}$ mode

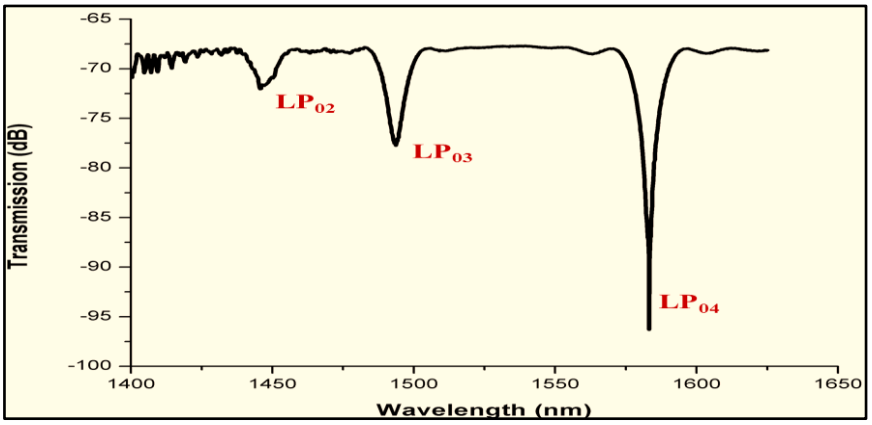


***Figure 2.6:*** *Transmission spectrum of LPG-1 fixed inside the glass cell with air as the surrounding medium.*

The transmission spectra of LPG-1 for various concentrations of cholesterol dissolved in petroleum ether is given below. The RI of pure petroleum ether used as solvent was measured as 1.341 at room temperature. As pure solvent, i.e. petroleum ether was introduced, a blue shift was observed for the peak of $LP_{04}$ mode along with a reduction in the amplitude. The $LP_{04}$ mode at 1583.27 nm shifted to1581.34 nm and the amplitude of the loss band

changed from -96.308 dB to -87.188 dB. This shift in wavelength and reduction in amplitude is as expected and is attributed to the increase in the SRI which changed from 1 (air) to 1.341 (petroleum ether).

The refractive indices of the prepared test solutions of cholesterol were found to vary from 1.341 to 1.346. Even though there was an increase in the RI of the sample solutions from 1.341 to 1.346 as the concentration of the cholesterol in the sample solution was varied from 0 ppm to 5000 ppm, the $LP_{04}$ resonant peak did not exhibit any considerable shift in wavelength or reduction in amplitude. This is because of the reduced LPG sensitivity in this range of RI, which is well below the RI value of the cladding material (1.456) of the fiber. Hence, it was concluded that, in order to have good sensitivity for an LPG based RI sensor, it is better to have the test samples with RI values more closer to that of the cladding.

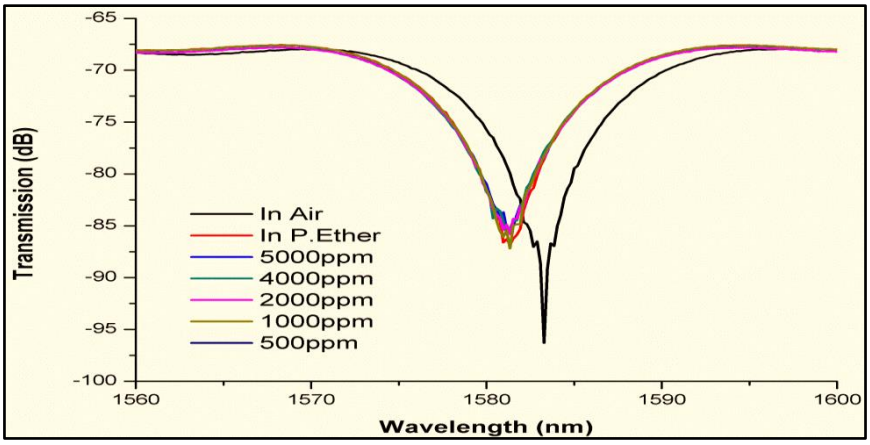


***Figure 2.7:*** *Transmission spectra of LPG-1 for different concentrations of cholesterol dissolved in petroleum ether*

In order to have higher sensitivity for LPG in these studies, it is necessary to choose a proper solvent for cholesterol such that, the RI of the test solution is nearer to that of the cladding. Literature suggests that, cholesterol is completely soluble in vegetable oils [69]. Therefore, it was

decided to take coconut oil, which can provide a RI near to that of the cladding, as the solvent. In addition, coconut oil is of low cost and easily available locally.

Coconut oil purchased from the market was found to have a RI value of 1.448, which is much closer to the LPG cladding RI value of 1.456. Test samples were prepared as described earlier. The refractive index values of the prepared test solutions were varying from 1.448 to 1.455. The experimental procedures adopted were the same as in the case of the experiments with petroleum ether as the solvent. The reference transmission spectra of LPG-2 with a period of 550 μm, fixed inside the glass cell is given below.

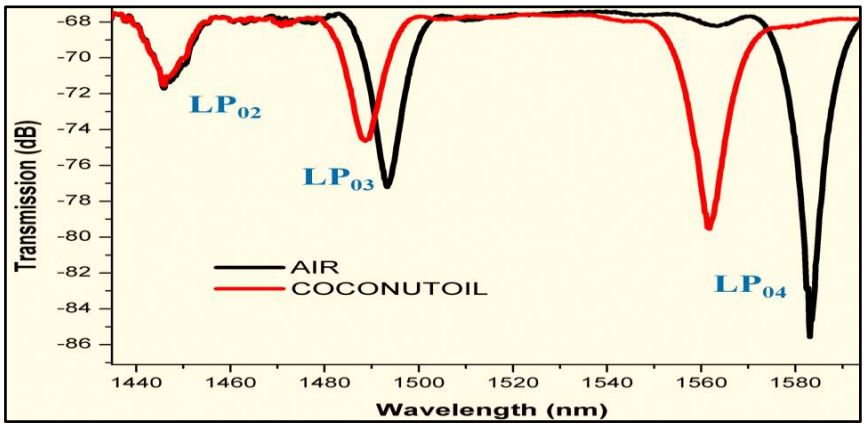


***Figure 2.8:*** *Transmission spectra of LPG-2 fixed in the cell with air and coconut oil as the surrounding medium*

For the LPG-2 used in this experiment, the power coupled to the cladding modes led to the development of resonant loss bands centered around 1445.83 nm ($LP_{02}$), 1493.28 nm ($LP_{03}$), and 1583.11 nm ($LP_{04}$), when air was the medium around the grating. As shown in Fig.2.7, the resonant peak of $LP_{04}$ mode exhibited maximum blue shift from 1583.11 nm to 1561.72 nm when the surrounding medium was changed pure coconut oil instead of air. Along with the blue shift in the wavelength, the dip of the resonant peak decreased

from -85.59 dB to -79.54 dB. As in the case of previous experiment, the $LP_{04}$ mode exhibited maximum response to the test conditions, compared to other resonant modes. The spectra of $LP_{04}$ mode at 1583.11 nm for various concentrations of cholesterol dissolved in coconut oil are given in Fig. 2.9.

It is clear from the spectra that, as the concentration of the cholesterol was varied from 0 ppm (pure coconut oil) to 5000 ppm, the $LP_{04}$ mode exhibited a blue shift in the wavelength. The shifts in the resonant peak was mainly due to the change in SRI and is a function of the pitch of the grating. The resonant peak of $LP_{04}$ mode shifted from 1561.72 nm to 1551.22 nm, to give a total blue shift was around 10.5 nm (± 0.01 nm), when the cholesterol level in the surrounding medium was increased up to 5000ppm.

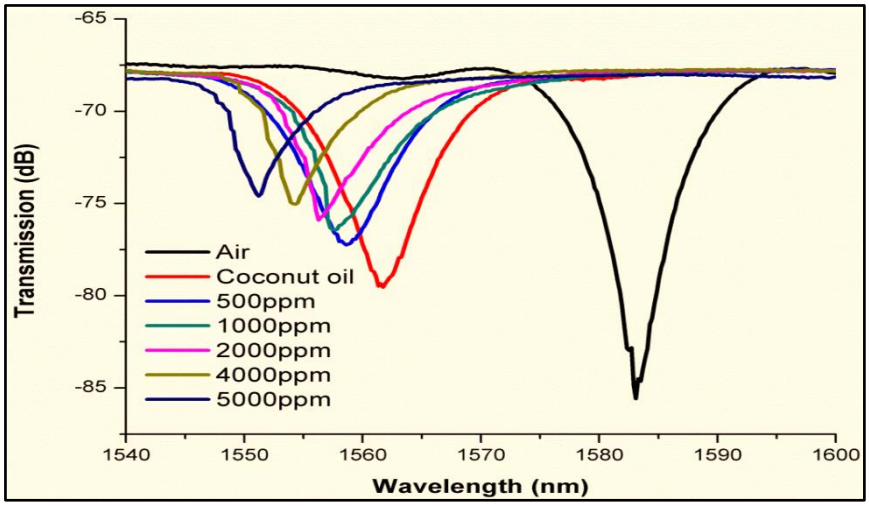


***Figure 2.9:*** *Transmission spectra of* $LP_{04}$ mode of *LPG-2 for various concentrations of cholesterol dissolved in coconut oil*

The average resolution corresponding to this spectral shift of 10.5 nm, observed for a RI range of 1.448 to 1.455 of the sample cholesterol solutions, was $6.7\times10^{-4}$ $nm^{-1}$. The sensitivity of the LPG, when used as a sensor for various concentrations of cholesterol is shown in Fig. 2.10. The overall sensitivity in the measurement range of the sensor was around 2 pm/ppm of

cholesterol. The sensitivity curve clearly depicts a linear response in the range of 1000 ppm to 4000ppm of cholesterol. The normal cholesterol levels in the blood of human beings i.e. 1400 ppm to 2000 ppm, falls within this linear range. This linearity is highly desirable for a commercial sensor for accurate measurements. In the higher ranges of measurements, above 4000 ppm, the RI of the sample solution is very much closer to the cladding RI of the fiber and the sensor head exhibited an increased sensitivity. When the SRI value approaches the RI of the cladding material, the LPG is having maximum sensitivity and the increased slope of the curve is as expected.

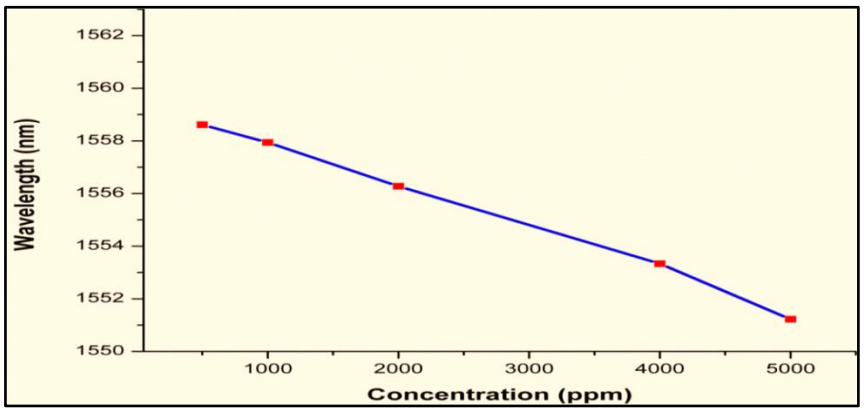


***Figure 2.10:*** *Resonant wavelength ($LP_{04}$) peak positions as a function of different concentrations of cholesterol.*

Apart from the wavelength shift, the intensity of the resonant peak decreased with the increase in the cholesterol levels. The transmittance at the resonant wavelength ($LP_{04}$) with respect to the different levels of cholesterol in the measured range is shown in Fig. 2.11.

The resonant wavelength peak amplitude decreased from -79.54 dB to -74.61 dB, when the cholesterol concentration was varied from 0 ppm to 5000 ppm. A linear response of the transmittance was observed in the measured range of cholesterol levels. This amplitude modulation can also be employed along with the wavelength coded information for confirmatory results in a

commercial sensor. The marginal error of ± 0.01 nm in the total wavelength shift, obtained for repeated experiments over a time of three weeks confirms the repeatability and reusability of the sensor head.

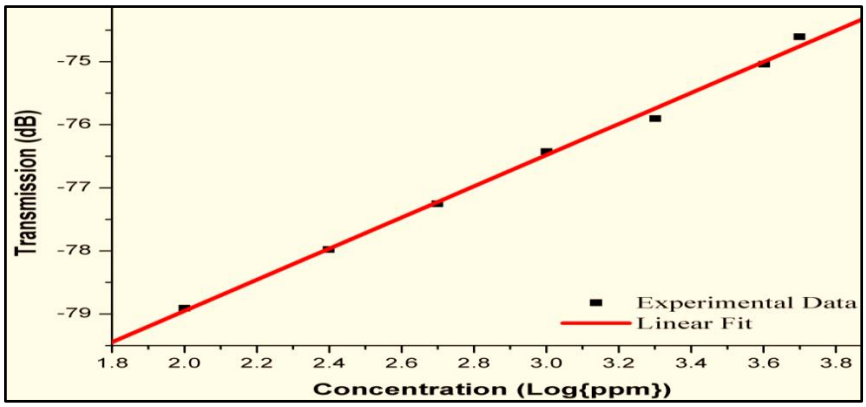


***Figure 2.11:*** *Transmittance at the resonant wavelength ($LP_{04}$) peak positions as a function of different concentrations of cholesterol.*

A comparison of the performance of the present sensor with that of other LPG based sensors and various types of cholesterol measuring sensors reported in literature can be analysed. The LPG based cadmium concentration probe had a limited measurement range of 0.01 to 0.04 ppm [70]. The intensity modulated plastic optic fiber cholesterol detection scheme proposed by M. Yunianto et al., had a linear response in the limited range of 140 mg/dL to 250 mg/dL [71]. The fiber bundle based intensity modulated cholesterol sensing probe had a very low sensitivity of 0.4 µV/ppm of cholesterol and a dynamic range of 0 ppm to 300 ppm [72]. The sensing probe also needs to be displaced during mesasurements, which may lead to misalignment and errors associated with it. An enzymatic fiber optic cholesterol sensor exhibited a linear response in a smaller range of 1700 ppm to 2000 ppm and had a large response time of 120s [73]. Another bifurcated fiber bundle based enzymatic cholesterol sensing probe exhibited a linear response in the range of 250 ppm to 2500 ppm, with a larger response time of 200s [74]. The method requires

heating of the sample, producing a pH dependent response and also was simple in terms of the components used. Apart from the fiber optic methods, other techniques like, voltametric [75, 76], and amperometric [77, 78] detection of cholesterol were also reported. These sensor heads are all, enzymatic and had a maximum linear range of measurements upto 500 ppm [75], 3000 ppm [76], and 4000 ppm [77].

In contrast, the LPG sensor head described in this chapter had a linear response for a wider range of 1000 ppm to 4000 ppm, which is equivalent to a range of 100 mg/dL to 400 mg/dL. Moreover, the LPG sensor head rely on wavelength modulation rather than intensity modulation which are prone to errors due to power fluctuations. Also, the LPG sensor head do not require any heating, or other chemical preparations and uses easily available solvent for the measurements. It also gave instantaneous results, which were independent of the pH variations in the samples.

### 2.5.5 Conclusions

A comparison of the performance of the LPG senor heads for the measurement of cholesterol dissolved in two solvents is given below.

| **Parameter** | **Solvent** | |
|---|---|---|
| | **Petroleum Ether** | **Coconut oil** |
| **Grating Pitch (μm)** | 515 | 550 |
| **Refractive Index Variation** | 1.31 – 1.346 | 1.448 – 1.455 |
| **Wavelength Shift ( $LP_{04}$, nm)** | < 1nm | 10.5 nm |
| **Sensitivity ($\times 10^{-4}$ $nm^{-1}$)** | Too low to be measured | 6.7 |

Table 2.1: Performance of LPG sensor heads for different solvents.

The results presented describe the application of fiber optic LPG based sensor system for the detection and measurement of cholesterol concentrations. Both the wavelength and intensity modulation characteristics of the sensor head can be employed in the design of cholesterol sensors. The sensor presented provides a real time response and requires only a small volume of the sample for analysis. Simplicity and high sensitivity are other added features of the sensor, which make it recommendable for medical diagnosis and clinical applications for the determination of cholesterol levels in humans with suitable modifications. The instantaneous and repeatable results, along with the wide range of linearity in the response makes the sensor head design attractive for commercial applications. The system can also be effectively deployed in the areas of drug development, chemical and biomedical sensing etc.

## 2.6 Summary

This chapter discussed, the theory of long period gratings and their applications. The chapter also presented the characteristics and the mode coupling mechanism in LPGs. A detailed study on the phase matching curve is given. Sensitivity of LPGs to external perturbations such as strain, temperature and RI were presented in detail.

A brief survey on the sensing applications of LPGs with an emphasis on RI sensing is presented in this chapter. Continuing with more practical aspects of RI sensing of LPG, design, development and demonstration of a cholesterol sensor is discussed. Cholesterol dissolved in two solvents namely, petroleum ether and coconut oil were subjected to investigations. LPG exhibited a higher sensitivity of 2 pm/ppm for test samples prepared in coconut oil. It is established that, the LPGs have higher RI sensitivity, when the RI of the test samples are closer to the cladding RI of the fiber. The results presented clearly establish the use of

LPGs for cholesterol sensing and measurements. It was also shown that the wavelength modulation as well as the intensity modulation of sensor output could be employed in realizing a RI sensor using LPGs.

The sensitivity of LPG can be enhanced by applying proper coatings around the grating region. A study of such an enhancement in the RI sensitivity of LPG, and its application for the detection and measurement of cholesterol are presented in the succeeding chapter.

## References

[1]. A M Vengsarkar, P J Lemaire, J B Judkins, V Bhatia, T Erdogan and J E Sipe, "*Long period fiber gratings as band rejection filters"*, J. Lightwave Technol., Vol. 14, no. 1, pp. 58-65 (1996).

[2]. A M Vengsarkar, P Lemaire, J Judkins, V Bhatia and J Sipe, "*Long period fiber rating based gain equalizers*", Optics Letters, Vol. 21, pp. 335-338 (1996).

[3]. V Bhatia and A M Vengsarkar, "*Optical fiber long period grating sensors*, Optics Letters, Vol. 21(9), pp. 692-694 (1996).

[4]. S W James and R P Tatam, "*Optical fiber long period grating sensors: characteristics and applications*", Measurement Science and Technology, Vol. 14 (5), pp 49-61 (2003).

[5]. V Bhatia, "*Applications of long period gratings to single and multi-parameter sensing*, Optics Express, Vol. 4, pp. 457-466 (1999).

[6]. Yi-Ping Wang, Limin Xiao, D N Wang and Wei Jin, "*Highly sensitive long period fiber grating strain sensor with low temperature sensitivity*", Optics Letters ,Vol. 31 (23), pp. 3414-3416 ( 2006).

[7]. F J O Flaherty, Z Ghassemlooy, P S Mangat and K P Dowker, "*Temperature characterization of long period gratings for sensor applications*", Microwave and Optical Technology Letters, Vol. 42 (5), pp. 402-405 (2004).

[8]. B H Lee and J Nishii, "*Bending sensitivity of in-series long period fiber gratings*", Optics Letters, Vol. 23, pp. 1624-1626 (1998).

[9]. X W Shu, L Zhang and I Bennion, "*Sensitivity characteristics of long period fiber gratings*", J. Lightwave Technol., Vol. 20, pp. 255-266 (2002).

[10]. C Ye, S James and R Tatam, "*Simultaneous temperature and bend sensing with long period fiber gratings*", Optics Letters, Vol. 25(14), pp. 1007-1009 (2000).

[11]. H Tsuda and K Urabe, "*Characterization of long period grating refractive index sensors and their applications"*, Sensors, Vol. 9, pp.4559-4571 (2009).

[12]. H J Patrick, A D Kersey and F Bucholtz, "*Analysis of the response of long period fiber gratings to external index of refraction*", J. Lightwave Technol., Vol. 16, pp. 1606–1612 (1998).

[13]. A P Zhang, L Y Shao, J F Ding and S L He, "*Sandwiched long period gratings for simultaneous measurement of refractive index and temperature*", IEEE Photonics Technology Letters 17(11), pp 2397-2399 (2005).

[14]. B H Lee, Y Liu, S B Lee, S S Choi and J N Jang, "*Displacements of the resonant peaks of a long- period fiber grating induced by a change of ambient refractive index",* Optics Letters, Vol. 22, pp. 1769-1771 (1997).

[15]. X W Shu, X M Zhu, S Jiang, W Shi, and D X Huang, "*High sensitivity of dual resonant peaks of long period fiber grating to surrounding refractive index changes*", Electronics Letters, Vol. 35(18), pp 1580-1581(1999).

[16]. Y Koyamada, "*Numerical analysis of core mode to radiation mode coupling in long period fiber gratings*", IEEE Photon. Tech. Letters., Vol. 13, pp. 308-310 (2001).

[17]. Olivier Duhem, Jean-Fraņois Henninot, Marc Warenghem and Marc Douay, "*Demonstration of long period-grating efficient couplings with an external medium of a refractive index higher than that of silica*", Applied Optics, Vol. 37, Issue 31, pp. 7223-7228.

[18]. T M Libish, "*Design and development of fiber grating based chemical and biosensors*", Ph.D. Thesis, Cochin University of Science and Technology, Kerala, India (2015).

[19]. Shu X and Huang D , "*Highly sensitive chemical sensor based on the measurement of the separation of dual resonant peaks in a 100 μm period fiber grating*", Opt. Commun., Vol. 171, pp.65–74 (1999).

[20]. T Allsop, L Zhang and I Bennion, "*Detection of organic aromatic compounds in paraffin by a long period fiber grating optical sensor with optimized sensitivity"*, Optics Communications, Vol. 191(3-6), pp181-190 (2001).

[21]. R Falciai, A G Mignani and A Vannini, "*Long period gratings as solution concentration sensors*", Sensors Actuators B, Vol. 74 (3), pp 74–77 (2001).

[22]. A Trouillet, E Marin, C Veillas and S Khaliq, "*Fiber gratings for hydrogen sensing*", Measurement Science and Technology, Vol. 17, pp 1124–1128 (2006).

[23]. S W James, and R P Tatam, "*Fiber optic liquid level sensor using a long period Grating*", Optics Letters, Vol. 26(16), pp 1224-1226 (2001).

[24]. C Silva, J Coelho, P Caldas, O Frazão, P Jorge and J Santos, "*Optical fiber sensing system based on long period gratings for remote refractive index measurement in aqueous environments"*, Fiber and Integrated Opt., Vol. 29 (3), pp 160-169 (2010).

[25]. J H Chong, P Shum, H Haryono, A Yohana, M K Rao, C Lu and Y Zhu, "*Measurements of refractive index sensitivity using long period grating refractometer*", Optics Communications, Vol. 229, pp. 65–69 (2004).

[26]. R Falate, R C Kamikawachi, M Muller, H J Kalinowski and J L Fabris, "*Fiber optic sensors for hydrocarbon detection*", Sensors and Actuators B-Chemical, Vol. 105 (2), pp 430-436 (2005).

[27]. R Falate, M Muller, J L Fabris and H J Kalinowski, "*Long period gratings in standard telecommunication optical fibers for fuel quality control*", Annals of Optics, Vol. 5, pp 1-4 (2003).

[28]. X Chen, L Zhang, K Zhou, E Davies, K Sugden, I Bennion, H M, Hine, "*A real-time detection of DNA interactions with long period fiber grating based biosensor"*, Opt. Lett., Vol. 32, pp 2541-2543 (2007).

[29]. E Brzozowska, M Smietana, M Koba, S Gorska, K Pawlik, A Gamian and W J Bock, "*Recognition of bacterial lipopolysaccharide using bacteriophage-adhesin coated long period gratings"*, J. Biosensors and Bioelectronics, Vol. 67, pp 93-99 (2015)

[30]. S M Tripathi, W J Boc, P Mikulic, R Chinnappan, N G Andy, M Tolba and M Zourob, "*Long period grating based biosensor for the detection of Escheichia coli bacteria"* , J. Biosensors and Bioelectronics, Vol. 35 (1), pp 308-312 (2012).

[31]. S M Tripathi, *Long period grating based bio sensor for rapid and accurate detection of E.coli bacteria in water*, Proc. Photonics 2016, OSA (2016).

[32]. Smietana, W J Bock, P Mikulic, N G Andy, R Chinnappan and Mohammed Zourob, "*Detection of bacteria using bacteriophages as recognition elements immobilized on long period fiber gratings"*, Opt. Exp., Vol. 19, No. 9, pp 7971-7978 (2011).

[33]. A Deep, U Tiwari, P Kumar, V Mishra, S C Jain, N Singh, P Kapur and L M Bharadwaj, "*Immobilization of enzyme on long period grating fibers for sensitive glucose detection",* Biosensors and Bioelectronics, Vol. 33(1), pp 190-195 (2012).

[34]. B Anjali, S Shivani, T Umesh, G Rani and K S Enakshi, "*Long period grating based sensor for the detection of triacylglycerides"*, Biosensors and Bioelectronics, Vol. 79, pp 693-700 (2012).

[35]. F Chiavaioli, P Biswas, C Trono, S Bandyopadhyay, A Giannetti, S Tombelli, N Basumallick, K Dasgupta and F Baldini, "*Towards sensitive label free immunosensing by means of turn around point long period fiber gratings"*, Biosensors and Bioelectronics, Vol. 60, pp 305-310 (2014).

[36]. F Chiavaioli, C Trono, A Giannetti, M Brenci and F Baldini, "*Characterization of a label free biosensor based on long period grating"*, J. Biophotonics, Vol. 7(5), pp 312–322 (2014)

[37]. X Chen, C Liu, M D Hughes, D A Nagel, A V Hine and L Zhang, "*EDC mediated oligonucleotide immobilization on a long period grating optical biosensor"*, Biosensors and Bioelectronics, Vol. 6 ( 2), pp 173 (2015).

[38]. R Kashyap, "*Fiber Bragg Gratings*", 2nd Edition, Academic Press (2010).

[39]. T Erdogan, "*Cladding-mode resonances in short and long period fiber grating filters*", Journal Optical Society of America, Vol. 14, pp. 1760-1773 (1997).

[40]. T Erdogan, "*Fiber grating spectra*", J. Lightwave Technology, Vol. 15, pp. 1277-1294 (1997).

[41]. C Tsao, "*Optical Fiber WaveguideAanalysis*", Oxford University Press (1992).

[42]. R J Black and L Gagnon, "*Optical Waveguide Modes: Polarization, Coupling and Symmetry*", Mcgrah-Hill (2010).

[43]. V Bhatia, "*Properties and Sensing Applications of Long period Gratings*", Ph.D. Thesis, Virginia Polytechnic Institute and State University, Blacksburg, Virginia (1996).

[44]. A V Brakel, "*Sensing characteristics of an optical fiber long period grating michelson refractometer*", Ph.D. Thesis, Rand Afrikaans University (2004).

[45]. Z J Zhang and W K Shi, "*Eigen value and field equations of three layered uniaxial fibers and their applications to the characteristics of long period fiber gratings with applied axial strain*", Journal of the Optical Society of America A-Optics Image Science and Vision, 22, pp. 2516-2526 (2005).

[46]. P Lalanne, I D Villar, I R Mat´ıas and F J Arregui, "*Optimization of sensitivity in long period fiber gratings with overlay deposition*", Optics Express, Vol. 13, pp. 56- 69 (2005).

[47]. Y Chung and U C Paek. "*Fabrication and performance characteristics of optical fiber gratings for sensing applications*", IEEE Transactions on Optical Fiber Sensors, Vol. 01, pp. 36-42 (2002).

[48]. A A Abramov, A Hale, R S Windeler and T A Strasser, "*Widely tunable long period fiber gratings*", Electronics Letters, Vol. 35, pp. 81- 82 (1999).

[49]. J Keith, S Puckett and G E Pacey, "*Investigation of the fundamental behavior of long period grating sensors*", Talanta, Vol. 61, pp. 417-421, (2003).

[50]. V Bhatia, D K Campbell, D Sherr, T G D Alberto, N A Zabaronick, G A Ten Eyck, K A Murphy and R O Claus, "*Temperature insensitive and strain insensitive long period grating sensors for smart structures*", Optical Engineering, Vol. 36, pp. 1872-1876 (1997).

[51]. V Bhatia, David Campbell, Richard O Claus, and Ashish M. Vengsarkar *"Simultaneous strain and temperature measurement with long period gratings",* Optics Letters , Vol. 22, No. 9 (1997).

[52]. X Shu, L Zhang and I Bennion, "*Sensitivity characteristics of long period fiber gratings*", J. Lightwave Technology, 20, pp. 255-266 (2002).

[53]. M N Ng and K S Chiang, "*Thermal effects on the transmission spectra of long period fiber gratings*", Optics Communication, 208, pp.321-327 (2002).

[54]. X Shu, T Allsop, B Gwandu, L Zhang and I Bennion, "*High-temperature sensitivity of long-period gratings in B-Ge co-doped fiber*", IEEE Photonics Technology Letters, 13, pp. 818-820 (2001)

[55]. X Shu, T Allsop, B Gwandu, L Zhang and I Bennion, "*Room temperature operation of widely tunable loss filter*", Electronics Letters, 37, pp. 216–218 (2001).

[56]. T Mizunami, T Fukuda and A Hayash, "*Fabrication and characterization of long-period grating temperature sensors using Ge–B co-doped photosensitive fiber and single mode fiber*", Measurement Sci. and Tech., Vol. 15, pp.1467-1473 (2004).

[57]. Yokouchi, Y Suzaki, K Nakagawa, M Yamauchi, M Kimura, Y Mizutani , S Kimura and S Ejima, "*Thermal tuning of mechanically induced long period fiber grating*", Applied Optics, Vol. 44, pp. 5024-5028 (2005).

[58]. S Khaliq, S W James and R P Tatam, "*Enhanced sensitivity fiber optic long period grating temperature sensor*", Measu. Sci. and Tech., Vol. 13, pp. 792-795 (2002).

[59]. C G Atherton, A L Steele and J E Hoad, "*Resonance conditions of long period gratings in temperature sensitive polymer ring optical fiber*", IEEE Photonics Technology Letters, Vol. 12, pp. 65-67 (2000).

[60]. K S Chiang, Y Liu, M N Ng and X Dong, "*Analysis of etched long period fiber grating and its response to external refractive index*", Electronics Letters, Vol. 36, pp. 966-967 (2000).

[61]. T H W Johnstone, G Stewart and B Culshaw, "*Surface plasmon polaritons in thin metal films and their role in fiber optic polarizing devices*", IEEE Journal of Lightwave Technology, Vol. 8, pp. 538 – 543 (1990).

[62]. T Hiroshi and K Urabe, "*Characterization of long period grating refractive index sensors and their applications*", Sensors, Vol. 9, pp. 4559-4571 (2009).

[63]. B H Lee, Y Liu, S B Lee, S S Choi and J N Jang, "*Displacements of the resonant peaks of a long period fiber grating induced by a change of ambient refractive index*", Optics Letters, Vol. 22, pp. 1769-1771 (1997).

[64]. A M Rios, D M Hernández and , I T Gomez, "*Highly sensitive cladding etched arc induced long period fiber gratings for refractive index sensing*", Optics Communications, Vol. 283, pp. 958-962 (2010).

[65]. O Duhem, J Fraņois Henninot, M Warenghem and M Douay, "*Demonstration of long period-grating efficient couplings with an external medium of a refractive index higher than that of silica*", Applied Optics, Vol. 37, pp. 7223-7228 (1998).

[66]. R Hou, Z Ghassemlooy, A Hassan, C Lu and K P Dowker, "*Modelling of long period fiber grating response to refractive index higher than that of cladding*", Measurement Science and Technology, Vol. 12, pp. 1709-1713 (2001).

[67]. D B Stegall and T Erdogan, "*Leaky cladding mode propagation in long period fiber grating devices*", IEEE Photonics Technology Letters, Vol. 11, pp. 343-345 (1999).

[68]. B Wang, J Huang, M Li, X Zhou, "*Multifunctional sensing film used for fiber optic cholesterol sensor*", Proc., SPIE, Vol. 7278 (2009).

[69]. G L Flynn, Y Shah, S Prakongpan, K H Kwan, W I Hguchi and A F Hofmann, "*Cholesterol solubility in organic solvents*", J. Pharm. Sci., Vol. 68, pp 1090-1097 (1979).

[70]. U S Raikar, A S Lalasangi, J F Akki, P Raikar, K G Manohar, T Srinivas, N M Badiger, P Radhakrishnan, "*Cd concentration sensor based on fiber grating technology*", Sens. and Act. B: Chemical, Vol. 161, pp. 818-823 (2012).

[71]. M Yunianto, A N Permata, D Eka, D Ariningrum, S Wahyuningsih and A Marzuki, "*Design of a fiber optic biosensor for cholesterol detection in human blood"*, IOP Conf. Series: Materials Science and Engineering, Vol. 176, 012014 (2017).

[72]. M Budiyanto, Suhariningsih and M Yasin, "*Cholesterol detection using optical fiber sensor based on intensity modulation*", Journal of Physics: Conf. Series, 853,012008 (2017).

[73]. D A R Medina, M T Durán and E A Méndeza, "*Cholesterol biosensor based on a plastic optical fiber with sol–gel: structural analysis and sensing properties"*, J. of Modern Optics, Vol. 65, Iss. 3, pp. 348-352 (2018).

[74]. J Huang, Y Liu, P Zhang, Yangjie Li and L Ding, "*A temperature triggered fiber optic biosensor based on hydrogel-magnetic immobilized enzyme complex for sequential determination of cholesterol and glucose"*, J. Biochem. Eng. Vol. 125, pp. 123–128 (2017).

[75]. A K Basu, P Chattopadhyay, U Roychoudhuri and R Chakraborty, "*Development of cholesterol biosensor based on immobilized cholesterol esterase and cholesterol oxidase on oxygen electrode for the determination of total cholesterol in food samples*", J. Bioelectrochemistry Vol. 70, Iss. 2, pp. 375–379 (2007).

[76]. K V Derina, E I Korotkova, E V Dorozhko , O A Voronovaa and D A Vishenkova, "*Voltammetric sensor for total cholesterol determination*", Procedia Chemistry, 10, pp. 513 – 518 ( 2014 ).

[77]. Q Wu, Y Hou, M Zhang, X Hou, L Xu, N Wang, J. Wang and W Huang, "*Amperometric cholesterol biosensor based on zinc oxide film at silver nanowires- graphene oxide modified electrode*", J. Anal. Methods, Vol. 8, pp. 1806- 1812 (2016).

[78]. X Lin, Y Ni and S Kokot, "*Electrochemical cholesterol sensor based on cholesterol oxidase and $MoS_2$-AuNPs modified glassy carbon electrode*", Sens. and Act. B: Chemical, Vol. 233, pp. 100-106 (2016).

Chapter 3

# Fabrication of Chitosan Coated Long Period Grating Sensor

*Abstract*

*This chapter gives a detailed discussion on chitosan coated fiber optic long period grating sensor for cholesterol measurements. The deposition of chitosan coating on the LPG sensor head by the method of dip coating is also discussed. The sensor head is employed for the detection and estimation of total cholesterol dissolved in coconut oil.*

1). ***C Bobby Mathews*** *et al., Optoelectronics Letters; Vol.12 (1), pp. 23-26 (2016).*

2). ***B Mathews C*** *et al., Proc. Photonics 2014: 12th Int. Conf. on Fiber Optics and Photonics, OSA Tech. Digest, OSA, S5A.22 (2014).*

## 3.1 Introduction

Long period gratings have good sensitivities to external perturbations like temperature, strain and SRI. A detailed discussion on the working principle and the sensitivity of LPG to SRI was given in chapter 2. It was also shown that this RI sensitivity of LPG could be utilized to determine the total cholesterol concentration

This section introduces the cholesterol sensing capabilities of chitosan coated long period gratings. Fabrication of the sensor head with chitosan coating is discussed initially. A brief description of the dip coating method used for the fabrication is described here. It is shown that chitosan has an affinity for cholesterol. It is also established that chitosan coating enhances the cholesterol sensitivity of the LPG sensor head.

## 3.2 Coated LPG for Sensing Applications

Several applications of LPGs in the field of sensing were discussed in chapter 2. For enhancing the sensitivity of the LPG in sensing applications, coatings with several materials are applied over the cladding around the LPG.

The deposition of overlay coatings onto optical fiber long period gratings (LPGs) has been in the limelight of researchers since the beginning of this century [1-4]. Rees et al. investigated the performance of LPGs with overlay films deposited by Langmuir-Blodgett technique in 2002 [1]. Electrostatic self-assembly method for the preparation of coatings on gratings was reported in 2005 [2]. In 2005, Cusano and team reported a LPG sensor head prepared by dip coating for chemical sensing [3]. A study on the modified RI response of LPGs when coated was presented by Ishaq et al. in the same year [5]. Optimization of the

sensitivities of LPG with overlay coatings was proposed by Lalanne et al. in 2005 [6]. Further, theoretical explanations for the overlay coated response of LPGs were developed by Villar et al. [7, 8] and Cusano et al. [9]. Influence of the SRI on the performance of the coated LPG sensor head was outlined in detail in the literature [5, 9, 10]. More on the application side, LPGs with coatings were demonstrated for physical parameter sensing like humidity [11-18], pH [19] etc. In the field of chemical sensing, LPG sensor heads with overlay coatings for ethylene glycol [5], copper ions [20], chloroform [21] etc., were also reported earlier. Overlay coatings with polystyrene and syndiotactic polystyrene on LPGs for chemical sensing was also demonstrated in 2005 [22].

LPG coated sensors were also employed in the field of biosensors. Kim et al. demonstrated a species-specific biosensor based on LPG with nanoscale, self-assembled polyelectrolyte layers and the immobilization of immunoglobulin G (IgG) in 2006 [23]. Wang et al. [24] and Helen et al. [25] have demonstrated ionic self-assembled multilayers (ISAMs) adsorbed on LPGs, functioning effectively as biosensors. Pierluigi et al. have reported research results relating to the development of a platform for label-free biosensing based on LPGs with overlay coatings [26-28].

In 2014, Chiavaioli et al. biofunctionalized LPG, to analyze antigen-antibody interaction [29]. His team also demonstrated an LPG based biosensor with sol-gel based titania-silica thin film overlay [30]. Bacteriophage-adhesin was coated over LPG by Brzozowska et al. [31], Tripathi et al. [32, 33] and Mateusz et al. [34], for the detection of bacteria. Deep et al. presented immobilization of enzymes on LPG in 2012, for the detection of glucose [35]. Anjali et al. in 2015 proposed, the detection of triacylglycerides using an LPG with immobilized enzymes [36]. DNA detection was reported using functionalised LPGs coated with peptide

nucleic acid [37]. Detection of DNA damaging agents was accomplished by Pacey and team using overlay coated LPG [38]. Several other applications of overlay coated LPGs in the area of biosensing were also published earlier [39, 40]. In the present studies, a cholesterol sensor exploiting the sensitivity of chitosan coated LPGs to the concentration of the sample solution under test is presented.

## 3.3 Cholesterol Sensor

An overlay coating of chitosan was made over the bare LPG in order to enhance the sensitivity of cholesterol sensing. As discussed in chapter 1, Chitosan is a polysaccharide, which can selectively bind with cholesterol [41]. The basic structure of chitosan coated LPG sensor head is shown in Fig.3.1. The three reactive functional groups, an amino/acetamido group as well as a primary and a secondary hydroxyl group present in chitosan, provide the necessary sites for the binding of cholesterol. The combined effects of electrostatic attraction, embedding, adsorption and entrapment are the probable mechanisms for the cholesterol binding effects of chitosan [42]. This binding of cholesterol in turn enhances the sensitivity of LPG to the SRI and this principle is used in the realization of the cholesterol sensor.

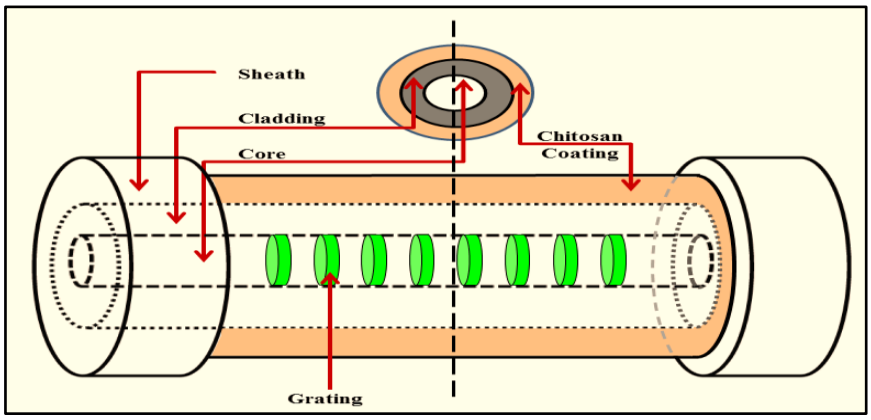


***Figure 3.1:*** *Structure of chitosan coated LPG sensor head*

As the cholesterol concentration level is increased, the amount of cholesterol getting attached to the chitosan layer increases. This increased binding of cholesterol on the surface of the LPG, enhances the effective RI of the cladding. This change in the effective index is manifested as shifts in the resonant wavelength and as changes in the depth (amplitude) of the loss bands in the LPG transmission spectrum. Cholesterol levels can be detected and measured by analyzing these spectral or amplitude changes.

### 3.3.1 LPG Fabrication

LPG with a grating period of 435 μm was fabricated at CGCRI, Kolkata, with KrF - Excimer laser source (248 nm), through point-by-point writing method on standard telecommunication SMF-28 (SMF-28e, Corning) fiber. The fiber used in this experiment had a core diameter of 8.2 micron, cladding diameter of 125 micron and a numerical aperture of 0.14. The index of refraction were 1.461 and 1.456, for the core and the cladding respectively.

The photosensitivity of the fiber was very low and was enhanced by the process of Hydrogen loading at a temperature of 100 $^0$C and 1500 psi pressure for 24 hours, prior to the fabrication of LPG. During the grating fabrication using UV exposure, photochemical reaction takes place, leading to the release of some of the Hydrogen molecules. Some Hydrogen molecules are retained inside the fiber after these photochemical reactions. This residual molecular Hydrogen was removed by the method of annealing, at a temperature of 200 $^0$C for 7 hours using a high temperature oven.

### 3.3.2 Sensor Head Fabrication

The sensor head was prepared by coating a thin layer of chitosan over the cladding of the fabricated LPG. In order to provide a coating on the LPG, 0.25gm of high molecular weight chitosan powder with 98% degree of deacetylisation, purchased from Sigma Aldrich, was stirred well with one

molar acetic acid with RI of 1.346, at room temperature for 5 hours to get a clear solution. Dip coating technique was used to coat the LPG with chitosan. A schematic of the dip coating setup is given in Fig. 3.2. The coating setup consists of a stepper motor driven moving arm mounted on a stand and an electronic control unit with provisions to adjust the speed and direction of the moving arm. The optical fiber with the LPG section was cleaned using distilled water and isopropyl alcohol several times and was fixed on the moving arm of the coating unit as shown.

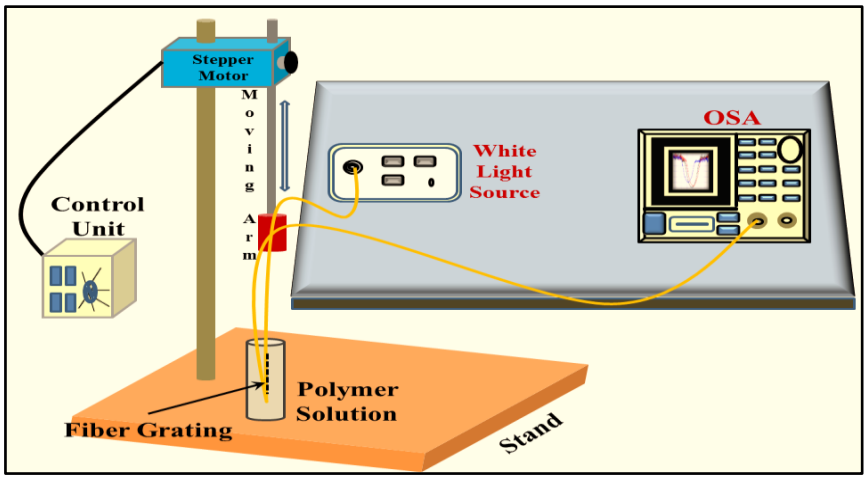


***Figure 3.2:*** *Dip coating setup*

The prepared chitosan solution for coating was taken in a test tube, mounted on the stand under the fiber with grating. The fiber with LPG was dipped and pulled out of the chitosan solution at an optimized uniform speed of 400 µm/s. The process of dip coating was optimized by varying the concentration of the chitosan solution and the speed of coating. The coated fiber was dried in air at room temperature to avoid cracks.

Scanning electron microscope (SEM) images were taken to confirm the presence of the chitosan coating and to determine the thickness of the layer coated. Fig. 3.3 shows the SEM images of the prepared chitosan coated

LPG sensor haed. Fig 3.3 (a) shows a portion of the cross-sectional view of the coated fiber tip, clearly showing a layer of chitosan over the fiber. The measured average thickness of the chitosan layer was found to be 1.461 µm. The image of the surface of the coating is presented in Fig. 3.3 (b). The image depicts the uniformity of the coating on the surface of the fiber.

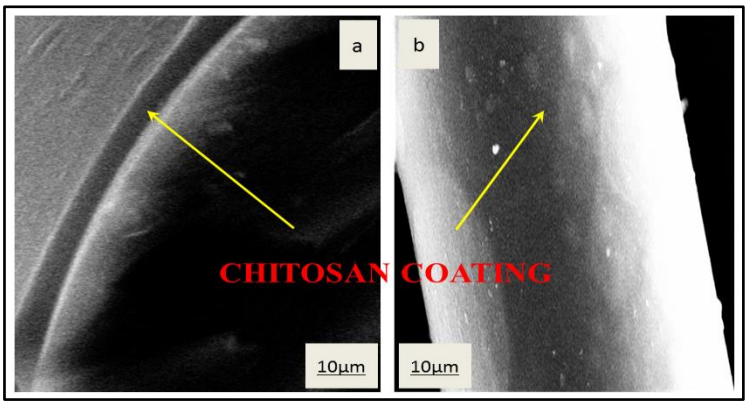


***Figure 3.3:*** *SEM images of the chitosan coated sensor head.*
*a). Side view of the fiber tip showing chitosan coated over the cladding.*
*b). Surface image of the fiber with a uniform layer of chitosan.*

When the sensor head was coated with more than one layer, the surface developed cracks and lost uniformity after the drying process. Hence, the number of chitosan layers coated on the LPG was restricted to one.

The prepared chitosan solution, which had RI of 1.394, was coated over a microscopic glass slide, by the method of dip coating described earlier. The speed of coating was kept the same as earlier and was dried in air at room temperature. The RI of the chitosan layer coated on the glass slide was analyzed by the method of Brewster angle measurement, using a 632 nm He-Ne laser and a silicon detector. The average of the measured RI of the chitosan film was found to be 1.446, which is very close to the reported value of 1.45 [43].

### 3.3.3 Experimental Setup

The experimental setup given in Fig. 2.5 was used for the investigations, after replacing the bare LPG with the chitosan coated LPG. The transmission spectrum of the LPG was studied with an optical spectrum analyzer (OSA) (Yokogawa - AQ 6319) and a white-light source (Yokogawa - AQ 4305) was used as the signal source. The procedure followed in setting up this experimental platform is same as that described in section 2.5.1.2 of chapter 2 of this thesis.

### 3.3.4 Materials and Methods

As explained in previous chapters, the cholesterol level in the blood of a normal human being is in the range of 1400 ppm to 2000 ppm [44]. Hence, the measurements were restricted to a maximum cholesterol concentration of 5000 ppm, which covers the normal levels of cholesterol in human blood. The procedures followed for the preparation of cholesterol samples with coconut oil as the solvent and the conduct of experiments are as described in section 2.5.1.3 of the previous chapter.

### 3.3.5 Results and Discussion

An LPG with a grating period of 435 μm was used in this experiment. The transmission spectrum of the bare LPG (without any coating) in air is given in Fig. 3.4. The transmission spectrum had resonant peaks corresponding to the $LP_{0m}$ modes, at 1419.31 nm ($LP_{03}$) 1473.12 nm ($LP_{04}$) and 1568.93 nm ($LP_{05}$).

Out of these modes the highest order mode, i.e., the $LP_{05}$ mode at 1568.93 nm, showed maximum sensitivity as expected. Hence, further investigations were centered around this resonant wavelength of $LP_{05}$ mode.

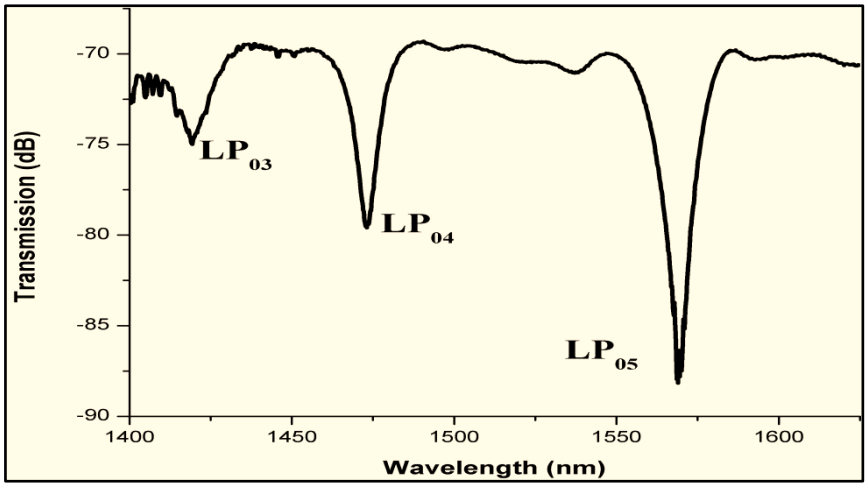


***Figure 3.4:*** *Transmission spectrum of bare LPG in air.*

The transmission spectrum of the LPG after coating a layer of chitosan is given in Fig 3.5. It was found that the $LP_{05}$ mode at 1568.93 nm of the bare LPG got blue shifted to 1565.37 nm with a reduction in the transmitted intensity, after the coating was given. This blue shift was expected, as the effective RI of the cladding was enhanced by the higher refractive index of the chitosan layer (1.446).

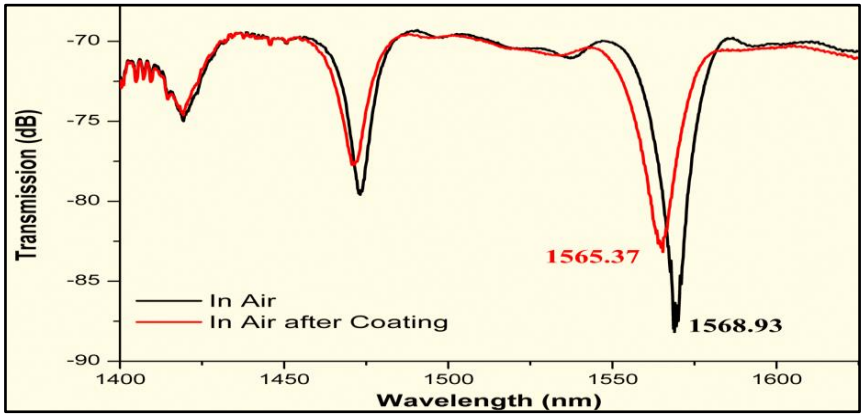


***Figure 3.5:*** *Transmission spectrum of LPG in air with and without coating*

Coconut oil purchased from the market for preparing the cholesterol solution was found to have a RI value of 1.448, which is much closer to the

LPG cladding RI value of 1.456. Test samples were prepared as described earlier in chapter 2. The refractive indices of the prepared cholesterol sample solutions were found to vary from 1.448 to 1.455. The experimental procedures were also the same as described in chapter 2. The transmission spectra corresponding to $LP_{05}$ mode of chitosan coated LPG for various concentrations of cholesterol dissolved in coconut oil is given in Fig. 3.6.

As the sample solution without any cholesterol (pure solvent) was introduced, a blue shift was observed for the resonant peak along with a change in the amplitude of the peak. The $LP_{05}$ mode at 1565.37 nm of the coated sensor head shifted to 1560.87 nm. This shift in wavelength is as expected and is attributed to the increase in the RI of the external environment. (SRI changed from 1 (air) to 1.448 (coconut oil)). It is clear from the spectra that, as the concentration of the cholesterol was varied from 0 ppm (pure coconut oil) to 5000 ppm, the $LP_{05}$ exhibited a blue shift in the wavelength. The resonant peak of $LP_{05}$ mode shifted from 1560.87 nm to 1535.75 nm, to give a total blue shift of approximately 25.12 nm (± 0.01 nm), when the cholesterol level in the surrounding medium was increased up to 5000ppm.

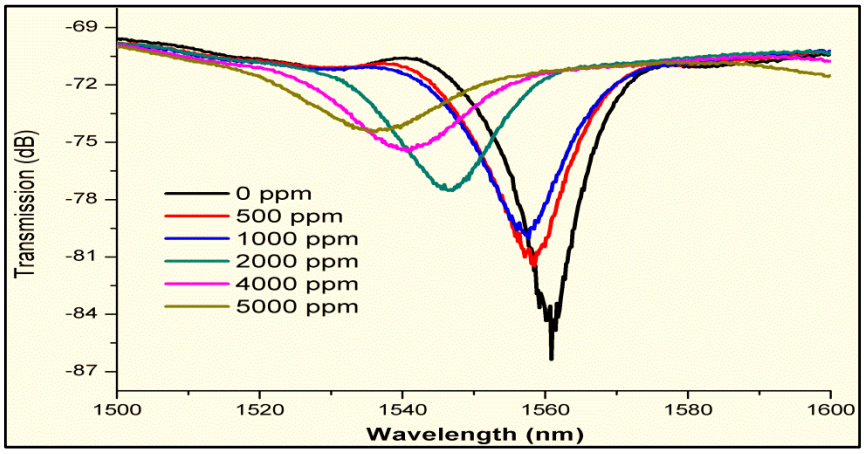


***Figure 3.6:*** *Transmission spectra of chitosan coated LPG sensor head for different concentrations of cholesterol dissolved in coconut oil.*

This spectral shift of 25.12 nm, noticed for a refractive index range of 1.448 to 1.455 of the sample solutions, corresponds to an average resolution $2.78\times10^{-4}$ $nm^{-1}$.

The transmitted intensity and the wavelength of the $LP_{05}$ resonant peak of the chitosan coated LPG sensor head, for various concentrations of cholesterol in the test sample, are tabulated in Table 3.1.

| **Cholesterol Concentration (ppm)** | **Refractive Index of Sample** | **$LP_{05}$ - Peak Wvelength (nm)** | **$LP_{05}$ Transmitted Intensity (-dB)** |
|---|---|---|---|
| **0** | 1.448 | 1560.87 | 86.38 |
| **500** | 1.450 | 1558.44 | 81.48 |
| **1000** | 1.452 | 1557.69 | 80.03 |
| **2000** | 1.453 | 1547.49 | 77.54 |
| **4000** | 1.454 | 1540.63 | 75.48 |
| **5000** | 1.455 | 1535.75 | 74.61 |

***Table 3.1:*** *Response of the chitosan coated LPG sensor head for various concentrations of cholesterol*

The sensitivity of the LPG, when used as a sensor for various concentrations of cholesterol is shown in Fig. 3.7. The overall sensitivity in the measurement range of the sensor was around 5 pm/ppm of cholesterol.

The sensitivity curve clearly depicts a linear response above 1000 ppm of cholesterol dissolved in coconut oil. The normal cholesterol levels in the blood of human beings i.e. 1400 ppm to 2000 ppm falls well inside this linear range. This linearity is highly desirable for a commercial sensor for accurate measurements.

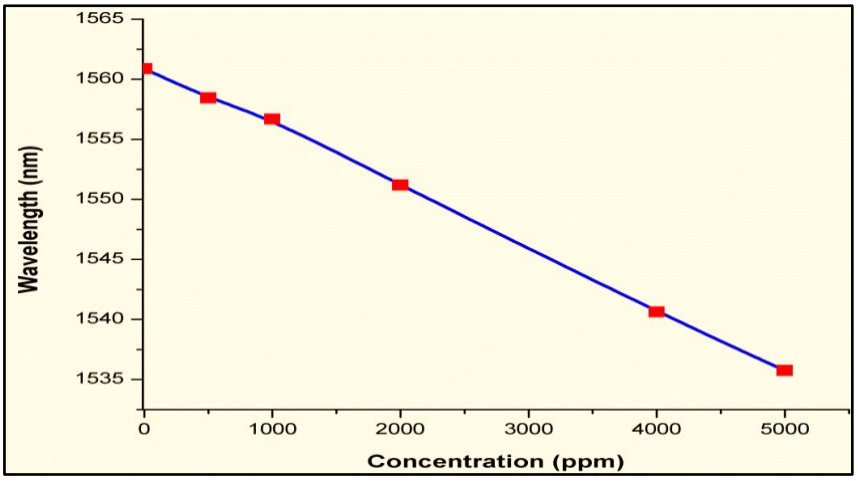


***Figure 3.7:*** *Resonant wavelength ($LP_{05}$) peak positions as a function of different concentrations of cholesterol.*

As given in Table 3.1, along with the wavelength shift, a reduction in the peak intensity of the resonance band was also observed with increasing cholesterol levels. The transmittance at the resonant wavelength ($LP_{05}$) with respect to the different levels of cholesterol dissolved in coconut oil in the measured range is given in Fig. 3.8.

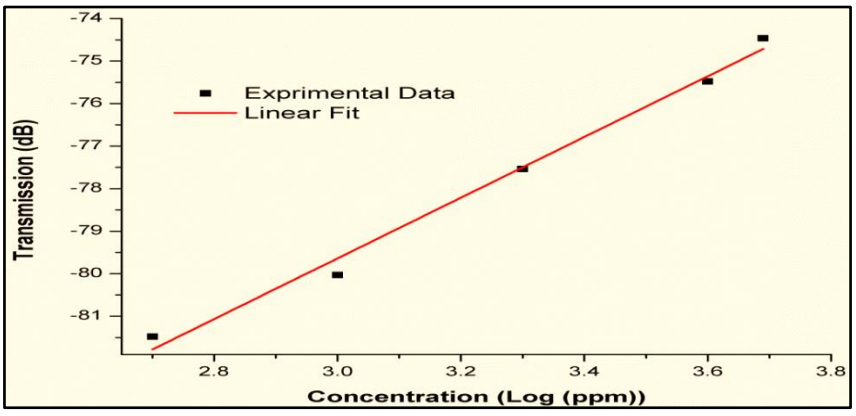


***Figure 3.8:*** *Transmittance of the resonant wavelength (LP05) peak positions as a function of different concentrations of cholesterol*

The amplitude of the resonant wavelength peak shifted from -86.38 dB to -74.61 dB as the concentration of cholesterol was varied from 0 ppm to 5000 ppm. A linear response of the transmittance was observed in the measured range of cholesterol levels. This intensity modulation can also be utilized along with the wavelength coded information for confirmatory results in a commercial sensor.

The marginal error of ± 0.01 nm in the wavelength measurements, obtained for repeated experiments over a time of three weeks confirms the repeatability and reusability of the sensor head.

### 3.3.6 Comparison with Uncoated LPG Sensor

A comparison of the performance of the LPG senor heads with and without chitosan coating for the detection of cholesterol is given in Table. 3.2. Form the values of the sensitivity, it is clear that the sensitivity of the chitosan coated sensor head has enhanced by 2.5 times approximately. This enhancement in the sensitivity of the chitosan coated sensor head compared to the uncoated LPG sensor is attributed to the alterations in the effective RI of the cladding of the LPG.

| **Parameter** | **Sensor Head** | |
|---|---|---|
| | **Bare LPG** | **Chitosan Coated LPG** |
| **Wavelength Shift (nm)** | 10.5 | 25.12 |
| **Amplitude Shift (dB)** | -79.54 to -74.61 | -86.38 to -74.61 |
| **Sensitivity (pm/ppm)** | 2 | 5 |

***Table 3.2:*** *Performance of LPG sensor heads with and without coating*

These alterations were introduced by the attachment of cholesterol to the coated chitosan polymer layer. This also clearly establishes the affinity of chitosan polymer coating for cholesterol.

The LPG sensor head coated with an enzyme, namely lipase, for the detection of triacylglycerides, displayed optimum response of one minute at a temperature of 37 °C and pH value of 7.4 [45]. Even though the sensor response was temperature and pH dependent, it had high sensitivity of 0.5 nm/mM. A generalized study on the refractive index sensitivity of LPGs in integration with colloidal gold nanoparticles reported an enhanced RI sensitivity of 759 nm/RIU [46]. Another LPG coated with a transparent composition of polycarbonate/cryptophane A was demonstrated as a methane concentration sensor with a maximum RI sensitivity of 3560 nm/RIU [47].

The reported intensity modulated cholesterol sensor using a bundle of optical fibers, requires displacement of the fiber bundle during the experimentation, and can lead to misalignment and errors associated with it [48]. Other characteristics of the senor were very low sensitivity of cholesterol detection (0.4 μV/ppm) and a limited range of 0 ppm to 300 ppm. A linear detection range of 180 mg/dL to 200 mg/dL of cholesterol was exhibited by the sol gel coated photonic crystal fiber employing, intensity modulated sensor head [49]. In spite of the pH dependent response, the voltametric non enzymatic cholesterol sensor proposed by S Alexander et al. had a wide linear measurement range of 0.01M to 0.1nM cholesterol [50].

The non enzymatic chitosan coated LPG sensor head described in this chapter had an instantaneous response and a sensitivity of 5nm/ppm (approximately 3590 nm/RIU); which is better than that reported in [46-48]. The response was repeatable and was also immune to pH in contrast with [45, 50]. The linear range of detection was found to be within 500 ppm to 5000

ppm of cholesterol which is much higher than that reported in [48, 49] but lower than that in [50].

### 3.3.7 Conclusions

The results presented illustrate the application of fiber optic chitosan coated LPG based sensor system for the detection and measurement of cholesterol concentrations. Both the wavelength and intensity modulation characteristics of the sensor head can be utilized in designing cholesterol sensors. The simple sensor presented provides a real time response with high sensitivity and requires only a small volume of the sample for analysis. The proposed technique can be suitably modified for field applications in clinical laboratories for the estimation cholesterol in blood of human beings. The results are instantaneous and repeatable, and cover a wide range of cholesterol levels. In addition, the linearity in the performance makes the sensor head design attractive for commercial applications like chemical and biomedical sensing, drug development, food processing etc.

## 3.4 Summary

This chapter discussed the fabrication of LPG sensor head with overlay coatings. The chapter also outlined the method of dip coating for the development of a polymer coated LPG sensor.

A brief survey on the sensing applications of LPG with overlay coatings of polymers with an emphasis on biosensing is presented in the introductory part of this chapter. Chitosan, which was identified as a polymer with an affinity to cholesterol was employed as an overlay coating around fiber optic LPG to develop a sensor head for cholesterol sensing application. It was established that, an overlay coating of chitosan around the optical fiber with LPGs could be developed by dip coating. With the solution of chitosan used in these experiments, it was found that a coating

layer of thickness 1.461 μm could be fabricated over an SMF 28 optical fiber at a coating speed of 400 μm/s. In our investigations, it was also found that, nonuniformities along with cracks were developed on the surface of the polymer coating around the LPG, when more than one layer was coated.

Chitosan coated LPG sensor head exhibited a sensitivity of 5 pm/ppm, for the test samples prepared by dissolving cholesterol in coconut oil. It was established that coating chitosan around LPG enhances the cholesterol sensitivity of the sensor head approximately by 2.5 times. It was also shown that, the wavelength modulation as well as the intensity modulation of sensor output could be employed in realizing a RI sensor using chitosan coated LPGs.

## References

[1]. Rees N D, James S W, Tatam R P, Ashwell G J "*Optical fiber long period gratings with Langmuir–Blodgett thin film overlays*", Opt. Lett., Vol. 27 (9), pp 686-699 (2002).

[2]. I Del Villar, M Achaerandio, I R Matias and F J Arregui "*Deposition of overlays by electrostatic selfassembly in long period fiber gratings*", Opt. Lett., Vol. 30, pp 720-722, (2005).

[3]. A Cusano, P Pilla, L Contessa, A Iadicicco, S Campopiano, A Cutolo "*High-sensitivity optical chemo sensor based on coated long period gratings for sub-ppm chemical detection in water*", Appl. Phys. Lett., Vol. 87, 234105 (2005).

[4]. S W James and R P Tatam, "*Fiber Optic Sensors with Nano-Structured Coatings*", J. Opt. A: Pure and Applied Optics, Vol. 8, S340, (2006).

[5]. I M Ishaq, A Quintela, S W James, G J Ashwell, L Higuera and R P Tatam, "*Modification of the refractive index response of long period gratings using thin film overlays*", Sens. Actuators B, Vol. 107, pp 738-741 (2005).

[6]. P Lalanne, I D Villar, I R Mat´ıas and F J Arregui. *"Optimization of sensitivity in long period fiber gratings with overlay deposition"*, Optics Express, Vol. 13, pp 56-69 (2005).

[7]. I Del Villar, I R Matias, F J Arregui and M Achaerandio *"Nanodeposition of materials with complex refractive index in long period fiber gratings"*, J. Lightwave Technol. 23, pp 4192-4199, (2005).

[8]. I Del Villar, I R Matias and F J Arregui, *"Influence on cladding mode distribution of overlay deposition on long period fiber gratings"*, OSA A, Vol. 23, pp 651-658, (2006).

[9]. A Cusano, A Iadicicco P Pilla, L Contessa, S Campopiano, A Cutolo and M Giordano, *"Cladding mode reorganization in high refractive index coated long period gratings: effects on the refractive index sensitivity"*, Opt. Lett Vol. 30, pp 2536-2538, (2005).

[10]. E Simõesb, I Abea, J Oliveirab, O Frazãoc, P Caldasc and J L Pintoa, *"Characterization of optical fiber long period grating refractometer with nanocoating*", Sensors and Actuators B, Vol. 153, pp 335–339 (2011).

[11]. K M Tan, C C Chan, L Mohanty and C Meng Tay, *"High relative humidity measurements using gelatin coated long period grating sensors*", Sens. Actuators B, Vol. 110, pp 335-341 (2005).

[12]. M Konstantaki, S Pissadakis, S Pispas, N Madamopoulos and N A Vainos *"Optical fiber long period grating humidity sensor with polyethylene oxide/cobalt chloride coating*", Appl. Opt., Vol. 45, pp 4567-4571 (2006).

[13]. J M Corres, I Villar, I R. Matias and F J. Arregui, *"Enhanced sensitivity in humidity sensors based on long period fiber gratings*", Proc. IEEE Sensors, EXCO, (2006).

[14]. K J Lee, D Wawro, P S Priambodo and R Magnusson, *"Agarose-gel based guided-mode resonance humidity sensor*", IEEE Sens. 7, pp 409–414 (2007).

[15]. L Wang, M Zhang, D Tu, X Mao and Y Liao, *"A relative humidity sensor using a hydrogel coated long period grating*", Meas. Sci. Technol. 18, pp 3131–3134 (2007).

[16]. J M Corres, I Villar, I R Matias and F J Arregui, *"Two layer nanocoatings in long period fiber gratings for improved sensitivity of humidity sensors*", IEEE Trans. Nanotechnology, Vol. 7, pp 394-400 (2008).

[17]. D Viegas, J Goicoechea, J M Corres, J L Santos, L A Ferreira, F M Araújo and I R Matias, *"A fiber optic humidity sensor based on a long period fiber grating coated with a thin film of SiO2 nanospheres*", Meas. Sci. Tech., Vol. 20, 034002 (2009).

[18]. Y Miao, K Zhang, Y Yuam, B Liu, H Zhang, Y Liu and J Yao, *"Agarose gel coated LPG based on two sensing mechanisms for relative humidity measurement*", Applied Optics, Vol. 52, No. 1 (2013).

[19]. J M Corres, I R Matias, I del Villar I and F J Arregui, *"Design of pH sensors in long period fiber gratings using polymeric nanocoatings*", IEEE Sens., Vol. 7, pp 455-463, (2007).

[20]. J Keith, L C Hess, W U Spendel, J A Cox and G E Pacey, *"The investigation of the behavior of a long period grating sensor with a copper sensitive coating fabricated by layer-by-layer electrostatic adsorption*", Talanta, Vol. 70, pp 818-822 ( 2006).

[21]. A Cusano, A Iadicicco, P Pilla, L Contessa, S Campopiano, A Cutolo, M Giordano and G Guerra, *"Coated long period fiber gratings as high-sensitivity opto-chemical sensors*", Lightwave Technol. Vol. 24, pp 1776-1786 (2006).

[22]. P Pilla, A Iadicicco, L Contessa, S Campopiano, A Cutolo, M Giordano, G Guerra and A Cusano, *"Optical chemo sensor based on long period gratings coated with δ form syndiotactic polystyrene"*, IEEE Photonics Technology Letters, Vol. 17, NO. 8 (2005).

[23]. D W Kim, Y Zhang, K L Cooper and A Wang, *"Fiber optic interferometric immuno sensor using long period grating"*, Electron. Lett., Vol. 42 (6), pp. 3245-325 (2006).

[24]. Z Wang, J R Heflin, K Van Cott , R H Stolen, S Ramachandran and S Ghalmi, *"Biosensors employing ionic self-assembled multilayers adsorbed on long period fiber grating"*, Sens. Actuators B Chem., Vol. 139 (2), pp 618-623 (2009).

[25]. H Shibru, Y Zhang and K L. Cooper *"Optimization of layer-by-layer electrostatic self-assembly processing parameters for optical biosensing"*, Optical Engineering, Vol. 45 (2) pp. 024401 (1-6) (2006).

[26]. P Pilla, C Trono, F Baldini, F Chiavaioli, M Giordano, and A Cusano, *"Giant sensitivity of long period gratings in transition mode near the dispersion turning point: an integrated design approach"*, Opt. Lett., Vol. 37 (19), pp. 4152-4154 (2012).

[27]. P Pilla, V Malachovská, A Borriello, A Buosciolo, M Giordano, L Ambrosio, A Cutolo and A Cusano, *"Transition mode long period grating biosensor with functional multilayer coatings"*, Opt. Express, Vol. 19 (2) (2011).

[28]. P Pilla, L Contessa, A Iadicicco, S Campopiano, A Cutolo, M Giordano and A Cusano *"Long period grating coated with high refractive index layer"*, Proc. IEEE/LEOS (2005).

[29]. F Chiavaioli, C Trono, A Giannetti, M Brenci and F Baldini, *"Characterization of a label free biosensor based on long period grating"*, Biophotonics Vol. 7 (5), pp 312-322 (2014)

[30]. F Chiavaioli, P Biswas, C Trono, S Jana, S Bandyopadhyay, N Basumallick, A Giannetti, S Tombelli, S Bera, A Mallick and F Baldini, *"Solgel based titania – silica thin film overlay for long period fiber grating based biosensors"*, Anal Chem, Vol. 87 (24), pp 12024-12031(2015).

[31]. E Brzozowska, M Smietana, M Koba, S Gorska, K Pawlik, A Gamian and W J Bock, *"Recognition of bacterial lipopolysaccharide using bacteriophage-adhesin coated long period gratings"*, Biosensors and Bioelectronics, Vol. 67, pp 93-99 (2015).

[32]. S M Tripathi, W J Boc, P Mikulic, R Chinnappan, N G Andy, M Tolba and M Zourob, "*Long period grating based biosensor for the detection of*

*Escheichia coli bacteria"* , J. Biosensors and Bioelectronics, Vol. 35 (1), pp 308-312 (2012).

[33]. S M Tripathi, *Long period grating based bio sensor for rapid and accurate detection of E.coli bacteria in water*, Proc. Photonics 2016, OSA (2016).

[34]. M Smietana, W J Bock, P Mikulic, N G Andy, R Chinnappan and Mohammed Zourob, "*Detection of bacteria using bacteriophages as recognition elements immobilized on long period fiber gratings"*, Opt. Exp., Vol. 19, No. 9, pp 7971-7978 (2011).

[35]. A Deep, U Tiwari, P Kumar, V Mishra, S C Jain, N Singh, P Kapur and L M Bharadwaj, "*Immobilization of enzyme on long period grating fibers for sensitive glucose detection",* Biosensors and Bioelectronics, Vol. 33(1), pp 190-195 (2012).

[36]. B Anjali, S Shivani, T Umesh, G Rani and K S Enakshi, "*Long period grating based sensor for the detection of triacylglycerides"*, Biosensors and Bioelectronics, Vol. 79, pp 693-700 (2012).

[37]. M Sozzi, A Cucinotta, R Corradini, R Marchelli, M Konstantaki, S Pissadakis and S.Selleri, *"Modification of a long period grating based fiber optic for DNA biosensing"*, Proc. SPIE, Vol. 7894, 78940J-2 (2011)

[38]. G E Pacey, S D Puckett , L Cheng, S K Shahidi and J A Cox, *"Detection of DNA damaging agents using layer-by-layer assembly*", Anal. Chem. ACTA, Vol. 533, pp 135-139 (2005).

[39]. F Chiavaioli, P Biswas, C Trono, S Bandyopadhyay, A Giannetti, S Tombelli, N Basumallick, K Dasgupta and F Baldini, "*Towards sensitive label free immunosensing by means of turn around point long period fiber gratings",* Biosensors and Bioelectronics, Vol. 60, pp 305-310 (2014).

[40]. X Chen, C Liu, M D Hughes, D A Nagel, A V Hine and L Zhang, *"EDC mediated oligonucleotide immobilization on a long period grating optical biosensor"*, Biosensors and Bioelectronics, Vol. 6 ( 2), pp 173- (2015).

[41]. Y I Cho, H K No and S P Meyers, *"Physicochemical characteristics and functional properties of various commercial chitin and chitosan products*", Agric. Food Chem., Vol. 46, pp.3839-3843 (1998).

[42]. W Xia, P Liu, J Zhang and J Chen, "*Biological activities of chitosan and chitooligosaccharides*", Food Hydrocolloids, Vol. 25 (2), pp 170-179 (2010).

[43]. J Mathew, K J Thomas, V P N Nampoori and P Radhakrishnan, "*A comparative study of fiber optic humidity sensors based on chitosan and agarose*", Sensors & Transducers, Vol.84 (10), pp. 1633-1640 ( 2007).

[44]. B Wang, J Huang, M Li and X Zhou, "*Multifunctional sensing film used for fiber optic cholesterol sensor*", Proc. of the SPIE, Vol. 7278 (2009).

[45]. B Anjali, S Shivani, T Umesh, G Rani and K S Enakshi, "*Long period grating based sensor for the detection of triacylglycerides*", Biosensors and Bioelectronics, Vol. 79, pp 693-700 (2015).

[46]. F Tian, X Li, J Kanka and H Du , "*Fiber optic index sensor enhanced by gold nanoparticle assembly on long period grating*", Optik – Int. J. for Light and Electron Opt., Vol. 132, , pp. 445-449 (2017).

[47]. J Yang, L Zhou, J Huang, C Tao, X Li and W Chen, "*Sensitivity enhancing of transition mode long-period fiber grating as methane sensor using high refractive index polycarbonate/cryptophane A overlay deposition*", Sens. and Act. B: Chemical, Vol. 207, Part A, pp. 477-480 (2015).

[48]. M Budiyanto, Suhariningsih and M Yasin, "*Cholesterol detection using optical fiber sensor based on intensity modulation*", Journal of Physics: Conf. Series, 853,012008 (2017).

[49]. D A R Medina, E A Méndeza and M T Durán, "*Thin film of sol-gel deposited in photonic crystal fiber for cholesterol detection*", Proc. SPIE Vol. 9434, pp. 943417-1-6 (2015).

[50]. S Alexander, P Baraneedharan, S Balasubrahmanyan and S Ramaprabhu, "*Modified graphene based molecular imprinted polymer for electrochemical nonenzymatic cholesterol biosensor*", European Polymer J. Volume 86, pp. 106-116 (2017).

Chapter 4

# Development of Etched Fiber Bragg Grating Sensor

*Abstract*

*This chapter gives a detailed discussion on the principle of operation of Fiber Bragg gratings. It also deals with the sensitivities of FBGs to external perturbations like, temperature and strain. It includes a review of the sensing applications of FBGs with emphasis on refractive index sensors for various applications. A study on the etching of FBGs, as a method to make it sensitive to surrounding refractive index (SRI), is given. This chapter also provides the development of cholesterol sensors working on the basis of refractive index sensitivity of etched FBG.*

**C Bobby Mathews** et al. *"Etched fiber Bragg grating sensor for the measurement of total cholesterol", (Communicated).*

## 4.1 Introduction

Hill et al. discovered photosensitivity in optical fibers in 1978 [1]. His team created a spatially periodic refractive index perturbation in the fiber core and demonstrated the first application of optical fiber Bragg grating as a reflection filter. Since then, numerous applications of FBGs have been reported in literature. This section introduces the basic theory behind the working of FBGs. The sensitivities of FBGs to external perturbations are also covered. In order to make FBG sensitive to external RI variations, the section of the fiber containing the grating was chemically etched to reduce the cladding diameter. The process of FBG etching and its application for RI sensing are discussed in this chapter.

### 4.2. FBG: Basic Principle of Operation

A Bragg grating is made up of alternate low and high RI regions in the core of the optical fiber. Several factors like the wavelength used for writing the grating, the magnitude of the RI change induced, the pitch or period of the grating written on the optical fiber, the RI pattern formed, length of the grating etc., determine the response characteristics of FBGs. The theory and working principle of FBGs with grating planes perpendicular to the axis of the fiber and uniform periodicity is discussed in this section.

The RI modulation induced in the fiber core due to the exposure to UV radiations during the process of FBG fabrication can be expressed as: [2, 3].

$$n_{eff}(x, y, z) = n_o(x, y, z) + \Delta n(x, y, z) \cos\left(\frac{2\pi z}{\Lambda}\right) \ldots\ldots\ldots\ldots\ldots\ldots \quad (4.1)$$

where, $n_0$ is the average RI of the fiber core, $\Delta n$ is the amplitude of the induced refractive index perturbation, z is the distance along the fiber's longitudinal axis and $\Lambda$ is the grating period. Considering only one direction,

i.e. the direction of propagation of light inside the fiber, the above equation can be simplified as [3]:

$$n_{eff}(z) = n_o + \Delta n \cos\left(\frac{2\pi z}{\Lambda}\right) \quad \text{..... (4.2)}$$

As the light launched into the optical fiber travels through the induced RI perturbations (FBG), a small portion of the incident light is reflected backwards from the grating planes. Out of these reflections, the wavelength satisfying the Bragg condition adds up to form a strong reflected signal, as illustrated in Fig.4.1. This wavelength, reflected from the FBG, is termed as the Bragg wavelength ($\lambda_B$) [2-8].

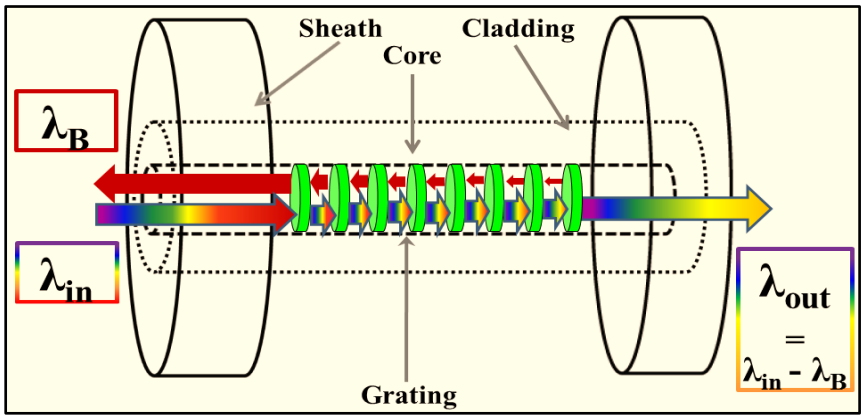


***Figure 4.1:*** *Illustration - Light coupling in fiber Bragg grating.*

Typical transmission and reflection spectra of an FBG are given in Fig.4.2.

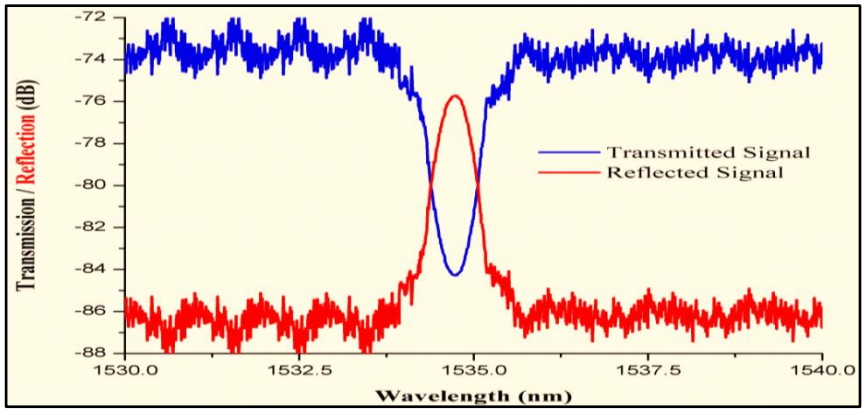


***Figure 4.2:*** *Typical spectra of fiber Bragg grating.*

### 4.2.1 FBG: Reflected Bragg Wavelength

FBGs work by coupling the forward propagating core modes to the back propagating core modes whereas in LPGs, the coupling is between the forward propagating core modes and the co-propagating cladding modes. In an optical fiber grating, the phase matching condition is given by [4 - 8]:

$$\beta_1 - \beta_2 = \Delta\beta = \frac{2\pi}{\Lambda} \quad \text{(4.3)}$$

where, $\beta_1$and $\beta_2$ denotes the propagation constants of the coupled modes and $\Lambda$ is the grating pitch. For an FBG, these propagation constants are of same magnitude, as the forward and backward propagating modes are travelling through the same medium, but are given opposite signs accounting the direction of their travel.

Hence, $\beta_1 = -\beta_2 = \beta$ (4.4)

This leads the phase matching condition to:

$$\beta - (-\beta) = \Delta\beta = \frac{2\pi}{\Lambda} \quad \text{(4.5)}$$

$$2\beta = \frac{2\pi}{\Lambda} \quad \text{(4.6)}$$

In FBG, the propagation constant ($\beta$) of the reflected or the back propagating core mode is given by:

$$\beta = \left(\frac{2\pi n_{eff}}{\lambda_B}\right) \quad \text{(4.7)}$$

Substituting the value of $\beta$ in equation 4.6 and rearranging yields the expression for the reflected Bragg wavelength as:

$$\lambda_B = 2\, n_{eff}\, \Lambda \quad \text{(4.8)}$$

where, $\lambda_B$ represents the Bragg wavelength and $n_{eff}$ is effective RI of the core and $\Lambda$ is the grating period. The rest of the reflected wavelengths, which do not satisfy the above condition, are cancelled out eventually as these reflected wavelengths from each subsequent grating plane become out of phase gradually. All the other wavelengths except the $\lambda_B$, travel in the forward

direction through the grating and are received at the output end of the optical fiber, without much attenuation.

### 4.2.2 FBG: Mode Coupling

The working of FBG can be explained using the coupled mode theory proposed in 1981 by Lam and Garside [8]. Coupled mode theory was extensively used to explain the wave propagation in FBGs [2-8]. As mentioned earlier, the reflectivity of FBGs is an important parameter, which determines its quality. By using coupled mode theory, the reflectivity of a uniform FBG or the fraction of the reflected power from a uniform FBG can be expressed as:

$$R(L,\lambda) = \frac{\Omega^2 \sinh^2(sL)}{\Delta k^2 \sinh^2(sL) + s^2 \cosh^2(sL)} \quad \text{(4.9)}$$

where, $R(L,\lambda)$ is a function of the length of the grating L and wavelength $\lambda$, with values limited between 0 and 1. $\Omega$ is coupling coefficient, $\Delta k$ is the detuning factor given by $\Delta k = \beta - \pi/\Lambda$, with $\beta$ the propagation constant and $s = \sqrt{\Omega^2 - \Delta k^2}$. For a sinusoidal RI modulation in the core, the coupling coefficient is given by:

$$\Omega = \frac{\pi \Delta n \, \eta(V)}{\lambda} \quad \text{(4.10)}$$

where, $\Delta n$ denotes the magnitude of the induced RI variation at a particular wavelength ($\lambda$) and $\eta$ (V) is a function of the normalized frequency (V) of the fiber. It is a measure of the mode power contained in the core, $\eta(V) \approx 1 - 1/V^2$. The normalized frequency, V of an optical fiber is given by the expression [9]:

$$V = \frac{2\pi}{\lambda} a \left(n_{co}^2 - n_{cl}^2\right)^{1/2} \quad \text{(4.11)}$$

where, a is the radius of the core of the fiber, $n_{co}$ and $n_{cl}$ are the refractive indices of the core and cladding respectively. For all wavelengths, if the value of $V \leq 2.405$, then the fiber is a single mode fiber [10]. In an FBG, at the Bragg

wavelength, there is no detuning and hence, $\Delta k = 0$ and $s = \Omega$. The expression for the reflectivity therefore reduces to:

$$R(L,\lambda) = \tanh^2(\Omega L) \quad \text{……..……..…..} \quad (4.12)$$

From equation 4.12, it is clear that the spectral reflectivity of an FBG can be related to two factors, Ω and L. Normally; gratings are fabricated with a typical length (L) of few centimeters. As given in equation 4.12, the spectral reflectivity (R) can be increased by increasing the length of the grating [3]. The equation also suggests that the reflectivity of FBGs can be enhanced by increasing the value of Ω, which is directly proportional to the magnitude of the induced refractive index variation (Δn). Hence, the reflectivity can be increased by enhancing the grating depth or strength [3]. In other words, FBGs with approximately 100% reflectivity can be fabricated by properly designing the grating length (L) and the grating strength or depth (Δn).

Full width at half maximum (FWHM), is another parameter used to specify an FBG. The FWHM bandwidth of a grating [11, 12] is a measure of the selectivity of the FBG and is defined as the difference between wavelengths in the reflected spectra, where reflectivity drops to the half of its maximum value. An illustration showing how the FWHM is determined from the reflected spectrum of an FBG is given in Fig. 4.3.

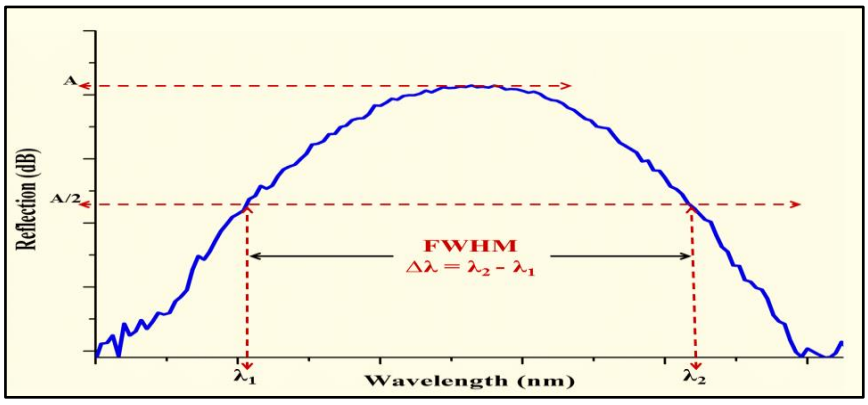


***Figure 4.3:*** *FWHM* of f*iber Bragg grating*

An approximate mathematical expression for FWHM of FBGs is:

$$\Delta\lambda_{FWHM} = \lambda_B \alpha \sqrt{\left(\frac{1}{2}\frac{\Delta n}{n}\right)^2 + \left(\frac{1}{N}\right)^2} \quad \text{(4.13)}$$

where, N represents the number of grating planes present in grating structure, $\alpha \approx 1$ for strong gratings (for grating with reflectivity ≈ 100%) and $\alpha \approx 0.5$ for weaker gratings [13]. Equation 4.13 suggests that, for an FBG, the bandwidth can be reduced by decreasing the grating strength or depth ($\Delta n$) and by increasing the value of N.

The value of N can be enhanced by increasing the grating length (L), which in turn increases the reflectivity of an FBG. However, the dependence of reflectivity (R) and FWHM on the grating strength ($\Delta n$) is opposing. Hence, an optimum value of $\Delta n$ is chosen to fabricate an FBG with the desired values of bandwidth and reflectivity.

## 4.3. FBG: Sensing Principle

FBGs are widely used in various fields like communication, lasers and sensing applications. The narrow band operation of FBG, clubbed with the inherent advantages of fiber optic sensors made it a lead runner in the field of sensors. They are being employed as the sensing elements to monitor physical, chemical as well as biological parameters.

The reflected Bragg wavelength of an FBG is a function of the grating pitch ($\Lambda$) and the effective refractive index ($n_{eff}$) of the fiber core and is given by equation (4.8). From this equation it is clear that, a shift in $\lambda_B$ can be induced by either a change in the $n_{eff}$ or $\Lambda$ or both these parameters. This shift in the reflected Bragg wavelength ($\lambda_B$) under the influence of external perturbations forms the basis of FBG sensors. Physical parameters like strain ($\varepsilon$), temperature (T) and SRI or surrounding RI ($n_{sur}$) are the possible external

perturbations which can initiate changes in $n_{eff}$ or $\Lambda$ or both. This can be mathematically expressed as [1]:

$$\Delta\lambda_B = \frac{\partial\lambda_B}{\partial\varepsilon}\Delta\varepsilon + \frac{\partial\lambda_B}{\partial T}\Delta T + \frac{\partial\lambda_B}{\partial n_{sur}}\Delta n_{sur} \quad \text{(4.14)}$$

Substituting $\lambda_B = 2\, n_{eff}\, \Lambda$ in equation 4.14 and expanding, the above expression can be written as:

$$\begin{aligned} d\lambda_B = {} & 2\left(\Lambda\frac{\partial n_{eff}}{\partial\varepsilon} + n_{eff}\frac{\partial\Lambda}{\partial\varepsilon}\right)d\varepsilon \\ & + 2\left(\Lambda\frac{\partial n_{eff}}{\partial T} + n_{eff}\frac{\partial\Lambda}{\partial T}\right)dT \\ & + 2\left(\Lambda\frac{\partial n_{eff}}{\partial n_{sur}} + n_{eff}\frac{\partial\Lambda}{\partial n_{sur}}\right)dn_{sur} \end{aligned} \quad \text{(4.15)}$$

The three terms on the right hand side of the above equation represents the effect of strain, temperature and SRI respectively. Since, the grating pitch is not depending on SRI, the factor $\frac{\partial\Lambda}{\partial n_{sur}}$ in the third term reduces to zero.

Then, the above expression reduces to:

$$\begin{aligned} d\lambda_B = {} & 2\left(\Lambda\frac{\partial n_{eff}}{\partial\varepsilon} + n_{eff}\frac{\partial\Lambda}{\partial\varepsilon}\right)d\varepsilon \\ & + 2\left(\Lambda\frac{\partial n_{eff}}{\partial T} + n_{eff}\frac{\partial\Lambda}{\partial T}\right)dT \\ & + 2\left(\Lambda\frac{\partial n_{eff}}{\partial n_{sur}}\right)dn_{sur} \end{aligned} \quad \text{(4.16)}$$

Out of the three possible external perturbations, the basic factors that can directly tune the grating pitch are the strain and the temperature [3-5]. Strain and temperature are considered as the independent variables on which the Bragg wavelength depends [14, 15]. Then, equation 4.16 reduces to:

$$\begin{aligned} d\lambda_B = {} & 2\left(\Lambda\frac{\partial n_{eff}}{\partial\varepsilon} + n_{eff}\frac{\partial\Lambda}{\partial\varepsilon}\right)d\varepsilon \\ & + 2\left(\Lambda\frac{\partial n_{eff}}{\partial T} + n_{eff}\frac{\partial\Lambda}{\partial T}\right)dT \end{aligned} \quad \text{(4.17)}$$

Dividing equation 4.17 by $\lambda_B = 2\, n_{eff}\, \Lambda$, it becomes,

$$\begin{aligned} \frac{d\lambda_B}{\lambda_B} = {} & \left(\frac{1}{n_{eff}}\frac{\partial n_{eff}}{\partial\varepsilon} + \frac{1}{\Lambda}\frac{\partial\Lambda}{\partial\varepsilon}\right)d\varepsilon \\ & + \left(\frac{1}{n_{eff}}\frac{\partial n_{eff}}{\partial T} + \frac{1}{\Lambda}\frac{\partial\Lambda}{\partial T}\right)dT \end{aligned} \quad \text{(4.18)}$$

Equation 4.18 explains the Bragg wavelength shift under the impact of strain and temperature.

## 4.4 Sensitivities of FBG

### 4.4.1 Strain Sensitivity

Betholds et al. derived the strain-optic coefficient and put forward the idea of strain measurements using FBGs [16]. Strain sensing with FBGs rely on the measurement of the Bragg wavelength shift due to the strain applied on the sensor head. Considering the effect of strain alone on the FBG, equation 4.18 can be reduced to:

$$\frac{d\lambda_B}{\lambda_B} = \left(\frac{1}{n_{eff}}\frac{\partial n_{eff}}{\partial \varepsilon} + \frac{1}{\Lambda}\frac{\partial \Lambda}{\partial \varepsilon}\right) d\varepsilon \quad \text{..... (4.19)}$$

The first term on the right hand side of the above equation gives the changes in the effective RI of the core of the fiber due to the induced lattice stress. This is termed as the strain-optic effect or the photo elastic/Pockel's effect [17-19]. Straining FBGs cause stress in the lattice both in line and in perpendicular to the direction of the applied strain. In addition to the strain-optic effect, the periodicity of the grating also alters due to the change in the physical dimensions of the fiber. The second term represents the change in the grating pitch or lengthening of the fiber with respect to the applied strain. In other words, the induced strain stretches the fiber physically changing $\Lambda$ or separation between the grating planes. Thus, the change in the Bragg wavelength ($\lambda_B$) is the sum of the shifts due to strain-optic effect and change in pitch.

The strain induced shift in the Bragg wavelength of FBGs can also be expressed in terms of the photo elastic coefficient as given below [13, 16].

$$\Delta\lambda_B = (1 - p_e)\,\lambda_B \quad \text{..... (4.20)}$$

where, $\varepsilon$ denotes the axial strain experienced by the fiber, and $p_e$ is the photoelastic coefficient (effective strain-optic constant). The strain-optic

tensor relates the RI shifts along different crystal directions under the impact of the strain in each or a combination of directions. For cylindrical fibers, the Pockel's coefficients $p_{11}$ and $p_{12}$ are the only significant tensor components, describing the shift in RI of the two transverse polarizations for tension acting along the axis of the fiber. The photo elastic coefficient (effective strain-optic constant) $p_e$ of the fiber is given by [2, 20]:

$$p_e = \left(\frac{n_{eff}^2}{2}\right)\left[p_{12} - \upsilon(p_{11} + p_{12})\right] \quad \text{.....(4.21)}$$

where, $p_{11}$ and $p_{12}$ are the members of the strain-optic tensor, and $\upsilon$ is Poisson's ratio.

### 4.4.2 Temperature Sensitivity

Considering the effect of temperature alone, the shift in Bragg wavelength ($\lambda_B$) can be derived from equation 4.18 as [2]:

$$\frac{d\lambda_B}{\lambda_B} = \left(\frac{1}{n_{eff}}\frac{\partial n_{eff}}{\partial T} + \frac{1}{\Lambda}\frac{\partial \Lambda}{\partial T}\right) dT \quad \text{.....(4.22)}$$

A closer look at the above equation reveals that, Bragg wavelength shifts in response to the temperature arises due to two factors, the change in the $n_{eff}$ of the fiber due to the thermo optic effect and the change in the grating pitch due to thermal expansion of the fiber, represented as the two terms in the equation.

The thermo optic constant($\xi$), for the fiber can be positive or negative depending on the material composition. Silica, the basic constituent of the optical fibers exhibit both positive and negative thermo-optic constants depending on the type of dopant and their relative concentrations. The concentration of boron or germanium within the core, will determine its properties.

Equation 4.22 can be rewritten as: [2]

$$\Delta\lambda_B = \left(\frac{1}{\Lambda}\frac{\partial \Lambda}{\partial T} + \frac{1}{n_{eff}}\frac{\partial n_{eff}}{\partial T}\right)\lambda_B \Delta T \quad \text{.....(4.23)}$$

$$\Delta\lambda_B = (\alpha + \xi)\,\lambda_B\,\Delta T \quad \text{.....} \quad (4.24)$$

where, $\alpha = \left(\frac{1}{\Lambda}\right)\left(\frac{\partial\Lambda}{\partial T}\right)$ denotes the coefficient of thermal expansion, $\xi = \left(\frac{1}{n_{eff}}\right)\left(\frac{\partial n_{eff}}{\partial T}\right)$ denotes the thermo optic coefficient of the fiber and $\Delta T$ represents the change in temperature. Both these parameters $\alpha$ and $\xi$ are temperature dependent and behave non-linearly at high temperatures [18, 21].

### 4.4.3 Cross Sensitivity to Strain and Temperature

The independent sensitivities of FBGs to strain and temperature was discussed in sections 4.4.1 and 4.4.2. When FBGs are subjected to strain, the physical dimensions of the grating is altered which in turn changes the effective RI of the core of the fiber. The temperature sensitivity of an FBG results mainly due to the change in induced refractive index [2, 3]. One of the most important demerits of FBG sensor system is this dual sensitivity to temperature and strain. A sensor system designed to monitor strain, can lead to anomalous readings due to the temperature variations around the sensor head and vice versa. Hence, it is important to discriminate strain and temperature effects in order to determine the effect of individual parameter when they are acting simultaneously on an FBG.

The combined effect of strain and temperature acting simultaneously on an FBG can be considered as the sum of their individual effects. Then, the combined Bragg wavelength shift can be deduced from equation 4.20 and equation 4.24 as:

$$\Delta\lambda_B = [(1 - p_e)\varepsilon + (\alpha + \xi)\,\Delta T\,]\lambda_B \quad \text{.....} \quad (4.25)$$

The above equation can be expanded by substituting the values of $p_e$, $\alpha$ and $\xi$ to obtain the Bragg wavelength shift as:

$$\Delta\lambda_B = \begin{pmatrix} \left\{1 - \left(\frac{n_{eff}^2}{2}\right)\,[p_{12} - \upsilon(p_{11} + p_{12})]\right\}\varepsilon \\ + \\ \left\{\left(\frac{1}{\Lambda}\right)\left(\frac{\partial\Lambda}{\partial T}\right) + \left(\frac{1}{n_{eff}}\right)\left(\frac{\partial\, n_{eff}}{\partial T}\right)\right\}\Delta T \end{pmatrix}\lambda_B \quad \text{.....} \quad (4.26)$$

Several methods have been proposed to discriminate the cross sensitivity of FBG [22-28].

### 4.4.4 Refractive Index Sensitivity

In an FBG, the forward and backward propagating modes are strongly shielded by the cladding layer. This prevents the impact of the SRI on the guiding characteristics of the fiber. Since, the effective core refractive index of the fiber is not influenced by the SRI, there is no sensitivity to external medium refractive index. However, if cladding thickness around the grating is reduced partially or totally, the effective core refractive index can be influenced significantly by the surrounding medium [29-34]. Etching the cladding around the FBG, results in strong spectral changes in the response of the FBGs.

## 4.5 Sensing Applications of FBG

Fiber Bragg gratings are widely used in various applications. They are being employed in fiber optic communication systems [1], dispersion compensation [35-40], wavelength filtering devices [41-47], fiber amplifiers [48-54], laser systems [55-64], external cavity reflectors [65-67] and optical storage devices [68, 69].

In the field of sensors FBGs are employed for the measurement of various parameters like pressure [20, 70-81], strain [13, 15, 16-18, 21-24, 26-28, 90, 91], temperature [18, 24, 26-28, 82-86, 90, 91], displacement [70], radiation dose [92], liquid level [93, 94], humidity [74, 95-98] etc. Multiparameter measurements using FBGs were also reported in literature [82-86]. Polymers were also coated on FBGs to improve the sensitivity of measurements [72, 74, 79, 95, 104].

### 4.5.1 Etched FBG for RI Sensing

As explained in section 4.4.4, the RI sensitivity is absent in bare FBGs. However, FBGs can be made sensitive to the variations in SRI by the reduction of the diameter of the cladding of the fiber around the grating region [29-34]. Under this condition, the principle of operation depends on the interaction of the evanescent wave of the fundamental guided mode with the surrounding medium. Due to the reduction in the cladding diameter of the fiber, the highly shielded core modes get exposed to the influence of the external medium. The change in the RI of the external medium in turn affects the effective indices of these core modes, which is manifested as the shift in Bragg wavelength. This wavelength shift is also accompanied by a modulation of the reflected intensity. The change in the reflected amplitude for different values of RI of the external medium is due to the numerical aperture difference between the thinned and un-etched optical fibers [30, 31].The simplest technique to reduce the cladding thickness is by the method of uniform etching. In this method, the section of the fiber with the Bragg grating is dipped in hydrofluoric acid (HF) which dissolves the silica cladding.

Asseh et al. demonstrated the very first FBG refractometer based on chemically etched FBG for sensing applications in 1998 [99]. His team was successful in developing an etched FBG, protected by a thin Teflon tubing, for sucrose concentration measurements. Followed by this FBG based RI sensors were reported by several groups [100-107]. Schroeder et al. developed an FBG based RI sensor for online quality control of petrol products and in situ monitoring of salinity in bore holes [101]. Lu and team proposed a polyamide coated FBG sensor for the measurement of salinity [104]. Wei Liang et al. demonstrated the application of FBG for RI measurements of various liquids like, methanol, ethanol and isopropyl alcohol [106]. Several papers published earlier demonstrated the use of etched FBGs in sensing applications [29-34,

99]. Both etched and unetched FBGs were employed in varied applications in the field of bio sensing also [103, 108-113]. Chryssis et al. in 2005 demonstrated the first bio sensing application of etched FBG, in which DNA hybridization was detected [108]. Detection of DNA hybridization was also demonstrated using etched FBGs by S S Saini and team in 2007 [109]. In 2009, Ryu et al. functionalized FBG with a carbohydrate siloxane conjugate to realize a glucose biosensor with high specificity [110]. Simulated results of FBG based strain and temperature sensor for biomedical applications was reported in 2008 [111]. Mishra et al. reported a wide range of applications for FBG sensors in the field of medicine [112]. Protein concentration measurements, using DNA coated etched FBG sensor was reported by Libish et al. in 2015 [113].

## 4.6 Development of Etched / Thinned FBG Sensor Head

An FBG with a Bragg wavelength of $\lambda_B$ = 1561.616 nm was selected for the etching process. The FBG was fabricated at CGCRI, Kolkata, through phase mask method. The standard single mode optical fiber (SMF-28e) with a core diameter of 8.2 µm, cladding diameter of 125 µm and a numerical aperture value of 0.14 was used to fabricate the FBG. The fiber was hydrogen loaded for 24 hours at $100^0$C and 1500 psi pressure, prior to the fabrication. 248 nm laser output from a KrF excimer laser source was focused on to the phase mask by a cylindrical lens after multiple reflections. The resulting interference pattern of the diffracted first order beams were allowed to fall on the fiber to write the grating. The fiber with the grating was annealed in a high temperature oven at $200^0$C for 7 hours to remove the residual hydrogen. More detailed description and a schematic of the FBG fabrication set up is presented in chapter 1.

The need for the reduction of cladding radius for RI sensitivity of FBGs was discussed in the previous sections. The fabrication of etched FBG by the

process of chemical etching is discussed here. A schematic of the etched FBG is given in Fig. 4.4.

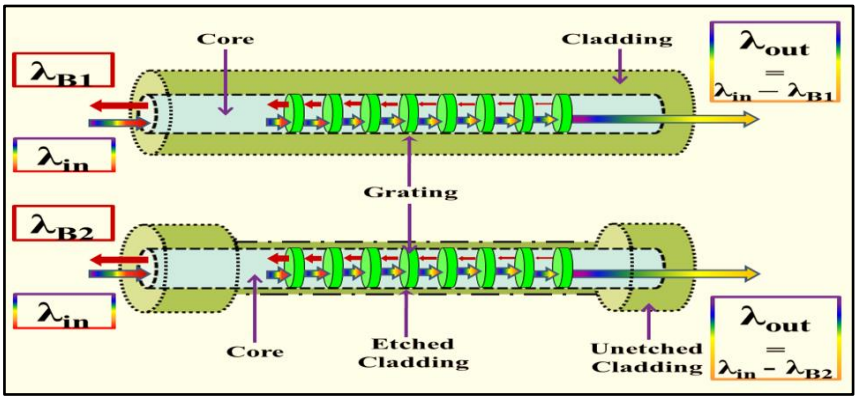


***Figure 4.4:*** *Schematic sketch - Etched FBG.*

Various concentrations of HF solutions were tried for the chemical etching process. Even though with higher concentrations of HF (typically 50%), the etching process was faster (around 22 minutes), it was difficult to control the process towards the end of the etching process. This led to the breakage of gratings towards the final stages of the process. The concentration of the HF solution was optimized at 30% and the entire process of etching took a time of 66.2 minutes.

The experimental setup used for the etching process is given Fig. 4.5. The grating region of the optical fiber was cleaned properly by washing repeatedly with distilled water and iso propyl alcohol. The prepared grating was placed horizontally in a Teflon mount as shown in the experimental setup, such that the grating is completely immersed in the etching solution. The output signals from a white light source (Yokogawa - AQ 4305) was coupled to the grating through a 3dB coupler and the reflected spectrum was monitored continuously with an OSA (Yokogawa - AQ 6319). The temperature around the set up was maintained at room conditions (around $27^0$C) throughout the process of etching.

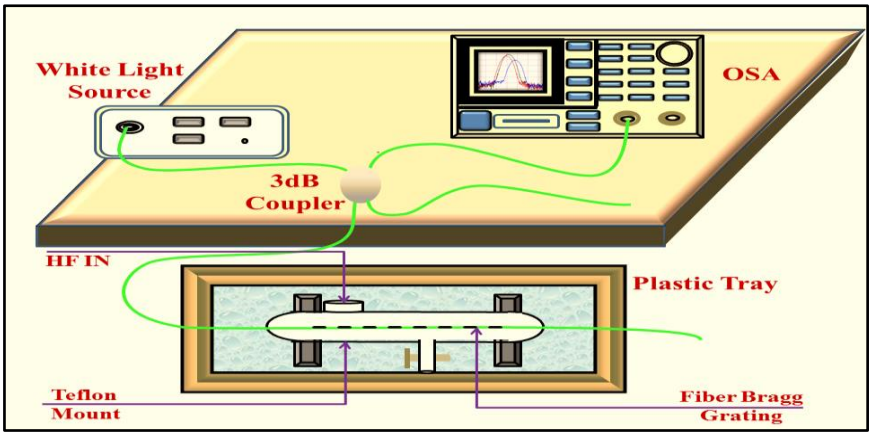


***Figure 4.5:*** *Experimental setup - FBG etching*

### 4.6.1 Evolution of the Reflected Spectrum

The initial spectrum with Bragg wavelength of $\lambda_B$ = 1561.616 nm was recorded after placing the grating in the Teflon mount. This was taken as the reference spectrum for the rest of the measurements taken during the etching process. Shift from this initial Bragg wavelength of $\lambda_B$ = 1561.616 nm of the FBG as a function of the time elapsed for the etching process was monitored and recorded in real time in order to study the progression of the grating spectrum. The reference spectrum of the FBG, recorded at t = 0 minutes is given in Fig. 4.6. The time just before the introduction of etching HF solution into the Teflon mount is defined as t = 0 minute.

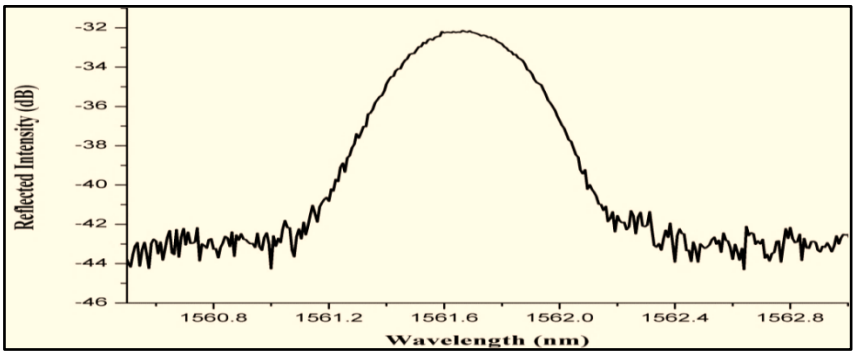


***Figure 4.6:*** *Reference spectrum of the FBG at t = 0 minute*

As mentioned earlier, the cladding over the FBG was etched in HF solution with a concentration of 30% for a time duration of 66.2 minutes. During the initial stages of the etching process, the spectrum gradually shifted towards higher wavelengths without any change in the intensity. This trend continued for a duration of 61 minutes after the introduction of the HF solution. The evolution of the reflected spectra of the FBG during the initial stages is shown in Fig. 4.7.

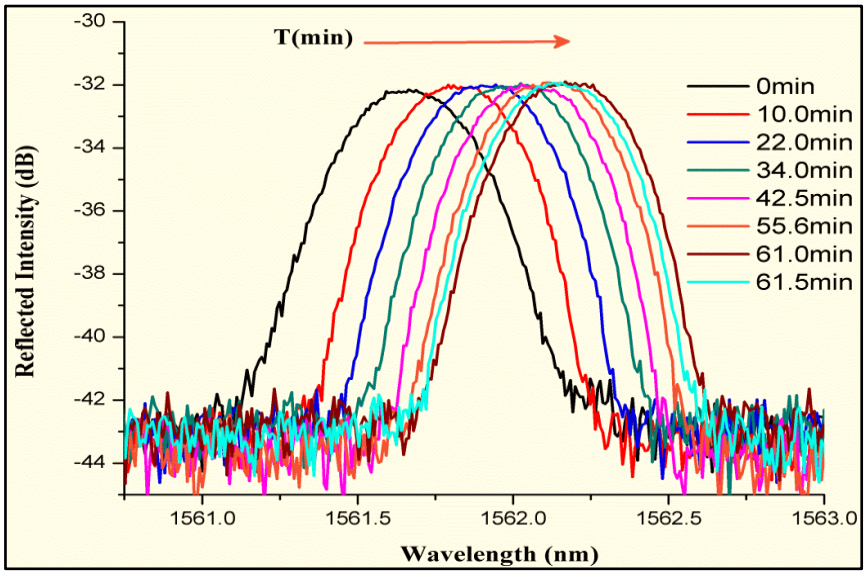


***Figure 4.7:*** *Evolution of the spectra of the FBG for the first 61.5 minutes*

A red shift of 0.552 nm in the Bragg wavelength, from $\lambda_B$ = 1561.616 nm at t = 0 minute to $\lambda_B$ = 1562.168 nm at t = 61 minutes, was noted during this stage. This increase in Bragg wavelength $\lambda_B$ is attributed to the heat generated during the chemical reaction of HF with silica. Increase in the temperature was reflected as the red shift in the reflected grating spectra. The change in strain during the etching process also adds to this early red shift to some extent [5, 9, 114].

After 61 minutes, the spectrum showed an abrupt change from the red shifting trend to gradual shifts towards shorter wavelengths. The progression of the reflected spectra of the FBG from 61 minutes to 66.2 minutes is shown in Fig. 4.8. The reflected Bragg wavelength of 1562.168 nm at t = 61 minutes, gets down shifted to 1561.568 nm at the end of etching after 66.2 minutes. This blue shift of 0.6 nm (t = 61 minutes to t = 66.2 minutes) in the reflected wavelength is attributed to the penetration of the optical core mode into the fiber cladding. This is due to the dominance of the effective RI change caused by reduction in the cladding diameter over the effect due to the variations in temperature produced during the reaction of silica cladding with HF [5, 9, 12, 13].

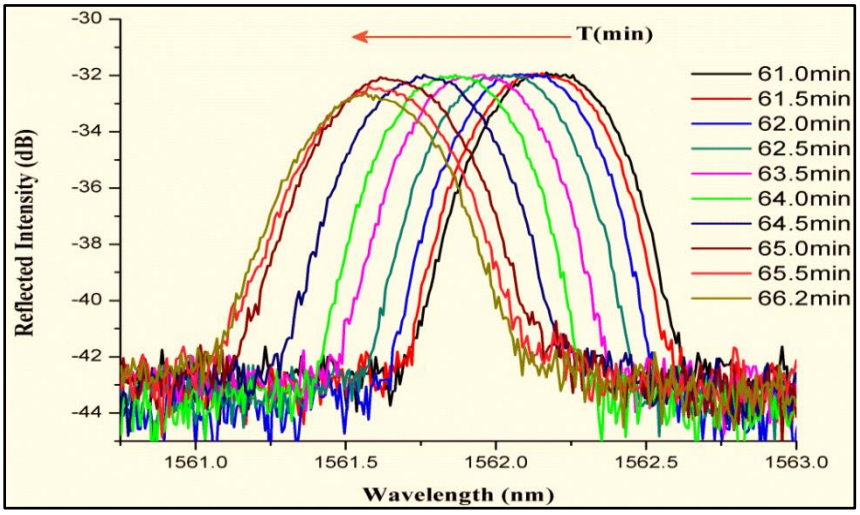


***Figure 4.8:*** *Evolution of the spectra of the FBG after 61 minutes*

Until 65 minutes, there was no change in the reflectivity of the grating or the amplitude of the reflected wavelength. However, after t = 65 minutes, the reflectivity of the grating was found to decrease gradually from the initial value of -32.056 dB at t = 0 minute. This is due to the difference in numerical aperture between the unetched fiber portion and the thinned region, which is a function of the RIs of core, cladding and the surrounding medium [13, 114].

This reduction in reflectivity is an indication that the etching has reached very close to the core cladding boundary or in other words, the fiber diameter around the grating approaches the fiber core diameter.

At this point, the etching process was interrupted by emptying the HF solution from the Teflon mount. Continued etching beyond this point will lead to the removal of core material and breakage of the fiber eventually. The FBG and the fiber was washed repeatedly 3 or 4 times with distilled water to ensure that, no residual HF is sticking on to the fiber.

The summary of the evolution of the reflected spectra of the FBG during the etching process is given in Fig 4.9. The Bragg wavelength of the bare FBG at 1561.616 nm, exhibited a red shift of 0.552 nm during the first 61 minutes of etching.

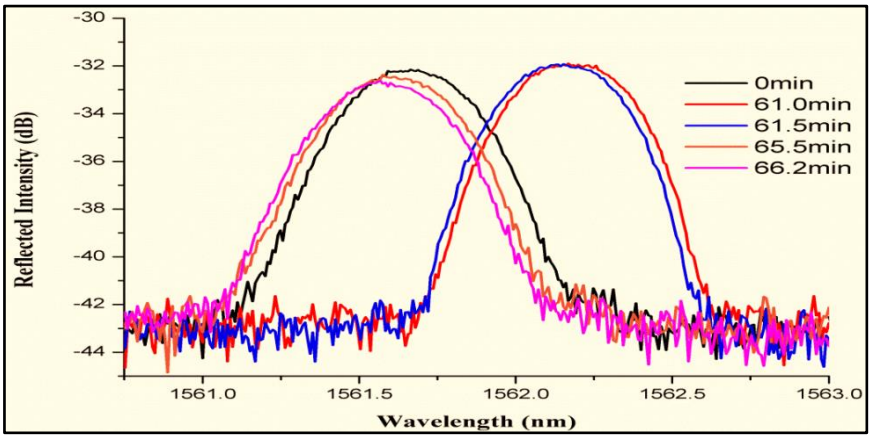


***Figure 4.9:*** *Bragg wavelength shifts during etching - Summary.*

Then, the peak wavelength blue shifted to 1561.568 nm at the end of the etching process after 66.2 minutes. The reflected intensity of -32.056 dB of the unetched FBG was reduced to a value of -32.624 dB after etching. Thus, the etching of the fiber led to a net blue shift of 0.048 nm in the reflected Bragg wavelength and a reduction of 0.568 dB in the reflected intensity.

## 4.7 Cholesterol Sensor

A cholesterol sensor exploiting the RI sensitivity of etched FBG to the concentration of the sample solution under test is presented in this section.

### 4.7.1 Experimental Setup

A schematic sketch of the setup for experimental analysis is given in Fig 4.10. The reflected FBG spectrum was analyzed with an optical spectrum analyzer (OSA) (Yokogawa - AQ 6319) and a white-light source (Yokogawa - AQ 4305) as the signal source.

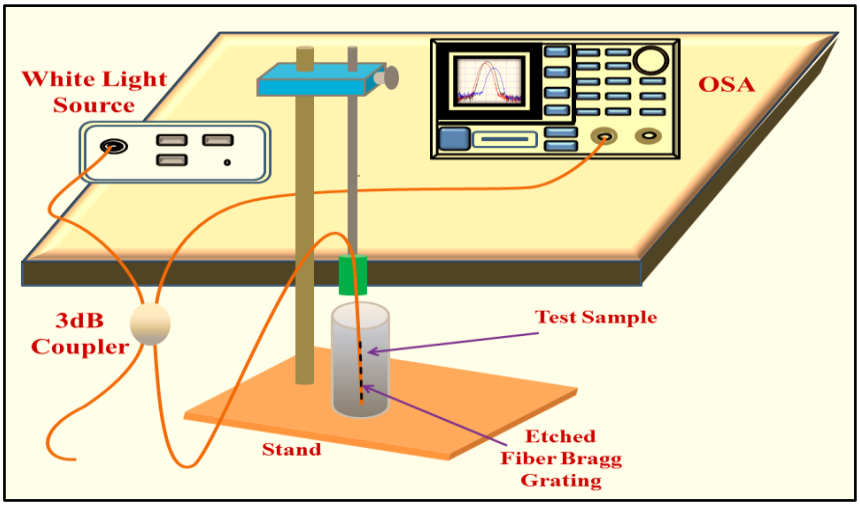


***Figure 4.10:*** *Etched FBG cholesterol sensor - Experimental set up.*

After the etching process, the etched FBG was coupled to the white light source through a 3 dB coupler. Without disturbing the etched grating, the other end of the fiber was properly cut at a length of 1 cm from the grating, using a cleaver. The prepared sensor head was fixed on a stand as shown above. The sample solution prepared was taken in a glass beaker for the experimental studies. Sufficient quantity, around 25 ml, of the test solution was used in all measurements so that the etched FBG section was completely immersed in the sample solution during the experimentation.

### 4.7.2 Materials and Methods

The cholesterol level in the blood of a normal human being is in the range of 1400 ppm to 2000 ppm [115]. Hence, the measurements were limited to a maximum of 5000 ppm of cholesterol in coconut oil, which covers the normal levels of cholesterol in human blood. The procedures followed for the preparation of cholesterol samples with coconut oil as the solvent is as described in section 2.5.1.3 of the chapter 2 of this thesis. After each measurement, the cholesterol test samples were removed from the beaker. The sensor head and the beaker were washed repeatedly 3 or 4 times with distilled water and iso propyl alcohol to remove any trace of residue left behind. This is to ensure that the initial spectrum of the etched FBG without any test sample in the beaker was reproduced.

### 4.7.3 Results and Discussion

The initial reflected spectrum of the etched FBG with air as the SRI, recorded after fixing it on the stand, is shown in Fig 4.11.

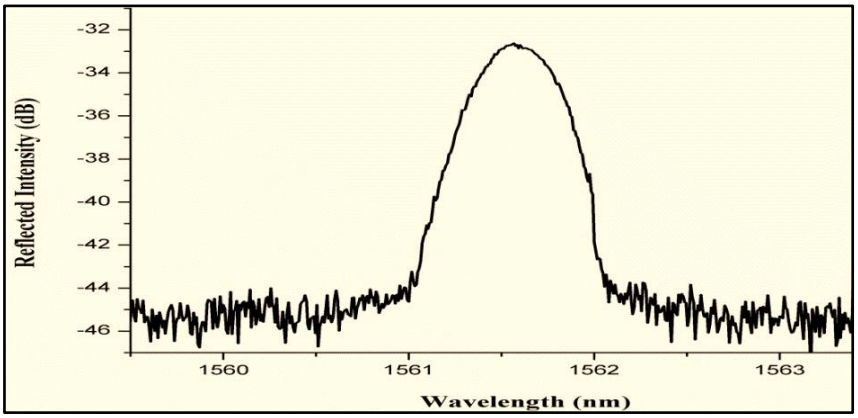


***Figure 4.11:*** *Reflected spectrum of etched FBG with air as the SRI.*

When coconut oil (solvent) was introduced into the beaker, the reflected Bragg wavelength got red shifted to 1561.584 nm along with a reduction in the reflected intensity. As soon as the test samples with increasing

concentrations of cholesterol dissolved in coconut oil were introduced into the beaker, more shifts towards higher wavelengths were observed in the reflected Bragg wavelength.

The reflected spectra of the sensor head for various cholesterol concentrations are given in Fig. 4.12. The peak of the reflected spectrum changed from 1561.584 nm to 1561.728 nm, when the concentration of cholesterol was varied from 0 ppm to 5000 ppm. The red shift in the Bragg wavelength is attributed to an increase in the effective index of the core under the influence of the SRI. As explained earlier, the principle of operation of etched FBG depends on the interaction between the evanescent wave of the fundamental guided mode and the medium around the grating. Hence, it is obvious that the reflected Bragg wavelength to shift according to the effective refractive index variations. As the cholesterol concentration was increased in the test sample, the SRI was increased, which in turn increased the effective RI of the grating. The red shift observed in the Bragg wavelength is attributed to this increased effective RI, as given by equation 4.16.

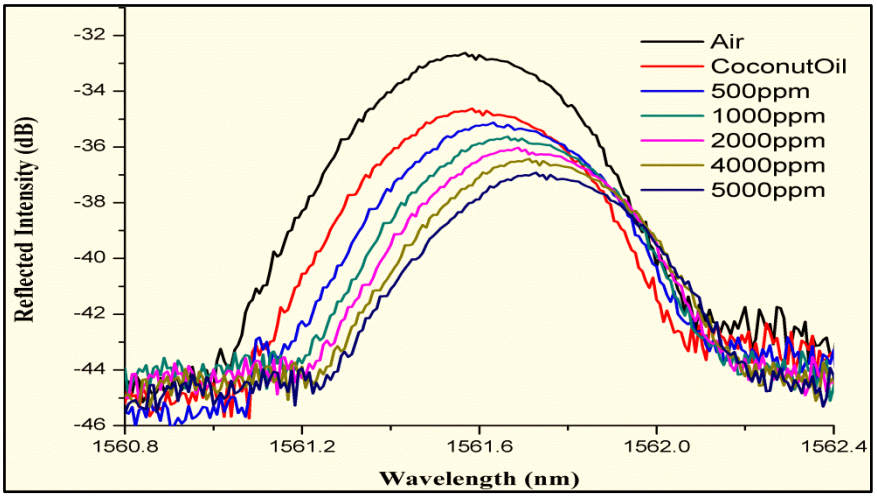


***Figure 4.12:*** *Reflected spectra of etched FBG sensor head for various concentrations of cholesterol dissolved in coconut oil.*

Along with this red shift of the Bragg wavelength, a reduction in the reflected intensity was also observed on increasing the concentration of cholesterol dissolved in coconut oil. In the measured range of concentrations, the reflected power from the sensor head reduced from a value of -34.635 dB to -36.926 dB, with increase in cholesterol concentration. This reduction in the transmitted intensity is due to the difference in the numerical aperture between the unetched and thinned sections of the optical fiber for different values of SRI [13, 114].

As the concentration of the cholesterol dissolved in coconut oil was varied from 0 ppm to 5000 ppm, the reflected Bragg wavelength was found to have a redshift of 144 pm. The wavelength sensitivity was calculated as the ratio of the shift in the reflected Bragg wavelength to the corresponding change in the concentration of cholesterol in the test samples. The shift of 144 pm corresponds to a wavelength sensitivity value of 0.028 pm/ppm of cholesterol dissolved in coconut oil.

## 4.8 Chitosan Coated Etched FBG Cholesterol sensor

The affinity of chitosan for cholesterol was established earlier in chapter 3. A cholesterol sensor employing a layer of chitosan coated around LPG was also discussed in chapter 3. Even though the etched FBG sensor head described in the last section exhibited good sensitivity to cholesterol, it is better to attempt for greater sensitivity. Development of an etched FBG sensor head with chitosan coating for enhanced cholesterol sensitivity is discussed below.

### 4.8.1 Sensor Head Fabrication

The etched FBG used in the earlier section for cholesterol measurement was used to fabricate the chitosan coated sensor head. The sensor head was fabricated by depositing a layer of chitosan biopolymer around the etched

FBG section. Dip coating method, as described in the section 3.3.1.2 of chapter 3 of this thesis, was employed in the fabrication process. The procedures and materials used for the dip coating were the same as explained in chapter 3. A schematic sketch of the etched FBG sensor head coated with chitosan is given in Fig. 4.13. The Bragg reflected wavelength of the etched FBG was at 1561.568 nm with a reflected intensity of -32.624 dB.

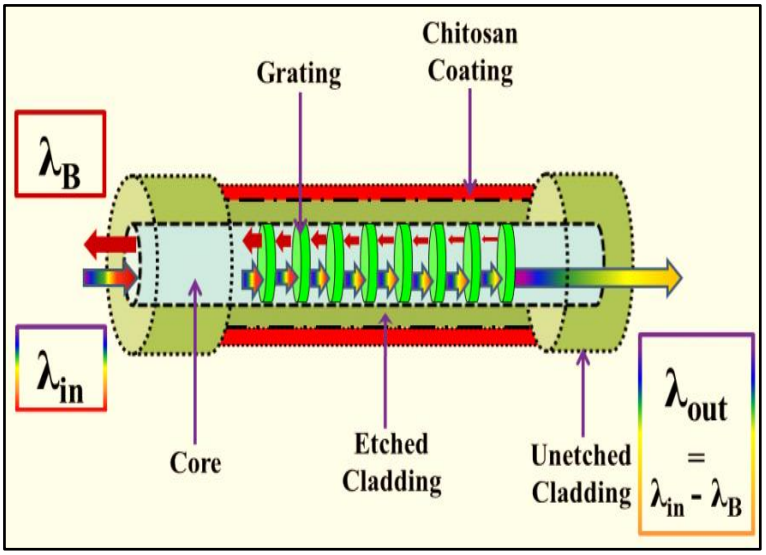


***Figure 4.13:*** *Schematic sketch - Chitosan coated etched FBG sensor head.*

After providing the overlay coating of chitosan biopolymer, the Bragg reflected wavelength shifted to 1561.848 nm with air as the SRI. The reflected spectrum of the fabricated chitosan coated etched FBG sensor head is given in Fig. 4.14.

This shift in the Bragg wavelength was along the expected lines, as the effective core refractive index of the FBG was enhanced due to the chitosan overlay coating. In addition, the amplitude of the reflected Bragg wavelength decreased to -34.287 dB.

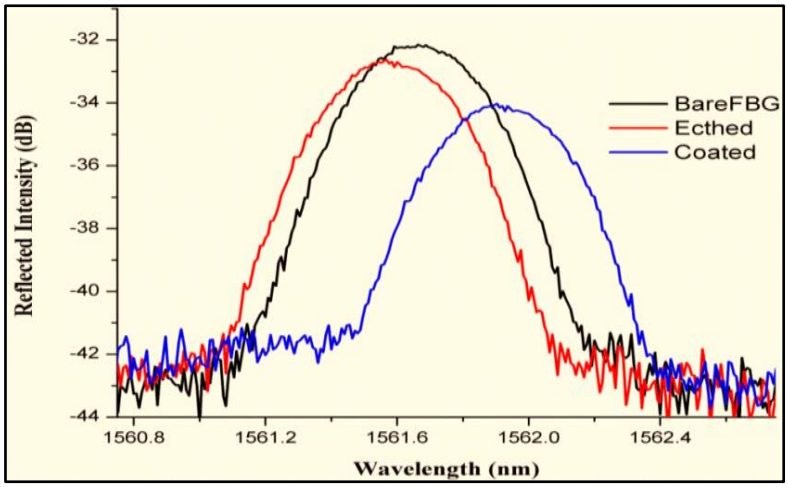


***Figure 4.14:*** *Reflected spectra of etched FBG sensor head in air before and after the coating*

### 4.8.2 Experimental Setup

The same experimental setup used in the cholesterol sensing experiments with etched FBG, discussed in section 4.7.1 was used for these experiments. The only difference is that, the etched FBG was replaced with the chitosan coated etched FBG as the sensor head.

### 4.8.3 Materials and Methods

The test samples for the experiments were prepared by dissolving definite amount of pure cholesterol in coconut oil. The method of preparation of samples and the procedures followed for the conduct of the experiments were the same as discussed in the previous sections.

### 4.8.4 Results and Discussion

The Bragg wavelength at 1561.848 nm showed a shift to 1561.904 nm, when pure coconut oil was introduced into the sample cell. As explained earlier, this red shift in the reflected Bragg wavelength is attributed to the

enhancement of the effective core refractive index of the fiber. A very small amount of strain induced by the coated layer also adds to this red shift. Along with this red shift in wavelength the peak intensity also reduced to a value of -34.913 dB.

Successive measurements were taken with different test samples of varying cholesterol concentration. The reflected spectra of the etched FBG sensor head with chitosan coating for various concentrations of cholesterol dissolved in coconut oil are presented in Fig. 4.15. When the concentration of the cholesterol in the test samples was increased, more and more cholesterol got attached to the coated chitosan layer. This attachment of cholesterol enhanced the RI of the coating, which in turn increased the effective RI of the core and was manifested as the red shift in the reflected Bragg wavelength. The strain exerted on the sensor head by the attachment of cholesterol on to the chitosan layer also contributes to the red shift to a small extent.

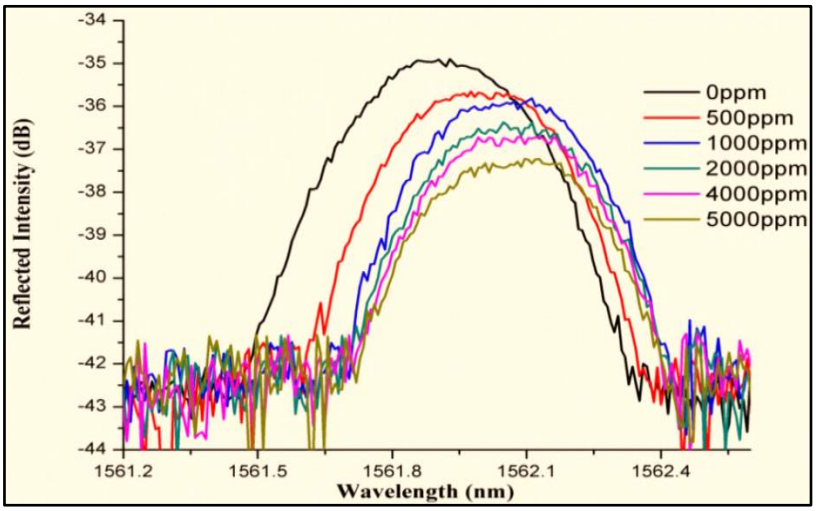


***Figure 4.15:*** *Reflected spectra of chitosan coated etched FBG sensor head for various concentrations of cholesterol dissolved in coconut oil.*

The reflected Bragg wavelength gradually shifted to 1562.220 nm for the maximum concentration of 5000 ppm used in this experiment. Along with

the red shift in the wavelength, the reflected intensity decreased to a value of -37.514 dB. A table showing the response of the chitosan coated etched FBG sensor head for various concentrations of cholesterol dissolved in coconut oil is given below.

| Cholesterol Concentration (ppm) | Refractive Index of Sample | Reflected Bragg Wavelength (nm) | | Reflected Intensity (- dB) | |
|---|---|---|---|---|---|
| | | Uncoated | Coated | Uncoated | Coated |
| **0** | 1.448 | 1561.584 | 1561.904 | 34.635 | 34.913 |
| **500** | 1.450 | 1561.602 | 1561.928 | 35.128 | 35.655 |
| **1000** | 1.452 | 1561.624 | 1561.950 | 35.623 | 35.995 |
| **2000** | 1.453 | 1561.648 | 1562.004 | 36.066 | 36.604 |
| **4000** | 1.454 | 1561.682 | 1562.118 | 36.423 | 36.915 |
| **5000** | 1.455 | 1561.728 | 1562.220 | 36.926 | 37.514 |

***Table 4.1:*** *Response of the chitosan coated etched FBG sensor heads for various concentrations of cholesterol*

Plots of the reflected wavelength peak with respect to the concentration of cholesterol dissolved in coconut oil for the etched FBG sensor head with and without chitosan coating are given in Fig 4.16.

The chitosan coated etched FBG sensor heads showed a sensitivity of approximately 0.063 pm/ppm of cholesterol dissolved in coconut oil, for the net red shift of 0.316 nm in the reflected Bragg wavelength. This is more than two times higher compared to that of the uncoated sensor head described earlier. This enhanced sensitivity compared to the uncoated sensor head is attributed to the affinity of the coated layer of chitosan biopolymer to cholesterol. The sensitivity curve also shows linearity in the measurements. The uncoated sensor exhibited linearity in the range of 1000 ppm to 4000 ppm whereas, the coated sensor showed linearity in an extended range of 0 ppm to

4000 ppm of cholesterol dissolved in coconut oil. As explained in the previous chapters these linear responses of the sensor heads cover the range of 1400 ppm to 2000 ppm cholesterol, which is the level of cholesterol in the blood of a normal human being.

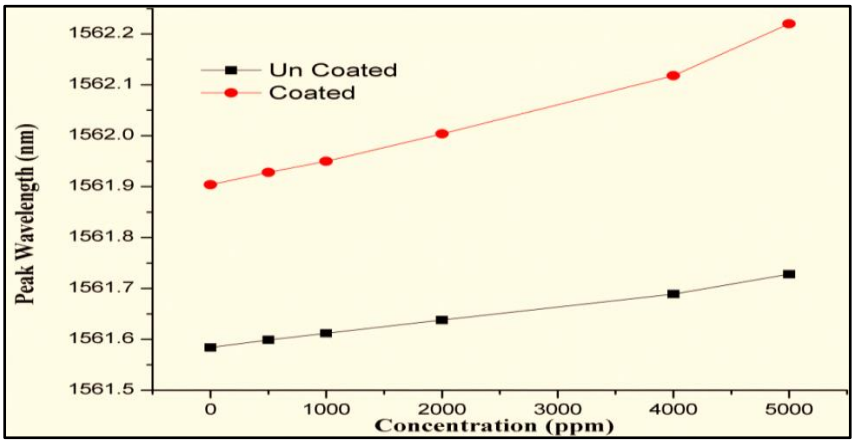


***Figure 4.16:*** *Reflected Bragg wavelength peak of the etched FBG sensor heads with and without chitosan coating*

At higher concentration levels of cholesterol, both the sensor heads showed a slightly increased sensitivity. At higher concentrations, the RI of the solution and hence the SRI is higher which in turn enhances the effective index of the fiber to a value nearer to the cladding refractive index thereby enhancing the sensitivity. Under these conditions, etched FBG sensor heads are expected to have higher sensitivities compared to the measurements with lower SRI values.

As mentioned earlier along with the red shift in the wavelength, the reflected intensity decreased to a value of -37.514 dB from the initial value -34.913 dB at 0 ppm of cholesterol. This reduction in amplitude is as expected and is attributed to the reduction in the reflectivity due to the difference in numerical apertures between the etched and unetched portions of the fiber [13, 114]. A plot of the reflected Bragg intensity of the chitosan coated sensor head

in comparison with that of the uncoated sensor head, for different concentrations of cholesterol is given in Fig. 4.17.

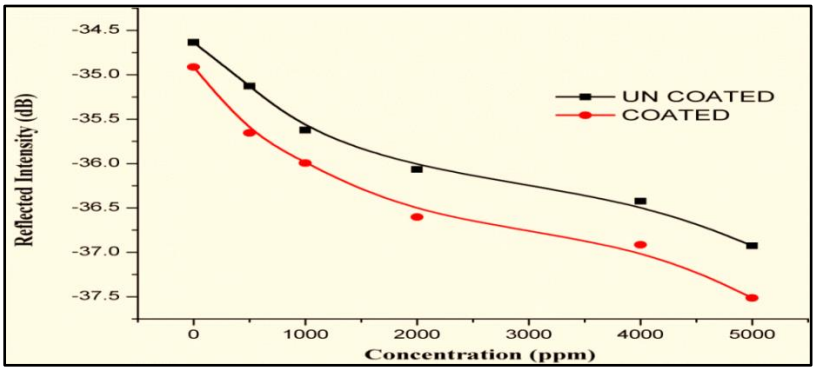


***Figure 4.17:*** *Reflected Bragg intensity of the etched FBG sensor heads with and without chitosan coating*

From the intensity plots, it is clear that the chitosan coated sensor head shows better performance when compared to the uncoated sensor. Both the sensor heads show increased reflectivity at lower concentration ranges, where the SRI values are low. This is also attributed to the difference in the numerical aperture values of the etched and unetched regions of the fiber, which leads to higher reflectivity at low values of SRI. A comparison of the performance of the etched FBG sensor heads with and without chitosan coating is given in Table 4.2.

| **Parameter** | **Etched FBG Sensor Head** | |
|---|---|---|
| | **Uncoated** | **Coated** |
| **Wavelength Shift for 0 – 5000ppm (pm)** | 144 | 316 |
| **Amplitude Shift (-dB)** | 34.635 – 36.924 | 34.913 - 37.514 |
| **Sensitivity (pm/ppm)** | 0.028 | 0.063 |

***Table 4.2:*** *Performance of FBG sensor heads with and without coating*

We have also demonstrated a DNA coated etched FBG based sensor for the estimation of protein concentrations [113]. The measurements were performed in a range of 50 μg/mL (ppm) to 300 μg/mL (ppm), which showed a maximum sensitivity of 0.820 pm/ppm. A sensitivity of 0.004 nm/ppm, for fluoride ions in a concentration range of 0.05 to 8 ppm [116] and 0.003 nm/ppm, for zinc ions upto a concentration of 4 ppm [117], have been reported for etched FBGs.

A sensitivity of 5.14 nm/ mM (13.2 pm/ppm), in the measurement range of 0 to 10 mM (0 – 3870 ppm) of cholesterol was reported by V Semwal et al. for a fiber optic cholesterol sensor based on surface plasmon resonance sensor head [118]. The sensing probe with enzyme, named cholesterol oxidase, bound over a layer of graphene oxide coated around optical fiber, exhibited pH dependent response and heating of the prepared sample was necessary for the measurements. Another fiber optic surface plasmon sensor for the detection of low density lipoprotein, a component of the total cholesterol, had a response time of 2 m and a sensitivity of 0.18 nm/ppm over a measurement range of 0 to 2000 ppm of cholesterol [119]. An enzymatic surface plasmon resonance sensor for the detection of cholesterol in a limited range of 0.12 to 10.23 mM (< 4000ppm) cholesterol has also been reported [120]. The sensors described above [118, 119] make use of metallic coatings around optical fiber for the detection of cholesterol. The sensors presented in [118, 120] were enzymatic. This makes the sensor head fabrication and handling complex and requires costlier equipment. Also, the measurement range is less than 4000 ppm. The sensor head described in this chapter makes use of a chitosan coating, and the range was also wider (0 to 5000 ppm). The response of the sensor head described in this chapter was found to be much more linear than that presented in [113].

## 4.9 Conclusions

The results presented illustrate the application of etched FBG based sensor systems for the detection and measurement of cholesterol concentrations. Both the chitosan coated and uncoated sensor heads can be utilized in designing cholesterol sensors. The simplicity of the sensors clubbed with its real time response and high sensitivity make them very attractive. The proposed techniques require only a small quantity of the test sample and can be suitably modified for field applications in clinical laboratories for the estimation of cholesterol in blood of human beings. The results are instantaneous and repeatable, and cover a wide range of cholesterol levels. In addition, the linearity in the performance makes the sensor head designs attractive for commercial applications in chemical, biomedical, drug development, food processing laboratories etc.

## 4.10 Summary

This chapter discussed, the fabrication of etched FBG based sensors. A detailed discussion on the principle of operation of FBG was provided. The response of FBGs to external perturbations like strain and temperature was discussed. The reason for the inherent low sensitivity of FBGs to SRI was outlined. A brief survey on the sensing applications of FBG, with an emphasis on bio sensing was also presented in the introductory part of this chapter.

The chapter also outlined the method of chemical etching to make the FBGs sensitive to RI variations. Evolution of the reflected spectra during the etching process was studied in detail. It was found that the RI sensitivity of FBGs written on SMF-28e fibers could be enhanced to a reasonably good level by the process of etching with 30% HF solution for a time duration of

approximately 66 minutes. It was shown that etched FBG can be employed as a RI sensor, specifically a cholesterol sensor.

For further enhancement of the RI sensitivity of the etched FBG, chitosan, which was identified as a biopolymer with an affinity to cholesterol, was employed as an overlay coating around the etched FBG to develop a sensor head for cholesterol sensing application. An overlay coating was prepared over the etched FBG by the process of dip coating. Etched FBG sensor head with chitosan coating exhibited more than two times higher sensitivity compared to the uncoated sensor for the test samples of cholesterol dissolved in coconut oil.

## References

[1]. K O Hill, Y Fujii, D C Johnson and B S Kawasaki, "*Photosensitivity in optical fiber waveguides: Application to reflection filter fabrication"*, Applied Physics Letters, Vol. 32, pp. 647-649 (1978).

[2]. A Othonos and K Kalli, *"Fiber Bragg Gratings: Fundamentals and Applications in telecommunications and sensing"*, Boston: Artech House (1999).

[3]. Andreas Othonos, "*Fiber Bragg gratings*", Review of Scientific Instruments, Vol. 68, pp. 4309-4341 (1997).

[4]. R. Kashyap, "*Fiber Bragg Gratings*", 2nd Edition, Academic Press (2010).

[5]. R Kashyap, J M L Higuera, "*Handbook of optical fiber sensing technology; Fiber Grating Technology: Theory, Photosensitivity, Fabrication and characterization*", John Wiley & Sons, pp. 349-377 (2002).

[6]. K O Hill and G Meltz, "*Fiber Bragg grating technology fundamentals and overview*", J. Lightwave Technology, Vol. 15, pp. 1263-1276 (1997).

[7]. T Erdogan, "*Fiber grating spectra*", J. Lightwave Technology, Vol. 15, pp. 1277-1294 (1997).

[8]. D K W Lam and B K Garside, "*Characterization of single mode optical fiber filters*", Appl. Optics, Vol. 20 (3), pp 440-445 (1981).

[9]. H G Limberger, P Y Fonjallaz and R P Salathe, "*Spectral characterization of photo induced high efficiency Bragg gratings in standard telecommunication fibers"*, Electronics Letters, Vol. 29, pp. 47-49 (1993).

[10]. G Meltz, W W Morey and W H Glenn, "*Formation of Bragg gratings in optical fibers by a transverse holographic method*", Optics Letters, 14, pp. 823-825 (1989).

[11]. I Bennion, J A R Williams, L Zhang, K Sugden and N J Doran, "*UV written in-fiber Bragg gratings"*, Optical and Quantum Electronics, Vol. 28, pp. 93-135 (1996).

[12]. P Russell, J L Archambault and L Reekie, "*Fiber gratings*", Physics World, Vol. 6, pp. 41-46 (1993).

[13]. Y J Rao, "*In-fiber Bragg grating sensors*", Measurement Science and Technology, Vol. 8, pp. 355-375(1997).

[14]. Y J Rao and D A Jackson, "*Recent progress in fiber optic low coherence interferometry*", Measurement Science and Technology, Vol. 7, pp. 981-999 (1996).

[15]. A D Kersey, M A Davis and H J Patrick, *"Fiber grating sensors",* J. Lightwave Technology, Vol. 15, pp. 1442 -1463 (1997).

[16]. A Bertholds and R Dandliker *"Determination of the individual strain optic coefficients in single mode optical fibers",* J. Lightwave Technology, Vol. 6, pp. 17-20 (1988).

[17]. L Ren, J Chen, H N Li, G Song and X Ji, "*Design and application of a fiber Bragg grating strain sensor with enhanced sensitivity in the small scale dam model*", Smart Materials and Structures, Vol. 18, pp. 035015 (2009).

[18]. S Pal, T Sun, K T V Grattan, S A Wade, S F Collins, G W Baxter, B Dussardier and Monnom G, "*Strain independent temperature measurement using a type I and type IIA optical fiber Bragg grating combination*", Review of Scientific Instruments,75, pp. 1327-1331(2004).

[19]. V M Murukeshan, P Y Chan, L S Ong and A Asundi, "*Intracore fiber Bragg gratings for strain measurement in embedded composite structures*", Applied Optics, Vol. 40, pp. 145-149 (2001).

[20]. B Budiansky, D C Drucker, G S Kino and J R Rice, "*Pressure sensitivity of a clad optical fiber"*, Appl. Opt. Vol. 18, 4085-4088, (1979).

[21]. W L Schulz, E Udd, J M Seim and G E McGill, "*Single and multiaxis fiber grating strain sensor applications for bridges and highways*", SPIE Proc., Vol. 3325, pp. 212-221(1998).

[22]. M G Xu, L Dong, L Reekie, J A Tucknott, and J L Cruz, "*Temperature-independent strain sensor using a chirped Bragg grating in a tapered optical fiber*", Electronics Letters, 31, pp. 823–825 (1995).

[23]. S Kim, J Kwon, and B Lee, "*Temperature-independent strain sensor using a chirped grating partially embedded in a glass tube*", Photonics Technology Letters, 12, pp.678-680 (2000).

[24]. S E Kanellopoulos, V A Handerek and A J Rogers, "*Simultaneous strain and temperature sensing with photo generated in-fiber gratings*", Optics Letters, Vol. 20, pp. 333-335 (1995).

[25]. Y Zhao and Y Liao, "*Discrimination methods and demodulation techniques for fiber Bragg grating sensors*", Optics and Lasers in Engineering, Vol. 41, pp. 1-18 (2004).

[26]. X Shu, Y Liu, D Zhao, B Gwandu, F Floreani, L Zhang and I Bennion, "*Dependence of temperature and strain coefficients on fiber grating type and its application to simultaneous temperature and strain measurement*", Optics Letters, Vol. 27, pp. 701-703 (2002).

[27]. W C Du, X M Tao and H Y Tam, "*Fiber Bragg grating cavity sensor for simultaneous measurement of strain and temperature*", Photonics Technology Letters, Vol. 11, pp. 105-107 (1999).

[28]. L A Ferreira, F M Arau Jo, J L Santos and F Farahi, *"Simultaneous measurement of strain and temperature using interferometrically interrogated fiber Bragg grating sensors"*, Opt. Eng., Vol. 39 (8), pp. 2226-2234 (2000).

[29]. A N Chryssis, S M Lee, S B Lee, S S Saini and M Dagenais, "*High sensitivity evanescent field fiber Bragg grating sensors*," Photonics Technology Letters, Vol. 17 (6), pp. 1253-1255 (2005).

[30]. A Iadicicco, A Cusano, A Cutolo, R Bernini and M Giordano, "*Thinned fiber Bragg gratings as high sensitivity refractive index sensor*", Photonics Technology Letters, Vol. 16, pp. 1149-1151 (20048, No. 9, pp. 2226-2234, (2000).

[31]. A Iadicicco, A Cusano, S Campopiano, A Cutolo and M Giordano, "*Thinned fiber Bragg gratings as refractive index sensors*", Sensors Journal, Vol. 5, pp. 1288-1295 (2005).

[32]. H Xue Feng, C Zhe Min, S Li Yang, C Ke Fa, S De Ren, C Jun and Z Hao, "*Design and characteristics of refractive index sensor based on thinned and microstructure fiber Bragg grating*", Applied Optics, Vol. 47, pp. 504-511 (2008).

[33]. G Tsigaridas, D Polyzos, A Ioannou, M Fakis and P Persephonis, "*Theoretical and experimental study of refractive index sensors based on etched fiber Bragg gratings*", Sensors and Actuators A: Physical, Vol. 209, pp. 9-15 (2014).

[34]. A Cusano, A Iadicicco, S Campopiano, M Giordano and A Cutolo, *"Thinned and micro structured fiber Bragg gratings: Towards new all fiber high sensitivity chemical sensors*", J. Opt. A: Pure Applied Optics, 7, pp. 734-741 (2005).

[35]. K O Hill, "*Aperiodic distributed parameter waveguides for integrated optics*", Appl. Opt., Vol. 13, pp. 1853-1856 (1974).

[36]. K O Hill, F Bilodeau, B Malo, T Kitagawa, S Th´eriault, D C. Johnson, J Albert, and K Takiguchi, "*Aperiodic in-fiber Bragg gratings for optical fiber dispersion compensation*", Proc. Optic. Fiber Commun., OFC'94, San Jose, CA (1994).

[37]. K O Hill, S Th´eriault, B Malo, F Bilodeau, T Kitagawa, D C Johnson, J Albert, K Takiguchi, T Kataoka, and K Hagimoto, "*Chirped in-fiber Bragg grating dispersion compensators: Linearization of the dispersion characteristic and demonstration of dispersion compensation in a 100 km, 10 Gbit/s optical fiber link*", Electron. Lett., Vol. 30, pp. 1755-1756 (1994).

[38]. J A R Williams, I Bennion, K Sugden, and N J Doran, "*Fiber dispersion compensation using a chirped in-fire Bragg grating*", Electron. Lett., Vol. 30, pp. 985-987 (1994).

[39]. R Kashyap, S V Chernikov, P F McKee, and J R Taylor, "*30 ps chromatic dispersion compensation of 400 fs pulses at 100 Gbits/s in optical fibers using an all fiber photoinduced chirped reflection grating*", Electron. Lett., Vol. 30, pp. 1078-1080 (1994).

[40]. K O Hill, F Bilodeau, B Malo, T Kitagawa, S Th´eriault, D C Johnson, J Albert, and K Takiguchi, "*Chirped in-fiber Bragg grating for compensation of optical fiber dispersion*", Opt. Lett., Vol. 19, pp. 1314-1316, (1994).

[41]. K O Hill, B Malo, F Bilodeau, S Th´eriault, D C Johnson, and J Albert, "*Variable-spectral-response optical waveguide Bragg grating filters for optical signal processing*", Opt. Lett., Vol. 20, pp. 1438-1440 (1995).

[42]. K O Hill, D C. Johnson, F Bilodeau, and S Faucher, "*Narrow bandwidth optical waveguide transmission filters: A new design concept and applications to optical fiber communications*", Electron. Lett., Vol. 23, pp. 465-466 (1987).

[43]. D C Johnson, K O Hill, F Bilodeau, and S Faucher, "*New design concept for a narrowband wavelength selective optical tap and combiner*", Electron. Lett., Vol. 23, pp. 668-669 (1987).

[44]. I Baumann, J Seifert, W Nowak, and M Sauer, "*Compact all-fiber add/drop multiplexer using fiber Bragg gratings*", Photon. Technol. Lett., Vol. 8, pp. 1331-1333 (1996).

[45]. L Dong, P Hua, T A Birks, L Reekie, and P S J Russell, "*Novel add/drop filters for wavelength division multiplexing optical fiber systems using a Bragg grating assisted mismatched coupler*", Photon. Technol. Lett., Vol. 8, pp. 1656-1658 (1996).

[46]. F Bilodeau, K O Hill, B Malo, D C Johnson, and J Albert, "*High return loss narrowband all-fiber bandpass Bragg transmission filter*", Photon. Technol. Lett., Vol. 6, pp. 80-82 (1994).

[47]. F Bilodeau, D C Johnson, S Th´eriault, B Malo, J Albert, and K O Hill, "*An all-fiber dense wavelength division multiplexer/demultiplexer using*

*photoimprinted Bragg gratings*", Photon. Technol. Lett., Vol. 7, pp. 388-390 (1995).

[48]. R Kashyap, R Wyatt, and P F McKee, "*Wavelength flattened saturated erbium amplifier using multiple sidetap Bragg gratings*", Electron. Lett., Vol. 29, pp. 1025-1026 (1993).

[49]. R Kashyap, R Wyatt, and R J Campbell, "*Wideband gain flattened erbium fiber amplifier using a photosensitive fiber blazed grating*", Electron. Lett., Vol. 24 (2), pp. 154-156 (1993).

[50]. C E Soccolich, V Mizrahi, T Erdogan, P J LeMaire, and P Wyscoki, "*Gain enhancement in EDFA's by using fiber grating pump reflectors*", Proc. Optic. Fiber Communication, OFC'94, San Jose, CA (1994).

[51]. V L da Silva, P B. Hansen, L Eskildsen, D L Wilson, S G Grubb, V Mizrahi, W Y Cheung, T Erdogan, T A Strasser, J E J Alphonsus, S J R and D J Di Giovanni, "*15.3 dB power budget improvement by remotely pumping an EDFA with a fiber grating pump reflector*", Proc. Optic Fiber Communication, OFC '95, San Diego, CA (1995).

[52]. J Capmany, D Pastor, and J Marti, "*EDFA gain equalizer employing linearly chirped apodized fiber gratings*", Microwave and Optic. Technol. Lett., Vol. 12, pp. 158-160 (1996).

[53]. C R Giles, T Erdogan and V Mizrahi, "*Simultaneous wavelength stabilization of 980 nm pump lasers*", Photon. Technol. Lett., Vol. 6, pp. 907-909 (1994).

[54]. B F Ventrudo, G A Rogers, G S Lick, D Hargreaves, and T N Demayo, "*Wavelength and intensity stabilization of 980 nm diode lasers coupled to fiber Bragg gratings*", Electron. Lett., Vol. 30, pp. 2147-2149 (1994).

[55]. G A Ball and W W Morey, "*Efficient integrated $Nd^{3+}$ fiber laser*", Photon. Technol. Lett., Vol. 3, pp. 1077-1078 (1991).

[56]. G A Ball and W W Morey, "*Continuously tunable single mode erbium fiber laser*", Opt. Lett., Vol. 17, pp. 420-422 (1992).

[57]. G A Ball, W W Morey, and W H Glenn, "*Standing wave monomode erbium fiber laser*", Photon. Technol. Lett., Vol. 3, pp. 613-615 (1991).

[58]. G A Ball, W H Glenn, W W Morey, and P K Cheo, "*Modeling of short, single-frequency, fiber lasers in high gain fiber*", Photon. Technol. Lett., Vol. 5, pp. 649-651 (1993).

[59]. G A Ball and W H. Glenn, "*Design of a single mode linear cavity erbium fiber laser utilizing Bragg reflectors*", J. Lightwave Technol., vol. 10, pp. 1338–1343 (1992).

[60]. M Sejka, P Varming, J Hubner, and M Kristensen, "*Distributed feedback $Er^{3+}$-doped fiber laser*", Electronics Letters, vol. 31, pp. 1445-1446 (1995).

[61]. G A Ball, G Hull-Allen, C Holton, and W W Morey, "*Low noise single frequency linear fiber laser*", Electron. Lett., Vol. 29, pp. 1623-1625 (1993).

[62]. J D Minelly, A Galvanauskas, M E Fermann, and D Harter, "*Femtosecond pulse amplification in cladding pumped fibers*", Opt. Lett., Vol. 20, pp. 1797-1799 (1995).

[63]. A Galvanauskas, P A Krug, and D Harter, "*Nanosecond to picosecond pulse compression with fiber gratings in a compact fiber based chirped pulse amplification system*", Opt. Lett., vol. 21, pp. 1049-1051 (1996).

[64]. M E Fermann, K Sugden, and I Bennion, "*High power soliton fiber laser based on pulse width control with chirped fiber Bragg gratings*", Opt. Lett., Vol. 20, pp. 172-174 (1995).

[65]. P A Morton, V Mizrahi, S G Kosinski, L F Mollenauer, T Tanbun- Ek, R A Logan, D L Coblentz, A M Sergent, and K W Wecht, "*Hybrid soliton pulse source with fiber external cavity and Bragg reflector*", Electron. Lett., Vol. 28, pp. 561-562 (1992).

[66]. P A Morton, V Mizrahi, P A Andrekson, T Tanbun-Ek, R A Logan, P Lemaire, D L. Coblentz, A M Sergent, K W Wecht, and P R Sciortino Jr., "*Mode locked hybrid soliton pulse source with extremely wide operating frequency range*", Photon. Technol. Lett., Vol. 5, pp. 28-31 (1993).

[67]. S M Lord, G W Switzer, and M A Krainak, "*Using fiber gratings to stabilise laser diode wavelength under modulation for atmospheric lidar transmitters*", Electron. Lett., Vol. 32, pp. 561-563 (1996).

[68]. T Erdogan, A Partovi, V Mizrahi, P J Lemaire, W L Wilson, T A Strasser, and A M. Glass, "*Volume gratings for holographic storage applications written in high quality germanosilicate glass*", Appl. Opt., Vol. 34, pp. 6738-6743 (1995).

[69]. K O Hill, T Kitagawa, S Th´eriault, F Bilodeau, D C Johnson, B Malo, and J Albert, "*Novel applications of photosensitivity in Ge doped silica: Bragg grating matched filtering for optical fiber dispersion compensation and multilayer optical storage medium*", Proc. 7th Annual. Meeting, IEEE Lasers and Electro-Opt. Soc., LEOS'94, Boston, MA (1994).

[70]. L S Pieter, M L Beatrys and A C Anatoli, "*Chirped fiber Bragg grating sensor for pressure and position sensing*", Opt. Eng., Vol. 44, 054402 (2005).

[71]. L Liu, Q Zhao, W Zhang, H Zhang, L Jin, L Zhao, Y Yan and S Gao, "*Fiber grating pressure sensor with enhanced sensitivity*", Proc. SPIE, Vol. 5623, pp. 16–19 (2005).

[72]. B K A Ngoi, J Paul, L P Zhao and Z P Fang, "*Enhanced lateral pressure tuning of fiber Bragg gratings by polymer packaging*", Opt. Communication, Vol. 242, pp.425-430 (2004).

[73]. M G Xu, L Reekie, Y T Chow and J P Dakin, "*Optical in-fiber grating high pressure sensor*", Electron. Lett., Vol. 29, pp. 398-399 (1993).

[74]. T L Yeo, T Sun, K T V Grattan, D Parry, R Lade and B D Powell, "*Characterization of a polymer coated fiber Bragg grating sensor for relative humidity sensing*", Sensors Actuators B, Vol. 110, pp. 148-55 (2005).

[75]. R M Measures, "*Structural Health Monitoring with Fiber Optic Technology*", New York: Academic (2001).

[76]. S H Jan, Y F Ming, C T Chiang, M L Chia, L W Fung and S B Sheau, "*High sensitivity pressure sensor based on a fiber Bragg grating*", Proc. SPIE, Vol. 5272, pp.248-254 (2004).

[77]. R R J Maier, J S Barton, J D C Jones, S McCulloch and G Burnell, "*Dual fiber Bragg grating sensor for barometric pressure measurement*", Meas. Sci. Technol. 14, pp. 2015–2020 (2003).

[78]. H J Sheng, M Y Fu, C C Tzu, W L Fung and B S Shong, "*A lateral pressure sensor using a fiber Bragg grating*", Photon. Technol. Lett., Vol. 16, pp. 1146-1148 (2004).

[79]. Y Zhang, D Feng, Z Liu, Z Guo, X Dong, K S Chiang and B C B Chu, "*High sensitivity pressure sensor using a shielded polymer coated fiber Bragg grating*", Photon. Technol. Lett., Vol. 13, pp. 618-619 (2001).

[80]. Dennison C R, Wild P M, Wilson D R and Cripton P A, "*A minimally invasive in-fiber Bragg grating sensor for intervertebral disc pressure measurements*", Meas. Sci. Technol., Vol. 19, 085201 (2008).

[81]. C R Dennison, P M Wild, M F S Dvorak, D R Wilson and P A Cripton "*Validation of a novel minimally invasive intervertebral disc pressure sensor utilizing in-fiber Bragg gratings in a porcine model: An ex vivo study*", Spine, Vol. 33, pp. E589-594 (2008).

[82]. C M Lawrence, D V Nelson and E Udd, "*Multi parameter sensing with fiber Bragg gratings*", Proc. SPIE, Vol. 2872, pp. 24-31 (1996).

[83]. E Udd, "*Fiber optic sensors An Introduction for Engineers and Scientists*", New York: Wiley-InterScience (1991).

[84]. Y Liu, Z Guo, Y Zhang, K Seng, C Dong and X Dong, "*Simultaneous pressure and temperature measurement with polymer coated fiber Bragg grating*", Electron. Lett. Vol. 36, pp. 564-566 (2000).

[85]. Nunes L C S, Valente L C G, Llerena R W A, Braga A M B and Triques A L C "*Simultaneous measurement of temperature and pressure using single fiber Bragg grating and fixed filter demodulation technique*", Proc. SPIE 5622 pp. 906–911 (2004).

[86]. A Sun, X G Qiao, Z A Jia, M Li and D Z Zhao, *"Study of simultaneous measurement of temperature and pressure using double fiber Bragg gratings with polymer package*", Opt. Eng., Vol. 44 (3), 034402 (2005).

[87]. S Huang, M LeBlanc, M M Ohn and R M Measures, "*Bragg intra grating structural sensing*", Appl. Opt., Vol. 34, pp. 5003–5009 (1995).

[88]. M G Xu, H Geiger and J P Dakin, "*Fiber grating pressure sensor with enhanced sensitivity using a glass bubble housing*", Electron. Lett., Vol. 32, pp. 128–129 (1996).

[89]. Abe I, Frazao O, Schiller M W, Nogueira R N, Kalinowski H J and Pinto J L, "*Bragg gratings in normal and reduced diameter high birefringence fiber optics*", Meas. Sci. Technol., Vol. 17, pp. 1477-1484 (2006).

[90]. Tran T V A, Han Y-G, Lee Y J, Kim S H and Lee S B, "*Performance enhancement of long distance simultaneous measurement of strain and temperature based on a fiber Raman laser with an etched FBG*", Photon. Technol. Lett. 17, pp. 1920–1922 (2005)

[91]. E Udd, C Lawrence and D Nelson, "*Development of a three axis strain and temperature fiber optic grating sensor*", Proc. SPIE, 3042, pp. 229-236 (1997).

[92]. A F Fernandez, B Brichard, F Berghmans and M Decreton, "*Dose rate dependencies in gamma irradiated fiber Bragg grating filters*", IEEE Trans. Nucl. Sci., Vol. 49, pp. 2874-2878 (2002).

[93]. D Sengupta, "*Study on discrete and continuous liquid level measurements using fiber bragg gratings*", Ph.D. Thesis, NIT, Warangal (2012).

[94]. D Sengupta, M S Shankar, P SReddy, R L N Sai Prasad, K Srimannarayana, "*Liquid level measurement using bragg grating sensor*", Optoelectronics and Advanced Materials – Rapid Communications Vol. 5, No. 7, pp. 742 – 744 (2011).

[95]. P Giaccari, H G Limberger and P Kronenberg, "*Influence of humidity and temperature on polyimide coated fiber Bragg gratings*", Proc. Trends in Optics and Photonics Series: Bragg Gratings, Photosensitivity, and Poling in Glass Waveguides vol 61, BFB2 (2001).

[96]. M Laylor, S Calvert, T Taylor, W Schulz, R Lumsden and E Udd, "*Fiber optic grating moisture and humidity sensors*", Proc. Smart Structures and Materials: Smart Sensor Tech. and Measurement System, Vol. 4694, pp. 210-217 (2002).

[97]. T L Yeo, T Sun, K T V Grattan, D Parry, R Lade and B D Powell, "*Polymer coated fiber Bragg grating for relative humidity sensing*", IEEE Sensors, Vol. 5, pp. 1082-1089 (2005).

[98]. P Kronenberg and P K Rastogi, P Giaccari and H G Limberger, "*Relative humidity sensor with optical fiber Bragg gratings*", Opt. Lett., Vol. 27 (16 0, pp. 1385-1387 (2002).

[99]. A Asseh, S Sandgren, H Ahlfeldt, B Sahlgren, R Stubbe and G Edwall, "*Fiber optical Bragg grating refractometer*", Fiber and Integrated Optics, Vol. 17, pp. 51-62 (1998).

[100]. A Iadicicco, S Campopiano, A Cutolo, M Giordano, and A Cusano, "*Self-temperature referenced refractive index sensor by nonuniform thinned fiber Bragg gratings*", Sensors and Actuators B, Vol. 120, pp. 231-237 (2006).

[101]. K Schroeder, W Ecke, R Mueller, R Willsch and A Andreev, "*A fiber Bragg grating refractometer*", Meas. Sci. Technol., Vol. 12, pp. 757-764 (2001).

[102]. G B Tait, G C Tepper, D Pestov, and P M Boland, "*Fiber Bragg grating multifunctional chemical sensor*", Proc. SPIE Vol. 5994, 599407 (2005).

[103]. B Scott, C Ma, G Pickrell, K Cooper, A Wang, and T Ooi, "*Novel chemical and biological fiber optic sensor*", Proc. SPIE, 6556, 65560F (2007).

[104]. P Lu, L Men, and Q Chen, "*Tuning the sensing responses of polymer coated fiber Bragg gratings*", J. Appl. Phys., Vol. 104, 116110, (2008).

[105]. K Zhou, Y Lai, X Chen, K Sugden, L Zhang, and I Bennion, "*A refractometer based on a micro slot in a fiber Bragg grating formed by chemically assisted femtosecond laser processing*", Opt. Express, Vol. 15, pp. 15848-15853 (2007).

[106]. W Liang, Y Huang, Y Xu, R K Lee, and A Yariv, "*Highly sensitive fiber Bragg grating refractive index sensors*", Appl. Phys. Lett., Vol. 86, 151122 (2005).

[107]. D A Pereira, O Frazao, and J L Santos, "*Fiber Bragg grating sensing system for simultaneous measurement of salinity and temperature*," Opt. Eng., Vol. 43 (2), pp. 299-304 (2004).

[108]. A N Chryssis, S S Saini, S M Lee, Y Hyunmin, W E Bentley and M Dagenais "*Detecting hybridization of DNA by highly sensitive evanescent field etched core fiber Bragg grating sensors*", IEEE J. Selected Topics: Quantum Electronics, Vol. 11, pp. 864-872 (2005).

[109]. S S Saini, C Stanford, S M Lee, J Park, . Deshong, W E Bentley and M Dagenais, "*Monolayer detection of Biochemical agents using etched core fiber Bragg grating sensors*", Photonics Technology Letters, Vol. 19, pp. 1341-1343 (2007).

[110]. G Ryu, M Dagenais, M T Hurley and P Deshong, "*High specificity binding of lectins to carbohydrate functionalized fiber Bragg gratings: A new model for bio sensing applications*", IEEE J. Quantum Electronics, Vol. 16, pp. 647-653 (2010).

[111]. G Gopalakrishnan, M Serene, R Jacob, G Amit, S K Sudheer, Z C Alex, S Abraham, S M Hardas and A R Krishnan, "F*iber Bragg grating based temperature and strain sensor simulation for biomedical applications*", Optoelectronics and advanced materials – Rapid communications, Vol. 2 (1), pp. 10 -14 (2008).

[112]. V Mishra, N Singh, U Tiwari and P Kapur, "*Fiber grating sensors in medicine: Current and emerging applications*", Sensors and Actuators A, Vol. 167, pp. 279-290 (2011).

[113]. T M Libish, M C Bobby, C L Linslal,, S Mathew,, C Pradeep, S Indu, P Biswas, S Bandhyopadyay, K Dasgupta, V P N Nampoori and P Radhakrishnan, "*Etched and DNA coated fiber Bragg grating based biosensor for protein concentration measurement*", Optoelectronics and Advanced Materials – Rapid Communications Vol. 9, no. 11-12, pp. 1401 – 1405 (2015).

[114]. B Kawasaki, K O Hill, D C Johnson and Y Fujii, "*Narrow band Bragg reflectors in optical fibers*", Optics Letters, Vol. 3, pp. 66-68 (1978).

[115]. B Wang, J Huang and M Li, X Zhou, "*Multifunctional sensing film used for fiber optic cholesterol sensor*", Proc. SPIE, Vol. 7278, (2009).

[116]. M S Jadhav, L S Laxmeshwar, J F Akki, P U Raikar, J Kumar, O Prakash and U S Raikar "*Fluoride contamination sensor based on optical fiber grating technology*", J. Opt. Fiber Tech., Vol. 38, pp. 136–141(2017).

[117]. L S Laxmeshwar, M S Jadhav, J F Akki, P U Raikar, J Kumar, O Prakash and U S Raikar, "*Highly sensitive fiber grating chemical sensors: An effective alternative to atomic absorption spectroscopy*", J. Opt. & Laser Tech., Vol. 91, pp. 27–31 (2017).

[118]. V Semwal and B D Gupta, "*LSPR and SPR based fiber optic cholesterol sensor using immobilization of cholesterol oxidase over silver nanoparticles coated graphene oxide nanosheets*", J. IEEE Sensors, Vol. 18, No. 3, pp.1039-46 (2018).

[119]. R Verma, S K Srivastava, and B D Gupta, "*Surface plasmon resonance based fiber optic sensor for the detection of low density lipoprotein*", J. IEEE Sensors, Vol. 12, No. 12, pp. 3460-3466 (2012).

[120]. G Kaur, M Tomar and V Gupta, "*Nanostructured zinc oxide thin film for application to surface plasmon resonance based cholesterol biosensor*", Proc. SPIE, Vol. 9667, pp. 966706-1-4 (2015).

# Chapter 5

# Tilted Fiber Bragg Grating Sensor

*Abstract*

*This chapter discusses Tilted Fiber Bragg Grating sensors for cholesterol measurements. The TFBG sensors have the benefit of intensity measurements, unlike wavelength measurements in the case of LPGs and FBGs. This makes the experimental procedures and analysis simpler at a lower cost. The sensor head with and without chitosan coating, employed for the detection and estimation of total cholesterol dissolved in coconut oil is detailed in this chapter.*

***C B Mathews** et al., Proc. Photonics 2016: 13th Int. Conf. on Fiber Optics and Photonics, OSA Tech. Digest, OSA, P1A5 (2016).*

## 5.1 Introduction

Optical fiber gratings are sensitive to external perturbations like temperature, strain and SRI. Several applications of fiber gratings were reported earlier employing their sensitivities to these parameters. Detailed discussion on the working principle and the sensitivities of LPG and FBG were presented in previous chapters. Total cholesterol concentration measurement techniques were presented in chapters 2, 3 and 4, exploiting the RI sensitivity of these optical fiber gratings. It was also demonstrated that the sensitivity of the grating sensor heads could be enhanced by the use of chitosan coating.

Since the invention of photosensitivity in optical fibers and demonstration of fiber grating by Hill et al. in 1978 [1], the discussions were centered around FBG and its applications in various fields. In 1990, the mode coupling model of tilted fiber Bragg grating (TFBG) was presented of for the first time by Meltz et al., at the Optical Society of America (OSA) conference on Optical Fiber Communication (OFC'90) [2]. In this paper, they discussed the radiation mode coupling. They also demonstrated the enhancement of mode coupling in phase gratings by the introduction of some tilt angle between the wave vector and fiber axis.

Unlike FBGs, the grating planes of TFBG are having a certain angle with respect to the fiber axis, making its structural properties different. These characteristics made TFBG a promising contender as fiber optic components with new functionalities and usages. Hence, TFBGs have been subjected to various studies right from its birth.

This section introduces the principle of operation of fiber optic tilted fiber Bragg grating. Subsequently total cholesterol concentration measurement using TFBG is detailed here. In order to improve the

sensitivity of cholesterol measurements, chitosan was coated around the TFBG. The results of cholesterol measurements with these sensor heads are described in this chapter. TFBG sensors have the advantage of amplitude or intensity measurements, rather than the wavelength modulation techniques used along with LPGs and FBGs. The costlier wavelength interrogators can be replaced with simpler power meters. This reduces the cost of the appliances required to a great extent and also makes the analysis of the experimental results easier.

## 5.2 TFBG: Basic principle of operation

A tilted Bragg grating is made up of alternate low and high RI bands in the core of the optical fiber just like an FBG. The only difference is that the grating planes are tilted at an angle to the axis of the fiber whereas in FBGs, the grating planes are perpendicular to the axis of the fiber.

All factors like the wavelength used for writing the grating, the magnitude of the RI change induced, the pitch or period of the optical fiber, the RI pattern formed, length of the grating etc., which determine the response characteristics of FBGs, also influence the characteristics of the TFBG. Along with these factors, the orientation or the tilt angle of the grating planes, also influence the response of a TFBG. The theory and working principle of TFBGs with uniform periodicity is discussed in this section.

Considering the cylindrical symmetry of the optical fiber, the RI modulation induced in the fiber core due to the exposure to UV radiations during the process of TFBG fabrication can be expressed as [3]:

$$n_{eff}^{co}(x,y,z) = n_o(x,y,z) + \Delta n(x,y,z)\cos\left[\left(\frac{4\pi}{\Lambda_g}\right)(z\cos\alpha) + (y\sin\alpha)\right] \ldots\ldots (5.1)$$

where, $n_0$ is the average RI of the fiber core, z represents the distance along the fiber axis, y is the radial distance from the axis, Δn denotes the amplitude of

the induced RI perturbation, $\Lambda_g$ is the period along the plane of the grating or the period of the UV pattern used for the fabrication of the grating and α is the tilt angle.

Considering only one direction, i.e. the direction of propagation of light inside the fiber, the above equation can be simplified as:

$$n_{eff}^{co}(z) = n_o + \Delta n \cos\left(\frac{4\pi z}{\Lambda_g}\cos\alpha\right) \quad \text{..... (5.2)}$$

As the light launched into the optical fiber travels through the induced RI perturbations (TFBG), a small portion of the incident light is reflected or coupled backwards inside the core of the fiber, from the grating planes. Out of these reflections in the core, the wavelength satisfying the Bragg condition adds up to form a strong reflected signal, as illustrated in Fig.5.1. This wavelength, which is reflected from the TFBG, is termed as the Bragg wavelength ($\lambda_B$) [4-9].

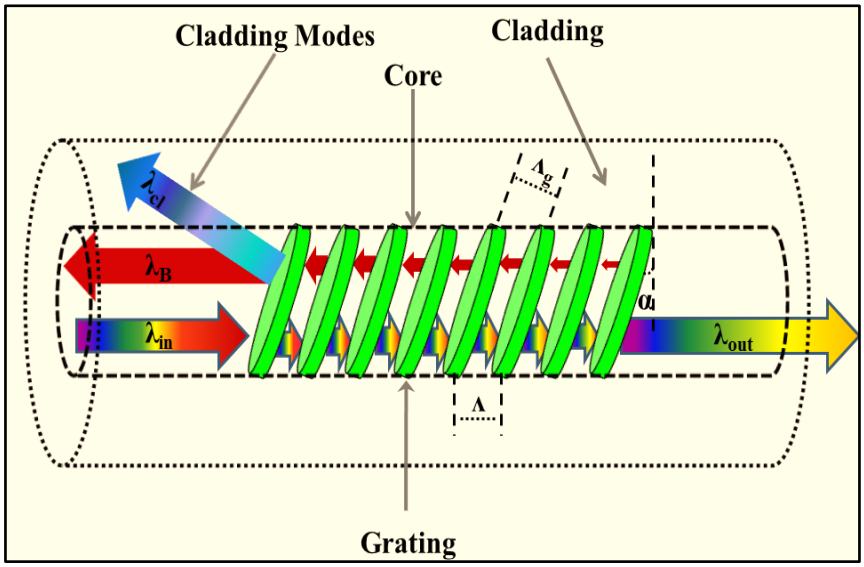


***Figure 5.1:*** *Illustration - Light coupling in Tilted FBG.*

Along with this Bragg reflection, another portion of the forward propagating core mode is also coupled to the cladding. Due to the presence

of the tilt in the grating planes, some reflections become off axis at these planes. Thus, each grating plane reflects a little bit of light towards the cladding. These off axis reflections contribute to the development of backward propagating cladding modes at the phase matched wavelengths. Typical transmission spectrum of TFBG plotted at Polytechnique, Montréal, Canada, is given in Fig.5.2.

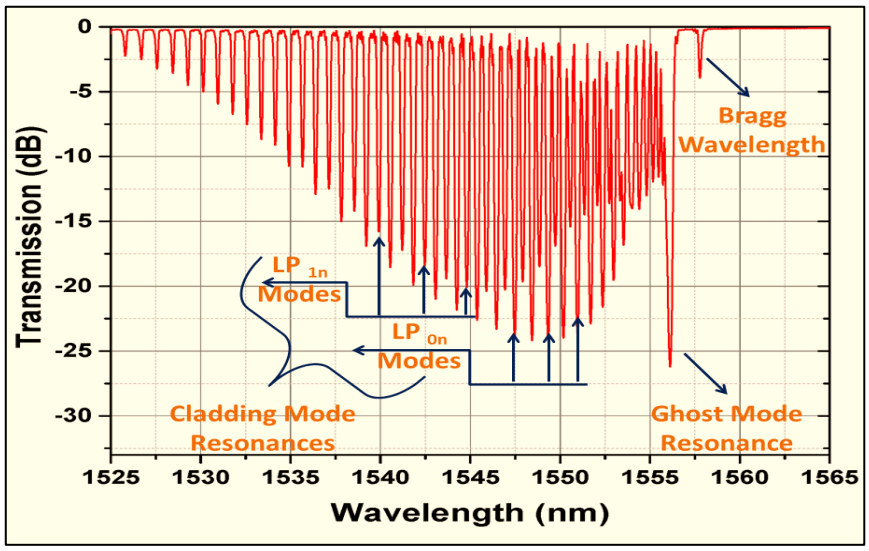


***Figure 5.2:*** *Typical transmission spectra of TFBG (Rrecorded at Polytechnique, Montréal, Canada).*

### 5.2.1 TFBG: Mode coupling

TFBGs work by coupling the forward propagating core modes to the back propagating core modes and cladding modes whereas in FBGs the coupling is only to the backward propagating core modes. These mode couplings in TFBG can be explained by the coupled mode theory developed in 1981 by Lam et al. [10]. To study the spectral characteristics and mode coupling in TFBG, Erdogan et al. in 1996, used coupled mode theory [3].

Further developments on mode coupling in TFBG were presented by A Bouzid and M A G Abushagur in 1997 [11].

The phase matching condition in an optical fiber grating is given by [3 – 12]:

$$\beta_1 - \beta_2 = \Delta\beta = \frac{2\pi}{\Lambda} \quad \text{(5.3)}$$

where, $\beta_1$ and $\beta_2$ denote the propagation constants of the coupled modes and $\Lambda$ represents the period of the grating along the axis. Accounting for the reflected core and cladding modes in a TFBG, the above expression can be more generalized as:

$$\beta_{\text{forward}} - (-\beta_{\text{backward}}) = \Delta\beta = \frac{2\pi}{\Lambda} \quad \text{(5.4)}$$

where, $\beta_{\text{forward}} = \frac{2\pi n_{\text{eff}}^{\text{co}}}{\lambda}$ denotes the propagation constant of the forward propagating core mode and $\beta_{\text{backward}} = \frac{2\pi n_{\text{eff}}^{\text{j}}}{\lambda}$ represents the propagation constant of the reflected core mode (denoted as j = co) or cladding mode (denoted as j = cl). '-' sign of $\beta_{\text{backward}}$ indicates the propagation of the reflected modes in the reverse direction.

Hence, equation 5.4 can be rewritten as:

$$\frac{2\pi n_{\text{eff}}^{\text{co}}}{\lambda} - \left(-\frac{2\pi n_{\text{eff}}^{\text{j}}}{\lambda}\right) = \Delta\beta = \frac{2\pi}{\Lambda} \quad \text{(5.5)}$$

i.e., $$\frac{n_{\text{eff}}^{\text{co}} + n_{\text{eff}}^{\text{j}}}{\lambda} = \Delta\beta = \frac{1}{\Lambda} \quad \text{(5.6)}$$

### 5.2.2 TFBG: Reflected Bragg Wavelength

For the reflected Bragg wavelength $\lambda = \lambda_B$, $n_{\text{eff}}^{\text{j}} = n_{\text{eff}}^{\text{co}}$, then equation 5.6 reduces to the Bragg condition of TFBG [11- 17]:

$$\lambda_B = 2n_{\text{eff}}^{\text{co}}\,\Lambda \quad \text{(5.7)}$$

where, $\lambda_B$ is the Bragg wavelength and $n_{eff}^{co}$ represents the effective RI of the fiber core and $\Lambda$ denotes the grating pitch along the axis of the fiber. By the fiber geometry:

$$\Lambda = \frac{\Lambda_g}{\cos\alpha} \quad \text{..... (5.8)}$$

Then $\lambda_B$ becomes:

$$\lambda_B = 2n_{eff}^{co}\frac{\Lambda_g}{\cos\alpha} \quad \text{..... (5.9)}$$

### 5.2.3 TFBG: Reflected Cladding Modes

Considering all the reflected cladding modes at $\lambda = \lambda_{cl,i}$, $n_{eff}^{j} = n_{eff,i}^{cl}$, equation 5.6 can be rewritten as [11, 12]:

$$\frac{n_{eff,i}^{co} + n_{eff,i}^{cl}}{\lambda_{cl,i}} = \Delta\beta = \frac{1}{\Lambda} \quad \text{..... (5.10)}$$

where, i = 1, 2, 3…..m (m is the total number of cladding modes), $n_{eff,i}^{co}$ is the effective refractive indices of core at each wavelength of the cladding mode. Substituting the value of $\Lambda = \frac{\Lambda_g}{\cos\alpha}$ and rearranging the expression for the reflected cladding modes in a TFBG can be expressed as [11- 17]:

$$\lambda_{cl,i} = \left(n_{eff,i}^{co} + n_{eff,i}^{cl}\right)\frac{\Lambda_g}{\cos\alpha} \quad \text{..... (5.11)}$$

These cladding modes are attenuated easily within a short distance from the grating and are not visible in the reflected spectrum [15]. However, these modes are clearly visible in the transmission spectrum as loss bands at definite wavelengths as in the case of the transmission spectrum of an LPG, as shown in Fig.5.2. Thus, the TFBG works by coupling the forward propagating core modes to the backward propagating core modes at the Bragg wavelength and to a large number of cladding modes ($LP_{0n}$, $LP_{1n}$, etc.) at definite wavelengths [16]. The spectrum of TFBG also consists of a strong loss peak named as the ghost mode resonance, just below the Bragg wavelength [17-19]. This ghost mode is made up of several lower order cladding modes.

## 5.3 TFBG: Sensing Principle

TFBGs are being employed as the sensing elements to monitor physical, chemical as well as biological parameters. From equation 5.9, it is clear that, the reflected Bragg wavelength ($\lambda_B$) of a TFBG is a function of the grating pitch ($\Lambda = \frac{\Lambda_g}{\cos\alpha}$) and the effective RI ($n_{eff}^{co}$) of the fiber core. Hence, a shift in $\lambda_B$ can be induced by a change in the $n_{eff}^{co}$ or $\Lambda$ or both these parameters. Physical parameters like strain ($\varepsilon$), temperature (T) and SRI ($n_{sur}$) are the possible external perturbations which can initiate changes in $n_{eff}^{co}$ or $\Lambda$ or both. This can be mathematically expressed as:

$$\Delta\lambda_B = \frac{\partial\lambda_B}{\partial\varepsilon}\Delta\varepsilon + \frac{\partial\lambda_B}{\partial T}\Delta T + \frac{\partial\lambda_B}{\partial n_{sur}}\Delta n_{sur} \quad \text{..... (5.12)}$$

Substituting $\lambda_B = 2n_{eff}^{co}\frac{\Lambda_g}{\cos\alpha}$ in equation 5.12 and expanding, the above expression can be written as:

$$\begin{aligned} d\lambda_B = {} & \frac{2}{\cos\alpha}\left(\Lambda_g\frac{\partial n_{eff}^{co}}{\partial\varepsilon} + n_{eff}^{co}\frac{\partial\Lambda_g}{\partial\varepsilon}\right)d\varepsilon \\ & + \frac{2}{\cos\alpha}\left(\Lambda_g\frac{\partial n_{eff}^{co}}{\partial T} + n_{eff}^{co}\frac{\partial\Lambda_g}{\partial T}\right)dT \\ & + \frac{2}{\cos\alpha}\left(\Lambda_g\frac{\partial n_{eff}^{co}}{\partial n_{sur}} + n_{eff}^{co}\frac{\partial\Lambda_g}{\partial n_{sur}}\right)dn_{sur} \quad \text{..... (5.13)} \end{aligned}$$

The above equation represents the effect of strain, temperature and SRI respectively on the Bragg wavelength shift. Since, the grating pitch is independent of the influence of SRI, the factor $\frac{\partial\Lambda_g}{\partial n_{sur}}$ in the third term reduces to zero.

Then, the above expression reduces to:

$$\begin{aligned} d\lambda_B = {} & \frac{2}{\cos\alpha}\left(\Lambda_g\frac{\partial n_{eff}^{co}}{\partial\varepsilon} + n_{eff}^{co}\frac{\partial\Lambda_g}{\partial\varepsilon}\right)d\varepsilon \\ & + \frac{2}{\cos\alpha}\left(\Lambda_g\frac{\partial n_{eff}^{co}}{\partial T} + n_{eff}^{co}\frac{\partial\Lambda_g}{\partial T}\right)dT \\ & + \frac{2}{\cos\alpha}\left(\Lambda_g\frac{\partial n_{eff}^{co}}{\partial n_{sur}}\right)dn_{sur} \quad \text{..... (5.14)} \end{aligned}$$

As explained in the previous chapter, the basic factors that can directly tune the grating pitch of a grating are the strain and the temperature. Then, equation 5.14 reduces to:

$$d\lambda_B = \frac{2}{\cos\alpha}\left(\Lambda_g \frac{\partial n_{eff}^{co}}{\partial \varepsilon} + n_{eff}^{co} \frac{\partial \Lambda_g}{\partial \varepsilon}\right) d\varepsilon + \frac{2}{\cos\alpha}\left(\Lambda_g \frac{\partial n_{eff}^{co}}{\partial T} + n_{eff}^{co} \frac{\partial \Lambda_g}{\partial T}\right) dT \quad \text{(5.15)}$$

Dividing equation 5.15 by $\lambda_B = 2n_{eff}^{co} \frac{\Lambda_g}{\cos\alpha}$, it becomes,

$$\frac{d\lambda_B}{\lambda_B} = \left(\frac{1}{n_{eff}^{co}} \frac{\partial n_{eff}^{co}}{\partial \varepsilon} + \frac{1}{\Lambda_g}\frac{\partial \Lambda_g}{\partial \varepsilon}\right) d\varepsilon + \left(\frac{1}{n_{eff}^{co}} \frac{\partial n_{eff}^{co}}{\partial T} + \frac{1}{\Lambda_g} \frac{\partial \Lambda_g}{\partial T}\right) dT \quad \text{(5.16)}$$

Equation 5.16 explains the shift of the Bragg wavelength of a TFBG under the influence of strain and temperature.

The influence of these parameters like strain (ε), temperature (T) and SRI or surrounding RI ($n_{sur}$), on the reflected cladding modes can be mathematically expressed as:

$$\Delta\lambda_{cl,i} = \frac{\partial \lambda_{cl,i}}{\partial \varepsilon} \Delta\varepsilon + \frac{\partial \lambda_{cl,i}}{\partial T} \Delta T + \frac{\partial \lambda_{cl,i}}{\partial n_{sur}} \Delta n_{sur} \quad \text{(5.17)}$$

Doing a mathematical treatment similar to that done earlier for the reflected Bragg wavelength, on equation 5.17, we get the expression for the shift in the wavelengths of these cladding modes as:

$$d\lambda_{cl,i} = \frac{1}{\cos\alpha}\left(\Lambda_g \frac{\partial (n_{eff,i}^{co} + n_{eff,i}^{cl})}{\partial \varepsilon} + (n_{eff,i}^{co} + n_{eff,i}^{cl}) \frac{\partial \Lambda_g}{\partial \varepsilon}\right) d\varepsilon + \frac{1}{\cos\alpha}\left(\Lambda_g \frac{\partial (n_{eff,i}^{co} + n_{eff,i}^{cl})}{\partial T} + (n_{eff,i}^{co} + n_{eff,i}^{cl}) \frac{\partial \Lambda_g}{\partial T}\right) dT + \frac{1}{\cos\alpha}\left(\Lambda_g \frac{\partial (n_{eff,i}^{co} + n_{eff,i}^{cl})}{\partial n_{sur}}\right) dn_{sur} \quad \text{(5.18)}$$

Proceeding further with similar mathematical treatment leads to the expression for the shift of the reflected cladding modes of a TFBG under the influence of strain, temperature and surrounding refractive index as:

$$\frac{d\lambda_{cl,i}}{\lambda_{cl,i}} = \left(\frac{1}{(n_{eff,i}^{co} + n_{eff,i}^{cl})} \frac{\partial(n_{eff,i}^{co} + n_{eff,i}^{cl})}{\partial\varepsilon} + \frac{1}{\Lambda_g}\frac{\partial\Lambda_g}{\partial\varepsilon}\right) d\varepsilon$$
$$+\left(\frac{1}{(n_{eff,i}^{co} + n_{eff,i}^{cl})} \frac{\partial(n_{eff,i}^{co} + n_{eff,i}^{cl})}{\partial T} + \frac{1}{\Lambda_g}\frac{\partial\Lambda_g}{\partial T}\right) dT$$
$$+\left(\frac{1}{(n_{eff,i}^{co} + n_{eff,i}^{cl})} \frac{\partial(n_{eff,i}^{co} + n_{eff,i}^{cl})}{\partial n_{sur}}\right) dn_{sur} \quad \text{(5.19)}$$

Equation 5.18 shows that, the cladding mode resonances are connected not only to the effective RI of the core mode, but also to the indices of the cladding mode resonances. The effective RI of the core mode is insensitive to SRI, as it is well shielded inside the core of the fiber. However, SRI has influences on the effective RI of the cladding modes. When the SRI changes, it will affect the coupling characteristics and transmission spectra of the cladding modes. This forms the basis of RI sensing with TFBG.

## 5.4 Sensitivities of TFBGs

### 5.4.1 Strain Sensitivity

Considering the effect of strain alone on TFBG, the reflected Bragg wavelength and the cladding modes shifts can be expressed as follows.

$$d\lambda_B = \frac{2}{\cos\alpha}\left(\Lambda_g \frac{\partial n_{eff}^{co}}{\partial\varepsilon} + n_{eff}^{co}\frac{\partial\Lambda_g}{\partial\varepsilon}\right) d\varepsilon \quad \text{(5.20)}$$

and $$d\lambda_{cl,i} = \frac{1}{\cos\alpha}\left(\Lambda_g \frac{\partial(n_{eff,i}^{co} + n_{eff,i}^{cl})}{\partial\varepsilon} + (n_{eff,i}^{co} + n_{eff,i}^{cl})\frac{\partial\Lambda_g}{\partial\varepsilon}\right) d\varepsilon \quad \text{(5.21)}$$

A closer look at equation 5.20 reveals that, the reflected Bragg wavelength behaves exactly similar to that of an FBG. The relative shift between the Bragg wavelength and cladding resonances with respect to the applied strain can be approximated as [20, 21]:

$$d(\lambda_B - \lambda_{cl,i}) = \frac{1}{\cos\alpha}\left[\frac{\partial\Lambda_g}{\partial\varepsilon}\left(n_{eff,i}^{co} - n_{eff,i}^{cl}\right)\right] d\varepsilon \quad \text{(5.22)}$$

This indicates that, for any cladding mode resonant wavelength, as the strain applied on the grating increases its separation from the Bragg wavelength increases, which in turn increases the value of $d(\lambda_B - \lambda_{cl,i})$.

### 5.4.2 Temperature Sensitivity

Considering the effect of temperature alone, the shift in Bragg wavelength ($\lambda_B$) and the cladding mode resonances can be derived from equations 5.15 and 5.18 as [21]:

$$d\lambda_B = \frac{2}{\cos\alpha}\left(\Lambda_g \frac{\partial n_{eff}^{co}}{\partial T} + n_{eff}^{co} \frac{\partial \Lambda_g}{\partial T}\right) dT \quad \text{..... (5.23)}$$

and $$d\lambda_{cl,i} = \frac{1}{\cos\alpha}\left(\Lambda_g \frac{\partial (n_{eff,i}^{co} + n_{eff,i}^{cl})}{\partial T} + (n_{eff,i}^{co} + n_{eff,i}^{cl}) \frac{\partial \Lambda_g}{\partial T}\right) dT \quad \text{..... (5.24)}$$

As the thermal expansion coefficient of silica is very small, the magnitude of $\frac{\partial \Lambda_g}{\partial T}$ is negligible when compared to $\frac{\partial n}{\partial T}$ terms in the above two equations. Then, the relative shift in the wavelengths $d(\lambda_B - \lambda_{cl,i})$ due to the effect of temperature becomes proportional to $\frac{d(n_{eff,i}^{co} - n_{eff,i}^{cl})}{dT}$ [21].

i.e. $$d(\lambda_B - \lambda_{cl,i}) \ \alpha \ \frac{d(n_{eff,i}^{co} - n_{eff,i}^{cl})}{dT} \quad \text{..... (5.25)}$$

Since the effect of temperature equally affect the effective indices of core and cladding modes, $(n_{eff,i}^{co} - n_{eff,i}^{cl})$ is a constant, so that, the relative shift in the reflected mode wavelengths is almost 0. In other words, the TFBG spectrum remains invariant under temperature changes, apart from a global shift of all the resonances [22]. This is highly helpful in eliminating the temperature cross sensitivity in the measurements, as it is sufficient to evaluate the relative wavelength shifts instead of absolute wavelengths.

### 5.4.3 Refractive Index Sensitivity

It is clear from equation 5.15 that, the reflected Bragg wavelength do not possess any RI sensitivity. The RI sensitivity of TFBG arises from the dependence of the reflected cladding mode resonances on the SRI. Considering the effect of SRI changes alone, the expression for the shift in the cladding mode resonant wavelengths can be derived from equation 5.18 as:

$$d\lambda_{cl,i} = \frac{1}{\cos\alpha}\left(\Lambda_g \frac{\partial(n_{eff,i}^{co} + n_{eff,i}^{cl})}{\partial n_{sur}}\right) dn_{sur} \quad \text{.....} \quad (5.26)$$

The above expression shows that, the cladding-mode resonances are connected to not only the effective RI of the core mode but also the cladding modes. The core mode, which is well shielded inside the core of the fiber, is insensitive to the variations in the SRI. However, SRI can influence the effective RI of the cladding modes, which in turn alters the coupling characteristics, and transmission spectra of the cladding modes.

Equation 5.11 suggests that, all the cladding modes get shifted with the variations in SRI. As the penetration depth of the evanescent field increases for higher order modes, the sensitivity of the effective index of the cladding modes to the SRI increases with mode order. Hence, the higher order cladding modes are first affected with a very small red shift in their resonance wavelength which eventually fade out, as the SRI increases, With further increase in SRI, more and more cladding modes get affected gradually until, only the two transmission peaks of ghost mode and core mode remain [18, 22]. Experimental investigations to study the relation between the SRI and the transmitted power revealed that the transmitted power decreases with the increase in SRI [23].

## 5.5 Sensing Applications of TFBG

The distinctive structure and mode coupling characteristics of TFBGs, made them very popular in optical fiber communication, fiber sensing technology, and related areas. In communication systems they are used as gain flattening filters for EDFA [24-26], filters & wavelength division multiplexing (WDM) [27-32], tuning polarization dependent loss [33- 35]etc.

Chen et al. [13, 20, 36] was the first to investigate on the applications of TFBG to measure the physical parameters like strain and temperature. Caucheteur et al. [13, 17, 36, 37] also worked in parallel on these sensing

applications of TFBG. Albert et al. [18, 20] and Baek et al. [38] proposed bending sensors using TFBG. Caucheteur et al. [39] presented simultaneous measurement of bending and temperature in 2005. Guo et al., proposed displacement sensors based on TFBG [40].

In 2001, Laffont et al. [16] proposed the very first refractometer using TFBG. They studied the influence of SRI on the spectral response of TFBG by evaluating the integral area of normalized cladding mode spectrum. In 2006, Zhao et al [41] achieved simultaneous measurement of RI and temperature based on different sensitivity of core and cladding modes in a TFBG. Zhou et al. proposed high RI sensitivity for TFBG with large tilt angle but rather insensitive to temperature [42]. An optical fiber based refractometer using the comb like spectrum of a TFBG was demonstrated by B Jiang et al. [43]. Recently, TFBG with superposed RI modulation written by a femtosecond laser and a phase mask employed for the measurement of RI and strain was demonstrated [44].

Chechura et al. described the impact of surface deposited nanostructure film, on the cladding mode resonance of TFBG [45]. Paladino et al. reported the spectral characteristics of TFBG with overlay coatings [46, 47]. X Chen et al. proposed multi angled TFBGs with and without gold coating for the measurement of RI [48] and A L Aldaba et al. demonstrated a pH sensor with polyaniline coated TFBG [49]. An etched TFBG coated with graphene oxide for the measurement of humidity was also proposed [50]. Y L Lu et al. cascaded TFBG with LPG for the simultaneous measurement of environmental temperature and RI [51].

In the field of bio sensing, label-free biosensor with bio functional materials coated on TFBG for sensing antibody and antigen was demonstrated by Maguis et al. in 2008 [52]. TFBG based biosensors using plasmonic resonance were also proposed in literature [53-55]. Guo et al. demonstrated

urinary protein variation measurement using TFBG, assisted by plasmonic nano coatings in 2016 [56].

## 5.6 Cholesterol Sensor

A cholesterol sensor exploiting the RI sensitivity of TFBG to the concentration of the sample solution under test is presented in this section.

### 5.6.1 TFBG Fabrication

TFBG with a reflected Bragg wavelength of 1557 nm and a tilt angle of $15^0$ was fabricated at Polytechnique, Montréal, Canada; through phase mask method on standard telecommunication SMF-28 (SMF-28e, Corning) fiber. The fiber used in this experiment had a core diameter of 8.2 micron, cladding diameter of 125 micron. The numerical aperture was 0.14, with the indices of refraction of the core and the cladding were 1.461 and 1.456 respectively.

### 5.6.2 Experimental Setup

A schematic sketch of the setup for experimental analysis is given in Fig 5.3. The fabricated TFBG was fixed in the middle of a glass cell using epoxy glue such that the grating region was straight without any bends. One end of the TFBG was connected to an erbium doped fiber amplifier (EDFA) (NeST - 2200s). The other end of the grating was connected to a digital power meter (Hewlett Packard - HP 8153A) through a 3dB coupler. The transmitted spectrum of the TFBG was also studied with an optical spectrum analyzer (OSA) (ANDO - AQ 6315 A).

The sample solutions prepared were introduced into the glass cell for the experimental procedures. Sufficient quantity, around 25 ml, of the test solutions were used in all measurements so that; the TFBG section was completely immersed in the sample solution during the experimentation.

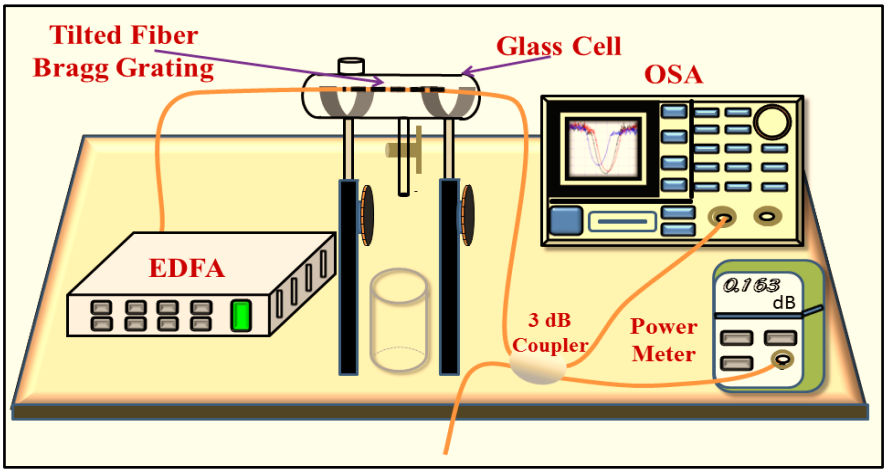


***Figure 5.3:*** *Experimental - TFBG cholesterol sensor*

### 5.6.3 Materials and Methods

As explained in the earlier chapters, the measurements were limited to a maximum of 5000 ppm of cholesterol in coconut oil, which covers the normal levels of cholesterol in human blood. The procedures followed for the preparation of cholesterol samples with coconut oil as the solvent was the same as described in section 2.5.1.3 of chapter 2 of this thesis. After each measurement, the cholesterol test samples were removed from the glass cell. The sensor head and the cell were washed repeatedly, 3 or 4 times, with distilled water and iso propyl alcohol to remove any trace of residue left behind. This is to ensure that the initial spectrum of the TFBG without any test sample in the glass cell was reproduced.

### 5.6.4 Results and Discussion

The initial transmission spectrum of the TFBG with air as the surrounding medium, recorded after fixing it in the glass cell, is shown in Fig 5.4. This was taken as the reference spectrum for the experiments with the TFBG sensor head.

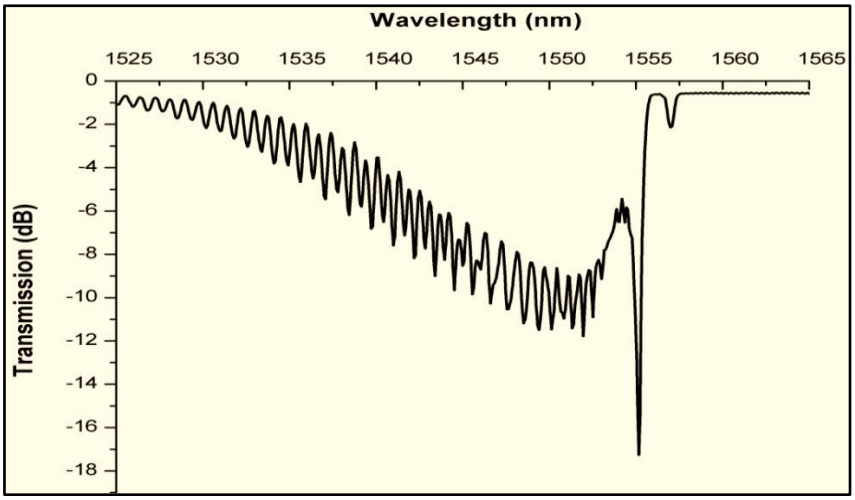


***Figure 5.4:*** *Transmission spectrum of TFBG with air as the SRI*

The transmitted spectrum had Bragg wavelength at 1557 nm and the ghost resonance peak at 1555.28 nm. The cladding mode resonances were distributed at wavelengths below the ghost resonance and their amplitudes decreased as the wavelength decreased. The cladding mode resonance with maximum intensity had a peak amplitude of -11.787 dB.

As soon as the test samples with increasing concentrations of cholesterol were introduced into the cell, the output power gradually decreased to a value of -8.36 dBm. Even though there was no considerable wavelength shift in the transmission spectra on account of the increase in concentration, the reduction in the swing of the cladding mode resonance peaks was noticeable as shown in Fig 5.5.

As the cholesterol concentration in the sample solution was increased, the RI of the samples increased. The RI of the prepared cholesterol samples were found to vary from 1.448 to1.455. When the concentration was increased, the cladding-mode resonance exhibited a slight red shift and the effective area of the transmission spectrum decreased gradually.

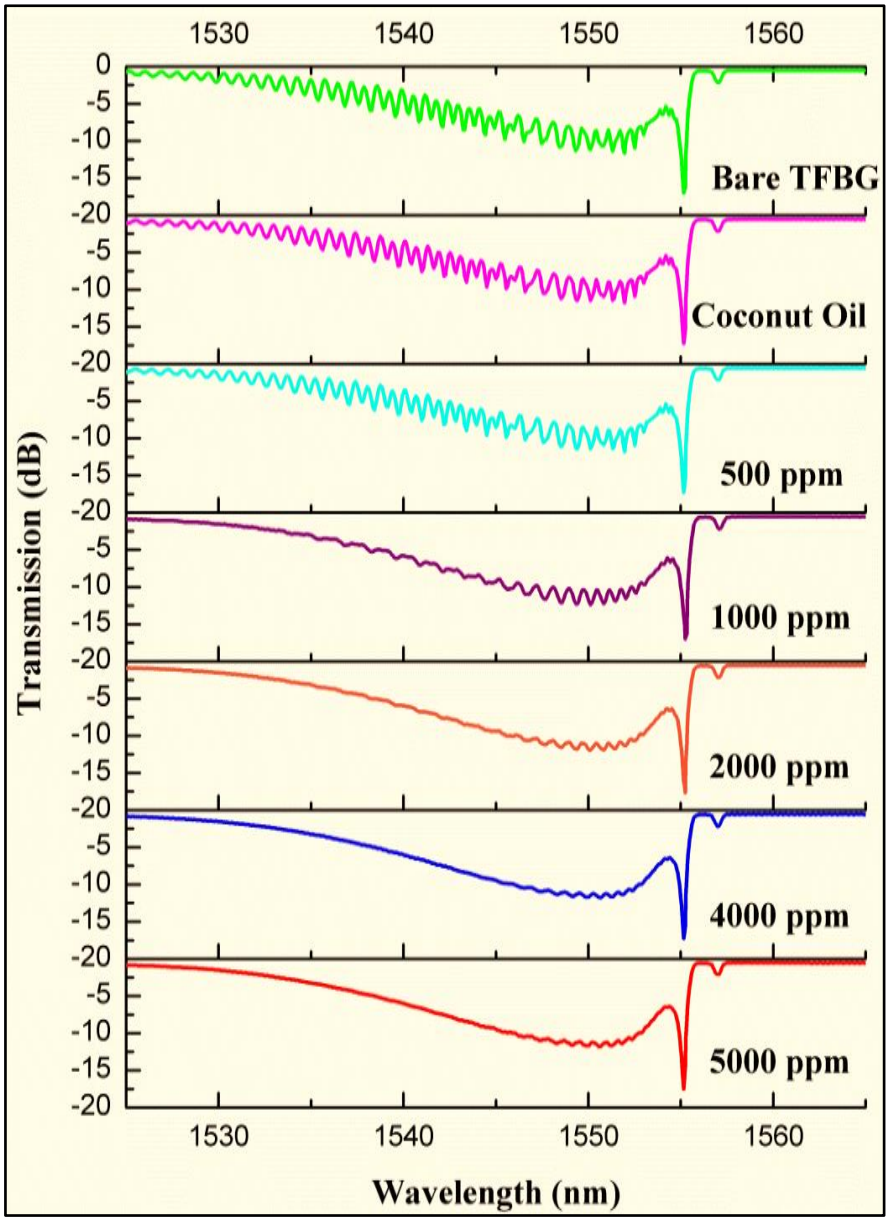


***Figure 5.5:*** *Transmission spectra of the TFBG sensor head for various concentrations of cholesterol dissolved in coconut oil.*

The amplitudes of the cladding mode resonance peaks progressively decreased, when the concentration was increased to 5000 ppm. The intensity

of the higher order cladding mode resonance located in the shorter wavelengths, began to decrease initially, followed by the lower order modes at the longer wavelengths. This is attributed to the smaller effective index values of higher order modes that are more susceptible to the SRI [23, 57, 58].

At SRI values nearer to that of the cladding, intensity of the cladding modes decreased by a large amount and is manifested as a smooth loss curve in the transmission spectrum. This can be explained by associating any discrete cladding mode resonance $\lambda_{cl,i}$ , to the corresponding effective refractive index $n_{eff,i}^{cl}$. When the SRI increases and reaches the value $n_{eff,i}^{cl}$, the mode located at $\lambda_{cl,i}$, becomes weakly guided due to the reduction in the overlap integral between the fundamental guided mode and the $i^{th}$ cladding mode. This in turn reduces the amplitude of the coupling coefficient and hence the amplitude of this transmitted peak [23, 50]. When SRI is equal or nearer to the effective cladding mode index $n_{eff,i}^{cl}$, the cladding mode is no longer guided and the coupling occurs to a continuum of radiation modes. This behavior is exhibited as the smoothing of the spectrum and reduction in the transmitted power. Thus, the more SRI increases, the more the transmitted spectrum becomes smoother, starting from the shortest wavelengths.

It may be noted that, these intensity variations were not considered for the calculation of sensitivity. The transmitted power measured using a power meter was used to calculate the sensitivity of the TFBG sensor head. As stated earlier, the value of the transmitted power decreased from -8.042 dBm to -8.36 dBm, as the concentration was increased up to 5000 ppm. The variation in the output power with respect to the concentration of cholesterol dissolved in coconut oil is presented in Fig 5.6.

This change of 0.318 dBm in the output power, for a concentration change of 5000 ppm, corresponds to a sensitivity of $0.06 \times 10^{-3}$ dBm/ppm.

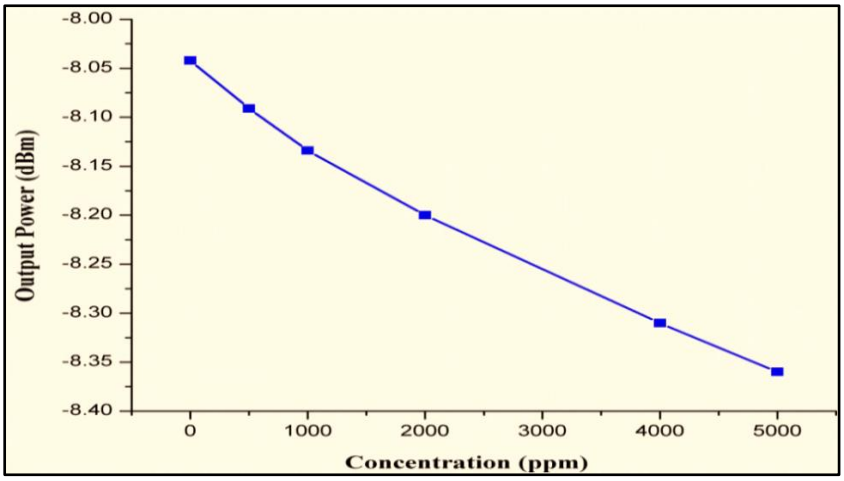


***Figure 5.6:*** *Transmitted power of the TFBG sensor head for various concentrations of cholesterol dissolved in coconut oil.*

## 5.7 Chitosan Coated TFBG for Sensing Cholesterol

As established in the previous chapters, chitosan has an affinity for cholesterol. Cholesterol sensors employing a layer of chitosan coated around LPG and etched FBG were presented in chapters 3 and 4. Even though the bare TFBG sensor head described in the last section exhibited good sensitivity to cholesterol, it is better to attempt for more sensitivity. A layer of chitosan was coated around the TFBG to enhance the sensitivity. Development of a TFBG sensor head with chitosan coating, for enhanced cholesterol sensitivity, is discussed in the following sections.

### 5.7.1 Sensor Head Fabrication

The TFBG for the cholesterol measurement experiments described above was used to fabricate the chitosan coated sensor head.

A schematic sketch of the etched FBG sensor head coated with chitosan is given in Fig. 5.7.

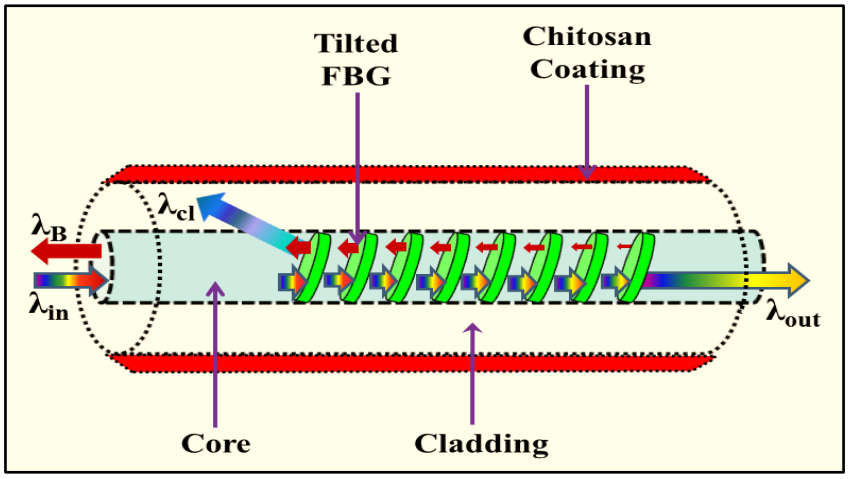


***Figure 5.7:*** *Schematic sketch - TFBG sensor head with chitosan coating*

The sensor head was fabricated by depositing a bio polymeric layer of chitosan around the TFBG section. Dip coating method, as described in the section 3.3.1.2 of chapter 3 of this thesis, was employed in the fabrication process. The procedures followed in the fabrication and the materials used for the dip coating were kept the same.

## 5.7.2 Experimental Setup

The same experimental setup employed with bare TFBG as described in section 5.6.2 was used for the analysis by replacing the bare TFBG with chitosan coated TFBG. The developed chitosan coated TFBG sensor head was fixed in the middle of the glass cell using epoxy glue such that, the grating region was straight without any bends and interrogated as in the case of uncoated TFBG sensor.

The sample solutions prepared were introduced into the glass cell for the experimental investigations. Sufficient quantity, around 25 ml, of the test solutions were used in all measurements so that; the TFBG section was completely immersed in the sample solution during the experimentation.

### 5.7.3 Materials and Methods

As explained in the earlier chapters, the measurements were limited to a maximum of 5000 ppm of cholesterol in coconut oil, which covers the normal levels of cholesterol in human blood. The procedures followed for the preparation of cholesterol samples with coconut oil as the solvent was as described in section 2.5.1.3 of the chapter 2 of this thesis. After each measurement, the cholesterol test samples were removed from the glass cell. The sensor head and the cell were washed repeatedly, 3 or 4 times, with distilled water and isopropyl alcohol to remove any trace of residue left behind. This is to ensure that the initial spectrum of the TFBG without any test sample in the glass cell was reproduced. The RI of the prepared cholesterol samples measured using Abbe refractometer was found to vary from 1.448 to1.455.

### 5.7.4 Results and Discussion

The bare TFBG had the Bragg wavelength at 1557 nm and the ghost resonance peak was at 1555.28 nm with a transmitted output power -8.042 dBm. When the prepared chitosan coated sensor head was fixed inside the glass cell, the Bragg wavelength has red shifted to 1557.08 nm while the ghost resonance peak remained unaffected at 1555.28 nm, with air as surrounding medium. This spectrum recorded as the reference for further experiments is given in Fig. 5.8. This shift in the Bragg wavelength is attributed to the small strain induced by the dried chitosan layer around the TFBG. As in the case of bare TFBG, the cladding mode resonances were distributed at wavelengths below the ghost resonance and their amplitudes decreased as the wavelength decreased. The peak amplitude of the cladding mode resonance with maximum intensity shifted to -10.738 dB from the initial value of -11.787 dB for the bare TFBG.

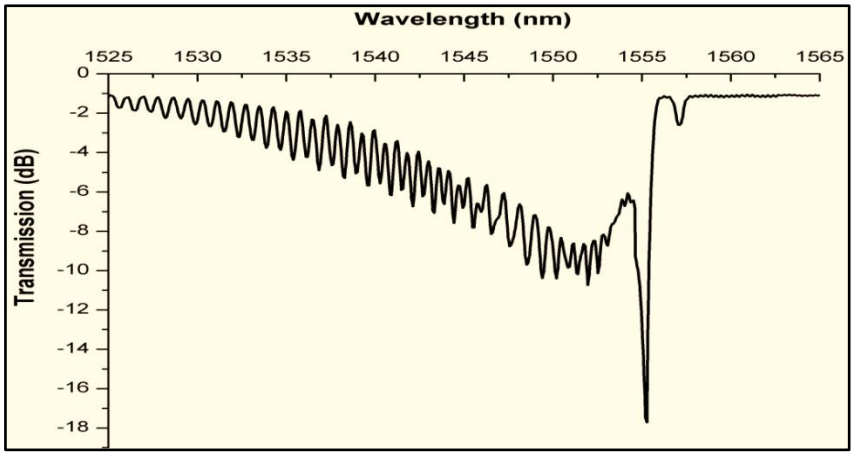


***Figure 5.8:*** *Transmission spectrum of chitosan coated TFBG in air.*

As explained earlier this reduction in the amplitude of the resonant cladding mode is attributed to the weaker guidance of the cladding mode due to the decrease of the overlap integral between the fundamental guided mode and the cladding mode [23, 50, 51]. This is due to the increased effective index of the cladding in the presence of the chitosan coating. This in turn reduced the amplitude of the coupling coefficient and hence the amplitude of this transmitted peak.

The transmitted output power was measured to be -8.113 dBm, without any sample solution in the glass cell. This reduction in the output power is attributed to the increased coupling to the radiation modes at the higher effective RI of the cladding due to the overlay coating of chitosan.

When the samples with increasing concentrations of cholesterol were introduced into the cell, the output power gradually decreased to a value of -8.912 dBm. As in the case of experiments with bare TFBG, there was no considerable wavelength shift in the transmission spectra with increase in concentration. The reduction in the swing of the cladding mode resonance peaks was noticeable as earlier and is given in Fig 5.9.

The changes in the spectral shape follow the same trend as explained earlier in section 5.6.4 for the bare TFBG. As the cholesterol concentration in the sample solution was increased, the RI of the samples increased. More the concentration of cholesterol, more of it gets attached to the chitosan overlay coating increasing its refractive index. This in turn increases the effective index of the cladding modes making them more and more weakly guided and thereby reducing the intensity of the resonant cladding modes. This is also accompanied by the smoothening of the spectra as the SRI value increases.

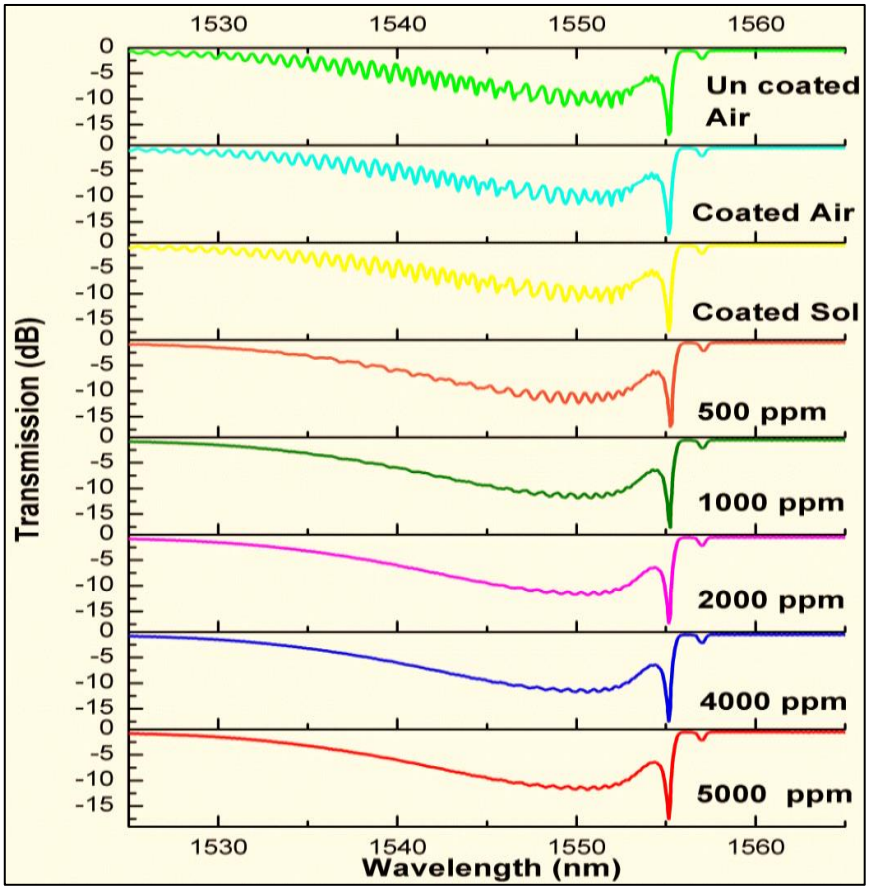


***Figure 5.9:*** *Transmission spectra of the chitosan coated TFBG sensor head for various concentrations of cholesterol dissolved in coconut oil.*

The transmitted power decreased from -8.113 dBm to -8.912 dBm, as the concentration was increased up to 5000 ppm. This variation in the output power with respect to the concentration of cholesterol dissolved in coconut oil for both the sensor heads are given in Fig 5.10.

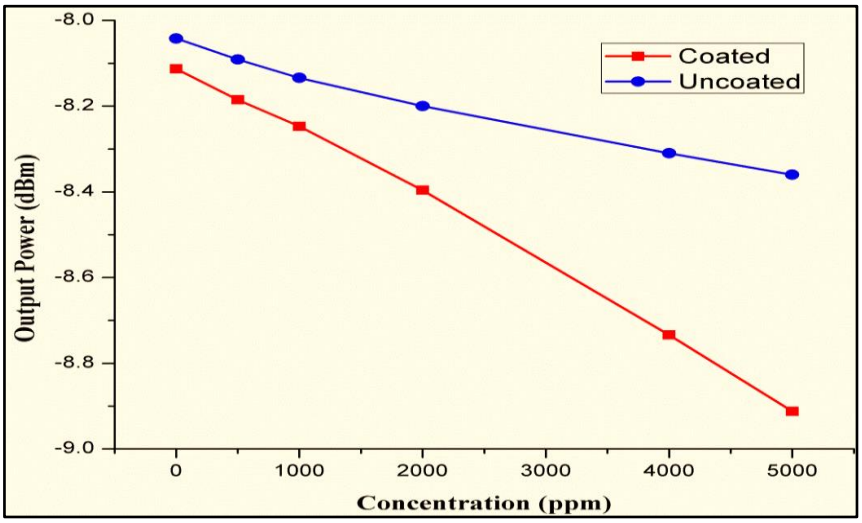


***Figure 5.10:*** *Transmitted power of the TFBG sensor heads for various concentrations of cholesterol dissolved in coconut oil.*

As explained earlier, the reduction in the transmitted power is attributed to increased coupling of the core modes to the radiation modes at higher values of SRI. The above plots clearly shows an increased slope for the coated sensor head and hence an increased sensitivity. The increase in sensitivity of the chitosan coated TFBG over the bare TFBG is attributed to the modulation of the effective cladding mode index due to the attachment of cholesterol on to the chitosan overlay coating. This change of 0.799 dBm in the output power, for a change in concentration of 5000 ppm, corresponds to a sensitivity of 0.16 $x10^{-3}$ dBm/ppm, which is two and a half times that of the bare TFBG.

A table showing the response of the chitosan coated TFBG sensor head for various concentrations of cholesterol dissolved in coconut oil is given below.

| Cholesterol Concentration (ppm) | Refractive Index of Sample | Output Power (-dBm) | |
|---|---|---|---|
| | | Uncoated | Coated |
| **0** | 1.448 | 8.042 | 8.113 |
| **500** | 1.450 | 8.091 | 8.185 |
| **1000** | 1.452 | 8.134 | 8.247 |
| **2000** | 1.453 | 8.20 | 8.396 |
| **4000** | 1.454 | 8.31 | 8.734 |
| **5000** | 1.455 | 8.36 | 8.912 |

***Table 5.1:*** *Response of the TFBG sensor head with and without chitosan coating for various concentrations of cholesterol*

Enzymatic bare fiber optic sensors for the measurement of cholesterol were reported earlier [59, 60, 61]. The enzymatic sensor head described in [59], with a linear response in a smaller measurement range of 1700 ppm to 2000 ppm of cholesterol, had a large response time of 120s. A photonic crystal fiber with a sol gel coating was used to develop an intensity modulated sensor head for the detection of cholesterol, with a linear detection range of 180 mg/dL to 200 mg/dL (1800-2000 ppm) [60]. Another enzymatic optical fiber probe based on fluorescence quenching and consumption of oxygen, exhibited a linear response in a limited range of 250 ppm to 2500 ppm, with a larger response time of 200s [62]. The method was simple in terms of the components used and required heating of the test samples, and the response was pH dependent.

The TFBG sensor head described in this chapter works linearly over a wider range of 500 to 5000 ppm of cholesterol. The sensor response was also instantaneous and no heating is required for the experimentation.

Unlike the pH dependent response of the cholesterol sensors reported earlier [62, 63, 64], the TFBG sensors described in this chapter are independent of pH alterations of the sample under test. All the wavelength modulated cholesterol measurement methods described in earlier chapters, make use of costlier instrumentation, while the TFBG sensor heads employ much easier power measurements with power meters. This in turn results in a considerable reduction in the cost of implementation of the sensing platform. In addition, due to the inherent characteristics of the TFBG, the sensor heads described in this chapter are not influenced by the changes in the ambient temperature.

## 5.8 Conclusions

The results presented illustrate the application of TFBG based sensor systems for the detection and measurement of cholesterol concentrations. Both the chitosan coated and uncoated sensor heads can be utilized in designing cholesterol sensors. The most important advantage of the above described sensors is that, the interrogation system uses simple power meters, which in turn can reduce the cost of experimentation and also make it easier. In addition, the measurements are independent of the fluctuations in the ambient temperature due to the characteristics of the TFBG itself.

The simple setup of the sensors clubbed with its real time and instantaneous response with high sensitivity makes them very attractive. The proposed techniques require only a small quantity of test sample and can be suitably modified for field applications in clinical laboratories for the estimation cholesterol in blood of human beings. The results are also repeatable, and cover a wide range of cholesterol levels. The linearity in the performance make the sensor head designs attractive for commercial applications. A comparison of the performance of the TFBG sensor heads with and without chitosan coating is given in Table 5.2.

| Parameter | TFBG Sensor Head | |
|---|---|---|
| | Uncoated | Coated |
| **Output Power Swing (-dBm)** | 0.318 | 0.799 |
| **Sensitivity ($\times 10^{-3}$dBm/ppm)** | 0.06 | 0.16 |

***Table 5.2:*** *Performance of TFBG sensor heads with and without coating*

In order to avoid damage of the TFBG, no attempt was made to fabricate etched TFBG sensor heads. However, etched TFBG sensor heads would have resulted in better sensitivity in the measurements of cholesterol.

## 5.9 Summary

This chapter discussed, the fabrication of TFBG based sensors. A detailed discussion on the principle of operation of TFBG was provided. The response of TFBGs to external perturbations like strain, temperature and surrounding refractive index was discussed. A brief survey on the sensing applications of TFBG was also presented in this chapter.

The chapter also outlined the method of RI sensing with TFBGs. It was shown that TFBG can be employed as a cholesterol sensor with reasonably good sensitivity.

For the enhancement of the RI sensitivity of the bare TFBG, chitosan, which was identified as a biopolymer with an affinity to cholesterol, was employed as an overlay coating around the grating to develop a sensor head for cholesterol sensing application. It was established that an overlay coating over the TFBG can be prepared by the process of dip coating. TFBG sensor head with chitosan coating exhibited two and a half times higher sensitivity compared to the uncoated sensor for the test samples of cholesterol dissolved in coconut oil.

## References


[1]. K O Hill, Y Fujii, D C Johnson and B S Kawasaki, "*Photosensitivity in optical fiber waveguides: Application to reflection filter fabrication*", Applied Physics Letters, Vol. 32, pp. 647-649 (1978).

[2]. G Meltz, W W Morey, and W H Glenn, "*In fiber Bragg grating tap*", Tech. Digest, Optical Fiber Communication (OFC '90), San Francisco, CA, pp. TUG1, (1990).

[3]. T Erdogan and J E Sipe, "*Tilted fiber phase gratings*", J. Opt. Soc. Am. A,Vol. 13, pp. 296-313 (1996).

[4]. R Kashyap, R Wyatt and R J Campbell, "Wideband gain flattened erbium fiber amplifier using a blazed grating", Electron. Lett., Vol. 24 (2), pp. 154-156 (1993).

[5]. A Othonos and K Kalli, *"Fiber Bragg Gratings: Fundamentals and Applications in Telecommunications and Sensing"*, Boston: Artech House (1999).

[6]. Andreas Othonos, "*Fiber Bragg gratings*", Review of Scientific Instruments, Vol. 68, pp. 4309-4341 (1997).

[7]. R. Kashyap, "*Fiber Bragg Gratings*", 2nd Edition, Academic Press (2010).

[8]. R Kashyap, J M L Higuera, "*Handbook of optical fiber sensing technology; Fiber Grating Technology: Theory, Photosensitivity, Fabrication and characterization*", John Wiley & Sons, pp. 349-377 (2002).

[9]. K O Hill and G Meltz, "*Fiber Bragg grating technology fundamentals and overview*", J. Lightwave Technology, Vol. 15, pp. 1263-1276 (1997).

[10]. D K W Lam and B K Garside, "*Characterization of single mode optical fiber filters*", Appl. Optics, Vol. 20,Iss 3, pp 440-445 (1981).

[11]. A Bouzid and M A G Abushagur, "*Scattering analysis of slanted fiber gratings*", Appl. Opt., Vol. 36 (3), pp. 558-562 (1997).

[12]. T Erdogan, "*Fiber grating spectra*", J. Lightwave Technology, Vol. 15, pp. 1277-1294 (1997).

[13]. C Chen, L Xiong, C Caucheteur, P Megret and J Albert, "*Differential strain sensitivity of higher order cladding modes in weakly tilted fiber Bragg gratings*", Proc. Photonic Applications for Aerospace Transportation, and Harsh Environments, Boston, MA, USA, pp. 63790E-7 (2006).

[14]. K S Lee and T Erdogan, "*Fiber mode coupling in transmissive and reflective tilted fiber gratings*", Applied optics, Vol. 39, pp. 1394-1404, (2000).

[15]. Chehura E, James, S W and Tatam R P, "*Temperature and strain discrimination using a single tilted fiber Bragg grating*", Opt. Com., Vol. 275, pp. 344-347 (2007).

[16]. G Laffont and P Ferdinand, "*Tilted short period fiber Bragg grating induced coupling to cladding modes for accurate refractometry*", Meas. Sci. Technol. Vol. 12, pp. 765-770 (2001).

[17]. C Caucheteur, C Chen, J Albert, P Mégret, "*Use of weakly titled fiber Bragg gratings for strain sensing purposes*", Proc. Symposium IEEE/LEOS Benelux Chapter, Eindhoven, pp. 61-66 (2006).

[18]. T Guo, A Ivanov, C K Chen and J Albert, "*Temperature independent tilted fiber grating vibration sensor based on cladding-core recoupling*", Opt. Lett., Vol. 33, pp. 1004-1006 (2008).

[19]. T Guo, F Liu, B Guan and J Albert, "*Tilted fiber grating mechanical and biochemical sensors*", Optics & Laser Technology, Vol. 78, pp. 19-33 (2016).

[20]. C Chen and J Albert, "*Strain optic coefficients of individual cladding modes of single mode fiber: Theory and experiment*", Electron. Lett., Vol. 42, pp. 1027-1028 (2006).

[21]. J Albert, LY Shao, and C Caucheteur, "*Tilted fiber Bragg grating sensors*", Laser Photonics Rev., pp. 1-26 (2012).

[22]. T Guo, C Chen, A Laronche and J Albert, "*Power referenced and temperature calibrated optical fiber refractometer*", Photonics Technology Letters, Vol. 20, pp. 635-637 (2008).

[23]. Y Miao, B Liu and Q Zhao, "*Refractive index sensor based on measuring the transmission power of tilted fiber Bragg grating*", Optical Fiber Technology, Vol. 15, pp. 233-236 (2009).

[24]. E Kerrinckx, A Hidayat, P Niay, Y Quiquempois, M Douay, I Riant, and C D Barros, "*Suppression of discrete cladding mode resonances in fiber slanted Bragg gratings for gain equalization*", Opt. Express, Vol. 14 (4), pp. 1388-1394 (2006).

[25]. R Kashyap, R Wyatt, and R J Campbell, "*Wideband gain flattened erbium fiber amplifier using a photosensitive fiber blazed grating*", Electron. Lett., Vol. 24 (2), pp. 154-156, (1993).

[26]. R Kashyap, R Wyatt, and P F Mckee, "*Wavelength flattened saturated erbium amplifier using multiple side tip Bragg gratings*", Electron. Lett., Vol. 29 (11), pp. 1025-1026 (1993).

[27]. C W Haggans, H Singh, W F Varner, Y Li, and M Zippin, "*Narrow band rejection filters with negligible back reflection using tilted photo induced gratings in single mode fibers*", IEEE Photon. Technol. Lett., Vol. 10 (5), pp. 690-692 (1998).

[28]. G Nemova, J Chauve, and R Kashyap, "*Design of side tap fiber Bragg grating filters*", Opt. Commu., Vol. 259 (2), pp. 649-654 (2006).

[29]. Y Liu, L Zhang, and I Bennion, "*Fabricating fiber edge filters with arbitrary spectral response based on tilted chirped grating structures*", Meas. Sci. Technol., Vol. 10 (1), pp. L1-L3 (1999).

[30]. E Marin, R Ghosh, J P Meunier, X Daxhelet, and S Lacoix, "*Bragg gratings in 2×2 symmetric fused fiber couplers: influence of the tilt on the wavelength response*", IEEE Photon. Technol. Lett., Vol. 11 (11), pp. 1434-1436 (1999).

[31]. R S Westbrook, K S Feder, P I Reyes, P Steinvurzel, B J Eggleton, R G Ernst, L A Reith, and D M Gill, "*Application of fiber Bragg grating filter/tap module to a wavelength locked low chirp directly modulated 10 GB/s RZ transmitter*", Proc. Optical Fiber Communication Conference, Anaheim, CA (2002).

[32]. K W Gaff, F Ladouceur, and J D Love, "*Two-wavelength planar add/drop WDM filter employing a three mode coupling Bragg grating*", Electron. Lett., Vol. 36, (13), pp. 1142-1144 (2000).

[33]. K Zhou, X Chen, A G Simpson, L Zhang, and I Bennion, "*High extinction ratio in-fiber polarizer based on 45°tilted fiber Bragg gratings*", Opt. Lett., Vol. 30 (11), pp. 1285-1287 (2005).

[34]. S J Mihailov, R B Walker, T J Stocki, and D C. Johnson, "*Fabrication of tilted fiber grating polarization dependent loss equalizer*", Electron. Lett., Vol. 37 (5), pp. 284-286 (2001).

[35]. P I D C Reyes and P S Westbrook, "*Tunable PDL of twisted tilted fiber gratings*", IEEE Photon. Technol. Lett., vol. 15, no. 6, pp. 828-830, (2003).

[36]. C Chen, C Caucheteur, P Mégret, and J Albert, "*The sensitivity characteristics of tilted fiber Bragg grating sensors with different cladding thickness*", Meas. Sci. Technol., Vol. 18 (10), pp. 3117-3122 (2007).

[37]. C Caucheteur, C Chen, J Albert, and P Mégret, "*Use of weakly tilted fiber Bragg gratings for sensing purpose*", Proc. Optical Sensors, Strasbourg, France (2008).

[38]. S Baek, Y Jeong, and B Lee, "*Characteristics of short period blazed fiber Bragg gratings for use as macro-bending sensors*", Appl. Opt., Vol. 41 (4), pp. 631-636 (2002).

[39]. C Caucheteur, K Chah, F Lhommé, M Blondel, and P Mégret, "*Simultaneous bend and temperature sensor using tilted FBG*", Proc., 17th Int. Conf. on Optical Fiber Sensors, Bruges, Belgium (2005).

[40]. T Guo, C K Chen and J Albert, "*Non uniform tilt modulated fiber Bragg grating for temperature immune micro displacement measurement*", Meas. Sci. and Technol. Vol. 20, 034007 (2009).

[41]. C Zhao, X Yang, M S Demokan, and W Jin, "*Simultaneous temperature and refractive index measurements using a 3°slanted multimode fiber*

*Bragg grating*", IEEE J. Lightwave Technol., Vol. 24 (2), pp. 879-883 (2006).

[42]. K Zhou, L Zhang, X Chen, and I Bennion, "*Optic sensors of high refractive index responsivity and low thermal cross sensitivity that use fiber Bragg gratings of >80°tilted structures*", Opt. Lett., Vol. 31 (9), pp. 1193-1195, (2006).

[43]. B Jiang, K Zhou, C Wang,Y Zhao, J Zhao,1 and L Zhang, "*Temperature calibrated high precision refractometer using a tilted fiber Bragg grating",* Optics Express, Vol. 25, No. 21, pp. 25910-25918 (2017).

[44]. X Y Zhang, C Chen, Y S Yu, W H Wei, Q Guo, Y Y Chen, X Zhang, L Qin, Y Q Ning, and H B Sun, "*High-order-tilted fiber Bragg gratings with superposed refractive Index modulation*", J. IEEE Photonics, Vol. 10, No. 1 (2018).

[45]. E Chechura, R P Murphy, S W. James, and R P Tatam, "*Tilted fiber Bragg gratings with nano structured overlays*", Proc. Optical Fiber Sensors, Cancún, Mexico (2006).

[46]. D Paladino, P Pilla, A Cutolo, S Campopiano, M Giordano, A Cusano, C Caucheteur, and P M´egret "E*ffects of thickness and external refractive index in coated tilted fiber Bragg gratings*", Proc. SPIE, Vol. 6619, pp. 68 (2007).

[47]. D Paladino, A Cusano, P Pilla, S Campopiano, C Caucheteur, and P M´egret "S*pectral behaviour in nano coated tilted fiber Bragg gratings: effect of thickness and external refractive index*", IEEE Phot. Technol. Lett., Vol. 19 (24), pp. 2051-2053 (2007).

[48]. X Chen, J Xu, X Zhang, T Guo and B O Guan, "*Wide range refractive index measurement using a multi-angle tilted fiber Bragg grating*", IEEE Photon. Technol. Lett., Vol. 29 ( 9), pp. 719-722 ( 2017).

[49]. A L Aldaba, A G Vila, M Debliquy, M L Amo, C.Caucheteur and D.Lahem, "*Polyaniline coated tilted fiber Bragg gratings for pH sensing"*, Sensors and Actuators B: Chemical, Vol. 254, pp. 1087-1093 (2018).

[50]. Y D Chiu, C W Wu and C C Chiang, "*Tilted Fiber Bragg Grating Sensor with Graphene Oxide Coating for Humidity Sensing*", Sensors, 17(9), 2129, (2017).

[51]. Y L Yu, H H Hung, S K Liaw, M H Shih, H Kishikawa, and N Goto, "*Simultaneously two-parameter measurement using tilted fiber grating and long period fiber grating",* Microwave and Opt. Tech. Let., Vol. 59, No. 5, pp. 1122-1125 (2017).

[52]. S Maguis, G Laffont, P Ferdinand, B Carbonnier, K Kham, T Mekhalif, and M C Millot, "*Biofunctionalized tilted fiber Bragg gratings for label free immunosensing*", Opt. Express, Vol. 16 (23), pp. 19049-19062 (2008).

[53]. Y Yanina, Y Shevchenko, and J Albert, "*Plasmon resonances in gold-coated tilted fiber Bragg gratings*", Opt. Lett., Vol. 32 (3), pp. 211-213 (2007).

[54]. T Allsop, R Neal, S Rehman, D J Webb, D Mapps and I Bennion, "*Characterization of infrared surface plasmon resonances generated from a fiber optical sensor utilizing tilted Bragg gratings*", J. Opt. Soc. Am. B, Vol. 25 (4), pp. 481-490 (2008).

[55]. A G Vila, A L Aldaba, D Kinet, P Megret, M L Amo and C.Caucheteur, "*Optical power based interrogation of plasmonic tilted fiber Bragg grating biosensors"*, Proc. SPIE, Vol. 10323, pp.103234V 1-4 (2017).

[56]. T Guo, F Liu, X Liang, X Qiu, Y Huang, C Xie, P Xu, W Mao, B Guan, J Albert, "*Highly sensitive detection of urinary protein variations using tilted fiber grating sensors with plasmonic nano coatings*", Biosensors and Bioelectronics Vol. 78, pp. 221–228 (2016).

[57]. Y Miao, B Liu, S Tian, and Q Zhao, "*Temperature insensitive refractive index sensor based on tilted fiber Bragg grating*", Microwave and Optical Technol. Lett., Vol. 51 (2), pp. 479-483 (2009).

[58]. Y Miao, B Liu, H Zhang, Y Li, H Zhou, H Sun, W Zhang, and Q Zhao, "*Relative humidity sensor based on tilted Bragg grating with polyvinyl alcohol coating*", IEEE Photon. Technol. Lett., Vol. 21 (7), pp. 441-443 (2009).

[59]. D A R Medina, M T Durán and E A Méndeza, "*Cholesterol biosensor based on a plastic optical fiber with sol–gel: structural analysis and sensing properties*", J. of Modern Optics, Vol. 65, Iss. 3, pp. 348-352 (2018).

[60]. D A R Medina, E A Méndeza and M T Durán, "*Thin film of sol-gel deposited in photonic crystal fiber for cholesterol detection*", Proc. SPIE Vol. 9434, pp. 943417-1-6 (2015).

[61]. V Semwal and B D Gupta, "*LSPR and SPR based fiber optic cholesterol sensor using immobilization of cholesterol oxidase over silver nanoparticles coated graphene oxide nanosheets*", J. IEEE Sensors, Vol. 18, No. 3, pp.1039-46 (2018).

[62]. J Huang, Y Liu, P Zhang, Yangjie Li and L Ding, "*A temperature triggered fiber optic biosensor based on hydrogel-magnetic immobilized enzyme complex for sequential determination of cholesterol and glucose*", J. Biochem. Eng. Vol. 125, pp. 123–128 (2017).

[63]. S Alexander, P Baraneedharan, S Balasubrahmanyan and S Ramaprabhu, "*Modified graphene based molecular imprinted polymer for electrochemical nonenzymatic cholesterol biosensor*", European Polymer J. Volume 86, pp. 106-116 (2017).

[64]. B Anjali, S Shivani, T Umesh, G Rani and K S Enakshi, "*Long period grating based sensor for the detection of triacylglycerides*", Biosensors and Bioelectronics, Vol. 79, pp 693-700 (2015).

# Chapter 6

# Conclusions and scope for future study

*Abstract*

*This chapter concludes the thesis by summarizing the results and providing suggestions for further work based on this research. This research work has focused on the study of fiber grating based sensing applications for the measurement of cholesterol.*

## 6.1 Summary

Design and development of optical fiber grating based sensors form the principal subject of this thesis. The applications of the developed sensors were oriented towards the detection and estimation of cholesterol.

An outline of the different types of fiber optic sensors with emphasis on optical fiber grating based sensors was given in the first chapter. Detailed discussions on the photosensitivity of optical fibers, methods to improve it and the process of grating fabrication were presented. This introductory chapter also presented various aspects of cholesterol and the importance of its sensing. Chitosan, the biopolymer used to enhance the sensitivity of the grating sensor heads was also introduced. The probable mechanism of its hypocholesterolaemic activity was also discussed.

The second chapter outlined the theory of operation and sensing principles of fiber optic LPG devices. The developed LPG sensor head was employed for the measurement of cholesterol, exploiting its RI sensitivity. It was found that the sensor head exhibited poor sensitivity when petroleum ether, with a low value of RI, was used as the solvent for cholesterol. Hence, coconut oil, which gave higher refractive index values for the test samples was used as the solvent. This sensor head exhibited an instantaneous and linear response with a total blue shift of 10.5 nm for the $LP_{04}$ mode showing a good sensitivity of 2 pm/ppm of cholesterol.

Chitosan was identified as cholesterol lowering agent and has been in use for several years. Chapter 3 sketched the development of a chitosan coated LPG sensor for the measurement of cholesterol exploiting the affinity of chitosan to cholesterol. A discussion on the sensing applications of LPG sensor heads with overlay coatings was presented. The method of dip coating was also detailed in this chapter. By providing the overlay

coating of chitosan around the LPG, measurement sensitivity could be enhanced by 2.5 times that of the uncoated sensor. The newly developed sensor head also showed reversible and repeatable performances.

In the fourth chapter, etching of FBG, in order to induce sensitivity to RI variations, was discussed. The chemical etching process of optical fibers using HF solution was studied in detail by analyzing the evolution of the grating spectra with time of etching. The etched sensor head was employed for the detection of cholesterol exploiting the RI sensitivity of etched FBGs. In order to further enhance the sensitivity of the sensor, a layer of chitosan was coated over the grating, to develop the chitosan coated etched FBG sensor. Both the sensor heads showed good response and the coated sensor exhibited 3 times enhancement in sensitivity.

Tilted FBGs have the advantage of intensity measurements with relatively higher sensitivities rather than wavelength interrogation. The use of low cost detectors makes the experiments and analysis simpler and easier. The fifth chapter provided the application of TFBGs with and without chitosan coating, for cholesterol measurement. It was established that, the chitosan coated sensor head could detect cholesterol with an enhanced sensitivity. The sensor heads developed exhibited a sensitivity of $0.06 \times 10^{-3}$ dBm/ppm for the uncoated sensor. The coated sensor offered a sensitivity of $0.16 \times 10^{-3}$ dBm/ppm, showing 2.5 times enhancement in the sensitivity.

Three different types of optical fiber gratings were fabricated and employed as a total cholesterol sensor, exploiting the sensitivity of these gratings to the changes in the SRI. A comparison of the performance of the different fiber grating sensor heads with and without chitosan coating for the measurement of cholesterol is given in Table 6.1.

| Sensor Head | Sensitivity | |
|---|---|---|
| | **Uncoated** | **Coated** |
| **LPG (pm/ppm)** | 2 | 5 |
| **Etched FBG (pm/ppm)** | 0.028 | 0.063 |
| **TFBG (x$10^{-3}$dBm/ppm)** | 0.02 | 0.16 |

***Table 6.1:*** *Performance of grating sensor heads with and without coating*

These grating based sensors working on different principles can be compared as follows.

- The chitosan coated sensor heads exhibited enhanced sensitivities compared to their uncoated versions.
- The LPG based sensor heads are easier to handle and exhibited good linear response.
- The fabrication and application of etched FBG based sensor is tedious.
- The sensitivity of the LPG sensor heads was found to be much better than that of the FBG sensor heads. The results are comparable with that published in the literature [1, 2].
- Unlike the spectral analysis followed for LPG and FBG, TFBG sensors rely on power measurements. This makes the experimentation simpler and less expensive.

## 6.2 Scope for Future Study

The main objective of this research work was to develop optical fiber grating based RI sensors and to employ them for cholesterol sensing application. A number of areas of future research have arisen from the experimental works and the most relevant of them are presented below.

- A sensor head for the measurement of cholesterol in human blood employing scratched plastic optical fiber has been reported earlier [3]. The sensor heads described in this thesis can also be deployed in clinical applications with proper modifications so that it is suited for the detection of total cholesterol in human blood samples.
- Further research can be extended in the direction of development of suitable and specific materials like chitosan that can be coated around the gratings in order to have more reliable, specific and selective measurement of cholesterol.
- Turn around LPGs show higher refractive index sensitivities compared to normal LPGs [4, 5]. Hence, better cholesterol sensor may be materialized with turn around LPGs.
- The sensitivity of LPG and TFBG based RI sensors can be increased significantly by etching the cladding of the fiber [6-8]. We believe that better performances of the designed sensors can be accomplished by the optimization of fundamental factors such as grating period, grating length and the thickness of cladding around the grating.
- The sensor heads presented in this thesis are non-enzymatic. Enzymatic detection of cholesterol provides more specificity and selectivity in the measurements. Incorporation of enzymes along with the advantages of gratings can be thought of in developing a cholesterol sensor, as proposed by Anjali et al. in 2015, for the detection of triacylglycerides [9].
- Even though total cholesterol is an indication of the probability of occurrence of diseases like arteriosclerosis, nowadays the clinical tests have become much more specific by including the measurement of LDL, HDL etc. Investigations can also be extended in this direction, to develop

sensor heads suitable for such specific and detailed measurement of various components of total cholesterol.

- The RI sensor based on etched FBGs exhibited good response with respect to its sensing characteristics. But, it is very difficult to fabricate and use the etched FBG sensor head. The etched fiber with such small diameters can be easily broken and extra care should be taken in handling the same. Hence, development of a proper protective packing for etched FBG sensor heads also assumes great importance.

## References

[1]. T M Libish, "*Design and development of fiber grating based chemical and biosensors*", Ph.D. Thesis, Cochin University of Science and Technology, Kerala, India (2015).

[2]. L S Laxmeshwar, M S Jadhav, J F Akki, P U Raikar, J Kumar, O Prakash and U S Raikar, "*Highly sensitive fiber grating chemical sensors: An effective alternative to atomic absorption spectroscopy*", J. Opt. & Laser Tech., Vol. 91, pp. 27–31 (2017).

[3]. M Yunianto, A N Permata, D Eka, D Ariningrum, S Wahyuningsih and A Marzuki, "*Design of a fiber optic biosensor for cholesterol detection in human blood*", IOP Conf. Series: Materials Science and Engineering, Vol. 176, 012014 (2017).

[4]. P Pilla, C Trono, F Baldini F Chiavaioli, M Giordano, and A Cusano, "*Giant sensitivity of long period gratings in transition mode near the dispersion turning point: an integrated design approach*", Optics Letters, Vol. 37 (19), pp. 4152-4154 (2012).

[5]. P Biswas, N Basumallick, K Dagupta and S Bandyopdhayay, "*Over coupled long period grating with enhanced sensitivity to refractive index higher than that of cladding*", Proc. Photonics '12, Int. Conf. on Fiber Optics and Photonics , OSA, pp. T2B3.1- T2B3.3(2012)

[6]. I D Villar, *"Ultrahigh-sensitivity sensors based on thin film coated long period gratings with reduced diameter, in transition mode and near the dispersion turning point",* Optics Express, Vol. 23, pp. 8389-8398 (2015).

[7]. S M Tripathi, W J Bock, P Mikulic and R Chinnappan, *"Long period grating based biosensor for the detection of Escherichia coli bacteria"*, Biosensors and Bioelectronics, Vol. 35, 308–312 (2012).

[8]. H Hen and Z Gu, "*Design of a gas sensor based on a cladding reduced long period fiber grating coated with a sensitive film*", Optik, Vol. 124, pp. 219-224 (2013).

[9]. B Anjali, S Shivani, T Umesh, G Rani and K S Enakshi, "*Long period grating based sensor for the detection of triacylglycerides*", Biosensors and Bioelectronics, Vol. 79, pp 693-700 (2015).

*"We still do not know one thousandth of one percent of*

*what nature has revealed to us"*

**Albert Einstein (1879-1955)**

# Appendix

---

*Selected publications related to this thesis are presented in the appendix.*

---

OPTOELECTRONICS LETTERS Vol.12 No.1, 1 January 2016

# A fiber optic biosensor for the detection of cholesterol levels based on chitosan coated long period grating

**C. Bobby Mathews[1,2]*, T. M. Libish[1], B. Kaushalkumar[3], V. Vivek[3], Radhakrishna Prabhu[3], and P. Radhakrishnan[1]**

*1. International School of Photonics, Cochin University of Science and Technology, Kochi 682022, India*

*2. Muslim Educational Society College of Engineering, Kuttippuram 679573, India*

*3. Robert Gordon University, Aberdeen AB10 7QB, UK*

(Received 17 November 2015)



A fiber optic sensor for the measurement of total cholesterol is designed and developed. The developed chitosan coated long period grating (LPG) sensor shows a sensitivity of $5.025\times10^6$ pm·mL/g in the measurement range of the sensor. The sensor also shows a linear response in the measured range of cholesterol levels, which is highly desirable for exploitation as a commercial cholesterol sensor.

**Document code:** A **Article ID:** 1673-1905(2016)01-0023-4

**DOI** 10.1007/s11801-016-5229-9

In the last three decades, many studies have revealed the relationship between the increased cholesterol concentration and the occurrence of cardiovascular diseases, like arteriosclerosis and hypertension. Hence, the detection and control of cholesterol have become highly significant in quality control of food products.

Many procedures, such as fluorescence detection[1,2], electrophoresis[3], Raman spectroscopy[4], high-performance liquid chromatography (HPLC)[5], gas-liquid chromatography[5,6] and using enzymes[7], have been reported earlier for the detection and estimation of cholesterol. However, the majority of these methods do not assure on-site monitoring of cholesterol. Even though enzymatic procedures ensure the specificity and selectivity required for these kinds of assays, the use of enzymes makes the fabrication and handling of the sensor head difficult and costly. Hence, the development of simple, inexpensive, direct and real-time cholesterol sensors is of continuing interest, because the traditional methods for cholesterol measurement require costlier laboratory analyses.

Optical fiber long period gratings (LPGs) are being used extensively in sensing applications for the last few decades. In this paper, we propose a cholesterol biosensor exploiting the sensitivity of chitosan coated LPGs to test the concentration of the cholesterol sample solution.

An LPG operates by the coupling of the fundamental core mode (i.e., the $LP_{01}$ mode) to the co-propagating cladding modes ($LP_{0m}$ mode with $m$= 2, 3, 4 ...) in the fiber. This coupling of power results in the formation of rejection bands around specific wavelengths (resonant wavelengths) in the transmission spectrum of the LPG. These resonant wavelengths are given by the phase-matching equation as

$$\lambda_m = (n_{\text{eff}}^{\text{co}} - n_{\text{eff},m}^{\text{cl}})\Lambda\,, \tag{1}$$

where $\lambda_m$ is the resonant wavelength corresponding to the coupling to the $m$th cladding mode, $\Lambda$ is the grating period, $n_{\text{eff}}^{\text{co}}$ is the effective refractive index of the fundamental core mode ($LP_{01}$), and $n_{\text{eff},m}^{\text{cl}}$ is the effective refractive index of the $m$th order cladding mode ($LP_{0m}$). External perturbations, like strain, temperature, bending and surrounding refractive index (SRI)[8], affect the coupling strength between the core and cladding modes, which leads to the amplitude changes as well as the wavelength shift of the resonant peaks in the LPG transmission spectrum.

The operation of the LPG based chemical sensor is based on the refractive index sensitivity of the LPG due to the dependence of the effective index of the cladding mode $n_{\text{eff},m}^{\text{cl}}$ on the SRI. The effect of SRI on the resonant wavelength[9] is determined by

$$\left(\frac{\mathrm{d}\lambda}{\mathrm{d}n_s}\right)_m = \left(\frac{\mathrm{d}\lambda}{\mathrm{d}n_{\text{eff},m}^{\text{cl}}}\right)\left(\frac{\mathrm{d}n_{\text{eff},m}^{\text{cl}}}{\mathrm{d}n_s}\right), \tag{2}$$

where $\mathrm{d}n_s$ is the change in SRI. It is known that the sensitivity of LPG to the SRI can be enhanced by providing one or more layers of coatings of reactive materials over the grating region[10,11].

In order to enhance the sensitivity of cholesterol sensing, a thin layer of chitosan was coated over the

* E-mail: mathewsbobby@gmail.com

LPG. Chitosan is a polysaccharide obtained by deacetylisation of chitin, which is the major constituent of the exoskeleton of crustaceous water animals[12]. Chitosan can selectively bind materials, such as cholesterol, fat, metal ion and protein[13]. Chitosan contains three types of reactive functional groups, which are an amino/acetamido group as well as a primary and a secondary hydroxyl groups. As the sample of cholesterol is introduced, the cholesterol gets attached to these active sites on the layer of coating. The combined effects of electrostatic attraction, embedding, adsorption and entrapment are the probable mechanisms for the cholesterol binding effects of chitosan[14]. This binding of cholesterol in turn enhances the sensitivity of LPG to the SRI, and this principle is used in the realization of the cholesterol sensor.

LPG with a grating period of 435 μm was fabricated by KrF excimer laser source (248 nm) through point-by-point writing method on SMF-28 (SMF-28e, Corning) fiber.

The sensor head was fabricated by coating the LPG with a thin layer of chitosan. 0.25 mg of high molecular weight chitosan powder with degree of deacetylisation of 98% was stirred well with 1 mol acetic acid at room temperature for 5 h to get a clear solution. Dip coating technique was used to coat the LPG with chitosan. The coated fiber was dried in air at room temperature to avoid cracks.

The scanning electron microscope (SEM) image of the coating shown in Fig.1(a) depicts a uniform surface layer of chitosan without any cracks. Fig.1(b) shows the end view of the fiber with coating. The chitosan coating on the fabricated sensor head has a thickness of 1.461 μm.

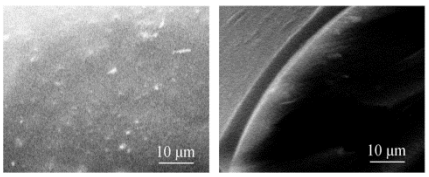


**Fig.1 SEM images of (a) the surface of chitosan coated layer and (b) the end view of the fiber with coating**

The chitosan coated LPG sensor head was fixed in a specially designed glass cell with epoxy as shown in Fig.2. Provisions for filling the sample and draining it out as and when desired were provided in the cell. The transmission spectrum of the LPG was studied with an optical spectrum analyzer (OSA) (Yokogawa-AQ6319) and a white-light source (Yokogawa-AQ4305). Accurate measurements were ensured by maintaining the temperature of the experimental setup and sample solution at 25.0 °C±0.5 °C. In addition, the test sample with a volume of 30 mL was used, so that the fiber section containing LPG was immersed completely in test sample throughout the experiments. The humidity around the test setup was also monitored to avoid the influence of humidity on the coating.

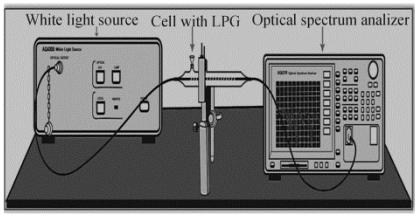


**Fig.2 Schematic diagram of experimental setup**

At the end of each measurement, the glass cell and the LPG sensor head were cleaned with distilled water and isopropyl alcohol repeatedly, followed by proper drying, so that the initial transmission spectrum of LPG in air was obtained.

Pure cholesterol ($C_{27}H_{46}O$) purchased from Sigma Aldrich was used for preparing the sample solutions with different cholesterol concentrations ranging from 0 g/mL to $5\times10^{-3}$ g/mL, by dissolving definite amount of cholesterol in coconut oil with refractive index of 1.448. The refractive indices of these sample solutions were found to vary from 1.448 to 1.455.

Fig.3 shows the transmission spectra of LPG with a period of 435 μm in air with and without the coating of the chitosan layer, and it also depicts the transmission spectrum of the coated LPG when it was immersed in pure coconut oil. For the used LPG, the maximum power coupling to the cladding mode was observed corresponding to the resonant peak of $LP_{04}$ mode at 1 568.93 nm in air. This resonant peak exhibits the maximum response at the test conditions, compared with other resonant modes.

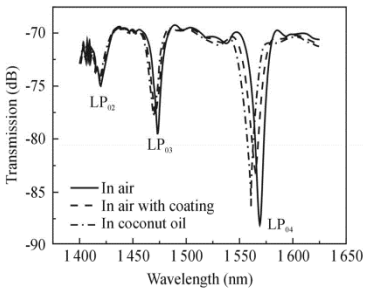


**Fig.3 Transmission spectra of LPG in air (with and without coating) and in solvent (with coating)**

The resonant peak of $LP_{04}$ mode at 1 568.93 nm in air was shifted to 1 565.37 nm after the prepared coat-

ing was dried. When pure solvent is introduced into the glass cell, the resonant peak of $LP_{04}$ shows a remarkable blue shift. The loss peak of $LP_{04}$ mode has a blue shift from 1 565.37 nm to 1 560.87 nm as the surrounding medium is altered from air to coconut oil. Along with the blue shift in the wavelength, the resonant peak amplitude is increased from −83.18 dB to −86.374 dB. Hence, further investigations will be centered on the $LP_{04}$ mode of the transmission spectra in the wavelength range 1 520 nm to 1 580 nm.

Fig.4 shows the transmission spectra of chitosan coated LPG sensor head with various cholesterol concentrations in coconut oil. When the concentration of the test solutions is increased, a blue shift of the $LP_{04}$ resonant peak is observed. The LPG exhibits a total blue shift of approximately 25.12 nm when the concentration of cholesterol is changed up to $5\times10^{-3}$ g/mL. This spectral shift of 25.12 nm, noticed for a refractive index range of the sample solutions from 1.448 to 1.455, corresponds to an average resolution of $2.78\times10^{-4}$ $nm^{-1}$.

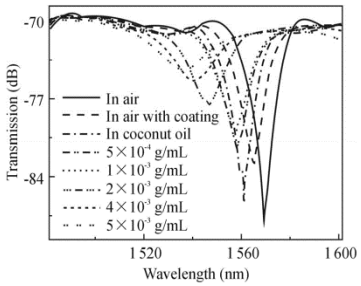


**Fig.4 Transmission spectra of chitosan coated LPG with different concentrations of cholesterol**

The sensitivity of the LPG is shown in Fig.5, when it is used as a sensor for various concentrations of cholesterol dissolved in coconut oil.

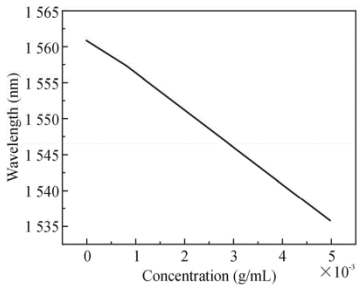


**Fig.5 Resonant wavelength ($LP_{04}$) peak positions as a function concentration of cholesterol**

The overall sensitivity in the measurement range of the sensor is around $5.025\times10^{6}$ pm·mL/g of cholesterol, which is more than double of that of the uncoated LPG sensor which was reported earlier[15]. Throughout the range of measurement, the sensor shows a linear response, which is highly appreciable for a commercial cholesterol sensor.

The transmitted intensity of the resonant wavelength ($LP_{04}$) with respect to the different concentrations of cholesterol in the measurement range is shown in Fig.6.

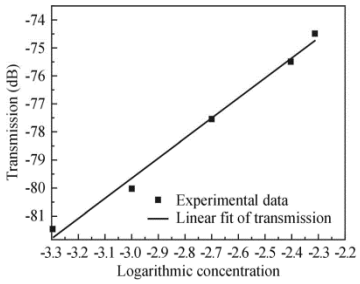


**Fig.6 Transmitted intensities at resonant wavelength ($LP_{04}$) peak as a function of logarithmic concentration of cholesterol**

As the cholesterol concentration increases, the SRI increases to approaching the cladding refractive index of the fiber, which can reduce the coupling between the core and cladding modes. This reduced coupling is attributed to the reduction in the amplitude of the $LP_{04}$ loss peak. In this experiment, the amplitude of the $LP_{04}$ resonant wavelength peak is decreased from −81.48 dB to −74.46 dB as the concentration of cholesterol in coconut oil is varied up to $5\times10^{-3}$ g/mL. A linear response of the transmitted intensity is also observed in the measurement range of cholesterol concentration. This intensity modulation can also be utilized along with the wavelength coded information to have better results for a commercial sensor.

The results shown in this paper depict the application of fiber optic LPG based system for the sensing and measurement of cholesterol concentration. The wavelength as well as the intensity modulation characteristics can be utilized in designing cholesterol sensors for commercial applications. The sensor presented here provides a real time response and requires only a small volume of the sample for analysis.

Added features of the sensor, like simplicity and high sensitivity, make it recommendable for medical diagnosis and clinical applications for the detection of cholesterol concentration in humans with suitable modifications. The system can be effectively employed in the areas of chemical and biomedical sensing, drug development, etc. The wide range and linear response are the other attractive features of the developed sensor.

**Acknowledgement**

We highly appreciate the support rendered by Fiber

Optics Laboratories, Central Glass and Ceramics Research Institute, Kolkata, which contributed greatly to this work. We thankfully remember the support rendered by the staff and students of Robert Gordon University, Aberdeen, UK. University Grants Commission, New Delhi is also acknowledged for the fellowships and for the financial assistance under the UKIERI project.

## References

[1] T. N. Flink, A. A. Oraevsky, F. K. Tittel, S. L. Thomsen and S. L. Jacques, Proceedings of SPIE **2679**, 34 (1996).

[2] Yan Y. H., Xu Y. H. and Li S. P., Chinese Journal of Biomedical Engineering **23**, 13 (2004).

[3] Lee I. N., Pinto D., Arriaga E. A., Zhang Z. and Dovichi N. J., Analytical Chemistry **70**, 4546 (1998).

[4] P. L. Cacheux, G. Menard, H. N. Quang, P. Weinmann, M. Jouan and N. Q. Dao, Applied Spectroscopy **50**, 1253 (1996).

[5] W. W. Wong, D. L. Hachey, L. L. Clark, S. Zhang, M. Llaurador and W. G. Piond, Applied Radiation & Isotopes **45**, 529 (1994).

[6] E. Agulló and B. Susna Gelós, Food Research International **29**, 77 (1996).

[7] G. Li, J. M. Liao, G. Q. Hu and N. Z. Ma, Biosensors Bioelectronics **20**, 2140 (2005).

[8] S. W. James and R. P. Tatam, Measurement Science & Technology **14**, 49 (2003).

[9] Jaw-Luen Tang and Jien-Neng Wang, Sensors **8**, 171 (2008).

[10] Ignacio Del Villar, Ignacio R. Matías and Francisco J. Arregui and Philippe Lalanne, Optics Express **13**, 56 (2005).

[11] Yinping Miao, Kaikiang Zhang, Yujie Yuam, Bo Liu, Hao Zhang, Yan Liu and Jianquan Yao, Applied Optics **52**, 90 (2013).

[12] Pesaramelli Karteek, International Journal of Pharmacy and Technology **2**, 186 (2010).

[13] Young In Cho, Hong Kyoon No and Samuel P. Meyers, Journal of Agricultural Food Chemistry **46**, 3839 (1998).

[14] Wenshui Xia, Ping Liu, Jiali Zhang and Jie Chen, Food Hydrocolloids **25**, 170 (2010).

[15] C. Bobby Mathews, T. M. Libish, J. Linesh, P. Biswas, S. Bandyopadhyay, K. Dasgupta and P. Radhakrishnan, A Biosensor for the Detection and Estimation of Cholesterol Levels based on Long Period Gratings, International Conference on Fiber Optics and Photonics, 1 (2013).

Sensors & Transducers, Vol. 149, Issue 2, February 2013, pp. 83-88

Sensors & Transducers



http://www.sensorsportal.com

# A Biosensor for the Detection and Estimation of Cholesterol Levels based on Long Period Gratings

**[1, 2*] C. Bobby MATHEWS, [1] T. M. Libish, [1] J. Linesh, [3] P. Biswas, [3] S. Bandyopadhyay, [3] K. Dasgupta, [1] P. Radhakrishnan**

[1] International School of Photonics, Cochin University of Science and Technology, Cochin-22, Kerala, India

[2] MES College of Engineering, Kuttippuram, Kerala, India

[3] Central Glass and Ceramics Research Institute, Kolkata-32, India

Tel.: +91 4842575848, fax: +91 4842576714

*E-mail: mathewsbobby@gmail.com

*Received: 8 November 2012 /Accepted: 14 February 2013 /Published: 28 February 2013*

**Abstract:** A Fiber Optic sensor for determining the total cholesterol has been designed and developed. The Long Period Grating (LPG) sensor developed showed good stability and repeatable performance. The sensor also showed good linear response in the range of 500 ppm to 4000 ppm of cholesterol levels. This is highly desirable for a commercial cholesterol sensor as the level of cholesterol for normal humans ranges from 1400 ppm to 2000 ppm. *Copyright © 2013 IFSA.*

**Keywords:** Biosensor, Cholesterol, Fiber optic, Long period grating.

## 1. Introduction

Cholesterol is a kind of lipid and a vital substance for animal life. Cholesterol is present in practically all cells of mammals, and is highly essential for the functioning of some glandules and interacts with many compounds such as the lipids from the membrane and other cell components. In addition, they are the basic components of nerve and brain cells [1] and are the precursors for other biological materials, such as bile acid and steroid hormones [2]. The cholesterol concentration in the blood of healthy people is in the range of 1400 to 2000 ppm [3]. When in excess, cholesterol may cause a number of health problems.

Hypercholesterolemia is one of the many independent risk factors for coronary heart diseases. Public concern about the risks of high cholesterol levels in blood began to rise in the 1980s. In the last three decades, numerous studies have brought out the relationship between increased cholesterol concentration and the occurrence of cardiovascular diseases like arteriosclerosis and hypertension. In quality control, determination of cholesterol and its derivatives in food is important as they may increase its level in the blood. For these reasons, cholesterol has become one of the main parameters to be determined in routine clinical, pharmaceutical, biomedical research and food processing laboratories. Consequently, a growing demand for cholesterol testing technology has been noticed in the last few years.

Several techniques developed for detection and estimation of cholesterol have been reported earlier,

Sensors & Transducers, Vol. 149, Issue 2, February 2013, pp. 83-88

such as, fluorescence detection [4, 5], electrophoresis [6], Raman spectroscopy [7], HPLC [8], gas-liquid chromatography [8, 9] etc. However, most of them do not assure on-site monitoring of cholesterol. Enzymatic procedures have practically replaced the chemical methods based on the classical Libermann-Burchard reaction [10]; which has been used traditionally for free total cholesterol determination, as enzymes ensure the specificity and selectivity required for these kinds of assays. Immobilized enzymes also offer advantages over free enzymes for their repeated use, ease of separation of enzyme and products, enhanced stability and significant reduction in the operation cost.

Cholesterol oxidase is one of the industrially important enzymes. It catalyzes the oxidation of cholesterol and forms equimolar amounts of cholest-4-en-3-one and hydrogen peroxide. The enzymatic methods are based on cholesterol oxidase for the determination of free cholesterol, which catalyze the following reaction.

$$Cholesterol + O_2 \xrightarrow{ChO_x} Cholest-4-en-3-one + H_2O_2 \quad (1)$$

Such enzymatic monitoring of cholesterol makes use of oxygen consumption or the production of hydrogen peroxide during the above mentioned enzymatic reaction. Enzymatic methods based on cholesterol esterase [11], cholesterol oxidase [11, 12], cytochrome P450scc [13], fiber optic [14], acoustic wave [15] etc. has been reported in the literature. The use of these enzymes makes the fabrication and handling of the sensor head difficult and is costlier. Hence, development of simple, inexpensive, direct and real-time cholesterol sensors is of continuous interest, as the traditional methods for cholesterol measurement require costlier laboratorial analyses.

In this context, fiber optic sensors offer very attractive solutions due to their intrinsic merits like high sensitivity, immunity to electromagnetic interference, small size, fast response etc. In recent years, Optical Fiber Long Period Grating (LPG) technology has gained great attention due to its numerous applications in fiber optic sensor [16] and communication systems. LPGs are fabricated by inducing a refractive index (RI) modulation in the core of a fiber with periodicities typically of hundreds of micrometers. Various features of LPGs are made used in its applications as sensors with a high degree of stability and reliability. The advantages of this type of grating sensor are their simple fabrication, ease of implementation, wavelength coded information, easy interrogation and the fact that it does not involve the use of toxic chemicals.

In this paper, we propose a cholesterol biosensor exploiting the sensitivity of LPGs to the concentration of the sample solution under test. As the cholesterol concentration levels are changed, a RI variation occurs, which in turn induce shifts in the resonant wavelength and change the depth (amplitude) of the loss bands in the LPG transmission spectrum. Cholesterol levels can be detected and measured by analyzing these spectral or amplitude changes. The device performance is analyzed in terms of its sensitivity and resolution.

## 2. Theory of Operation

An LPG operates by the coupling of the fundamental core mode (i.e. the LP01 mode) to the co-propagating cladding modes (LP0m mode with m = 2, 3, 4 . . .) in the fiber. As a result of this coupling, rejection bands around specific wavelengths (resonant wavelengths) are formed in the transmission spectrum of the LPG. The guided mode couples to the cladding modes at a wavelength [17], which can be obtained through the phase-matching equation (2):

$$\lambda_m = [n_{eff}^{co} - n_{eff,m}^{cl}]\Lambda \quad (2)$$

where $\lambda_m$ is the resonant wavelength corresponding to coupling to the m$^{th}$ cladding mode, $\Lambda$ is the grating period, $n_{eff}^{co}$ is the effective refractive index of the fundamental core mode ($LP_{01}$), $n_{eff,m}^{cl}$ is the effective refractive index of the m$^{th}$ order cladding mode ($LP_{0m}$).

The resonant wavelengths in the transmission spectrum of LPG are strong functions of external perturbations like strain, temperature, bending and surrounding refractive index (SRI) [18]. Any such external perturbations affect the coupling strength between the core and cladding modes, which leads to both amplitude and wavelength shift of the attenuation bands in the LPG transmission spectrum. Measurement of these spectral parameters such as amplitude and wavelength shift in response to environment, surrounding the grating region forms the basis of sensing with LPGs.

The LPG based chemical sensor operation is based on the variation of LPG transmission spectrum caused by changes in the SRI. The shift of the center wavelength of the attenuation peaks can occur towards longer or shorter wavelengths based on the SRI. The refractive index sensitivity of the LPG arises from the dependence of the effective index of the cladding mode ($n_{eff,m}^{cl}$) on the refractive index of the surrounding material. Thus, the LPG based sensor can be used for direct measurement of chemical concentrations, which determine the surrounding refractive index. The effect of refractive index of the surrounding medium on the resonant wavelength [19] is expressed by (3):

Sensors & Transducers, Vol. 149, Issue 2, February 2013, pp. 83-88

$$\left(\frac{d\lambda}{dn_s}\right)_m = \left(\frac{d\lambda}{dn_{cl,m}^{eff}}\right)\left(\frac{dn_{cl,m}^{eff}}{dn_s}\right), \quad (3)$$

where $dn_s$ is the change in the refractive index of the surrounding material.

For each cladding mode (m), the above expression is unique and is expected to have a strong dependence on the order of the coupled cladding mode. Higher order cladding modes tend to show greater sensitivity to the changes in external refractive index because these modes extend further out into the area exterior to the fiber [20, 21].

The spectral changes in the transmission spectrum of LPGs can be characterized in terms of external RI as follows. If the SRI is lower than the refractive index of the cladding ($n_s<n_{cl}$), mode guidance can be explained using total internal reflection. In this case, typically strong resonance peaks are observed and the attenuation bands shift towards shorter wavelengths (blue shift) with a reduction in the amplitude of the loss peak, as the external medium refractive index increases up to the fiber cladding refractive index [22, 23]. The closer the refractive index of the surrounding medium to that of the cladding material, the higher the grating sensitivity, which in turn leads to larger wavelength shift.

When the value of the ambient refractive index matches with that of the cladding, the cladding layer acts as an infinitely extended medium and hence supports no discrete cladding modes. In this case when $n_s = n_{cl}$, a broadband radiation mode coupling occurs with no distinct attenuation bands [24]. In short, when the external RI becomes equal to that of silica of the cladding, rejection bands disappear, and the transmission spectrum is flattened.

Once the SRI is higher than the refractive index of the cladding ($n_s > n_{cl}$), the cladding modes no longer experience total internal reflection and Fresnel reflection can be used to explain mode coupling characteristics. Then the resonance peaks reappear at slightly longer wavelengths (red shift) compared to those measured with air as the surrounding medium [25]. In this case, it is also observed that, the wavelength shift is very small with variation in RI, but changes in the amplitude of resonance dips are large.

## 3. Experiments

### 3.1. LPG Fabrication

The LPG was fabricated with a KrF - Excimer laser source (248 nm), through point-by-point writing method. The standard single mode Fiber, SMF-28 (SMF-28e, Corning) used for the LPG fabrication has a core diameter of 8.2 micron and cladding diameter of 125 micron and a numerical aperture of 0.14. The index of refraction were 1.46145 and 1.456, for the core and the cladding respectively. The photosensitivity of the fiber was enhanced by the process of Hydrogen loading at 1000 °C and 1500 psi of pressure for 24 hours prior to the fabrication of LPG. The residual molecular Hydrogen retained after the photochemical reactions during the process of grating writing was removed by annealing at a temperature of 2000 °C for 7 hours. LPG with a grating period of 550 μm was selected for the experimental investigation.

### 3.2. Experimental Setup

The LPG sensor head was fixed in a specially designed glass cell with provision for filling the sample and draining it out as and when desired. The transmission spectrum of the LPG was studied with an optical spectrum analyzer (OSA) (Yokogawa - AQ6319) and a white-light source (Yokogawa - AQ 4305) as the signal source. The transmission spectra of the LPGs were altered by the fluctuations of the external parameters like strain, temperature and bending. The effect of strain and bending were avoided by fixing the fiber in the glass cell with epoxy at its both ends such that, the grating section was kept at the center of the cell, without any bends. Accurate measurements were ensured by maintaining the temperature of the experimental setup and sample solution at 25.0 ± 0.5 °C. In addition, a volume of 22 ml of the test sample was used throughout the experiments. The resonant wavelength shift and amplitude changes of the LPG attenuation dips were measured with the fiber section containing the LPG immersed completely in samples. No protective coating was there on the fiber around the grating region, so that the external RI could easily affect the effective refractive index of the cladding modes. The fiber inscribed with LPG was connected to the light source on one end and to the OSA on the other side as shown in Fig. 1.

### 3.3. Materials and Methods

Pure cholesterol ($C_{27}H_{46}O$) was used for the studies. Coconut oil with a refractive index of 1.448 was chosen as the solvent for preparing the sample solutions, as its refractive index value is near to the cladding refractive index of the fiber used. Samples with different concentrations ranging from 0 ppm to 5000 ppm, prepared by dissolving definite amount of cholesterol in coconut oil, were subjected to investigation. The refractive indices of the sample solutions were found to vary from 1.448 to 1.455. Changes in the spectrum were observed as soon as the samples were introduced into the glass cell. All readings were taken one minute after the LPGs were immersed in the solution to have a stabilized output. The initial spectrum of the LPG in air was used as the primary reference for all the sample analysis. This is to ensure that the LPG attenuation dips return to the original wavelength after each measurement. At the

Sensors & Transducers, Vol. 149, Issue 2, February 2013, pp. 83-88

end of each sample measurement, the glass cell and the LPG sensor head was cleaned with distilled water and then with isopropyl alcohol repeatedly, followed by proper drying, so that the initial transmission spectrum of LPG in air was obtained.

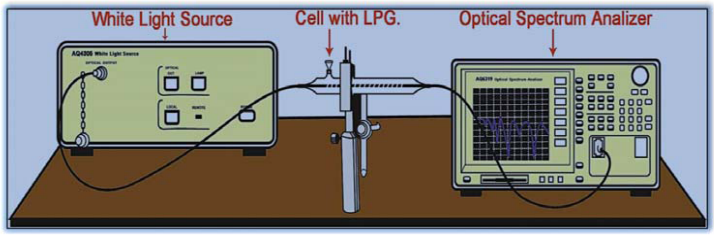


**Fig. 1.** Experimental Setup.

## 4. Results and Discussion

Fig. 2 shows the transmission spectra of LPG with period 550 μm in air and immersed in coconut oil. For the LPG used, power coupling to the cladding modes had resonant peaks at the wavelengths 1445.83 nm (LP02), 1493.28 nm (LP03), and 1583.11 nm (LP04) in air. The LP04 mode at 1583.11 nm exhibited maximum response to the test conditions, compared to other resonant modes.

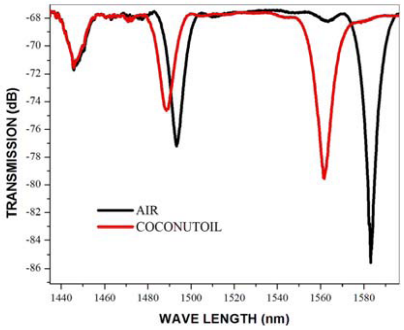


**Fig. 2.** Transmission spectra of LPG in air and coconut oil.

As the glass cell was filled with coconut oil, the resonant peaks of LP03 and LP04 showed a remarkable shift to the lower wavelength region. The loss peak of LP04 mode had maximum blue shift from 1583.11 nm to 1561.72 nm as the surrounding medium was altered from air to coconut oil. Along with the blue shift in the wavelength, the dip of the resonant peak decreased from -85.59 dB to -79.54 dB. Hence, further investigations were centered on the LP04 mode of the transmission spectra in the wavelength range of 1540 nm to 1580 nm.

Fig. 3 shows the transmission spectra of LPG for various concentrations of cholesterol. As the concentrations of cholesterol in the sample solutions were varied, a blue shift was observed in the LP04 resonant peak wavelength.

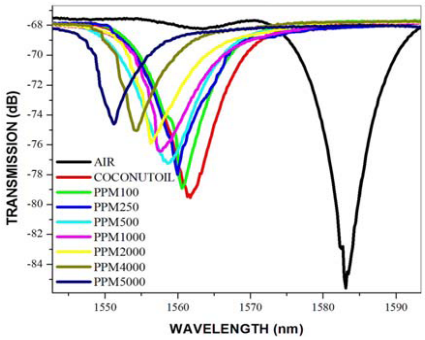


**Fig. 3.** Transmission spectra of LPG for different concentrations of cholesterol.

The LPG exhibited a total blue shift of approximately 10.5 nm when the cholesterol levels in the surrounding medium were changed up to 5000 ppm. This spectral shift of 10.5 nm, noticed for a refractive index range of 1.448 to 1.455 of the sample solutions, corresponds to an average resolution $6.7\times10^{-4}$ $nm^{-1}$. Apart from the wavelength shift with the changes in refractive index of the external medium, there was a reduction in the peak intensity of the resonance band with increasing cholesterol levels.

Sensors & Transducers, Vol. 149, Issue 2, February 2013, pp. 83-88

The sensitivity of the LPG, when used as a sensor for various concentration of cholesterol is shown in Fig. 4.
The overall sensitivity in the measurement range of the sensor was around 2.1 pm/ppm of cholesterol.

Fig. 5 shows the shift in peak of resonant wavelength (LP04) as a function of concentration of cholesterol.

The transmittance at the resonant wavelength (LP04) with respect to the different levels of cholesterol, in the measured range is shown in Fig. 6.

The amplitude of the resonant wavelength peak decreased from -79.54 dB to -74.61 dB as the concentration of cholesterol was varied from 0 ppm to 5000 ppm. A linear response of the transmittance was observed in the measured range of cholesterol levels. This intensity modulation can also be utilized along with the wavelength coded information to have better results for a commercial sensor.

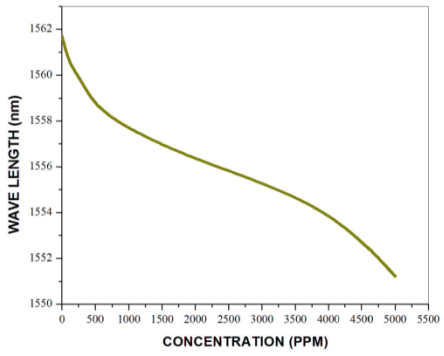


**Fig. 4.** Resonant Wavelength (LP04) Peak positions as a function of different concentrations of cholesterol.

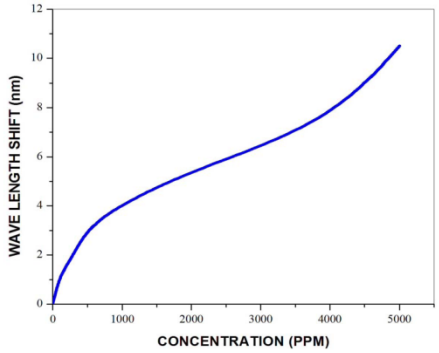


**Fig. 5.** Shift in Resonant Wavelength (LP04) Peak as a function of various concentrations of cholesterol.

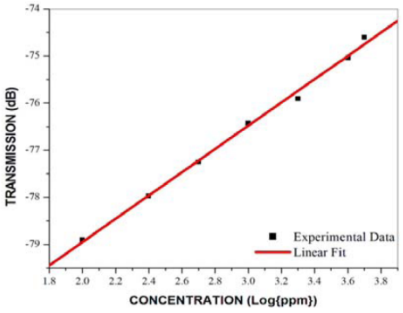


**Fig. 6.** Transmittance at Resonant Wavelength (LP04) Peak as a function of different concentrations of cholesterol.

## 5. Conclusions

The results showed in this work depict the application of fiber optic LPG based system for the sensing and measurement of cholesterol concentrations. Both the wavelength and intensity modulation characteristics can be utilized in designing cholesterol sensors for commercial applications. The sensor presented here provides a real time response and requires only a small volume of the sample for analysis. Added features like simplicity and high sensitivity of the sensor make it recommendable for medical diagnosis and clinical applications for the determination of cholesterol levels in humans with suitable modifications. The system can be effectively employed in the areas of chemical and biomedical sensing, drug development etc., as a number of substances can be detected, and different parameters can be measured.

## Acknowledgements

We highly appreciate and acknowledge the support rendered by Fiber Optics Laboratories, Central Glass and Ceramics Research Institute, Kolkata, which contributed greatly to this work. The author BMC acknowledges the Cochin University of Science and Technology, for the fellowship. He also thankfully remembers the sponsorship of MES College of. Engineering, Kuttippuram. We also acknowledge the University Grants Commission, New Delhi, for financial assistance through RFSMS. KSCSTE is also acknowledged for the financial assistance.

## References

[1]. N. B. Myant, The Biology of Cholesterol and Related Steroids, *Willium Heinemann*, London, 1981.

*Sensors & Transducers, Vol. 149, Issue 2, February 2013, pp. 83-88*

[2]. D. S. Fredrickson, R. I. Levy, J. B. Wyngarden, D. D. Fredrickson (Eds.), The Metabolic Basis of Inherited Disease, *McGraw-Hill*, New York, 1972, p. 545.
[3]. B Wang, J Huang, M Li, X Zhou, Multifunctional sensing film used for fiber optic cholesterol sensor, in *Proc. of the SPIE*, Vol. 7278, 2009.
[4]. Flink, T. N., Oraevsky, A., Jacques S. L., Autofluorescence detection of oxidized LDL in monocytes: a novel risk factor for the assessment of atherosclerosis ?, *Proc. of the SPIE*, Vol. 2679, 1996.
[5]. Yan, Y. H., Xu, Y. H., Li, S. P., Development of fiber optical biosensor of cholesterol based on fluorescence quenching, *Chinese Journal of Biomedical Engineering*, 23, 1, 2004, p. 13.
[6]. Lee, I. N., Pinto D., Arriaga, E. A., Zhang, Z., Dovichi, N., Picomolar Analysis of Proteins Using Electrophoretically Mediated Microanalysis and Capillary Electrophoresis with Laser-Induced Fluorescence Detection, *J. Anal. Chem.,* 70, 1998, p. 4546.
[7]. Cacheux, P. L., Menard, G., Quang, H. N., Weinmann, P., Jouan, M., Dao, N. Q., Quantitative Analysis of Cholesterol and Cholesterol Ester Mixtures Using Near-Infrared Fourier Transform Raman Spectroscopy, *Appl. Spectrosc*., 50, 1996, p. 1253.
[8]. Wong, W. W., Hachey, D. L., Clark, L. L., Zhang, S., Llaurador, M., Piond, W. G., An improved HPLC method to purify erythrocyte cholesterol for estimation of in vivocholesterol synthesis using the deuterium method, *Appl. Radial Isotopes*, 45, 1994, p. 529.
[9]. Agullo, E. and Susna, B., Gas-liquid chromatographic determination of total and free cholesterol in egg pastas, *Food Res. Int*., 29, 1996, p. 77.
[10]. M. D. Marazuela, B. de la Calle, A. Quejido, M. C. Moreno-Bondi, Free cholesterol fiber-optic sensor for serum samples with simplex optimization, *Biosens. Bioelectron*., 12, 1997, pp. 233-241.
[11]. Lia G., Liao, J. M., Hu G. Q., Ma, N. Z, Wu P. J. Study of carbon nanotube modified biosensor for monitoring total cholesterol in blood, *Biosens. Bioelectron.,* 20, 2005, pp. 2140–2144.
[12]. Tan X., Li M., Cai, P., Luo L., Zou X, An amperometric cholesterol biosensor based on multiwalled carbon nanotubes and organically modified sol-gel/chitosan hybrid composite film, *Anal. Biochem.,* 337, 2005, pp. 111–120.
[13]. Shumyantseva U., Deluca G., Bulko T., Carrara S., Nicolini C., Usanov S. A., Archakov, A, Cholesterol amperometric biosensor based on cytochrome P450scc, *Biosens. Bioelectron.,* 19, 2004, p. 971.
[14]. Kim S. H., Nam S. M., Byun G. S., Yun S. Y., Hong, S, Determination of Cholesterol by a Diode Laser/Fiber Optic Colorimetric Spectrometer, *Bull. Korean Chem. Soc.,* 21, 2000, p. 389.
[15]. Martin, S. P., Lamb, D. J., Lynch, J. M., Reddy, S. M, Enzyme-based determination of cholesterol using the quartz crystal acoustic wave sensor, *Anal. Chim. Acta,* 487, 2003, pp. 91–100.
[16]. S. A. Vasil'ev, O. I. Medvedkov, I. G. Korolev, A. S. Bozhkov, A. S. Kurkov, E. M. Dianov, Fibre gratings and their applications, *Quantum Electronics,* Vol. 35, No. 12, 2005, pp. 1085 -1103.
[17]. T. M. Libish, J. Linesh, M. C. Bobby, B. Nithyaja, S. Mathew, C. Pradeep, P. Radhakrishnan, Glucose Concentration Sensor Based on Long Period Grating Fabricated from Hydrogen Loaded Photosensitive Fiber, *Sensors & Transducers*, Vol. 129, Issue 6, June 2011, pp. 142-148.
[18]. S. W. James, R. P. Tatam, Optical fiber long period grating sensors: characteristics and applications, *Meas. Sci. Technol*., Vol. 14, No. 5, 2003, pp. 49-61.
[19]. Jaw-Luen Tang, Jien-Neng Wang, Chemical Sensing Sensitivity of Long-Period Grating Sensor Enhanced by Colloidal Gold Nanoparticles, *Sensors*, 8, 2008, pp. 171-184.
[20]. V. Bhatia, A. M. Vengsarkar, Optical fiber long period grating sensors, *Opt. Lett.,* Vol. 21, No. 9, 1996, pp. 692-694.
[21]. H. J. Patrick, A. D. Kersey, F. Bucholtz, Analysis of the response of long period fiber gratings to external index of refraction, *J. Lightwave Technol.,* Vol. 16, No. 12, 1998, pp. 1606–1612.
[22]. X. W. Shu, L. Zhang, I. Bennion, Sensitivity characteristics of long-period fiber gratings, *J. Lightwave Technol.,* Vol. 20, No. 2, 2002, pp. 255-266.
[23]. B. H. Lee, Y. Liu, S. B. Lee, S. S. Choi, J. N. Jang, Displacements of the resonant peaks of a long period fiber grating induced by a change of ambient refractive index, *Opt. Lett.,* Vol. 22, No. 23, 1997, pp. 1769-1771.
[24]. Y. Koyamada, Numerical analysis of core-mode to radiation-mode coupling in long-period fiber gratings, *IEEE Photon. Technol. Lett.,* Vol. 13, No. 4, 2001, pp. 308-310.
[25]. O. Duhem, J. Franois Henninot, M. Warenghem, M. Douay, Demonstration of long- period-grating efficient couplings with an external medium of a refractive index higher than that of silica, *Appl. Opt.,* Vol. 37, No. 31, 1998, pp. 7223-7228.